CHALMERS

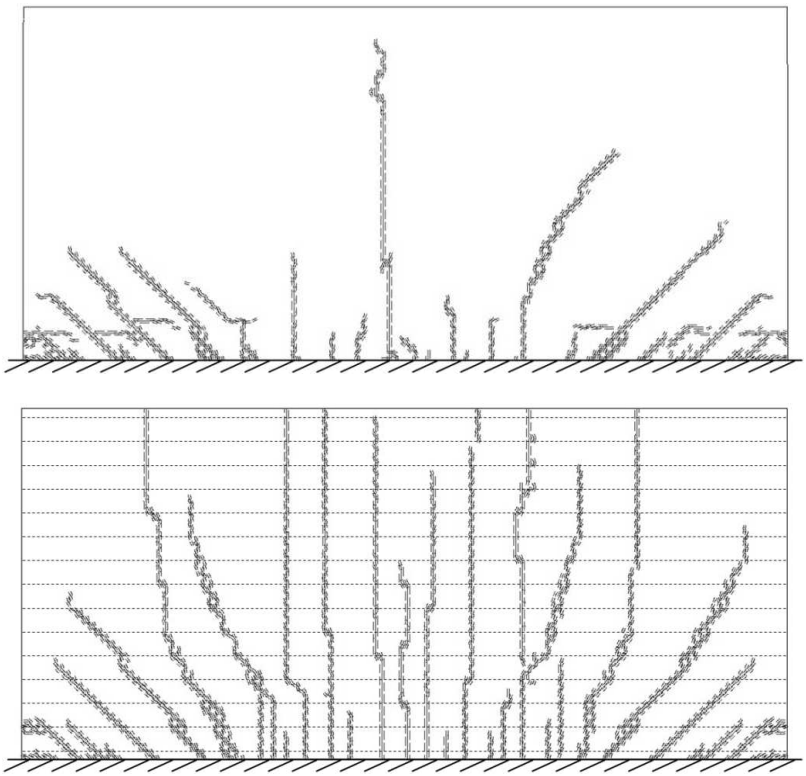

Crack Control of Concrete Structures Subjected to Restraint Forces

Influence of Fibre Reinforcement

Master of Science Thesis in the Master's Programme Structural Engineering and Building Performance Design

BRUNO ANTONA
RICHARD JOHANSSON

Department of Civil and Environmental Engineering
Division of Structural Engineering
Concrete structures
CHALMERS UNIVERSITY OF TECHNOLOGY
Göteborg, Sweden 2011

Master's Thesis 2011:70

MASTER'S THESIS 2011:70

Crack Control of Concrete Structures Subjected to Restraint Forces

Influence of Fibre Reinforcement

Master of Science Thesis in the Master's Programme Structural Engineering and Building Performance Design

BRUNO ANTONA

RICHARD JOHANSSON

Department of Civil and Environmental Engineering
Division of Structural Engineering
Concrete structures
CHALMERS UNIVERSITY OF TECHNOLOGY

Göteborg, Sweden 2011

Crack Control of Concrete Structures Subjected to Restraint Forces
Influence of Fibre Reinforcement

Master of Science Thesis in the Master's Programme Structural Engineering and Building Performance Design

BRUNO ANTONA
RICHARD JOHANSSON

Examensarbete / Institutionen för bygg- och miljöteknik,
Chalmers tekniska högskola 2011:70

Department of Civil and Environmental Engineering
Division of Structural Engineering
Concrete structures
Chalmers University of Technology
SE-412 96 Göteborg
Sweden
Telephone: + 46 (0)31-772 1000

Cover:
Crack patterns for the retaining wall with plain concrete (top figure) and ordinary reinforcement concrete (bottom figure), see Section 5.3.1.

Chalmers Reproservice / Department of Civil and Environmental Engineering
Göteborg, Sweden 2011

Crack Control of Concrete Structures Subjected to Restraint Forces
Influence of Fibre Reinforcement

Master of Science Thesis in the Master's Programme Structural Engineering and Building Performance Design

BRUNO ANTONA & RICHARD JOHANSSON

Department of Civil and Environmental Engineering
Division of Structural Engineering
Concrete structures
Chalmers University of Technology

ABSTRACT

When concrete is subjected to shrinkage, a need for deformation will occur. If this deformation is restrained, restraint forces will appear. When a concrete member is cast against an existing concrete member restraint forces may occur due to different needs of movement, which may lead to cracking. Two specific cases are when edge beams on concrete bridges are replaced and when concrete retaining walls are cast against an existing concrete foundation slab. Even though cracks are natural in reinforced concrete during the service state, they can cause durability problems if they become too large. Increased reinforcement amount and addition of fibre reinforcement to the concrete are two possibilities to control the cracking. However, guidance of how to design restrained members with regards to crack widths is insufficient in codes used today. Therefore, non-linear finite element analyses were performed in order to increase the understanding of the cracking response in restraint situations and how to design in these situations.

Results from non-linear finite element analyses were compared with test results on tie-rod tests carried out on concrete specimens with ordinary and fibre reinforcement. When using uniform material properties determined from tests, good agreement was achieved for the case with ordinary reinforcement. For the fibre reinforced concrete it was necessary to take into account the heterogeneity of the combined material. A new model, showing good agreement with test results, was proposed to simulate the behaviour of fibre reinforced concrete. When the modelling technique had been verified, it was also used to investigate the cracking response in other applications.

Investigations on the edge beam and the retaining wall showed that continuous edge restraint helps to create more and narrower cracks close to the restraint edge. However, reinforcement is still needed to keep crack widths at a sufficiently low level. The standard reinforcement configuration normally used today for bridge edge beams has been concluded to be acceptable. However, a configuration where reinforcement is concentrated at a certain distance away from the restraint edge was suggested to control crack widths in retaining walls cast on foundation slabs.

Applying fibre reinforcement has been found to be a good solution to improve the crack control in edge beams and retaining walls as this increases the number of cracks, and thus, reduces their crack widths. Ordinary reinforcement, though, is still needed.

Keywords: Crack control, restraint forces, fibre reinforced concrete, non-linear finite element analysis, shrinkage strain, tie-rod, edge beam, retaining wall.

Sprickbegränsning hos betongkonstruktioner utsatta för tvångskrafter
Inverkan av fiberarmering
Examensarbete inom Structural Engineering and Building Performance Design
BRUNO ANTONA & RICHARD JOHANSSON
Institutionen för bygg- och miljöteknik
Avdelningen för konstruktionsteknik
Betongbyggnad
Chalmers tekniska högskola

SAMMANFATTNING

När betong krymper uppkommer ett behov av deformation. Om denna deformation förhindras uppkommer tvångskrafter. När ett betongelement gjuts mot en existerande betongkonstruktion kan tvångskrafter uppstå på grund av olika rörelsebehov, vilket kan leda till sprickbildning. Två typiska exempel är när kantbalkar på betongbroar byts ut och när stödmurar gjuts mot en befintlig grundplatta. Även om det är naturligt att sprickor uppkommer i en armerad betongkonstruktion under dess livslängd kan de orsaka beständighetsproblem om de blir för stora. Att öka armeringsmängden eller att använda fiberarmering i betongen är olika sätt att begränsa och kontrollera sprickbildningen. Anvisningar för hur man dimensionerar konstruktioner utsatta för tvång med hänsyn till sprickbredder är otillräckliga i dagens regelverk. Därför har olinjära finita elementanalyser utförts för att öka förståelsen för sprickbildningsprocessen i tvångssituationer samt för hur man bör dimensionera i sådana situationer.

Resultat från finita elementanalyser har jämförts med resultat från experiment utförda på armerade och fiberarmerade dragbelastade betongstavar. Vid användning av konstanta materialegenskaper utvärderade från experimenten fanns en god överensstämmelse i fallen med armerad betong. För fiberarmerad betong var det dock nödvändigt att ta hänsyn till det sammansatta materialets heterogenitet. En ny modell som bättre simulerar verkningssättet hos fiberarmerad betong föreslogs och visade sig ge god överensstämmelse med testresultaten. Efter att denna modelleringsteknik verifierats användes den för att undersöka sprickbildningsprocessen i olika mer realistiska tillämpningar.

Undersökningar av kantbalkar och stödmurar visade att kontinuerligt tvång utefter en kant hjälper till att framtvinga fler och finare sprickor nära den inspända kanten. Vanlig armering behövs dock fortfarande för att hålla sprickbredderna på en tillräckligt låg nivå. En slutsats var att den standardutformning av armering av kantbalkar som vanligtvis används idag är tillfredställande. En förbättrad armeringsutformning där armering koncentrerats på ett visst avstånd från den inspända kanten har föreslagits för få effektivare sprickbreddbegränsing i stödmurar.

Fiberarmering visade sig vara ett bra sätt att begränsa sprickbredder i kantbalkar och stödmurar eftersom antalet sprickor ökar och därmed minskar sprickbredderna. Emellertid visade det sig att även vanliga armeringsstänger fortfarande behövs.

Nyckelord: Sprickbegränsning, tvångskrafter, fiberarmerad betong, olinjära finita elementanalyser, krympning, sprickbredd, betongstav, kantbalk, stödmur.

Contents

Preface

In this master's project, the cracking behaviour of concrete structures with ordinary and fibre reinforcement were studied. Structures with continuous edge restraint subjected to restraint forces were investigated by non-linear finite element analyses. The project was a cooperation between Reinertsen Sverige AB, Thomas Concrete Group AB and the Division of Structural Engineering, Concrete Structures, at Chalmers University of Technology, Sweden. The work was carried out at Reinertsen Sverige AB from January to June 2011.

First of all, we would like thank our three supervisors. Morgan Johansson, Reinertsen Sverige AB, who initiated this project, we wish to thank for all the guidance and the valuable discussions we have had during the project. We also thank Björn Engström, Chalmers, who also was the examiner, for his much appreciated comments and guidance. Further thanks to Ingemar Löfgren, Thomas Concrete Group AB, who shared his deep knowledge in fibre reinforcement.

This thesis was a continuation of three previous master theses carried out by Johan Nesset and Simon Skoglund, 2007, Helena Alfredsson and Johanna Spåls, 2008, and Patrik Johansson and Håkan Lantz, 2009. We would like to thank them all for sharing their results and FE files with us. Special appreciation is due to Patrik Johansson and Håkan Lantz who have shared their experience throughout the project. We also wish to thank the staff at Reinertsen Sverige AB, Göteborg, for their support and for providing a good working climate.

Furthermore, we would like to thank our opponent Thomas Åhnberg for his feedback and comments during this project.

We also want to show our gratitude to Anette Jansson for sharing the results from tests carried out as a part of her Ph.D. project at Chalmers.

Göteborg, June 2011

Bruno Antona & Richard Johansson

Notations

Roman upper case letters

A_{s1}	Total top reinforcement area
A_{s2}	Total bottom reinforcement area
A_{surf}	Surface area
E_c	Young's modulus for concrete
$E_{c,ef}$	Young's modulus for concrete, effective value
E_s	Young's modulus for steel
F_b	Bond force
F_{fm}	Bond force, mean value
L	Length
L_f	Length of a fibre
N	Normal force
N_{cr}	Cracking load of concrete
N_y	Yield force of reinforcement
P	Pull out force
R	Restraint degree
G_f	Fracture energy
T	Temperature
V_f	Fibre volume

Roman lower case letters

a_s	Distance from concrete face to the centre of the reinforcement level
b	Width of the cross-section
f_{cd}	Concrete compressive strength, design value
f_{ck}	Concrete compressive strength, characteristic value
f_{cm}	Concrete compressive strength, mean value
f_{cpt}	Concrete post tensile strength
f_{ct}	Concrete tensile strength
f_y	Yield strength of steel
f_{yd}	Yield strength of steel, design value
f_{yk}	Yield strength of steel, characteristic value
f_{ym}	Yield strength of steel, mean value
h	Height of the cross section
l_{el}	Element length
l_t	Transmission length
$l_{t,max}$	Maximum transmission length
n_{bar}	Number of reinforcement bars
s	Slip
s_N	Standard deviation of a sample
t	Width of the interface between edge beam and boundary
u	Imposed displacement
w	Crack width
w_c	Critical crack width
w_{max}	Maximum crack width
w_u	Ultimate crack width

Greek letters

α_{cT}	Coefficient of thermal expansion for concrete
δ	Displacement
ε	Strain
ε_c	Concrete strain
ε_{cT}	Thermal strain
ε_{ct}	Concrete tensile strain
ε_{cu}	Ultimate concrete tensile strain
ε_{cs}	Concrete shrinkage strain
$\varepsilon_{c,tot}$	Total concrete strain
ε_{pl}	Plastic strain
λ_f	Fibre aspect ratio
ξ	Input parameter in ADINA used to describe the ultimate concrete tensile strain
ρ_l	Longitudinal reinforcement ratio
ρ_t	Transversal reinforcement ratio
σ_c	Concrete stress
σ_{cd}	Concrete normal stress, design value
σ_{cm}	Concrete normal stress, mean value
σ_{ct}	Concrete tensile stress
τ_b	Bond stress
τ_{fd}	Mobilised shear stress, based on design values
τ_{fm}	Mobilised shear stress, based on mean values
$\tau_{fu,d}$	Shear stress at s = 2.0 mm, design value
$\tau_{fu,m}$	Shear stress at s = 2.0 mm, mean value
τ_{lim}	Limit value of bond stress
τ_{max}	Maximum bond stress
ϕ	Diameter of reinforcement bar
φ	Creep coefficient

1 Introduction

1.1 Background

When a reinforced concrete structural member is subjected to temperature changes and/or shrinkage, i.e. stress independent strains, a need for movement will occur. If this deformation is restrained, restraint forces will occur. Even though these restraining forces may not be large enough to cause failure of the structure by themselves, they may become important in the design for the serviceability limit state as they will lead to cracking if the concrete tensile strength is reached.

Cracking of reinforced concrete is natural while the structure is under service, i.e. the service state. However, cracks are intolerable if the crack widths impair the appearance, serviceability, function, or resistance of the structure. For instance, cracks may expose the reinforcement to the environmental conditions and because of presence of moisture and oxygen steel bars may start to corrode. This corrosion process can result in severe durability problems, which in the long way affect the load bearing capacity and safety of the structure. Therefore it is of great importance to keep the crack width below a certain value depending on the actual exposure. Increasing the number of cracks is a way to reduce the crack width, as the total need for deformation in the member will be the same independently of the number of cracks that have developed. Increased reinforcement amount is one way to achieve this, but also to add fibre reinforcement to the concrete, since it gives concrete a more ductile behaviour and acts as a 'distributed' reinforcement.

In order to increase the knowledge about how reinforced concrete structures behave while subjected to restrained forces and how to design them in order to keep the crack widths acceptable, three master theses have recently been carried out at Reinertsen Sverige AS. Nesset and Skoglund (2007) studied the cracking behaviour and crack pattern of a member with fixed short ends, see Figure 1.1 (a). Alfredsson and Spåls (2008) investigated the influence of different parameters in a continuously restrained edge beam, see Figure 1.1 (b), while Johansson and Lantz (2009) looked deeply into the influence of restraint cracking and crack widths in a continuous edge beam of a bridge, see Figure 1.1 (c). This thesis is a continuation of their work.

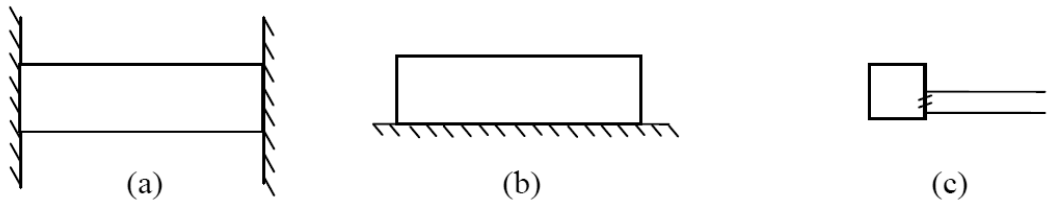

Figure 1.1 Examples of (a) short end restraint; (b) continuous edge restraint; (c) edge beam at a bridge.

A special situation where cracks can appear due to restraint forces is when a new concrete member is cast against an existing concrete member. The concrete in the two members will have different needs of movement and, due to this restraint situation, restraint forces will appear. One case where this problem occurs is when edge beams on concrete bridges are replaced, which usually is done a number of times during the lifetime of a bridge. Another similar case is when concrete retaining walls are cast against an existing concrete slab, schematically shown in Figure 1.2. Guidance of how to design these members regarding restraint forces and crack widths is insufficient in

codes used today. Therefore it is of interest to perform finite element analysis, in order to increase the knowledge on how to design in these situations.

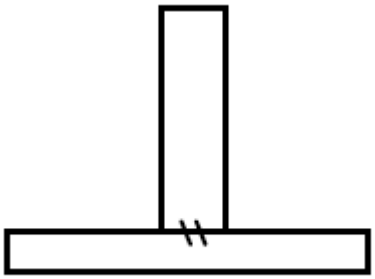

Figure 1.2 Concrete wall cast against a concrete slab.

1.2 Aim

The general aim of this thesis is to increase the knowledge of how to design reinforced concrete structures with regard to restraint forces that are obtained due to stress-independent strains. Focus will be put on the effect of different parameters on the crack widths of concrete structures with continuous edge restraint. It is of special interest to study the effects on the cracking process of adding fibre reinforcement. Investigations using non-linear finite element analysis will be carried out on bridge edge beams and retaining walls.

The different goals for this project are listed below:

- Verify the finite element modelling procedure, used in this and previous theses to describe concrete structures subjected to restraint forces, by comparing with test results from Jansson (2011).
- Investigate the applicability of the finite element model for cases with fibre reinforcement.
- Increase the parametrical study done by Johansson and Lantz (2009) on a bridge edge beam.
- Study the effect of size and reinforcement amount in other applications with continuous edge restraint such as retaining walls cast against a concrete slab.
- Check the possibility to reduce crack widths by adding fibre reinforcement to concrete in various applications with continuous edge restraint.

1.3 Method

The beginning of the project consisted of literature studies to increase the knowledge on restraint forces and the cracking behaviour of concrete. Further on, literature studies were also made concerning fibre reinforcement and its influence of the cracking process.

Tie rod tests on specimens with ordinary and fibre reinforcement carried out by Jansson (2011) were simulated by non-linear finite element analyses in order to verify the reliability of the type of model used in the present work and previous theses; i.e. Nesset and Skoglund (2007), Alfredsson and Spåls (2008) and Johansson and Lantz (2009). The analyses were carried out in the commercial FE software ADINA (2010).

Further on, non-linear finite element analyses were performed on various applications with continuous edge restraint subjected to shrinkage.

1.4 Limitations

The specimens modelled in this thesis project were assumed to have fully developed concrete strength, i.e. the 28-days strength. All material properties were time independent, including the creep coefficient. Due to limitations in ADINA fibre reinforced concrete was modelled with multi-linear behaviour, just affecting the ductility of concrete. No initial stresses or strains from casting were considered. No external loads have been included in the analyses except the effect of restrained shrinkage strain.

1.5 Outline of the thesis

In Chapter 2, a theoretical background to the subject is presented. It includes a short introduction to restraint forces, the cracking process and motivates why it is needed to control crack widths. Material behaviour of ordinarily reinforced concrete and fibre reinforced concrete is introduced. Recommendations from CEB-FIP Model Code (1993) and CEB (1997) publications on how to model the interaction between reinforcement and concrete and at concrete interfaces are also shown.

Chapter 3 presents different tests carried out by Jansson (2011) and their results are compared to results from finite element analysis in order to verify the model for concrete specimens with ordinary and fibre reinforcement.

In Chapter 4 non-linear finite element analyses on a bridge edge beam are presented. Analyses comprehend studies on how the crack pattern and crack widths are affected by the reinforcement arrangement and other parameters such as the fracture energy and the creep coefficient. The effect of adding fibre reinforcement is also presented.

Chapter 5 presents non-linear finite element analyses on a retaining wall cast on top of an existing concrete slab. Different reinforcement arrangements and geometries of the wall were analysed.

Finally, in Chapter 6, conclusions drawn from this thesis project and suggestions for further research are presented.

2 Restraint forces and material behaviour

2.1 Introduction

This chapter gives a theoretical background to the concepts of restraint forces, restraint cases, restraint degrees and the material behaviour of steel, concrete and fibre reinforced concrete. The interaction between concrete and steel and the cracking behaviour of reinforced concrete is also presented.

2.2 Restraint forces

It is of great importance to understand the difference between the concepts of applied load and restraint forces. Applied loads are loads or imposed displacements that are applied at the boundaries of a structural concrete member.

On the other hand, restraint forces appear in a concrete member when it has a need to move, but the movement is prevented to some degree. The restraint forces in the structure cause stress dependent strain, which is added to the stress independent strain. The sum represents the final deformation that takes place. Strain due to shrinkage and/or temperature changes are examples of such stress independent strains.

2.2.1 Restraint cases

There are several different types of restraint cases that fully or partially prevent movements. However, the different cases can be divided into external and internal restraints.

A structural member that is prevented to move freely due to its support conditions and natural surroundings is subjected to external restraints. A concrete member fully fixed at both short ends, shown in Figure 2.1 (a), or with a continuous fixation along an edge, shown in Figure 2.1 (b), are two examples of external restraints.

Internal restraints are commonly caused by different needs for movement of different parts of the cross-section. If, as an example, a reinforced concrete member is subjected to shrinkage, the reinforcement will not have the same need for movement as the concrete, see Figure 2.1 (c), thus the reinforcement gives rise to internal restraint. Internal restraints also appear due to different need for shrinkage when new concrete is cast on mature concrete, such as schematically shown in Figure 2.1 (d).

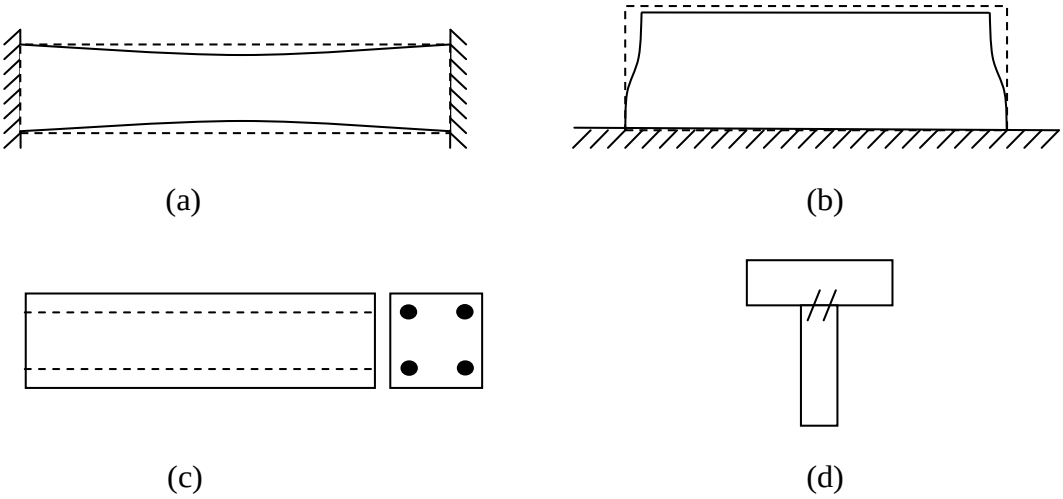

Figure 2.1 Example of external, (a) and (b), and internal restraints, (c) and (d).

2.2.2 Stress independent strains

Stress independent strains are those which result in just deformations and not in stresses when a structural concrete member is allowed to deform freely. This can be caused, for instance, by concrete shrinkage or temperature changes. Constant or linear variations of, e.g., temperature will cause the same distribution of stress independent strains across the cross-section, as can be deduced from Figure 2.2.

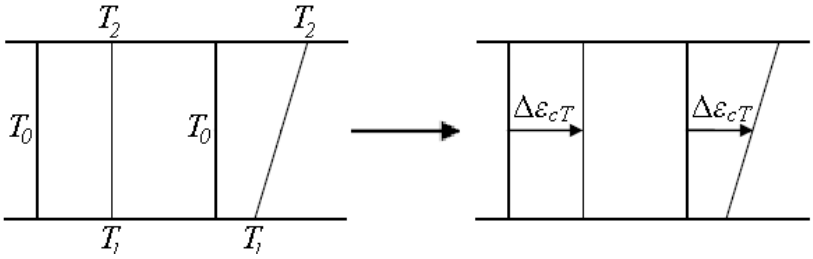

Figure 2.2 Different stress independent strain distributions across the same cross-section caused by temperature change.

2.2.3 Stress dependent strains

Stress dependent strains are caused by external loads, but also as a result of external or internal restraints acting on a structural concrete member subjected to stress independent strains. As can be seen in Figure 2.3, the same stress independent strain distribution can cause very different stress distributions depending on the restraint case. For example a rectangular distribution of stress independent strain can develop to a rather complex distribution of stress dependent strain, as shown in Figure 2.3 (b).

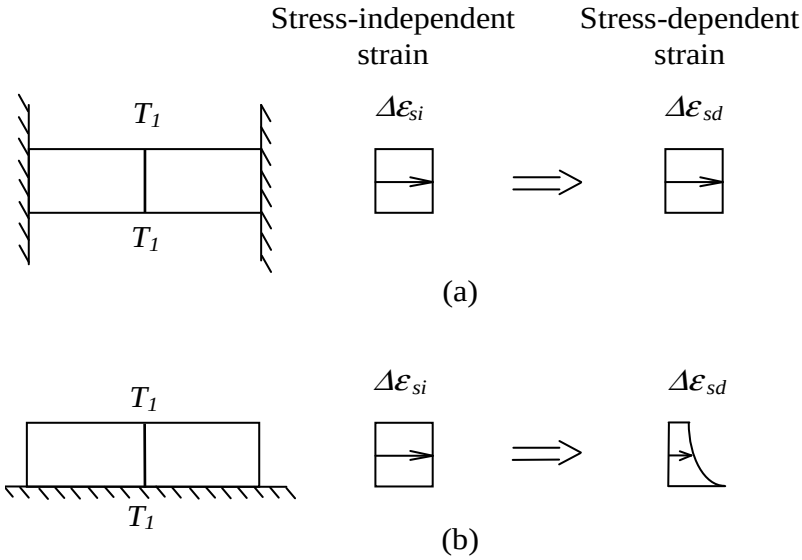

Figure 2.3 Stress dependent strains caused by stress independent strains for (a) fixed end restraints; and (b) continuous edge restraint.

2.2.4 Restraint degree

If stress independent strains appear, there will be a need for deformations. This need for movements can be satisfied in mainly three different ways:

- There is no restraint, thus all movements needed are satisfied, resulting in that no stress dependent strains will appear.
- No movements are allowed by full restraint. Stress dependent strains will appear and since all deformations are prevented, they will be of the same magnitude as the stress independent strain but with opposite sign.
- Free movements are partly restrained. The stress dependent strains will not be equal to the stress independent strains, as some deformation of the boundaries or the member itself is permitted.

To what extent a structure is prevented to move freely is described by the restraint degree, R. This is defined as the relation between the actual imposed strain, i.e. stress dependent strain caused by restraint, and the imposed strain in case of full restraint, see Equation (2.1) and Equation (2.2).

$$restraint\ degree = \frac{actual\ imposed\ strain}{imposed\ strain\ in\ case\ of\ full\ restraint} \tag{2.1}$$

$$R = \left|\frac{\varepsilon_c}{-\varepsilon_{cT}}\right| \tag{2.2}$$

In case of a member between fully fixed end supports, as in Figure 2.1 (a), and since no movement is allowed in the longitudinal direction, there is a full restraint and $R = 1$. If, however, the supports are flexible to some extent the restraint degree will be lower, $R < 1$.

This report especially treats cases with continuous base restraints. If a member with this kind of restraint has a need of longitudinal shortening, the restraint degree will

vary within the cross-section. This can be seen in the example in Figure 2.4, where the upper part of the member is almost free to move while the areas close to the fixed edge are more or less fully restrained. The actual variation of the restraint degree depends on the relation between the length and the height of the member.

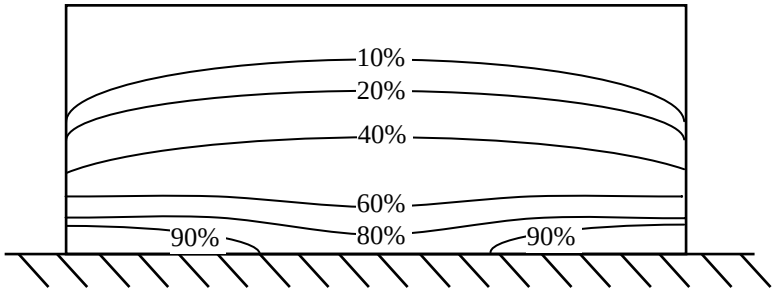

Figure 2.4 Example of variation of restraint degree in member with continuous base restraint, Svensk byggtjänst (1994).

2.3 Material behaviour

2.3.1 Concrete

Concrete has different material behaviours depending on whether it is loaded in compression or tension, as schematically shown in Figure 2.5. The failure modes for both cases are also different. When concrete is loaded in compression, evenly distributed microcracks will form and finally lead to crushing failure. On the other hand, a concrete member subjected to tension will also form microcracks, but these will localise into narrow zones and form macrocracks. Concrete in tension is considered, simplified, to be a linear elastic material until it cracks. However, once the tensile stress is reached, a localised crack zone or failure zone is initiated and its behaviour becomes non-linear and non-linear fracture mechanics needs to be used to describe its behaviour, Plos (2000).

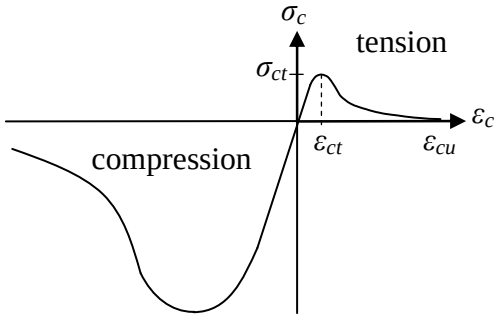

Figure 2.5 Typical material response for concrete.

In Figure 2.6 (a), post cracking behaviour of concrete is shown as a stress-displacement relation. In order to capture the behaviour of deformations independently of the specimen length, the specimen is subdivided into two parts. In Figure 2.6 (b), the stress-strain relation outside the fracture zone is shown and the stress-crack width relation of the fracture zone can be seen in Figure 2.6 (c). The area under the stress-crack width curve represents the fracture energy, G_f, and it represents

the energy that is consumed in order to form a fully developed crack in a concrete member.

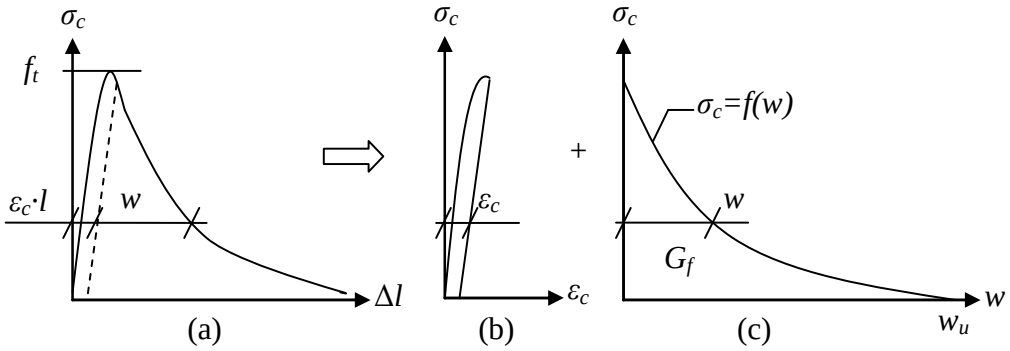

Figure 2.6 (a) Stress-displacement relation, (b) stress-strain relation and (c) stress-crack width relation. Based on Plos (2000).

The crack width development in a concrete prism subjected to uniaxial tension can be seen in Figure 2.7. Microcracks are formed in weaker points. When tensile strength is reached, microcracks will connect and form a continuous crack at the weakest section, see Figure 2.7 (c). No larger stress can be transferred through this crack and the deformation within the fracture zone will increase with decreasing load, see Figure 2.7 (d). The concrete stress will be equal to zero when the crack opening has reached its ultimate value, w_u, see Figure 2.7 (e).

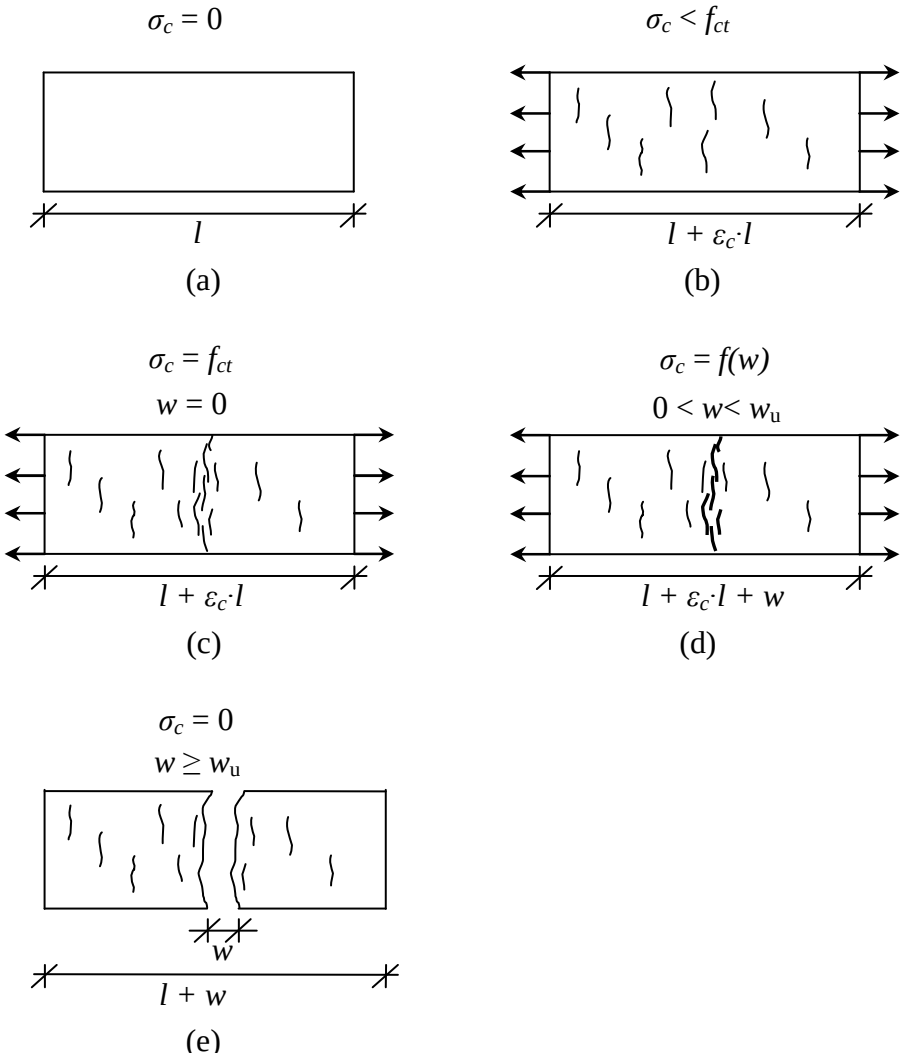

Figure 2.7 Fracture development of a concrete specimen subjected to tension till failure. Based on Johansson (2000).

2.3.2 Steel fibre reinforced concrete

2.3.2.1 Introduction to fibre technology

Fibre reinforced concrete (FRC) is a composite material that results from adding fibres (discontinuous material) to a concrete mix (continuous matrix). This is usually done during the mixing process and the amount of fibres added to a concrete mix is expressed as the volume fraction, V_f, of the total volume of the composite typically ranging from 0.1 % to 2 %. However, by using SIFCON (Slurry Infiltrated Fibre Concrete) technology for which the fibres are placed in the mould before casting, fibre volumes of up to 12 % can be achieved, Fall and Nielsen (2010).

Fibres can be obtained from different materials and they can be categorised in two main groups; natural fibres (e.g. bamboo, cellulose, wollastonite and asbestos fibres) and manufactured fibres (e.g. metallic, glass and synthetic fibres). Some examples of different commercial fibres can be seen in Figure 2.8.

Figure 2.8 Examples of commercially available fibres obtained from different materials, Löfgren (2005).

For most structural purposes, steel fibres are the most commonly used. Therefore, in this thesis, focus will be on steel fibre reinforced concrete (SFRC). However, synthetic fibres (e.g. polypropylene and nylon) are also commonly used for other purposes, such as controlling early cracking in slabs (plastic shrinkage cracks) and to prevent spalling of concrete during fire, Bentur and Mindess (1990).

Independently of the fibre material, fibres are produced with different shapes and sizes. Some examples of typical shapes are seen in Figure 2.9.

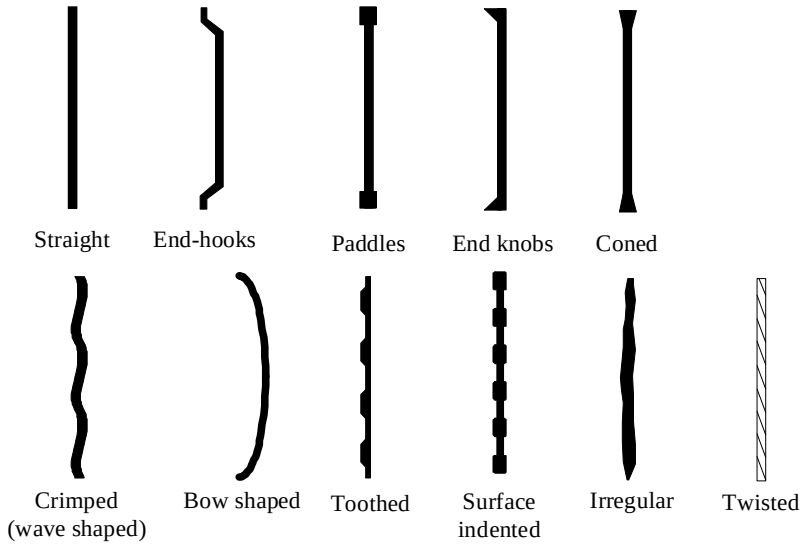

Figure 2.9 Examples of some typical fibre shapes, from Löfgren (2005).

Adding fibre reinforcement does not show a large improvement on the tensile strength of ordinary concrete, why it is generally used as secondary reinforcement combined

with a conventional reinforcement system that provides the required structural resistance. However, the post cracking behaviour is highly affected, making the material much more ductile. This results in increased number of cracks and therefore, it helps to reduce their crack widths. Because of this, it is broadly used for structural elements that need to keep crack widths at very low levels, such as structures that need to be waterproof or are subjected to a high pressure (e.g. dams, water tanks, channel and tunnel linings). Fibre reinforcement is also commonly used for non load bearing concrete elements that need to present a uniform surface without large cracks (e.g. pavements and slabs lying directly on the ground). For these special cases, crack control can be achieved without any primary reinforcement, which will lead to decreased building time and costs.

2.3.2.2 Material response of SFRC

The effect of adding steel fibres on the compressive and tensile strength of the concrete can be divided into two opposite influences. A large amount of pores in the matrix decreases its original compressive strength, but randomly spread fibres across the micro cracks bridge them together and, therefore, also increase their resistance to concentrate into macro cracks. Depending on the concrete mixture and the kind and amount of fibres, the concrete tensile and compressive strength may be increased, decreased or kept at the same values as in ordinary concrete, Schumacher (2006).

If microfibres (fibres whose length is smaller than the maximum aggregate size) are used, the development of micro cracks into macro cracks may be delayed and the tensile and compressive resistance is then increased, Löfgren (2005).

On the other hand, fibres are of great importance for the post cracking behavior. Response of SFRC is a result of the combined action of single responses from ordinary concrete and fibres. This can be clearly seen in Figure 2.10, where the material response of a fibre reinforced concrete member loaded in uni-axial tension is obtained from the addition of the material responses of concrete and fibres when loaded separately in uni-axial tension. SFRC shows a ductile behavior allowing cracks to transfer larger stresses than plain (unreinforced) concrete, which has a brittle fracture.

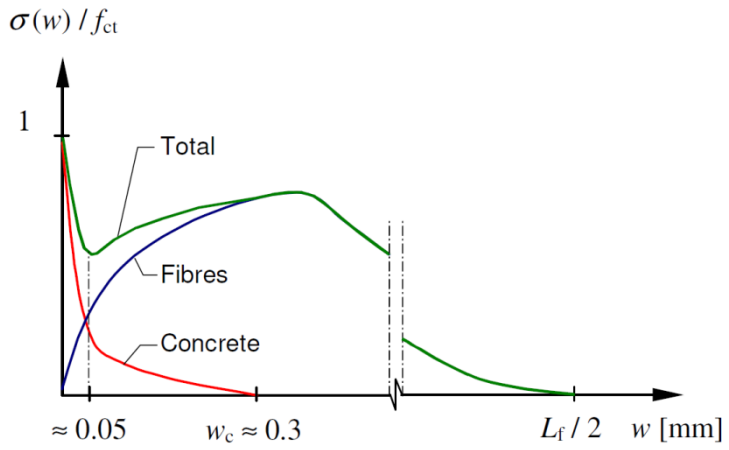

Figure 2.10 Fibre reinforced concrete response when loaded in uni-axial tension, Löfgren (2005).

The ductility increase is a result of the load needed to pull out a fibre from the concrete matrix when the crack width increases. In Figure 2.11, pull-out loads are compared for different fibre geometries. It is observed that higher loads are needed to pull out end-hooked fibres, or any other engineered geometries seen in Figure 2.9, than straight ones. This is due to some energy needed to create plastic hinges in the end hook, as well as the energy needed to overcome friction and break the fibre-concrete bond at the interface.

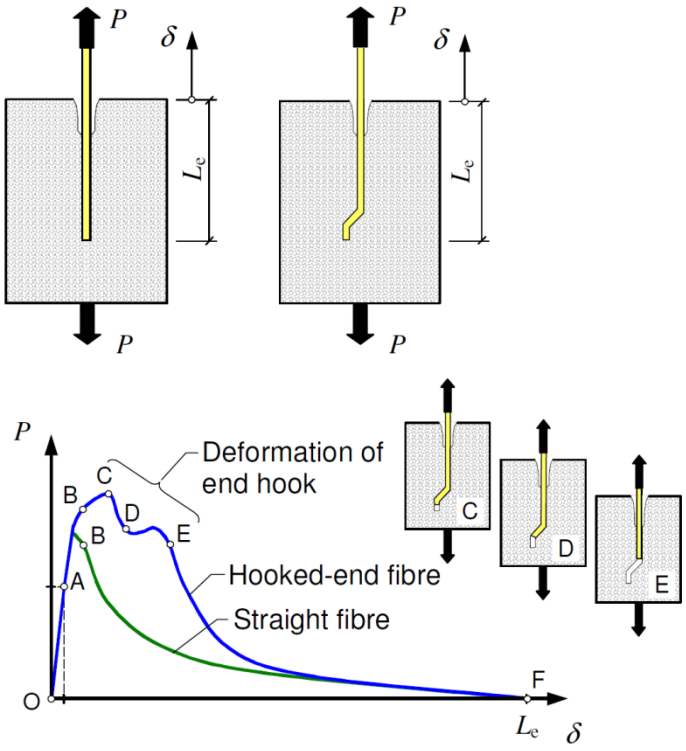

Figure 2.11 Relation between pull-out load and end slip for a straight fibre and an end-hooked fibre, based on Löfgren (2005).

Two major cases can be observed when studying the tensile behaviour; strain-softening and strain-hardening. Strain-hardening behaviour, where post cracking strength is larger than the cracking strength (see Figure 2.12), can be obtained for some special cases and they are called high-performance fibre-reinforced concrete (HPFRC). This performance is achieved by different methods, such as using a very high fibre volume or a densified matrix, using engineered cementitious composites, combining use of micro and macro fibres or by using some engineered fibres (e.g. Torex fibres), Jansson (2008). However, these are not very common cases, and in this thesis just the strain-softening behaviour will be studied.

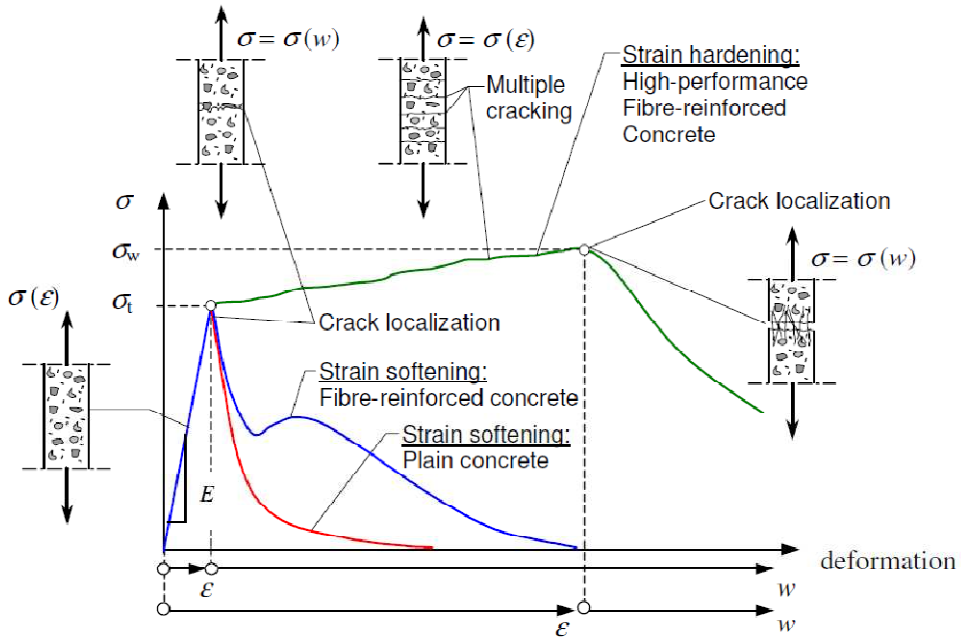

Figure 2.12 Classification of tensile behaviour of cement-based materials, from Löfgren (2005).

It is generally agreed that steel fibres also increase the ductility of concrete in compression as well as the strain at which the maximum compressive strength is reached, Schumacher (2006). However, since the focus in this thesis is on restrained structures mainly subjected to tensile stresses, the effect of fibres on the behaviour in compression is not further considered in this report.

2.3.3 Steel

A typical stress-strain relation for reinforcing steel is shown in Figure 2.13 (a). It is generally assumed that steel has a linear behaviour until yielding is reached, where plastic deformations start to occur. However, it is generally simplified to a bilinear elastic-plastic material, as can be seen in Figure 2.13 (b) and (c). If the load is removed before reaching yielding, no plastic deformations will remain. However, if the yield stress is reached some plastic deformation will still remain after unloading. In this thesis, all analyses concern the service state and steel subjected to small loads will only act in the elastic part of the curve. Hence, the bilinear behaviour assumption corresponds, in this study, with the real behaviour of reinforcing steel.

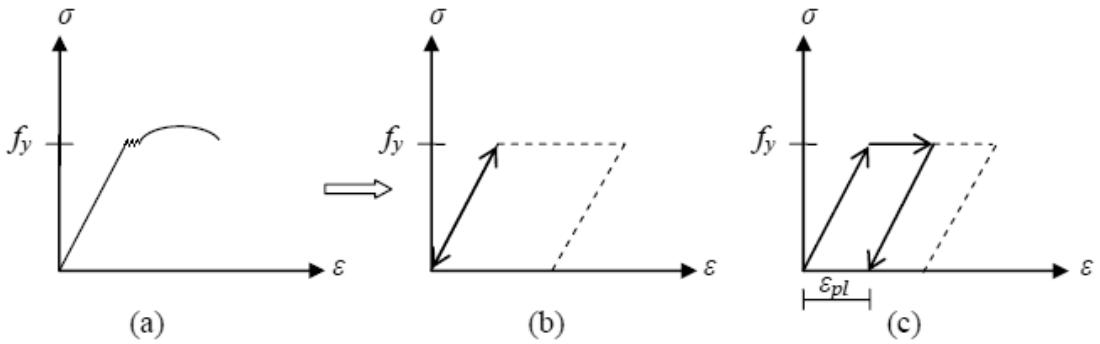

Figure 2.13 (a) Typical material response of reinforcing steel, (b) simplified response when unloading before reaching yield stress and (c) simplified response while unloading after yielding in reinforcing steel.

2.4 Cracking process

The cracking process of ordinarily reinforced concrete consists of three principal stages: uncracked stage, crack formation and stabilised cracking. The different stages are schematically shown in Figure 2.14 for a reinforced concrete member loaded in pure tension.

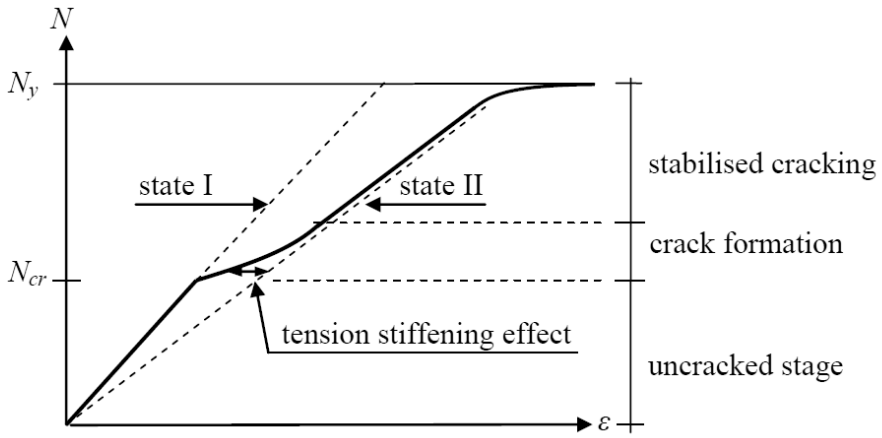

Figure 2.14 Global average response of a reinforced concrete region at various cracking stages.

While the tensile stresses in reinforced concrete have not reached the tensile strength of concrete, f_{ct}, the concrete is uncracked. At this stage both concrete and reinforcement behave in a linear elastic manner and the strains are almost equal for the two materials.

The first crack appears when the concrete tensile strength is reached in a section of the reinforced concrete member. Due to the fact that not all sections of the concrete member cracks in the crack formation stage, the stiffness of the uncracked regions between the cracks contribute to the overall stiffness; a phenomenon called the tension stiffening effect, see Figure 2.14.

While looking at a reinforced concrete member axially loaded in tension, see Figure 2.15, the cracking behaviour can be described. After formation of the first crack, the member can be considered as divided into two parts. In each part new

cracks may form outside a certain distance from the first crack. When a crack is forming, the reinforcement immediately takes over the tensile force in the cracked section. Due to bond action between steel and concrete, tensile force is transferred to the concrete between adjacent cracks. The redistribution of forces takes place within a certain length from the crack; the transmission length, l_t. A new crack is able to form at a distance no shorter than the maximum transmission length, $l_{t,max}$, from the first crack, as seen in Figure 2.15.

No further cracks can appear when the distance between all cracks is less than two times the maximum transmission length. The stabilised cracking is then reached. At this stage a further increase in load will not cause any more cracks, but rather increase the crack widths of already existing cracks.

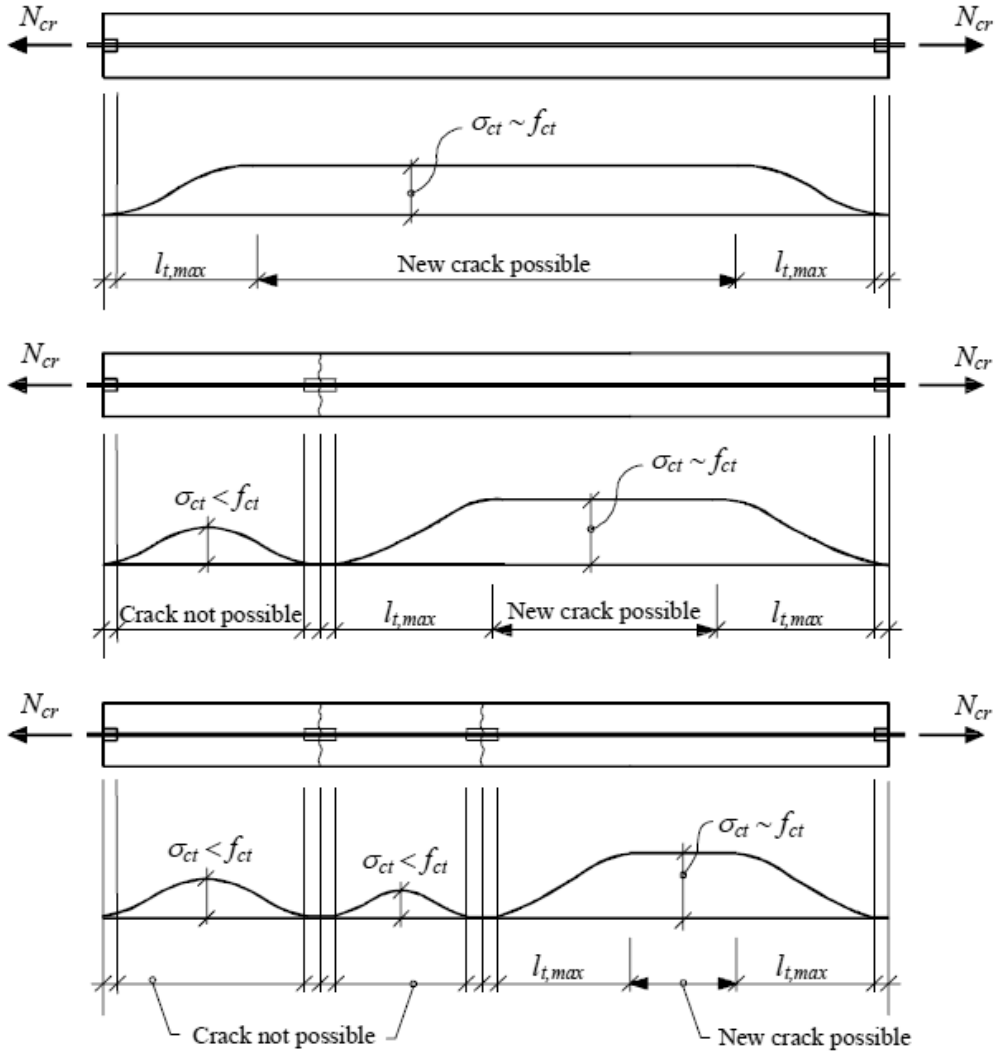

Figure 2.15 Cracking process of a reinforced concrete member axially loaded in tension. From Engström (2008).

When looking at the crack formation there are two different responses of the structure depending on how the load is applied. If a reinforced concrete member is loaded with a tensile force, the deformation for each new crack increases instantaneously, see Figure 2.16 (a). If, on the other hand, the member is subjected to an imposed

elongation, the force decreases instantaneously for each new crack, see Figure 2.16 (b).

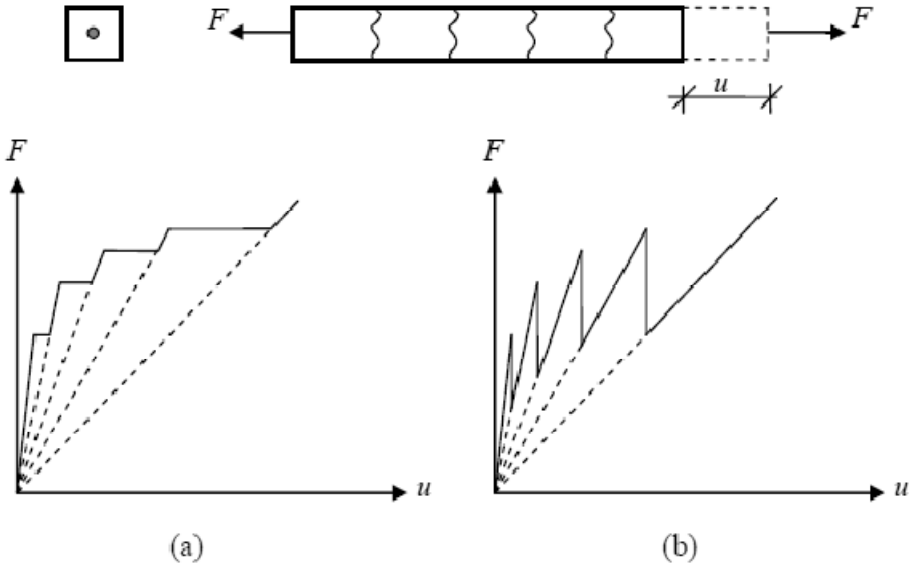

Figure 2.16 Response of a reinforced concrete member subjected to (a) applied load and (b) imposed elongation.

The inclination of the lines in Figure 2.16 represents the global stiffness of the member. The inclination decreases with formation of each new crack, hence the global stiffness decreases with each new crack.

The same cracking stages presented in Figure 2.14 are observed during cracking of fibre reinforced concrete too. However, cracks do not reach the fully developed state as they, due to the presence of fibres, are still able to transfer stresses. Therefore, the difference between the stresses in cracked and uncracked sections is smaller and the transmission length is decreased, which allows the creation of more cracks closer to each other. Further, as fibre reinforced concrete has some ductile behaviour, no such drastic drops in the reaction force are produced as shown for ordinary concrete in Figure 2.16 (b). Tension stiffening effect has also been reported to be higher than for ordinary concrete, Jansson (2011) and Bischoff (2003).

2.5 Design for crack control

Cracking of concrete is natural during the service life of a reinforced concrete structure. However, cracks are openings where moisture and oxygen can penetrate the structure and if the reinforcement is exposed to the environmental conditions, steel bars may start to corrode. This corrosion process can result in severe durability problems and in the long run affect the load bearing capacity and safety of the structure. Therefore, it is important to keep the crack width below certain values, depending on the exposure. Maximum crack widths for general buildings according to Eurocode, CEN (2004), are shown in Table 2.1. For a reinforced concrete structure placed in the most severe environmental conditions, crack widths will need to be kept below 0.3 mm. However, this limit value may change depending on the function and location of the structure. It shall be mention as well that other values may be stated by national codes, e.g. Swedish code put higher demands on crack widths.

Table 2.1 Recommended values of w_{max} in mm, from CEN (2004).

Exposure class	Reinforced members and prestressed members with unbounded tendons	Prestressed members with bonded tendons
	Quasi-permanent load combination	Frequent load combination
X0, XC1	0.4[1]	0.2
XC2, XC3, XC4	0.3	0.2[2]
XD1, XD2, XS1, XS2, XS3		Decompression

Note 1: For X0, XC1 exposure classes, crack width has no influence on durability and this limit is set to guarantee acceptable appearance. In the absence of appearance conditions, this limit may be relaxed.

Note 2: For these exposure classes, in addition, decompression should be checked under the quasi-permanent combination of loads.

Steel fibres will also corrode when used in aggressive environments. If crack widths are limited to values shown in Table 2.1, corrosion will mostly take place close to the surface, which can impair the appearance. However, light corrosion may occur on the fibres bridging cracked regions without reducing their cross-section. Then, strength of fibres can even be increased since rust on their surface makes it more difficult for them to slip out of the concrete matrix, Granju and Balouch (2005).

Guidance on how to limit crack widths is given by Eurocode, CEN (2004), for cases where stabilised cracking is reached. In case of external loading, all cracks will form under a small load increase above the tensile strength; assumed to be 30% according to *fib* (2009). Reinforcement is designed in order to be able to transfer the tensile load across the cracks until stabilised cracking is obtained without yielding.

However, when the cracks are formed due to restraint loading, restraint forces depend on the structural stiffness and the restraint conditions. The stiffness of the structure and the restraint forces are decreased during cracking, see Figure 2.16 (b), and thus, there is no known force to design the reinforcement for. Restraint forces may even decrease so much that no further cracks are able to appear after formation of the first crack. Then, the cracking process may be stopped before stabilised cracking is reached and crack widths cannot be determined for cases with restraint loading by the method presented in CEN (2004).

For such cases, a method to estimate the number of cracks and crack widths based on the restraint degree was presented in Engström (2010). Johansson and Lantz (2009) also introduced a simplified method to estimate the mean crack width of an edge beam based on their results from non-linear finite element analyses for different cross-sections. However, influence of more parameters should be included in order to develop their method and be able to use it in design.

2.6 Bond behaviour

2.6.1 Interaction between concrete and reinforcement

If there is a different need for longitudinal deformation between reinforcing steel and concrete, shear stresses will appear at the interface between the two materials. These shear stresses are called bond stresses and they are associated with a local slip between steel and concrete. The bond stress, τ_b, is dependent of the local slip, s, and a typical relation for ribbed reinforcement bars can be seen in Figure 2.17 (a).

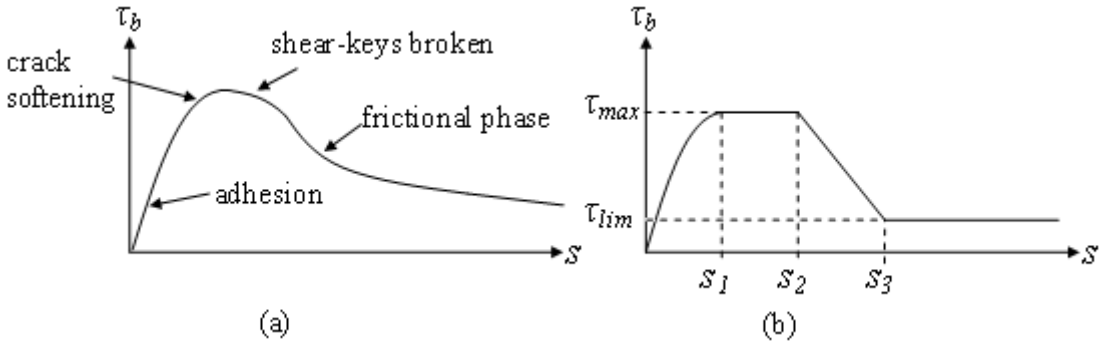

Figure 2.17 (a) Typical and (b) simplified, according to CEB-FIP (1993), bond stress-slip relation between reinforcing steel and concrete.

A schematic relationship to be used in calculations is provided in CEB-FIP Model Code 1990, (CEB-FIP (1993)) and it can be observed in Figure 2.17 (b). This curve is defined for confined concrete with good bond conditions by Equations (2.3) to (2.6).

$$\tau_b(s) = \tau_{max} \cdot \left(\frac{s}{s_1}\right)^{0.4} \quad \text{if } s \leq s_1 \tag{2.3}$$

$$\tau_b(s) = \tau_{max} = 2.5 \cdot \sqrt{f_{ck}} \quad \text{if } s_1 < s \leq s_2 \tag{2.4}$$

$$\tau_b(s) = \tau_{max} - (s - s_2) \cdot \frac{\tau_{max} - \tau_{lim}}{s_3 - s_2} \quad \text{if } s_2 < s \leq s_3 \tag{2.5}$$

$$\tau_b(s) = \tau_{lim} = 0.4 \cdot \tau_{max} \quad \text{if } s > s_3 \tag{2.6}$$

where:

τ_b = Bond stress

f_{ck} = Concrete compression strength, characteristic value

s = Slip, should be inserted in mm

τ_{max} = Maximum bond stress

τ_{lim} = Final value of bond stress

s_1 = 1.0 mm, according to CEB-FIP (1993)

s_2 = 3.0 mm, according to CEB-FIP (1993)

s_3 = Clear rib spacing, should be inserted in mm

An alternative way to calculate the first branch of the curve in Figure 2.17 (b) was proposed by CEB (1997). This part of the curve can be calculated by Equation (2.7) and the maximum bond stress is obtained at s = 1 mm.

$$\tau_b(s) = 0.22 \cdot f_{cm} \cdot s^{0.21} \quad (2.7)$$

where: f_{cm} = Concrete compression strength, mean value

s = Slip, should be inserted in mm

Possible effect on the bond interaction between concrete and ordinary reinforcement by adding fibres has been studied by different authors in the literature but no general agreement has been reached. In case of pull-out bond failure, conclusions vary from confirming an increase in bond strength to have no effect at all. However, it is accepted that the bond strength in case of splitting bond failure is increased by adding fibres, but no relation has been found with the fibre volume, Bigaj-van Vliet (2001).

In the same way, there are contradictory opinions about the influence of fibre content in the bond stiffness before the maximum bond stress is reached. It is more evident that the post-peak behavior is affected and it becomes more ductile when fibres are added, particularly in case of splitting bond failure, Bigaj-van Vliet (2001).

2.6.2 Interaction at concrete interfaces

Concrete cast against old concrete creates some resistance to relative displacements at the interface between the different members in contact. This can be regarded as a reinforcing effect and therefore it will help to distribute smaller cracks in the member subjected to stress independent strains. CEB-FIP (1993) gives some guidelines about how to calculate the mobilised shear stress-slip relation, $\tau_{fd}(s)$, when the slip is smaller than 2.0 mm, see Equations (2.8) to (2.10).

$$\tau_{fd} = 5 \cdot \tau_{fu,d} \cdot s \quad \text{if } s < 0.1 \text{ mm} \quad (2.8)$$

$$\left(\frac{\tau_{fd}}{\tau_{fu,d}}\right)^4 - 0.5\left(\frac{\tau_{fd}}{\tau_{fu,d}}\right)^3 = 0.3 \cdot s - 0.03 \quad \text{if } 0.1 \leq s < 2.0 \text{ mm} \quad (2.9)$$

$$\tau_{fu,d} = 0.40 \cdot {f_{cd}}^{2/3} \cdot (\sigma_{cd} + \rho_t \cdot f_{yd})^{1/3} \quad (2.10)$$

where τ_{fd} = Mobilised shear stress

s = Slip, should be inserted in mm

$\tau_{fu,d}$ = Design value of shear stress at s = 2.0 mm

f_{cd} = Design value of concrete compressive strength

σ_{cd} = Design value of concrete normal stress

ρ_t = Transversal reinforcement ration

f_{yd} = Design value of yield strength of steel

In Johansson and Lantz (2009) a modified way of calculating the ultimate mobilised shear stress was used. This modified relation, $\tau_{fm}(s)$, was based on mean values instead of design values and it was obtained by replacing in Equations (2.8) and (2.9) $\tau_{fu,d}$ with $\tau_{fu,m}$, as defined by Equation (2.11).

$$\tau_{fu,m} = 0.50 \cdot {f_{cm}}^{2/3} \cdot (\sigma_{cm} + \rho_t \cdot f_{ym})^{1/3} \quad (2.11)$$

where $\tau_{fu,m}$ = Mean value of shear stress at s = 2.0 mm

f_{cm} = Mean value of concrete compressive strength

σ_{cm} = Mean value of concrete normal stress

ρ_t = Transversal reinforcement ratio

f_{ym} = Mean value of yield strength of steel

In order to be able to compare the results in this report with those obtained by Johansson and Lantz (2009), the bond-slip relation based on the mean values, i.e. Equation (2.11), will be used when defining the concrete interface properties.

3 Verification of FE model using tie-rod tests

3.1 Introduction

Finite element analyses are nowadays commonly used in research as well as industry as they can save a lot of costs and time when used early in design. In previous theses in this field, non-linear analyses have been used to predict the behaviour of concrete structures, while subjected to restraint forces. The finite element modelling technique used in this thesis, based on the work of the previous theses, is presented in this chapter. In order to verify this modelling technique and check the applicability in case of fibre reinforced concrete structures, non-linear analyses were made in order to simulate tie-rod tests carried out by Jansson (2011). The material data used in the finite element analyses was based on experimental results from uni-axial tensile tests and bar pull-out tests carried out by Jansson (2011).

3.2 Tests

Three different types of tests were carried out by Jansson (2011) on concrete specimens with different fibre volumes, V_f = [0 %, 0.25 %, 0.5 %, 0.85 % and 1.0 %]. Material properties were determined by uni-axial tensile tests, where the influence of the fibre content in the stress-crack opening relation was measured. Bar pull-out tests were carried out to check possible effects of fibre reinforcement on the bond-slip response at the interface between reinforcement and concrete. Furthermore, tensile tests were performed on reinforced concrete tie-rods with a centric reinforcement bar and with different fibre dosages. Results of these later tests were used to verify the finite element model for only two cases; the one with no fibre reinforcement and the case with a fibre volume of 0.85 %.

Self-compacting concrete was used for both mixes, and for the fibre reinforced mix end-hooked steel fibres from Bekaert were used. These fibres have a tensile strength of 1100 MPa, a length of 35 mm and an aspect ratio (relation between length and diameter) of 65.

Apart from the tests presented in this thesis, compressive tests following the Swedish standard SS-EN 12390-3:2009 were performed on cylindrical specimens resulting in a mean compressive strength of 64.5 and 54.1 MPa for ordinary and fibre reinforced concrete, respectively.

3.2.1 Uni-axial tensile tests

Uni-axial tests of cylindrical concrete specimens in tension were made according to Figure 3.1. A crack was forced to occur in a notched section where the crack opening was measured by three displacement transducers placed around the concrete specimen and spaced from each other by 120°. The test was carried out as displacement controlled with a constant rate of 0.005 mm/min. The load was transferred through a glued connection between the concrete specimen and the loading plates of the machine. For each fibre volume, five specimens were tested.

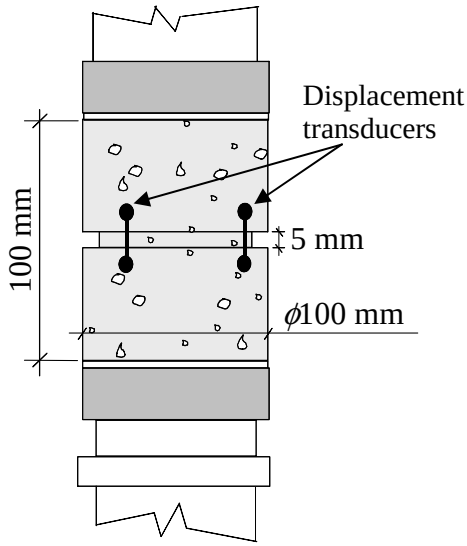

Figure 3.1 Geometry and setup of uni-axial tensile tests by Jansson (2011).

The displacement across the crack (crack opening) was evaluated as the mean value of the elongations measured by the three different transducers. Stress-displacement curves resulting from the tests made in ordinary concrete can be observed in Figure 3.2.

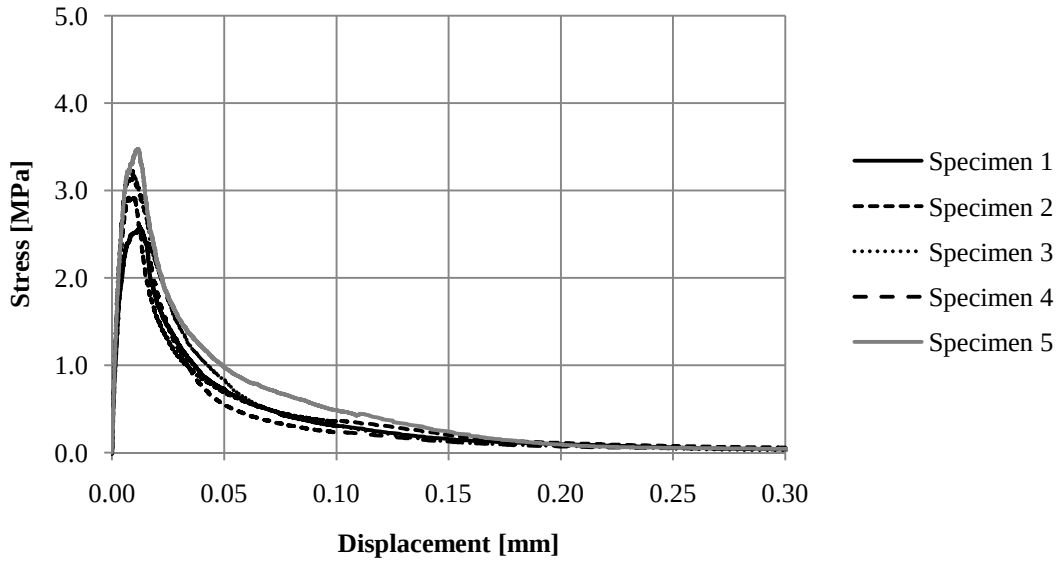

Figure 3.2 Stress-displacement curves for specimens with V_f = 0 %.

As explained in Section 2.3.1, the stress-crack opening relation can be obtained by stress-displacement graphs by subtracting the elastic deformation just before cracking. By doing so, stress-crack opening curves obtained for each specimen can be seen in Figure 3.3.

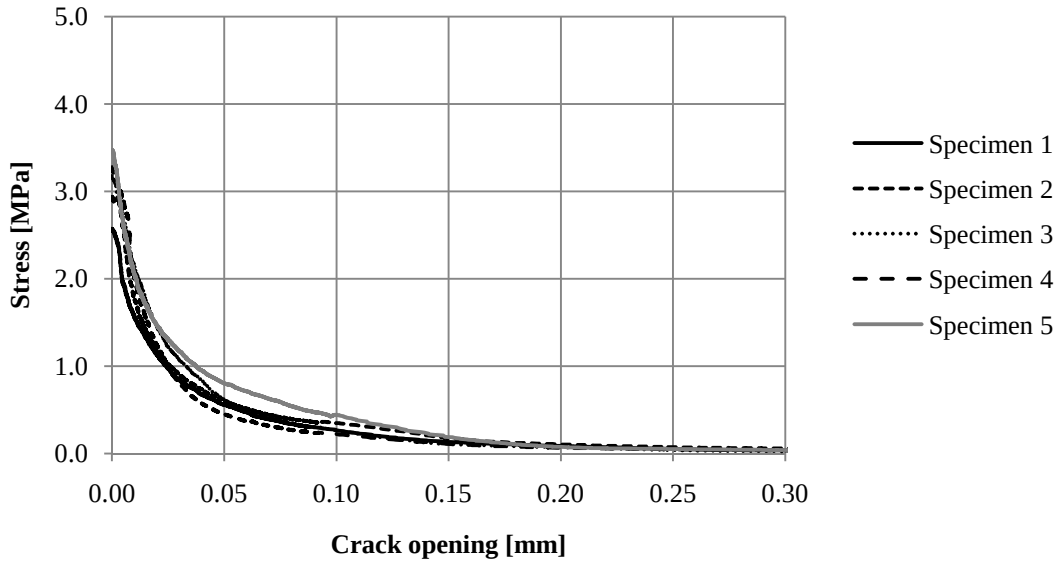

Figure 3.3 Stress-crack opening curves for specimens with V_f = 0 %.

The fracture energy can be graphically understood as the area below the stress-crack opening curve. Therefore it can be obtained for each specimen by integrating the functions shown in Figure 3.3. A summary of the test data and mean values for the specimens with V_f = 0 % is shown in Table 3.1.

Table 3.1 Summary of test data obtained from uni-axial tensile testing of ordinary concrete.

Specimen	1	2	3	4	5	Mean
f_{ct}	2.57 MPa	2.94 MPa	3.17MPa	3.27 MPa	3.47 MPa	3.09 MPa
G_F	101 N/m	132 N/m	113 N/m	103 N/m	139 N/m	118 N/m

In Figure 3.4 stress-displacement relations for fibre reinforced specimens with V_f = 0.85 % are shown. It can be clearly seen that the stresses transferred through the crack zone (fracture zone) at a certain displacement are much higher than for ordinary concrete. At the same time, higher displacements were achieved without reaching a fully developed crack. Two different behaviours are observed: specimens 3, 4 and 5 show strain softening behaviour, while specimens 1 and 2 were able to carry higher stresses after having cracked.

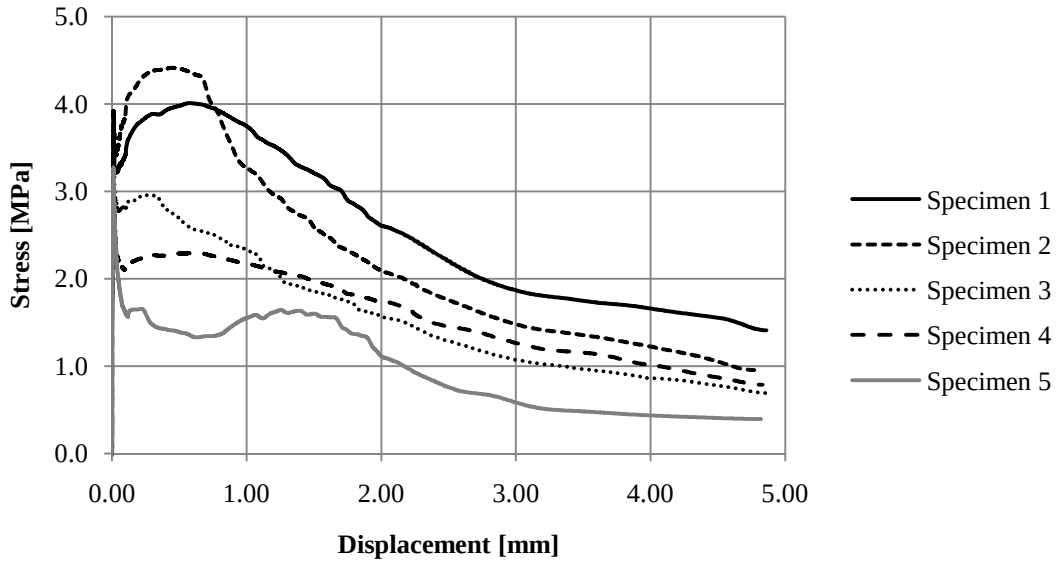

Figure 3.4 Stress-displacement curves for specimens with V_f = 0.85 %.

In the same way as for ordinary concrete, stress-crack opening curves were calculated and are shown in Figure 3.5. The first millimeter has been zoomed in, since for fibre reinforced concrete just the first part of the curve is of interest, as cracks usually will not reach those large values in a real structure. While magnifying this zone, it is easier to notice that the stress that was transferred dropped quickly to an almost constant value once the crack had been initiated.

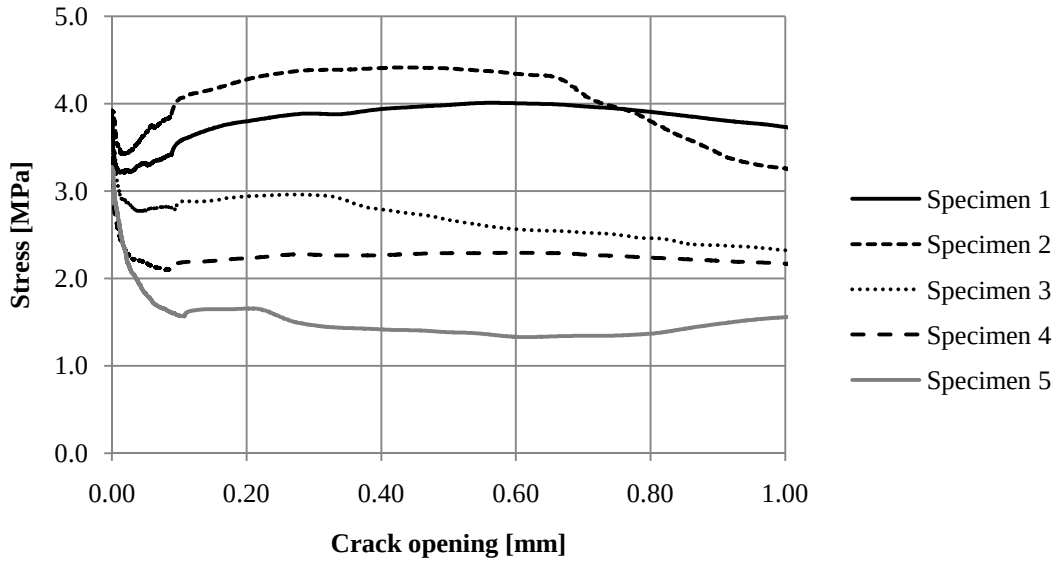

Figure 3.5 Stress-crack opening curves for specimens with V_f = 0.85 %.

As the displacement transducers were not able to record any displacement greater than 5 mm, the fracture energy was calculated assuming a constant slope from 5 mm till zero stress and equal to the slope of the stress-crack opening curve between 3 and 5 mm. The calculated fracture energy values together with the tensile strength of the fibre reinforced concrete specimens obtained by uni-axial testing are summarised in Table 3.2.

Table 3.2 Summary of test data obtained during uni-axial tensile testing of fibre reinforced concrete (V_f = 0.85 %).

Specimen	1	2	3	4	5	Mean
f_{ct}	3.71 MPa	3.37 MPa	3.27 MPa	3.89 MPa	3.92 MPa	3.63 MPa
G_f	9 009 N/m	9 172 N/m	5 527 N/m	15 627 N/m	12 461 N/m	10 359 N/m

3.2.2 Bar pull-out tests

Pull-out tests of reinforcement bars in ordinary and fibre reinforced concrete were carried out by Jansson (2011) according to Figure 3.6. One ϕ16 reinforcement bar was pulled out from one end until ultimate failure was achieved. The concrete specimen was supported at the same end, forcing the bar to slip along the embedded length. The relative displacements between the steel bar and the concrete specimen were measured by displacement transducers at the top and at the bottom faces. When the embedded length is small it is possible to assume that the slip is constant along this length. Therefore, it was decided to determine the slip of the bar at its passive steel, which needs not to be corrected due to the elastic deformation of the bar. The same consideration was taken by Magnusson (2000).

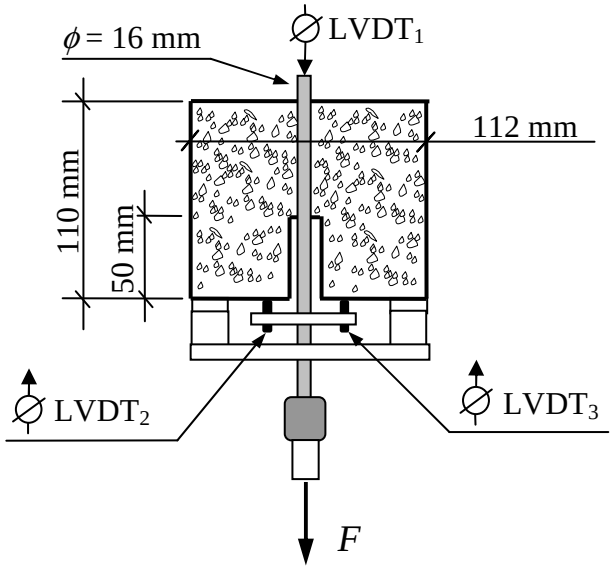

Figure 3.6 Geometry and setup of bar pull-out tests by Jansson (2011).

Some results from these tests are shown in Figure 3.7 and Figure 3.8 for ordinary and fibre reinforced concrete, respectively. Mean values were determined by calculating the mean bond stress at certain discrete slip values within the range before failure had occurred in any specimen.

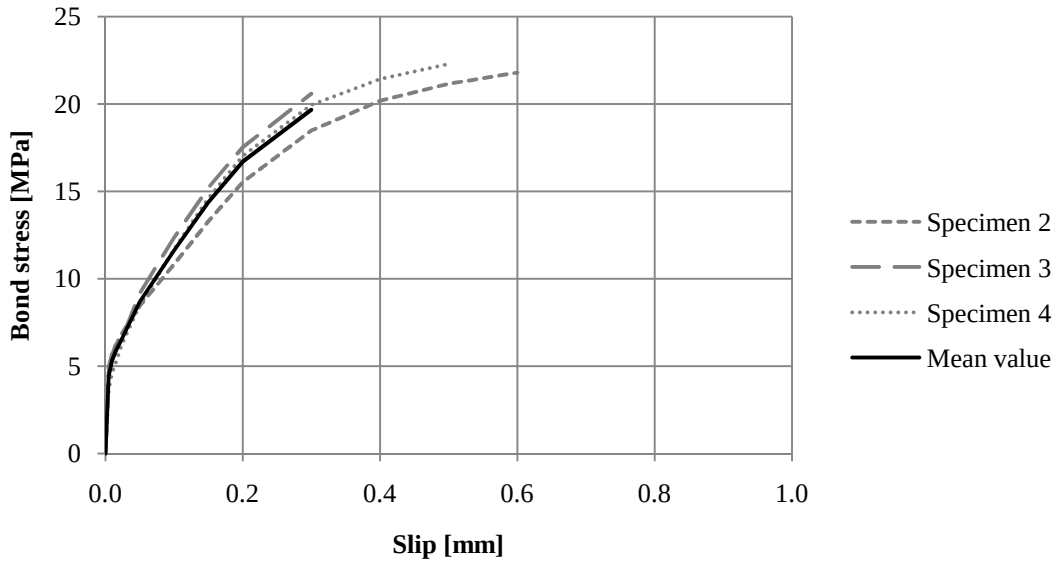

Figure 3.7 Experimental bond stress-slip relation for ordinary concrete (V_f = 0 %).

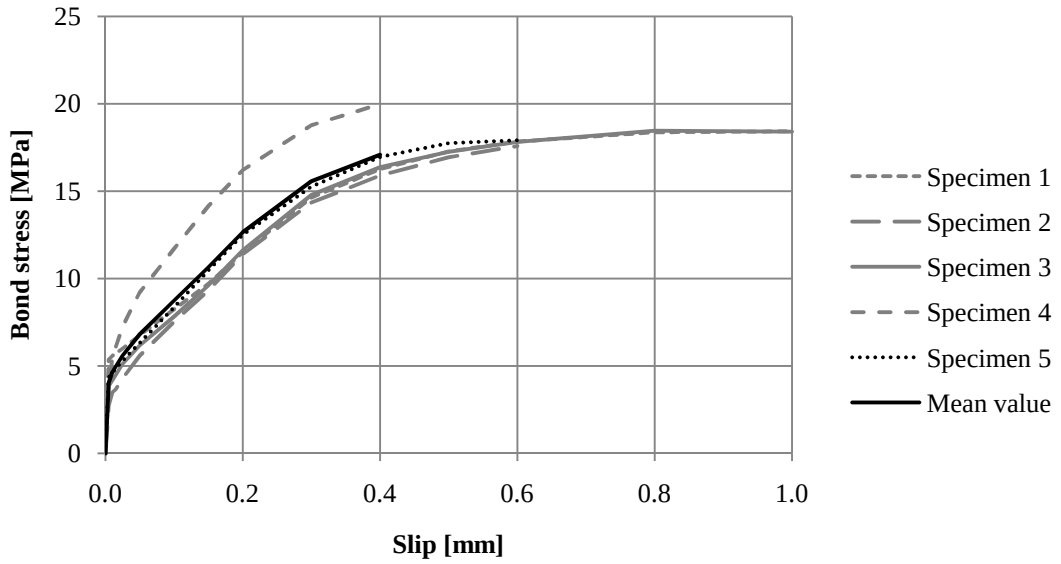

Figure 3.8 Experimental bond stress-slip relation for fibre reinforced concrete (V_f = 0.85 %).

Comparisons of the experimental results with bond stress-slip models suggested in CEB-FIP (1993) and CEB (1997) are shown in Figure 3.9 and Figure 3.10. For both concrete specimens with ordinary and fibre reinforcement, the experimental results show good agreement for slips smaller than 0.1 mm with the bond stress-slip relation proposed in CEB (1997). Model Code 1990 suggests using a less stiff behaviour for the bond stress at lower slips; however, it provides a maximum bond stress that corresponds better with the values observed during testing. This is due to that proposal in CEB (1997) is only aimed to be used for predictions of the service behaviour and the final point of the first branch should not be understood as corresponding to a bond failure.

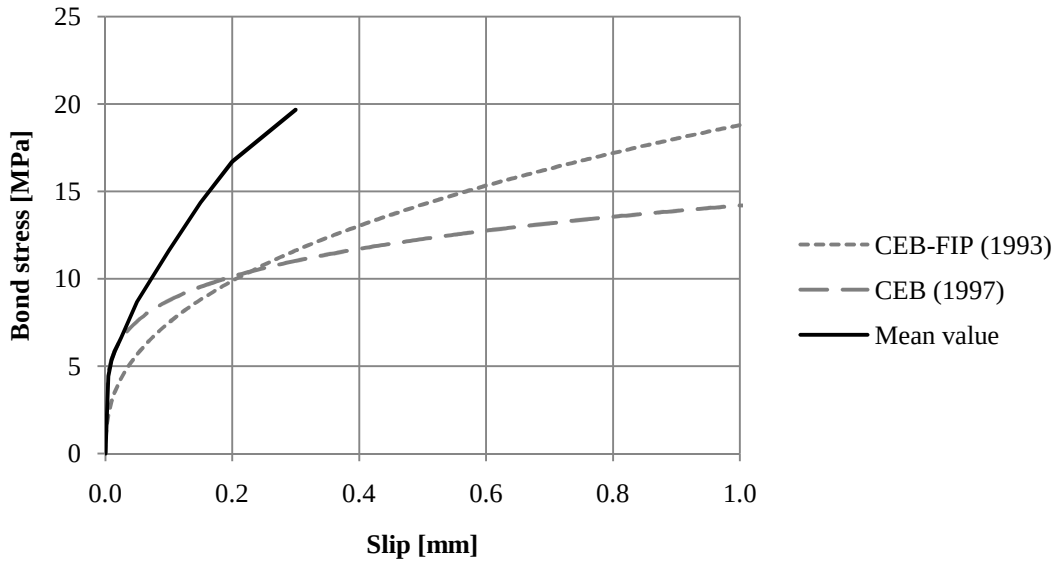

Figure 3.9 Comparison of mean experimental bond stress-slip curve and proposed schematic relations for ordinary concrete (V_f = 0 %).

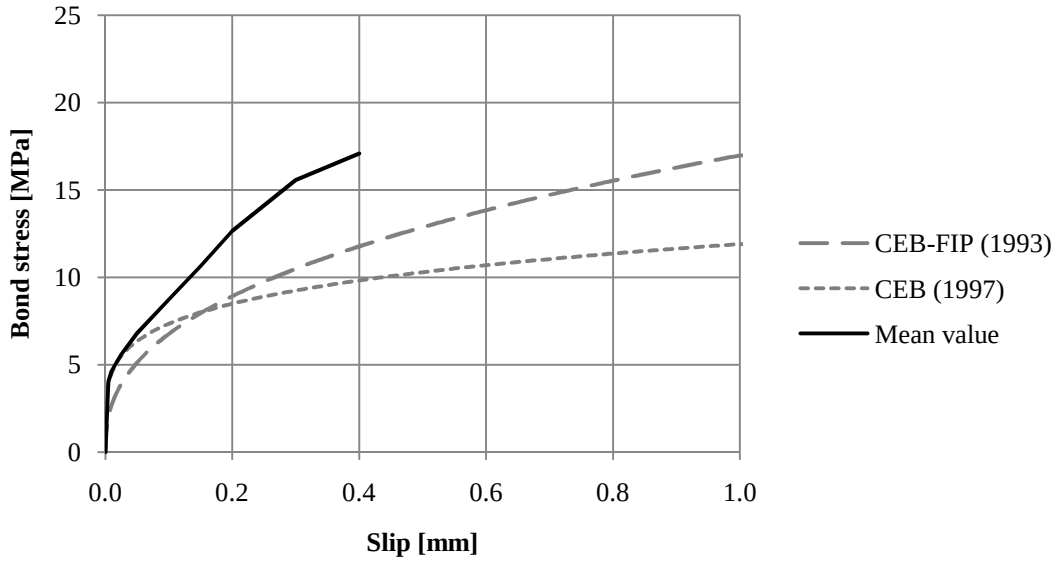

Figure 3.10 Comparison of mean experimental bond stress-slip curve for fibre reinforced concrete specimens (V_f = 0.85 %) and proposed schematic relations for ordinary concrete.

Both CEB-FIP (1993) and CEB (1997) suggest relations where the bond stress is a function of the concrete strength. Then, in order to check the effect of fibre reinforcement in the bond stress-slip relations, it is needed to normalise the results to the actual concrete strength, since the ordinary and fibre reinforced concrete mixes had different compressive strengths. Assuming a linear relation with the mean compressive strength, as in CEB (1997), normalised curves are shown in Figure 3.11. No clear effect of including fibre reinforcement to the mix is observed, since all specimens show similar behaviour with respect to stiffness and peak value. There is a slight tendency in fibre reinforced specimens, though, to show lower stiffness at small

slips and to produce higher slips without failure. However, fibre reinforced specimen number 4 is an exception. No final conclusions were drawn, and also contradictory opinions on this are reported in literature, see Bigaj-van Vliet (2001).

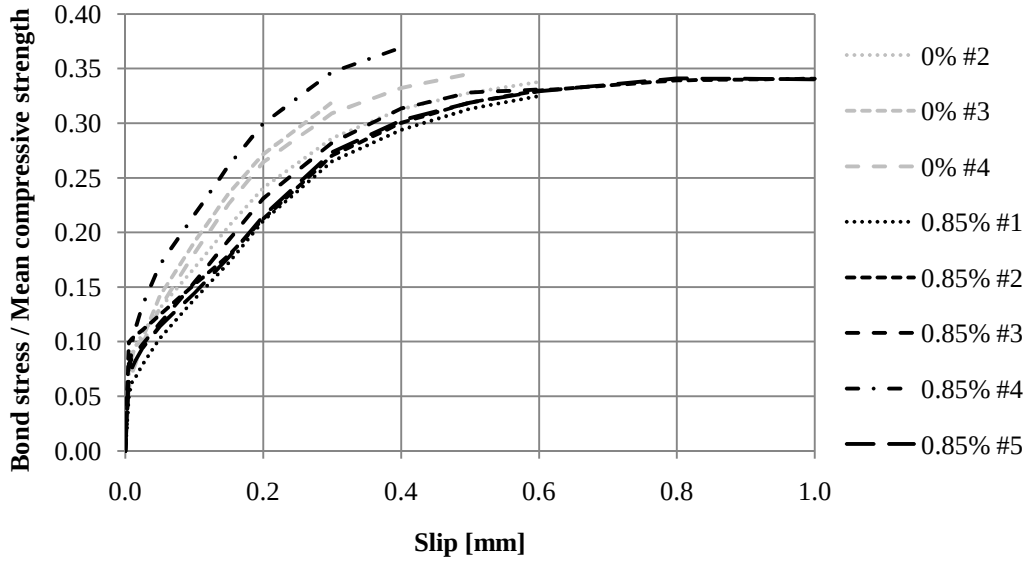

Figure 3.11 Normalised bond stress-slip experimental curves for ordinary (V_f = 0 %) and fibre reinforced concrete (V_f = 0.85 %).

3.2.3 Tie-rod tests

Tensile tests were carried out on reinforced concrete prisms with square section. A ϕ16 mm reinforcing bar was placed in the centre of the cross-section. The dimensions of the cross-section were the same as for the bar pull-out test, in order to be able to use those results for finite element analysis. The load was applied as an imposed displacement on both ends of the reinforcement bar and it was increased at a constant rate of 0.007 mm/min till yielding of the steel reinforcement. Two displacement transducers were placed on each end of the specimen and its was calculated by addingthe mean values at each end. The setup of the test can be seen in Figure 3.12.

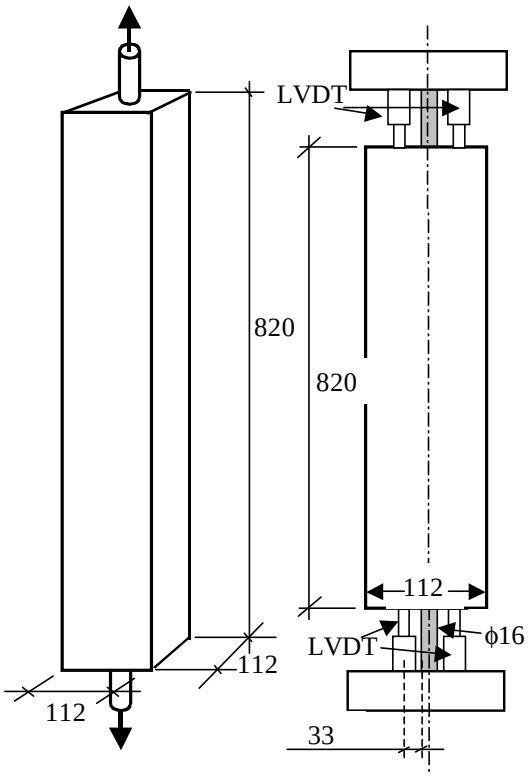

Figure 3.12 Geometry and setup of tie-rod tests by Jansson (2011). All dimensions in mm.

For each fibre volume, five specimens were tested. Specimens with ordinary or fibre reinforced concrete (with $V_f = 0.85$ %) after testing can be seen in Figure 3.13 (a) and (b), respectively. By looking at the developed cracks, it can be stated that the fibre reinforced specimens present more cracks and that the crack spacing is smaller, compared to the specimens with ordinary concrete. It is also observed that not the whole section is cracked in some regions. The number of cracks ranges from 3 to 4 for ordinary concrete and from 5 to 6 for fibre reinforced concrete.

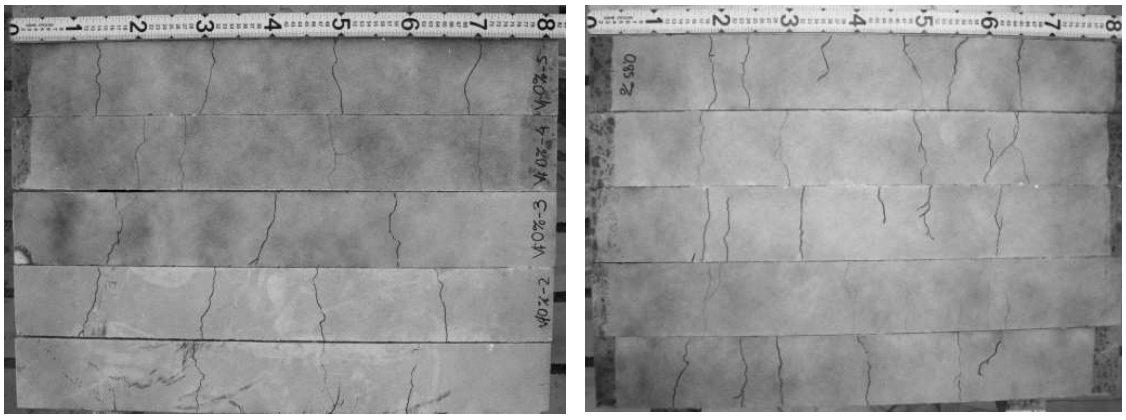

(a) Ordinary concrete, $V_f = 0\%$ (b) Fibre reinforced concrete, $V_f = 0.85\%$

Figure 3.13 Crack pattern on tested specimens for ordinary (a) and fibre reinforced concrete with $V_f = 0.85$ % (b).

The load elongation response during testing is shown for each specimen in Figure 3.14. As can be seen it is a significant difference in behaviour between the two series. The fibre reinforced concrete specimens needed higher loads to obtain the same elongation as ordinary concrete. The response curves do not show as many drops as for ordinary concrete specimens because of the fibres were able to transfer stresses across them. The ability of transferring stresses even through large cracks also increased the tension stiffening effect.

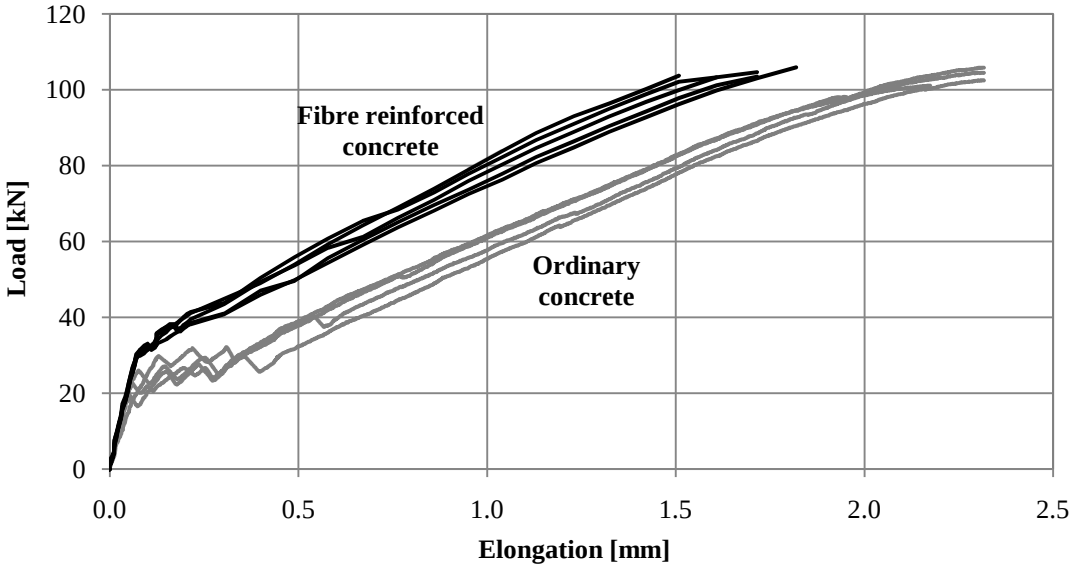

Figure 3.14 Load-elongation curves during testing of tie-rods with ordinary or fibre reinforced concrete (V_f = 0.85 %).

3.3 FE model

3.3.1 Software

The non-linear finite element simulations of the tie-rod tests were carried out in the commercial FE software ADINA (2010), where ADINA stands for Automatic Dynamic Incremental Non-linear Analysis.

3.3.2 Geometry

The concrete specimens tested in the tie-rod tests were modelled as a prism with square section with a ϕ16 mm reinforcement bar in the centre of the cross-section. The dimensions of the model are shown in Figure 3.15 and are the same as explained in Section 3.2.3, except for the length of the specimen, which was decreased 4 mm in order to make the meshing of the model easier and uniform over the specimen with an element length of 8 mm.

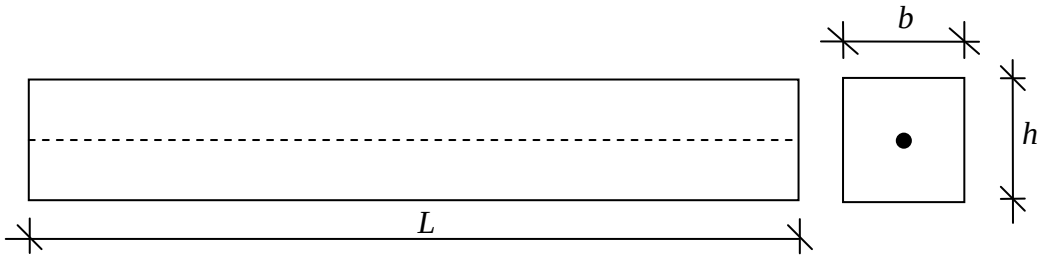

Dimensions
h = 112 mm
b = 112 mm
L = 816 mm

Figure 3.15 Geometry modelled in ADINA for the simulation of the tie-rod tests.

3.3.3 Material models

3.3.3.1 Concrete

In this thesis, the concrete properties were defined by using an existing material model called CONCRETE in ADINA. This model has a material response that is multi-linear on the tensile side, see Figure 3.16 (b), and non-linear in compression, as can be seen in Figure 3.16 (a).

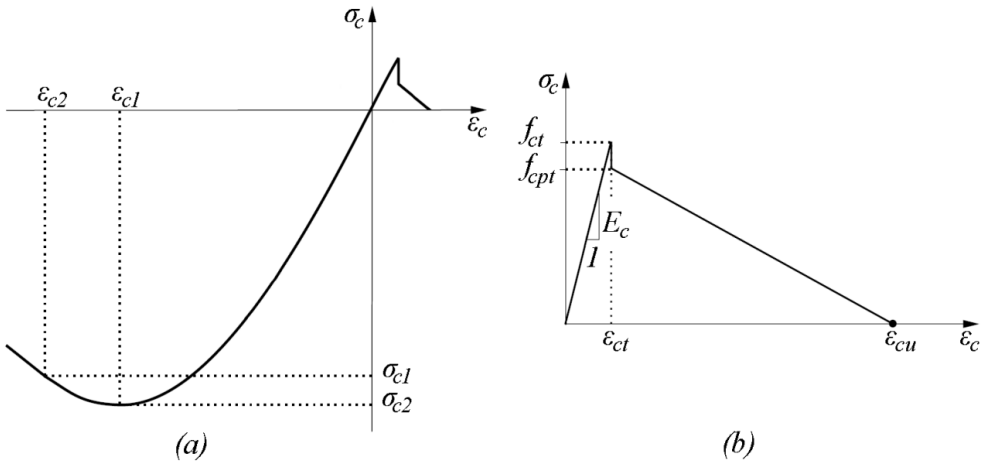

Figure 3.16 (a) Concrete material model used in ADINA, (b) enlargement of the tensile side.

With regard to the different geometries, loads and boundary conditions used in this thesis project, concrete compression failure was not expected to occur. However, some numerical problems were discovered by Alfredsson and Spåls (2008). In order to avoid this, the compressive capacity was considerably increased, which should not influence the results. The values used in ADINA for the compressive parameters defined in Figure 3.16 (a) are shown in Table 3.3.

Table 3.3 Inserted values of concrete compressive parameters defined in Figure 3.16 (a).

i	1	2
σ_{ci}	-100 MPa	-97 MPa
ε_{ci}	-10.0 ‰	-13.5 ‰

The behaviour after having reached the maximum tensile stress, f_{ct}, is of great importance for the cracking process of fibre reinforced concrete. At this tensile stress concrete starts to crack and there is a sudden drop in the ability to transfer stresses across the crack zone, see Figure 3.16 (b). The maximum stress that the cracked zone is able to transfer is called the post-tensile strength, f_{cpt}. When the strain continues to increase, the stress being transferred through the crack zone decreases linearly until it reaches the ultimate concrete strain, ε_{cu}, where a fully developed crack is reached and no stress can any longer be transferred.

The relation between ε_{cu} and ε_{ct} is defined in ADINA by using a parameter ξ as it is seen in Equation (3.1).

$$\varepsilon_{cu} = \xi \cdot \varepsilon_{ct} \tag{3.1}$$

where ε_{ct} is obtained by the relation in Equation (3.2).

$$\varepsilon_{ct} = \frac{f_{ct}}{E_c} \tag{3.2}$$

For the smeared crack approach of reinforced concrete members, considering a bond-slip, the crack zone is assumed to concentrate in just one element row, which means that the ultimate strain is related to the element length, l_{el}, and the crack width, w_u (see Section 2.3.1), by Equation (3.3).

$$\varepsilon_{cu} = \frac{w_u}{l_{el}} \tag{3.3}$$

In Section 2.3.1, the fracture energy, G_f, was explained as the area below the stress-crack opening curve. If we assume a linear relation as in Figure 3.16 (b), its value is obtained by using Equation (3.4).

$$G_f = \frac{f_{cpt} \cdot w_u}{2} \tag{3.4}$$

By combining Equations (3.1) to (3.4), an expression based on geometrical and material properties for the parameter ξ can be derived, and it is shown in Equation (4.5).

$$\xi = \frac{2 \cdot G_f \cdot E_c}{l_{el} \cdot f_{ct} \cdot f_{cpt}} \tag{3.5}$$

For ordinary concrete with no fibre reinforcement it is commonly assumed that the stress being transferred through a crack zone decreases linearly with increasing strain, see Figure 3.17 (a) and (b). This is due to the fact that ordinary concrete has small fracture energy and therefore the crack development until a fully open state is achieved within a small strain interval, which makes the shape of this descending branch less significant than the total fracture energy in the crack zone.

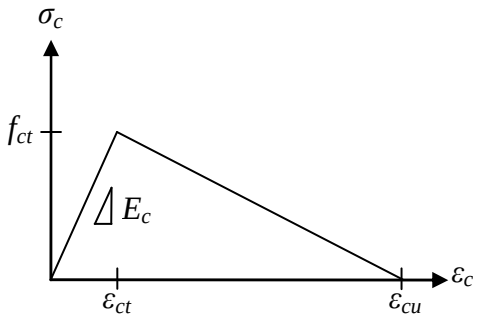

Figure 3.17 Enlargement of the tensile side of the material model used for ordinary concrete.

In ADINA this is defined by setting the post tensile strength equal to the tensile strength. In the same way as explained before, the fracture energy is determined by the parameter ξ, which then can be calculated by Equation (3.6)

$$\xi = \frac{2 \cdot G_f \cdot E_c}{l_{el} \cdot f_{ct}^2} \tag{3.6}$$

In the modelling the material properties of concrete were determined according to the test results shown in Section 3.2.1. Mean values of tensile strength and fracture energy were used for both ordinary and fibre reinforced concrete. In order to determine the post tensile strength of fibre reinforced concrete, mean stress values were calculated at certain crack openings and adjusted by a linear relation as can be seen in Figure 3.18. Mean values were taken for only the first milimeter, as it is only the behaviour in this interval which is of interest as no larger crack widths are expected to occur. If the resulting slope is extrapolated to the whole post-cracking model seen in Figure 3.16 (b), a post tensile strength of 3.12 MPa and a fracture energy equal to 10 659 N/m are obtained. This seems reasonable with regard to the mean experimental value of the fracture energy, which was 10 359 N/m.

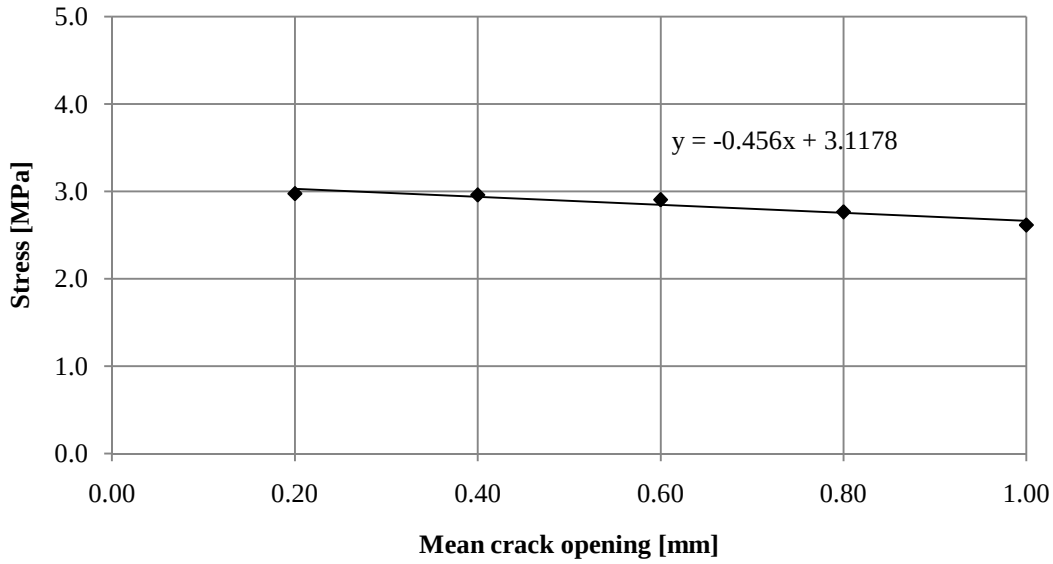

Figure 3.18 Mean post tensile stress values observed in testing of fibre reinforced concrete (V_f = 0.85 %).

The material properties used in the analysis to characterise the material behaviour of ordinary and fibre reinforced concrete according to Figure 3.17 (b) and Figure 3.16 (b), respectively, are summarised in Table 3.4.

Table 3.4 Material properties used in modelling ordinary and fibre reinforced concrete.

Ordinary concrete (V_f=0%)	
f_{cm}	64.5 MPa
f_{ct}	3.08 MPa
f_{cpt}	3.08 MPa
E_c	30 GPa
G_f	118 N/m
α_{cT}	$1.0 \cdot 10^{-5}$ 1/°C

Fibre reinforced concrete (V_f=0.85%)	
f_{cm}	54.1 MPa
f_{ct}	3.63 MPa
f_{cpt}	3.12 MPa
E_c	30 GPa
G_f	10 500 N/m
α_{cT}	$1.0 \cdot 10^{-5}$ 1/°C

3.3.3.2 Reinforcement

The material response of reinforcing steel was modelled as bilinear in both compression and tension. The yield strength, f_{yk}, and Young's modulus, E_s, for the actual steel type are shown in Table 3.5.

Table 3.5 Material properties for reinforcing steel

Reinforcing steel B500B	
f_{yk}	500 MPa
E_s	200 GPa

A small strain hardening effect was included in the material model. This is reflected in the final stress-strain relation used for reinforcing steel shown in Figure 3.19.

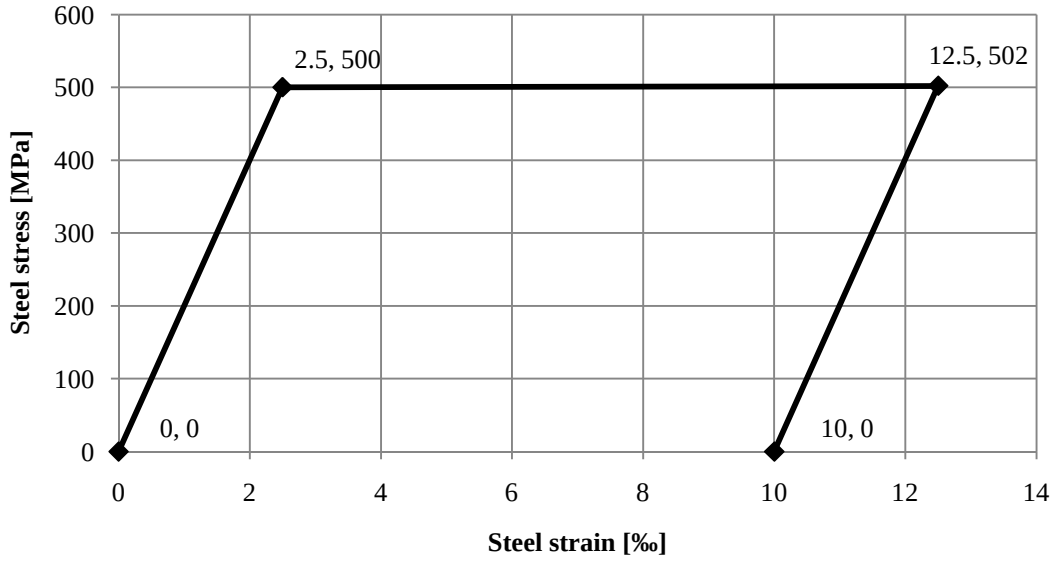

Figure 3.19 Material model for reinforcing steel B500B.

3.3.3.3 Bond between concrete and reinforcement

The bond behaviour was modelled in ADINA by defining spring elements with non-linear properties between concrete and reinforcement nodes. The non-linear properties are defined as a force-slip relation, which can be calculated from the bond stress-slip relation, as seen in Equation (3.7).

$$F_b(s) = \tau_b(s) \cdot A_{surf} = \tau_b(s) \cdot \pi \cdot \phi_{bar} \cdot l_{el} \tag{3.7}$$

Consequently, two different spring properties were defined to simulate the bond behaviour. These were based on the results from bar pull-out tests made on specimens with ordinary or fibre reinforced concrete previously shown in Section 3.2.2. When a new crack is formed, the surrounding concrete will slip towards opposite directions and, hence, it is also necessary to define spring properties for negative slips, see Figure 3.20.

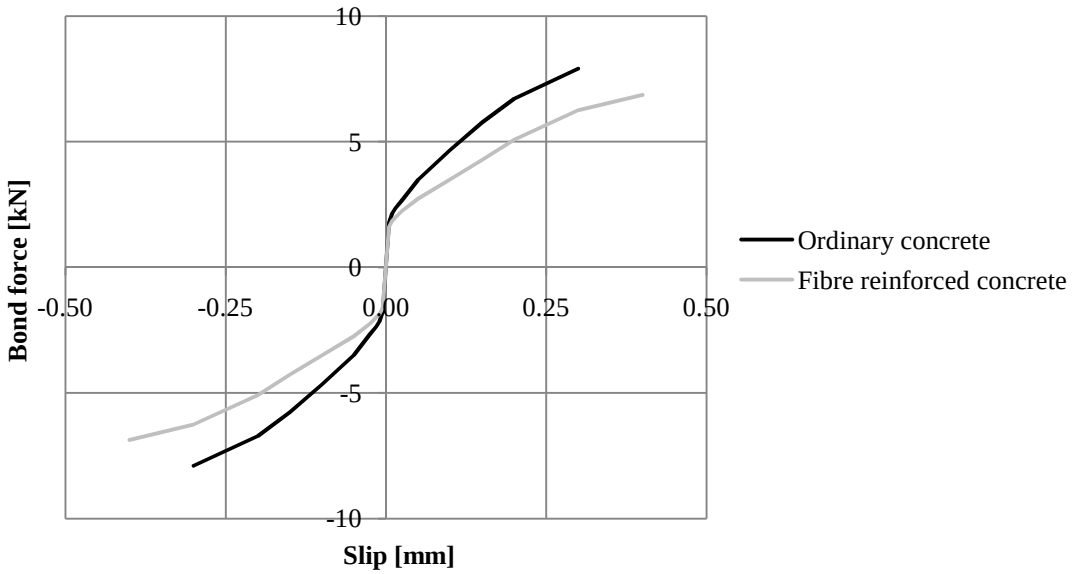

Figure 3.20 Spring properties as defined in ADINA to simulate bond behaviour between concrete and reinforcement.

For the end node of the reinforcement bar spring properties considering just half of the element length were defined for each case, as these nodes are just surrounded by one element in the longitudinal direction.

3.3.4 Boundary conditions and load

The boundary conditions were defined on the concrete prism as described in Figure 3.21. During the real testing the concrete specimens were pulled from both ends of the reinforcement bar. However, as the model needs to have at least one fixed point, the test was modelled as imposed displacement acting on one reinforcement bar end, the other end being fully fixed. In order to capture the slip behaviour, reinforcement nodes were constrained to have the same displacement in z-direction as its surrounding concrete nodes. As a consequence, there can only be relative displacement between concrete and reinforcement nodes in y-direction, which is controlled by the springs explained in Section 3.3.3.3.

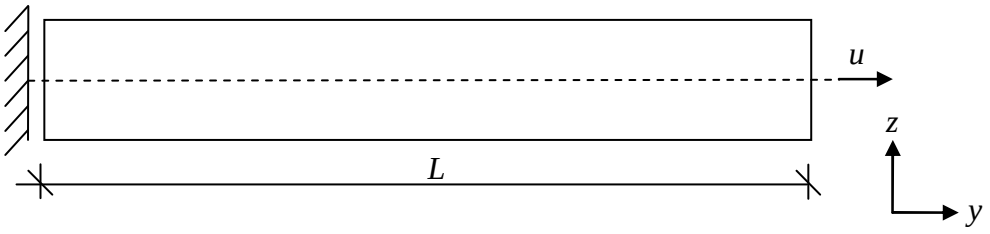

Figure 3.21 Boundary conditions used on the FE-simulation of the tie-rod tests.

The load was applied as a horizontal displacement increasing with time at a constant rate till yielding of the steel bar was reached. A maximum positive displacement of the right end node of the bar of 5 mm was defined.

3.3.5 Mesh

The concrete was modelled with 2D solid plane stress elements that define a 2D surface with a considered thickness of 112 mm. The concrete elements were meshed with a right-angled triangular mesh. A triangular mesh type was preferred rather than a quadratic mesh, since analyses carried out by Alfredsson and Spåls (2008) showed some difficulties to develop inclined cracks in a quadratic mesh. An element length of l_{el} = 8 mm was chosen, see Figure 3.22.

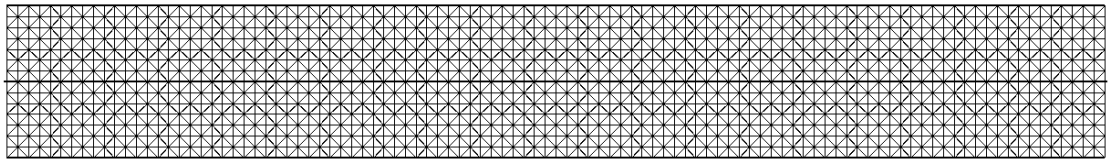

Figure 3.22 Right-angled triangular mesh with element size l_{el} = 8 mm.

Two node pipe elements, with the same element length as used for the concrete elements, were used to model the reinforcing steel. This type of element was chosen rather than truss elements as it is not possible to apply thermal strains on truss elements. Therefore, the model is able to simulate different load cases, such as including shrinkage or thermal effects.

3.3.6 Method

In this thesis static analysis were carried out. The iteration method used was Broyden, Fletcher, Goldfarb and Shanno (BFGS-Method). This method was used since Alfredsson and Spåls (2008) found some numerical and convergence problems while using the full Newton and modified Newton iteration methods. The applied displacement was divided in 1000 steps and, hence, each step corresponds to a positive displacement increment of 0.005 mm.

The results obtained by non-linear finite element analysis are shown by crack widths and crack pattern graphs. The crack widths in this thesis project were calculated according to Equation (3.8). The concrete strain was measured in ADINA at different reinforcement layers and crack widths at these points were obtained by multiplying the total concrete strain by the element length.

$$w = \varepsilon_c \cdot l_{el} \tag{3.8}$$

In order to be able to compare the crack widths with each other in one specimen, the crack widths at a certain level are plotted against the length of the specimen at the final step of the analyses, i.e. when the reinforcing bar has started to yield, see example in Figure 3.23.

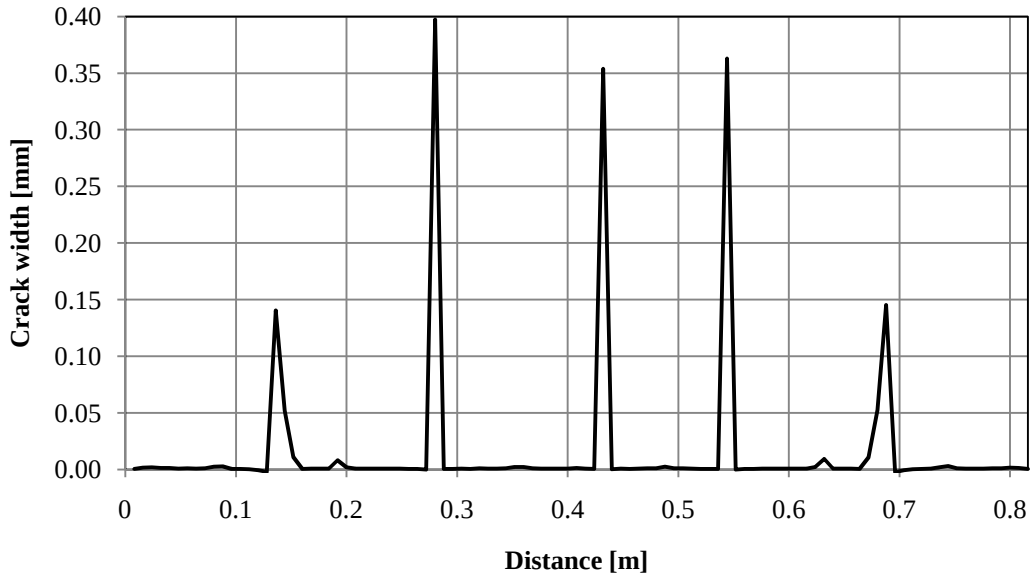

Figure 3.23 Example of graph showing crack widths along the specimen length.

While studying crack patterns it is possible to obtain cracks at different stages of crack development from ADINA. Looking at Figure 3.24, when concrete reaches its tensile strength, micro cracks start to form, i.e. 0 % open cracks. These will increase for higher strains until the crack zone is not able to carry any further load, and it is assumed at this point that cracks are 100 % fully developed. Any intermediate state between these two points corresponds to crack zones that are still able to carry some stresses.

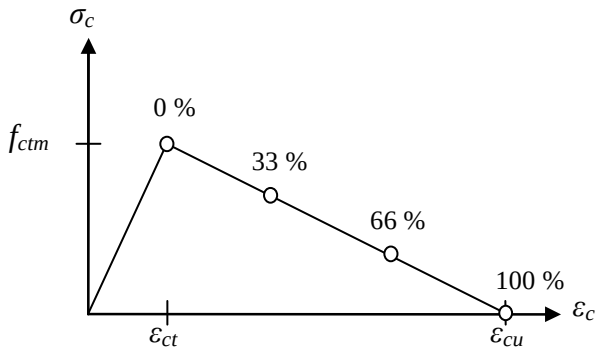

Figure 3.24 Percentage of total crack opening.

While looking at the crack patterns at different stages shown in Figure 3.25, it is easy to see that there is not much difference between 33 % and 100 % fully developed crack states. For this reason, in this and in the following sections, focus will be just on crack formation and fully open crack states. When we refer to crack formation patterns this is related to 0 % fully developed open cracks, and fully open cracks pattern will just show cracks which strains are larger than the ultimate strain, i.e. 100 % fully developed cracks.

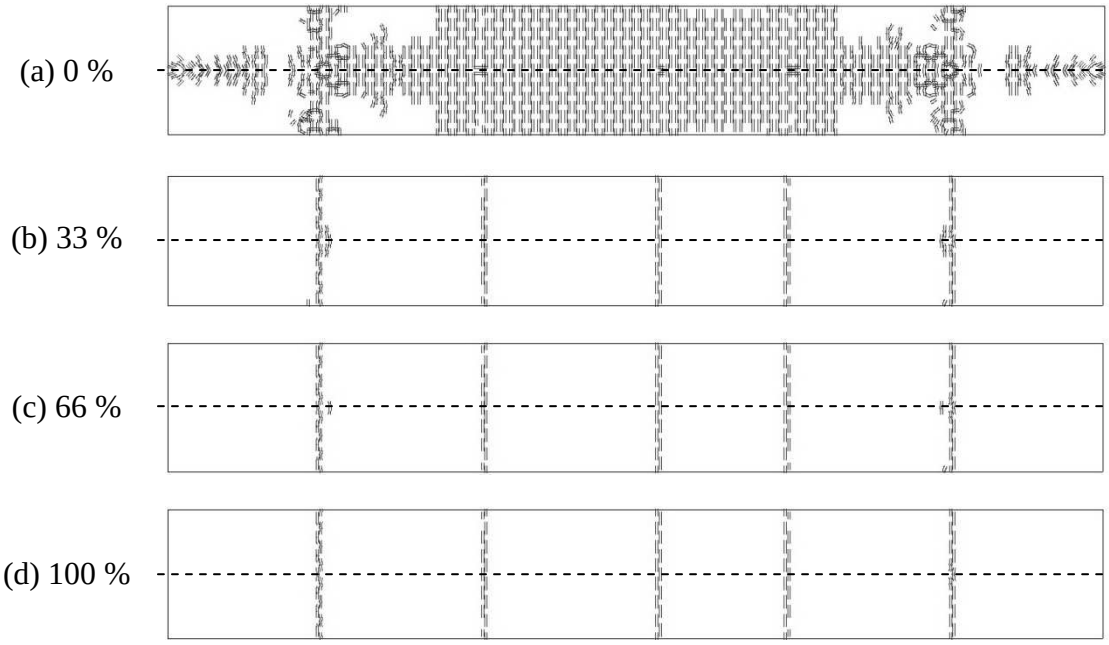

Figure 3.25 Crack pattern graphs for different percentages of crack opening.

When looking at crack patterns for fibre reinforced concrete, 100% open cracks does not refer to their actual ultimate strain. In case of high fracture energies fully opened cracks are not reached for the maximum imposed displacement. The same strain value as the ultimate strain for ordinary concrete was used instead in order to be able to compare crack patterns with different fracture energies, see Figure 3.26.

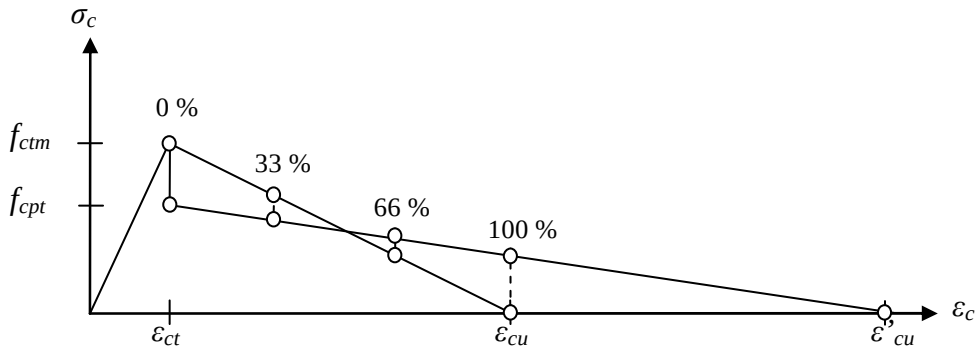

Figure 3.26 Definition of 33 %, 66 % and 100 % open cracks for fibre reinforced concrete compared to ordinary concrete.

3.4 Comparison of results

3.4.1 Uniform material properties

The crack pattern obtained by simulation of tie-rod tests for ordinary concrete is shown in Figure 3.27. It is clearly seen that five through cracks have appeared and they are almost symmetrically and equally spaced. Mean value of 4.2 cracks was counted on the surface of ordinary concrete specimens. In the analyses some skew cracks also formed close to the ends but they were not fully developed.

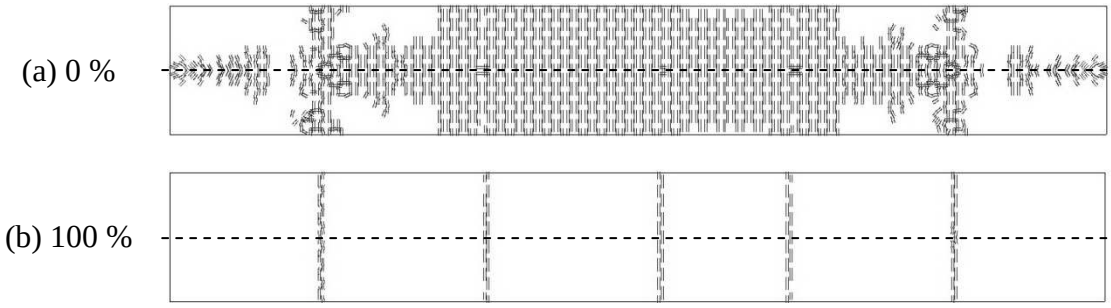

Figure 3.27 Crack pattern obtained by finite element analysis of tie-rod test with ordinary concrete for u = 1.49 mm.

In Figure 3.28, where crack widths at the steel level are plotted, it is possible to observe that inner cracks are larger than the ones close to the ends of the specimens. Crack widths range from 0.15 to 0.40 mm.

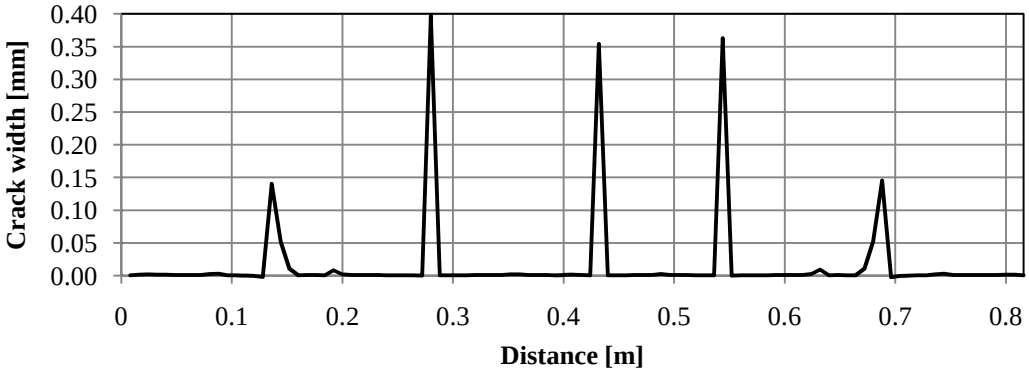

Figure 3.28 Crack widths at steel level obtained by finite element analysis of ordinary concrete for u = 1.49 mm.

In Figure 3.29, the load-elongation relation, obtained by finite element analysis, is compared with the relations observed during testing of specimens with ordinary concrete. The relation obtained by simulation shows a good agreement in stiffness before cracking and in the state of stabilised cracking (when all cracks have formed). However, cracking is delayed in the analyses and the cracking load is higher than the mean value observed in the tests. This increase of the initial crack load could be caused by ignoring possible shrinkage induced stresses, or having used the mean tensile strength in the whole model. There may also have been some geometrical imperfections in the specimens that could create second order bending moment and reduce the cracking load.

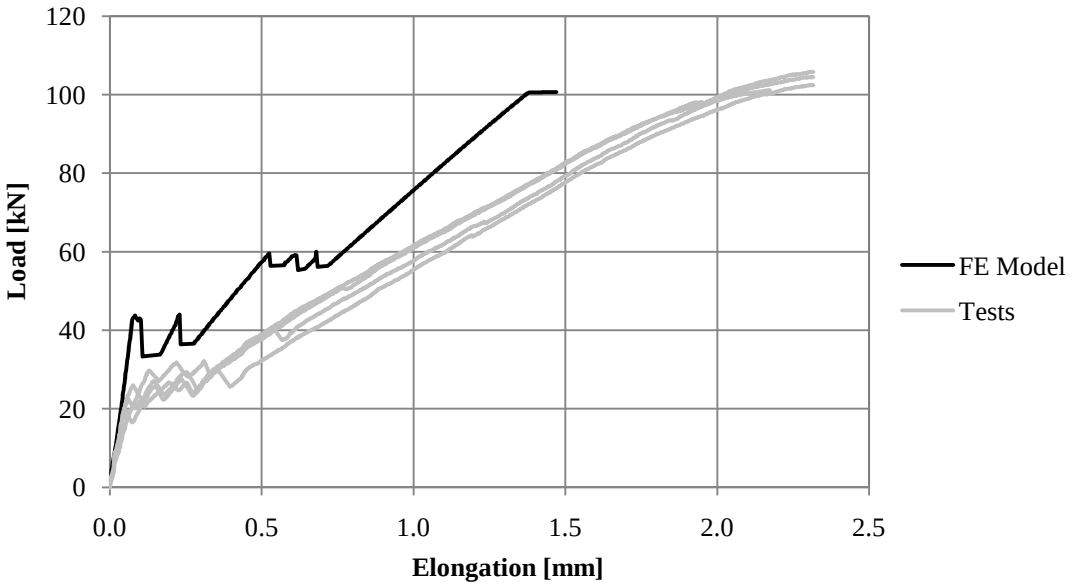

Figure 3.29 Load-elongation relation obtained by finite element analysis of specimen with ordinary concrete in comparison with test results.

Finite element analyses were also carried out to simulate the tie-rod tests of specimens with fibre reinforced concrete. When using homogeneous material properties as explained in Section 3.3.3.1, the crack pattern shown in Figure 3.30 was obtained. It can be observed that no 100 % open cracks were formed. However, almost every section of the model has started to crack. This is also apparent in Figure 3.31, where crack widths along the reinforcing bar are plotted. The crack width is very small but constant along the central part of the model, i.e. where the reinforcing bar has been able to transfer tensile stress to the surrounding concrete. Since a material with very ductile behaviour was applied to all elements in the model, all crack zones are able to transfer high stresses through themselves and an almost uniform tensile stress state was achieved in the model. Then, not large enough stresses can be redistributed in the cracked sections from the concrete to the bar to cause localization of cracks.

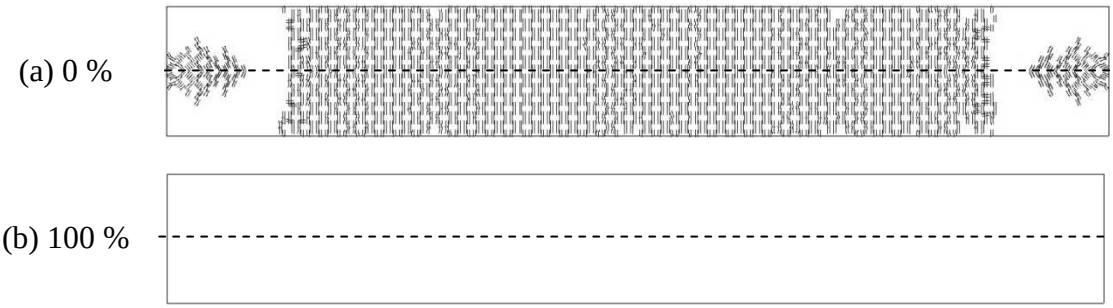

Figure 3.30 Crack pattern obtained by finite element analysis of fibre reinforced concrete for u = 1.03 mm.

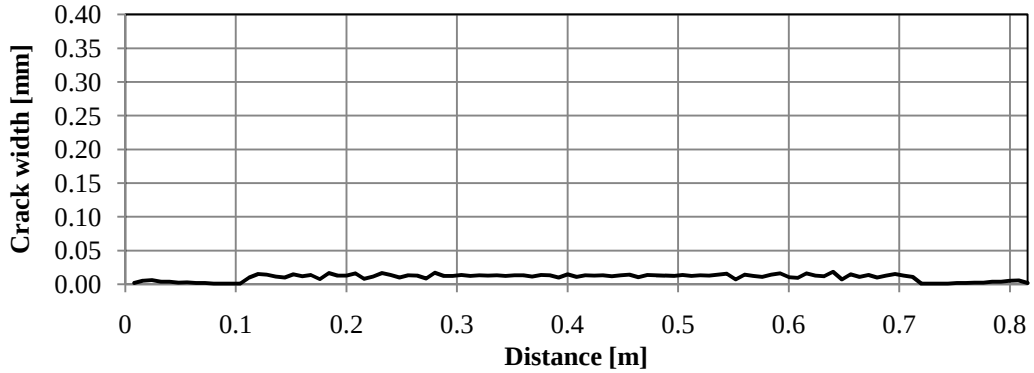

Figure 3.31 Crack widths at steel level obtained by finite element analysis of specimen with fibre reinforced concrete for u = 1.03 mm.

These difficulties to localise cracks and reproduce the real behaviour of fibre reinforced concrete are also apparent from Figure 3.32, where some numerical problems can be observed in the stage where the whole model starts to crack at once. The predicted load-elongation curve shows unrealistic values from the initiation of cracking to an elongation of about 0.3 mm.

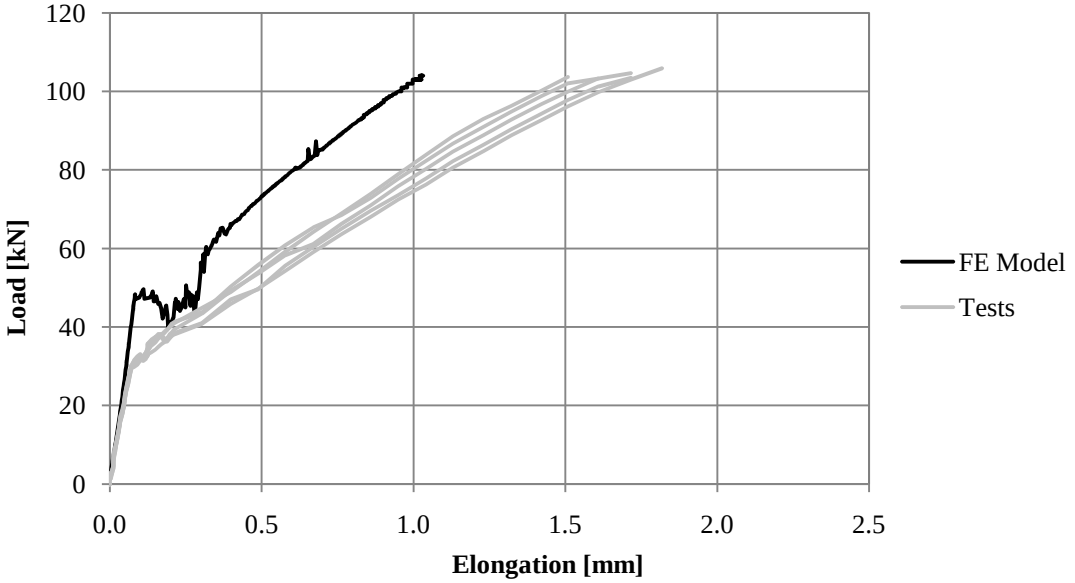

Figure 3.32 Load-elongation relation obtained by finite element analysis of specimen with fibre reinforced concrete in comparison with test results.

3.4.2 Heterogeneous material approach

As seen in Section 3.4.1, when using uniform material properties in the simulation of tie-rod tests on fibre reinforced concrete specimens, there were some problems to localise cracks. Therefore, analyses on fibre reinforced concrete specimens with random material properties were carried out, see Appendix A. The tensile strength was randomized following a normal distribution based on the mean and standard deviation values obtained in the uni-axial tensile tests of fibre reinforced concrete specimens. The parameter ξ, see Equation 3.6, was varied in order to have the same fracture energy in every case. These new analyses showed an improved behaviour,

having some element rows where cracks were concentrated. However, all elements had very high fracture energy and, thus, high stresses could still be transferred through the cracks. Hence, no significant stress redistribution due to crack formation took place.

Due to this, another approach to simulate fibre reinforced concrete was considered. Till now, material data from tests had been used to describe the material behaviour in all elements in the model. However, as seen in Figure 2.10, fibre reinforced concrete behaviour in tension is a result of the combined effect of the individual behaviour of ordinary concrete loaded in tension and response of fibres when pulled out from the concrete matrix.

In order to simulate this, two different material properties with the same tensile strength were defined, see Figure 3.33, and applied randomly all over the model with the same probability of appearance. One material property had the same fracture energy as observed during testing of ordinary concrete specimens and simulates plain concrete elements. The other one had the same material properties that were used for modelling fibre reinforced concrete with uniform properties, but with the aim to simulate just the fibres themselves. Three different material distributions were analysed; results from these analyses are shown in Appendix B.

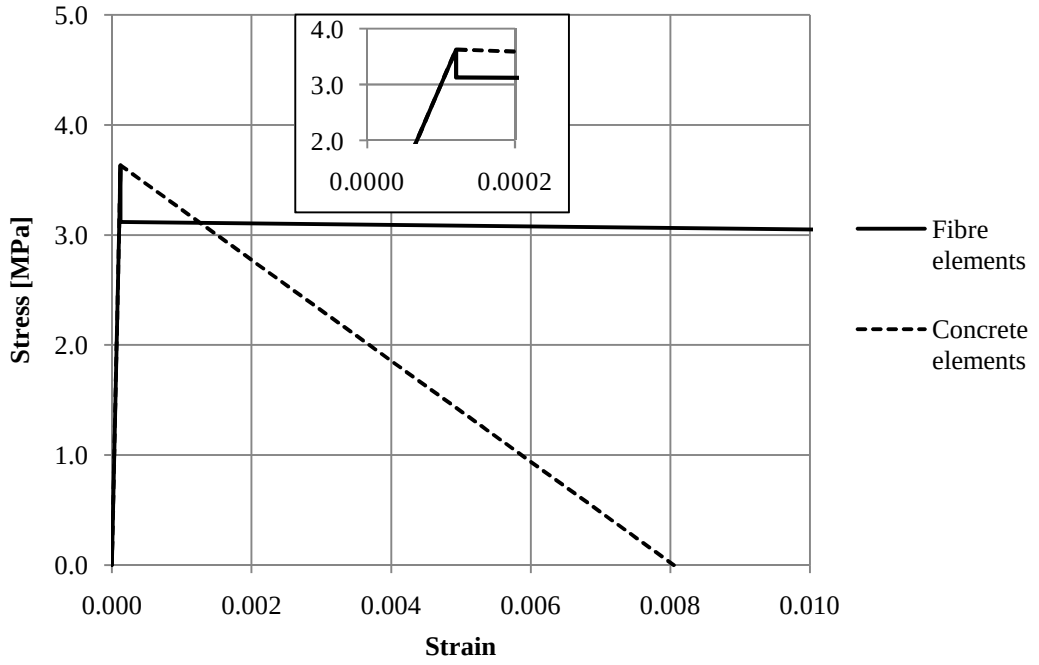

Figure 3.33 Material properties as defined in ADINA for fibre and concrete elements.

It shall be mentioned that this approach does not correspond exactly to the material behaviour shown in Figure 2.10, since it underestimates the material properties. This is further discussed in Section 3.5. However, by using this new approach of modelling fibre reinforced concrete specimens, a better behaviour was captured. Elements with concrete behaviour loose stresses once they are cracked and this allows cracks to grow in concentrated element rows. At the same time, there are still stresses being transferred through fibre elements, which decreases the transmission length and therefore, initiate more cracks than in ordinary concrete, see Figure 3.34. Some of these cracks did not develop to through cracks and were concentrated towards one

face only, which was also observed during the tests on fibre reinforced concrete specimens shown in Section 3.2.3.

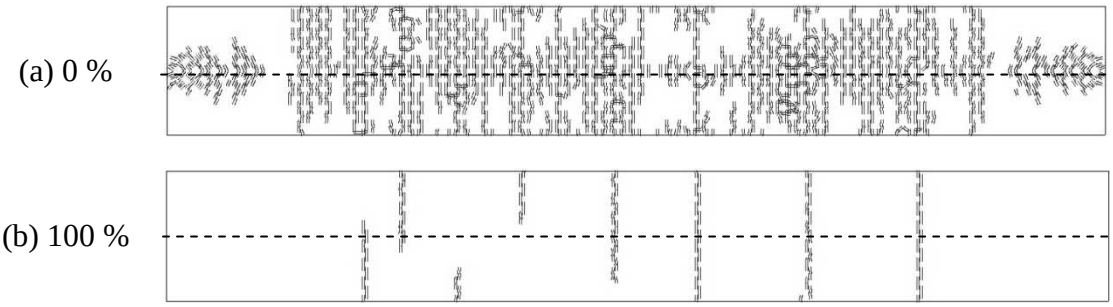

Figure 3.34 Crack pattern obtained for specimen with fibre reinforced concrete analysed with heterogeneous material distribution R1 for u = 1.10 mm.

Since weaker elements were randomly distributed across the model, cracks may not form through the whole specimen. In order to be comparable with the test results it was obtain the crack widths at the surfaces in the model, i.e. the top and bottom faces. In Figure 3.35 and Figure 3.36 predicted crack widths at the top and bottom face, respectively, of the fibre reinforced concrete specimen can be seen. It can be observed that cracks differ in position and width from one face to the other. The mean number of visible cracks obtained on all faces of the three different material distributions analysed was 6.5, which is reasonable as a mean value of 6.2 cracks were determined at the tested fibre reinforced concrete specimens.

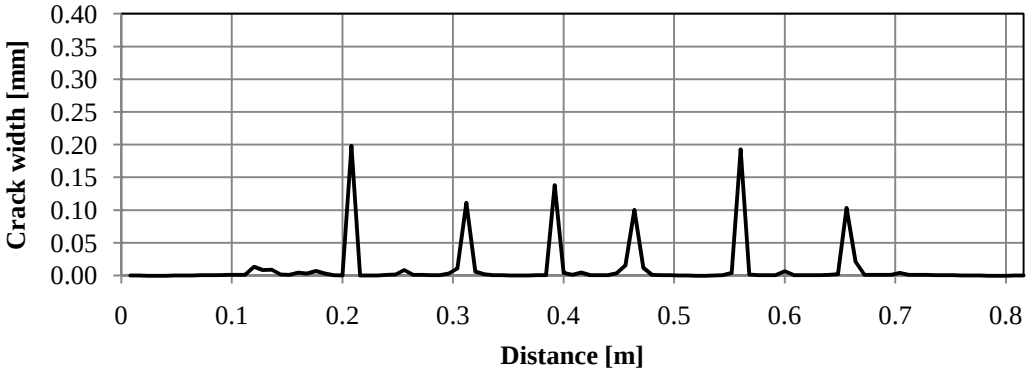

Figure 3.35 Predicted crack widths at the top face obtained for fibre reinforced concrete specimen analysed with heterogeneous material distribution R1 for u = 1.10 mm.

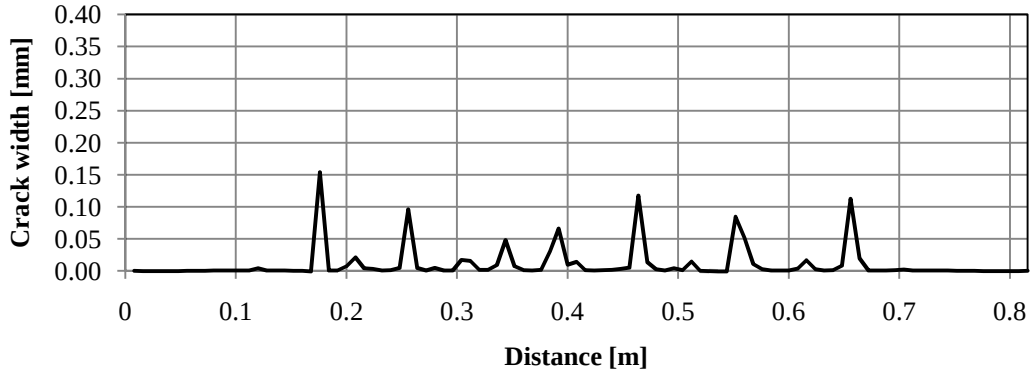

Figure 3.36 Predicted crack widths at the bottom face obtained for fibre reinforced concrete specimen analysed with heterogeneous material distribution R1 for u = 1.10 mm.

The relation between load and elongation obtained by the analysis with heterogeneous material properties is shown in Figure 3.37 in comparison with experimental results. With regard to stiffness a very good agreement before and after cracking is observed. However, the cracking load is too large in the analyses compared to that observed in the tests. As discussed concerning the analysis of ordinary concrete specimen with homogenous material properties, the reason may be that shrinkage effect on the real specimens before testing was not considered in the analysis.

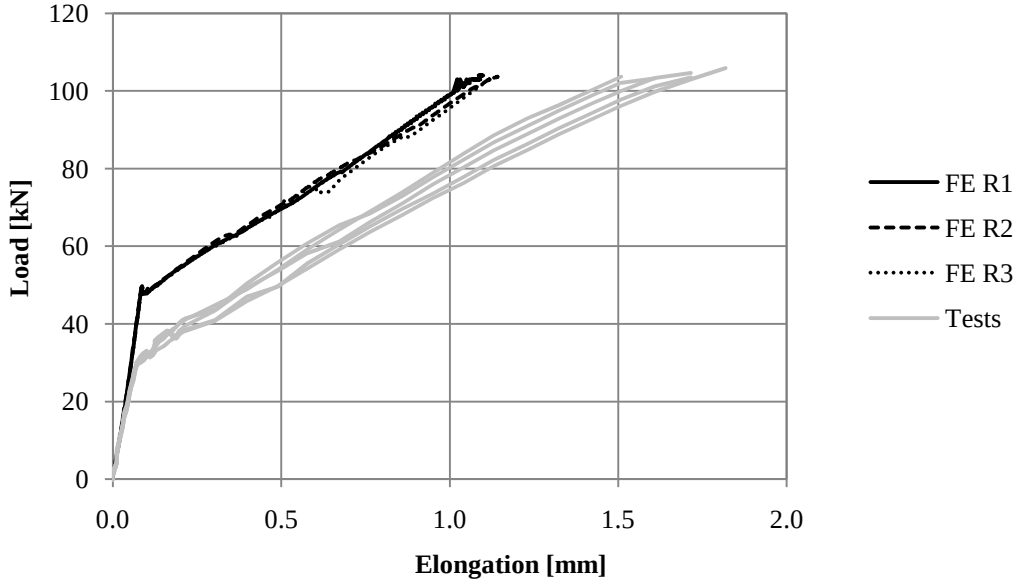

Figure 3.37 Predicted load-elongation relation for specimen with fibre reinforced concrete modelled with different heterogeneous material properties distributions in comparison with experimental results.

3.5 Concluding remarks

The model used to simulate tie-rod tests on specimen with ordinary concrete showed a good agreement with the test results. In average 4.2 cracks per tie-rod specimen were observed in the test series with ordinary concrete, while 5 cracks were formed in the finite element simulation, see Figure 3.38. As it can be seen in Figure 3.27, good correlation was shown between predicted and observed load-elongation curves, except concerning the cracking load, for which possible sources of error were explained in the previous sections. Therefore, for ordinary concrete it seems to be appropriate to assume uniform material properties obtained during testing in order to reproduce a realistic behaviour.

However, while trying to simulate tie-rod tests on fibre reinforced concrete it was not appropriate to assume uniform material properties resulting from the tests. Due to the presence of two materials with different behaviours, in Section 3.4.2 it was suggested to model the average material response as a combination of the individual behaviour of both of them. This approach gave a better agreement between the model and the test results and was also used in Jansson (2011). In the tie-rod test an average of 6.2 cracks per specimen was observed for cracks having appeared at any face, while in the finite element simulation a mean value of 6.5 100 % fully open cracks were formed at the faces of the three different samples, see Figure 3.38. The stiffness of the load-elongation response obtained from finite element analysis also showed very good agreement with the observed before and after cracking. However, cracking was initiated at a higher load in the model, see Figure 3.37.

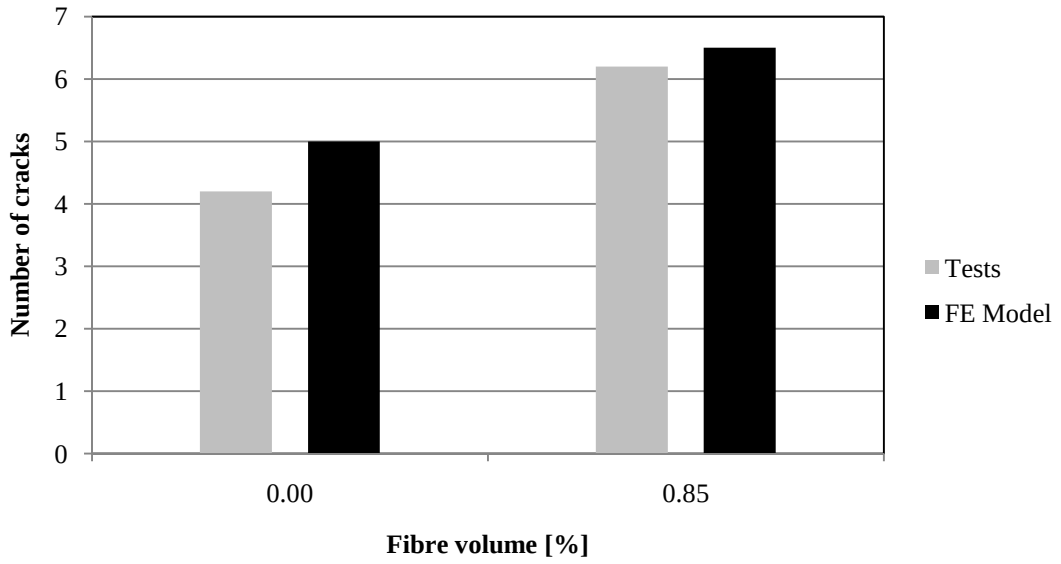

Figure 3.38 Comparison of average number of cracks in the tested specimens and the finite element analysis.

The approach with two different materials has been used in this thesis project as a way to understand the behaviour of fibre reinforced concrete and check its possible effects on various structural elements with continuous edge restraint. However, in this project, due to limitations in ADINA, fibre elements have been modelled as very ductile concrete. This assumption has shown good agreement with the tests results concerning the number of cracks appeared. However, the mean material response

added to the model does not correspond to the material behaviour obtained during testing as the total fracture energy is underestimated. Analyses using this model would help to understand the behaviour of fibre reinforced concrete, but will not correspond to any specific fibre dosage. In order to reproduce a more realistic behaviour, it would be necessary to use a more suitable material model for fibre elements, as it is shown in Figure 2.10. Also, the probability of appearance of concrete and fibre elements should be specified in order to, after adding the weighted contribution from fibre and concrete elements, getting the same fracture energy as in the tests. Weighting values could also be determined by the expected number of fibres per unit area for a certain fibre volume.

4 Non-linear FE analyses of edge beams with continuous edge restraint

4.1 Introduction

One type of structural component with continuous edge restraint of special interest is edge beams of bridges. Due to being highly exposed to an aggressive environment, edge beams often need to be replaced during the service life of a bridge. When a new edge beam is cast to an existing concrete bridge deck, there will be different thermal and shrinkage strains in the two members and the new concrete may crack due to the need for movement in combination with a continuous restraint. Because of the importance of protecting reinforcement against the environment, it is necessary to take restraint cracking into account during the design process.

In order to understand how the cracking process develops, Alfredsson and Spåls (2008) carried out some finite element analyses on edge beams. They studied the influence of beam length, boundary conditions, stiffness of the joint in plain concrete edge beams subjected to a temperature decrease and also the effect of adding reinforcement to it. A typical reinforcement configuration for a bridge edge beam, shown in Figure 4.1, was chosen to be analysed in their thesis project. Johansson and Lantz (2009) continued their work by studying different reinforcement configurations and their effects on crack widths and crack patterns. Influence of beam length, transversal reinforcement ratio and width of the joint between different concrete members, in reinforced edge beams, was also analysed.

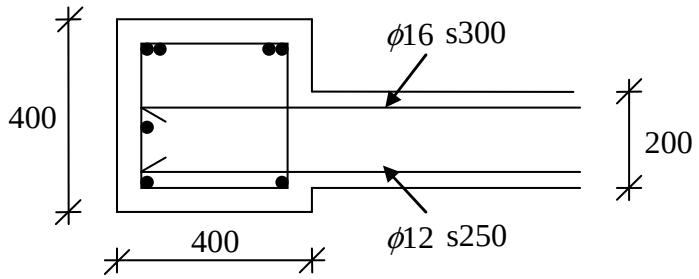

Figure 4.1 Sketch over a typical edge beam, based on Vägverket (2001).

One aim of the actual project was to expand the previous work; and therefore the following parameters were studied.

- Possible rearrangement of the main reinforcement, while increasing the transversal reinforcement ratio.
- Effect of using different bar diameters, while keeping the same longitudinal reinforcement ratio.
- Influence of the thickness of the concrete cover.
- Effect of using concrete with different fracture energies.
- Influence of adding fibre reinforcement.
- Effect of concrete creep.

This study on bridge edge beams is presented in the following sections.

4.2 FE model

4.2.1 Introduction

The non-linear finite element analyses on edge beams were carried out according to the modelling methodology explained in Section 3.3, which showed good correlation with experimental results for concrete specimens with ordinary reinforcement. Basic studies on how fibre reinforcement affects crack widths were also carried out according to the same approach as presented in Section 3.4.2.

4.2.2 Geometry

A reference case was defined with a reinforcement configuration consisting of 4ϕ16 mm reinforcement bars in the top and 3ϕ16 mm reinforcement bars at the bottom, which corresponds to a longitudinal reinforcement ratio, ρ_l, of 0.88 %. This configuration seemed to give the best results according to the reinforcement study made by Johansson and Lantz (2008). The geometry of the reference case is shown in Figure 4.2, where A_{s1} and A_{s2} are the total steel areas at the top and bottom level, respectively, as they were defined in the FE model. Transversal reinforcement, as seen in Figure 4.1, was defined with a reinforcement ratio, ρ_t, of 0.62 % with regard to the area of the interface with the width *t*.

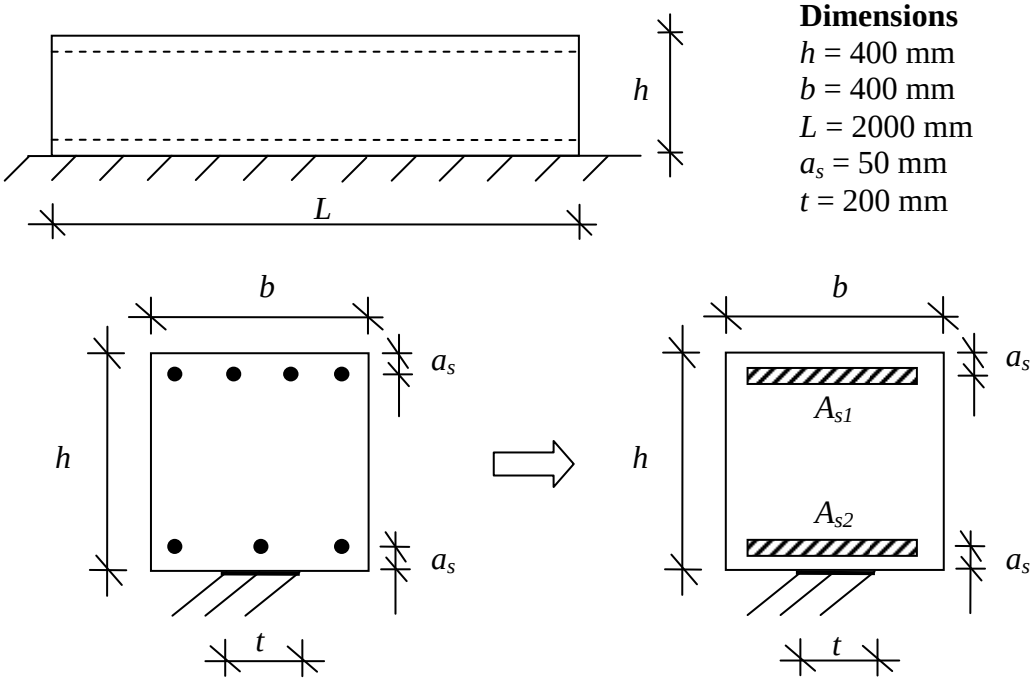

Figure 4.2 Geometry of the edge beam for the reference case.

4.2.3 Material model

4.2.3.1 Concrete

Concrete material properties were defined as for ordinary concrete according to Section 3.3.3.1, see Figure 3.17. It was decided to use concrete of strength class C30/37 in the analysis in order to be able to compare with results from previous

works. The material properties for this concrete class are shown in Table 4.1. In order to avoid numerical problems and since the model will be subjected mainly to tensile stresses, the compressive strength was also increased to the same values as introduced in Section 3.3.3.1.

Table 4.1 Material properties for the reference case.

Concrete class C30/37	
f_{cm}	38 MPa
f_{ct}	2.9 MPa
f_{cpt}	2.9 MPa
E_c	33 GPa
G_f	100 N·/m
α_{cT}	$1.0 \cdot 10^{-5}$ 1/°C

When studying the effect of adding fibre reinforcement, the same heterogeneous material approach as described in Section 3.4.2 was used. The material properties shown in Table 4.1 were applied to concrete elements. For fibre elements, based on the material behaviour observed in the tie-rod tests with fibre reinforced concrete, the post-tensile strength was assumed to 85% of the tensile strength and the fracture energy was increased to 10500 N/m.

4.2.3.2 Reinforcement

Reinforcing steel was modelled as a bilinear material in both compression and tension with material properties as defined in Table 3.5.

4.2.3.3 Bond between concrete and reinforcement

In Figure 3.9, a comparison was made between test data and bond-stress slip relations suggested by CEB-FIP (1993) and CEB (1997) for ordinary concrete. It was observed that the experimental results had a better agreement with the relation proposed by CEB (1997) for slips lower than 0.2 mm. In absence of experimental data for the concrete strength class presented in Table 4.1, the bond stress-slip relation recommended by CEB (1997) was used in the analyses for slips up to 1.0 mm. For larger slips the bond stress-slip relation recommended by CEB-FIP (1993) was used. This combined relation is shown in Figure 4.3.

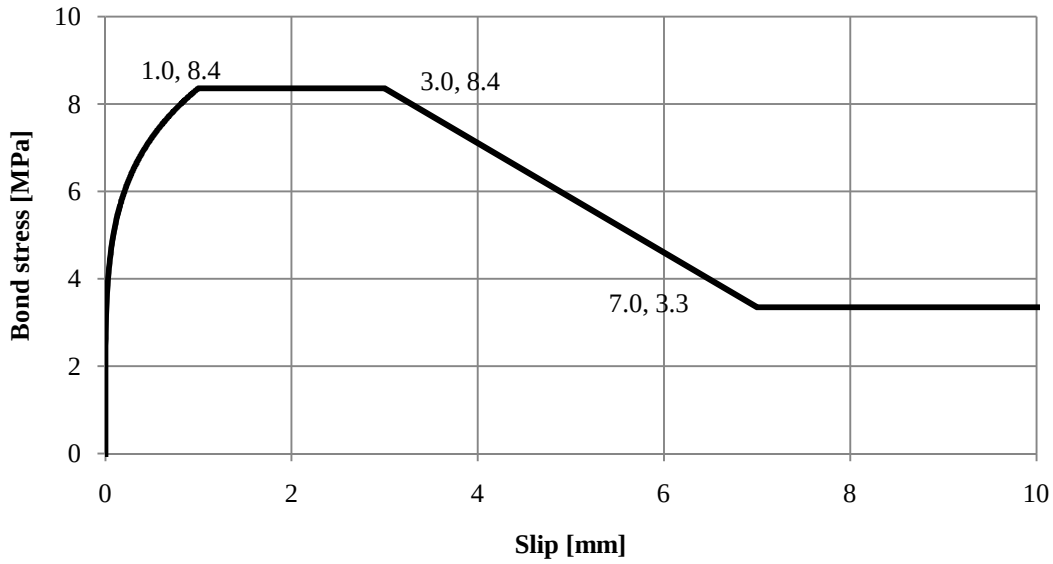

Figure 4.3 Assumed bond stress-slip relation between concrete and reinforcement.

The bond behaviour was modelled by non-linear springs between concrete and reinforcement nodes at each reinforcement layer. Therefore, spring properties should be defined as seen in Equation (4.1), where the number of reinforcing bars at each layer is taken into account, cf. Equation (3.7).

$$F_b(s) = \tau_b(s) \cdot A_{surf} = \tau_b(s) \cdot n_{bar} \cdot \pi \cdot \phi \cdot l_{el} \tag{4.1}$$

The corresponding force-slip relation for the case of one ϕ16 mm reinforcement bar is shown in Figure 4.4.

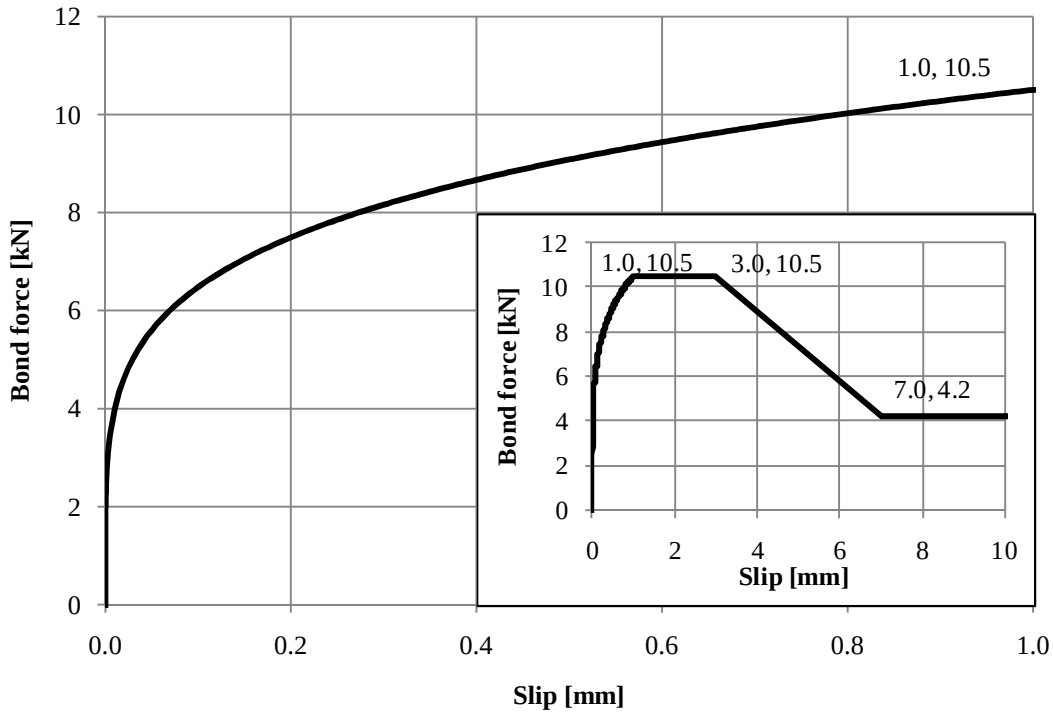

Figure 4.4 Bond force-slip relationship for element length 25 mm and one ϕ16 mm reinforcement bar .

4.2.3.4 Shear transfer at the joint interface

The interaction at the joint interface between the edge beam and the concrete bridge deck is described by the bond stress-slip relation introduced in Section 2.6.2. This relation for the material properties used in the reference case is shown in Figure 4.5.

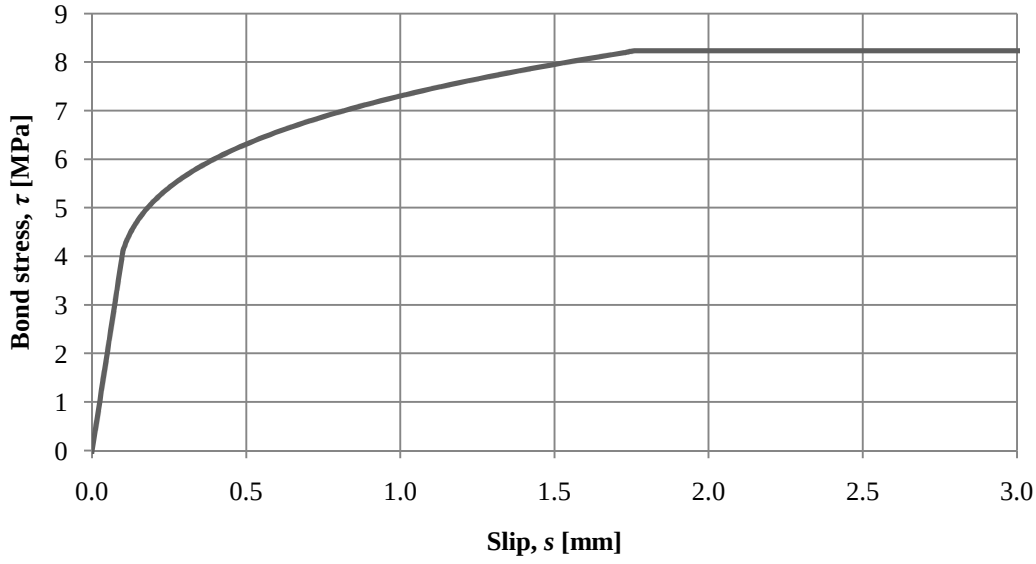

Figure 4.5 Bond stress-slip relation at the joint interface for the reference case.

As for the concrete-reinforcement interaction, for describing the bond behaviour at the joint interface, springs with non-linear properties were defined connecting nodes at the joint interface with auxiliary nodes. The corresponding bond force-slip relation can be obtained from Equation (4.2), where *t* is the width of the joint between the beam and the bridge deck.

$$F_{fm}(s) = \tau_{fm}(s) \cdot A_{surf} = \tau_{fm}(s) \cdot t \cdot l_{el} \tag{4.2}$$

The bond force-slip relation for the reference case and an element length of 25 mm can be observed in Figure 4.6.

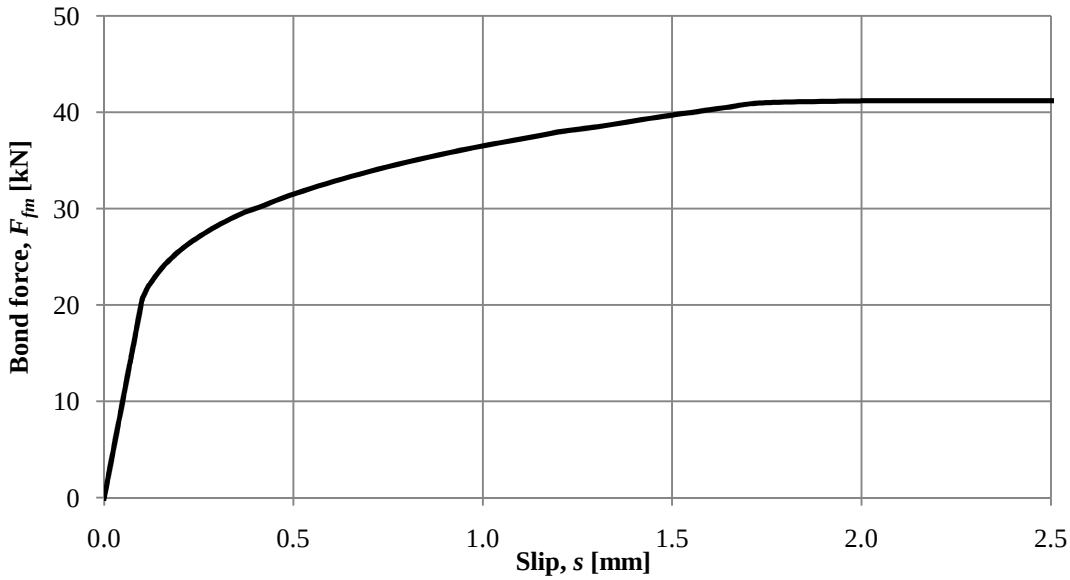

Figure 4.6 Bond force-slip relation at the joint interface with an element length l_{el} = 25 mm.

4.2.4 Boundary conditions and load

The boundary conditions were defined on the edge beam as described in Figure 4.7. Just half of the edge beam was modelled because of symmetry conditions being applied on the left boundary. Auxiliary nodes, where the springs defined in Section 4.2.3.4 were attached, were set as fully fixed.

Reinforcement nodes were constrained to have the same displacement in z-direction as its surrounding concrete nodes. The displacement in y-direction was restrained at the end nodes of the each bar. In this way, the model simulates the behaviour of an uncracked edge beam region between two fully open cracks spaced *L* m, where the reinforcement is taking the entire load.

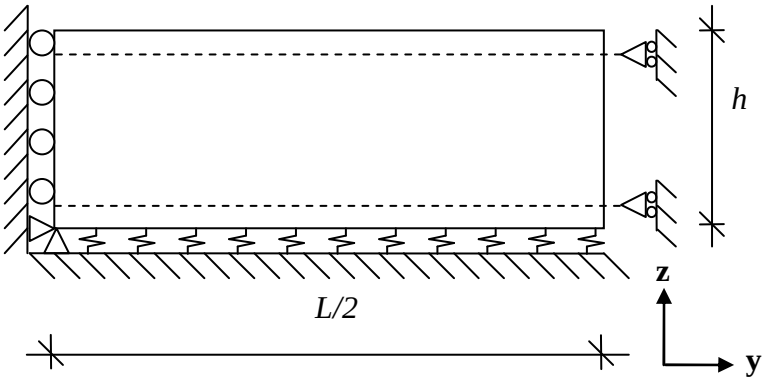

Figure 4.7 Boundary conditions for the edge beam with continuous edge restraint.

The edge beam was analysed to check effects of shrinkage induced deformations. This was modelled in ADINA by a temperature decrease acting on the whole model. Since no shrinkage strain develops in steel, the coefficient for thermal expansion, α_{sT}, was set to zero for the steel material. A total temperature decrease of ΔT=100 °C was applied during the analysis, corresponding to a final shrinkage strain of ε_{cs}=1.00 ‰, which is about three to four times higher than what would be expected.

4.2.5 Mesh

The concrete specimen was modelled with 2D solid plane stress elements that define a 2D surface with a thickness of 0.4 m for the reference case. The concrete elements for the reference case were meshed with a right-angled triangular mesh and an element length of l_{el}=0.025 m, see Figure 4.8. Two node pipe elements, with the same element length as used for the concrete elements, were used to model the reinforcing steel.

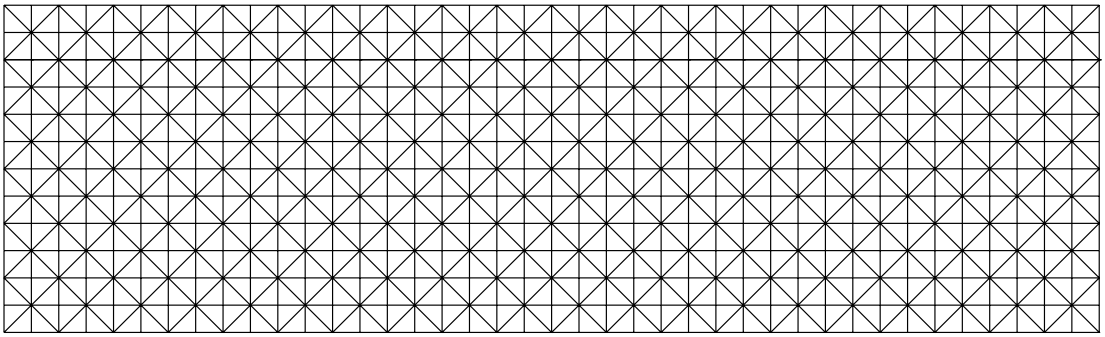

Figure 4.8 Right-angled triangular mesh with element size l_{el} = 25 mm.

4.2.6 Method

The BFGS-Method was used in the analyses. The applied temperature decrease was divided in 1000 steps and, hence, each step corresponded to a negative temperature change of 0.1 °C.

The results concerning crack patterns show the 100% open cracks in the same manner explained in Section 3.3.6. However, when showing results for fracture energies larger than 100 N/m it shall be stated that 100% open cracks does not refer to the actual ultimate strain. In order to get comparable results, the same value of the

ultimate strain as for the reference case (G_f = 100 N/m) was used to define the crack development stages, see Figure 4.9.

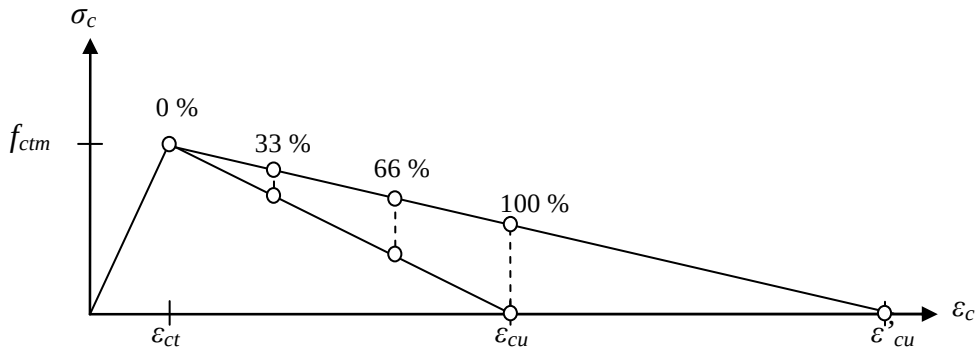

Figure 4.9 Definition of 33 %, 66 % and 100 % open cracks states used during investigations with fracture energies larger than 100 N/m.

In order to show and understand the formation of cracks with increasing shrinkage strain, each crack will in the following sections be numbered referring to the order of appearance in the analyses. This is exemplified in Figure 4.10, where the first crack appears close to the symmetry line, the second crack appears at the middle of the modelled beam and the third and fourth cracks form in the regions between previous cracks and free edges.

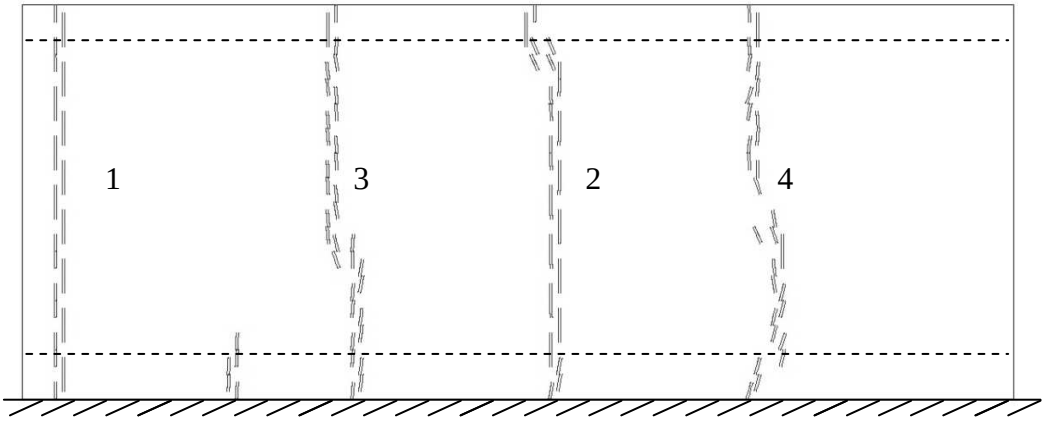

Figure 4.10 Example of crack pattern.

The shrinkage strain needed for each crack to appear will in the following be shown in graphs like the one in Figure 4.11. These figures show approximately the shrinkage strain for which a new fully open crack has developed and this is a clear way to compare the effect of different parameters.

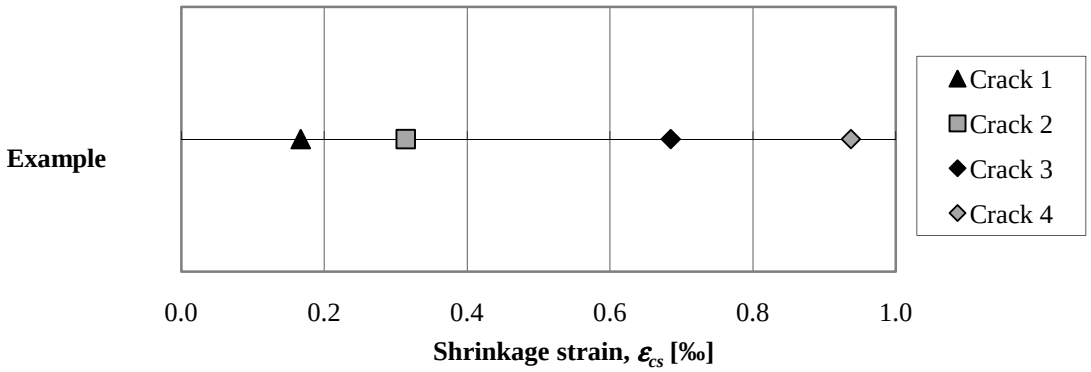

Figure 4.11 Example of graph showing the shrinkage strain at which fully open cracks have developed.

Since the concrete member was subjected to shrinkage strain the crack widths were calculated according to Equation (4.3). The total concrete strain was measured at the top and bottom reinforcement layers and the crack widths at these points were obtained by multiplying the difference between the total concrete strain obtained from ADINA and the applied shrinkage strain times the element length.

$$w = (\varepsilon_{c,tot} - \varepsilon_{cs}) \cdot l_{el} \tag{4.3}$$

In some cases, it can be important to know how the crack widths develop with increasing shrinkage strain. For that reason, and in order to be able to compare the edge beam results with the results obtained by Johansson and Lantz (2009), crack width developments are shown in this chapter as in Figure 4.12. Crack widths have similar values at the top and bottom reinforcement levels and crack width graphs at both levels for each analysis are shown in its respective appendices. However, just crack widths at the bottom reinforcement level are presented in the report, as it was chosen as well by Johansson and Lantz (2009). Crack numbers are related to the order of appearance and they correspond to the numbers shown in the crack pattern figures, shown in Figure 4.10.

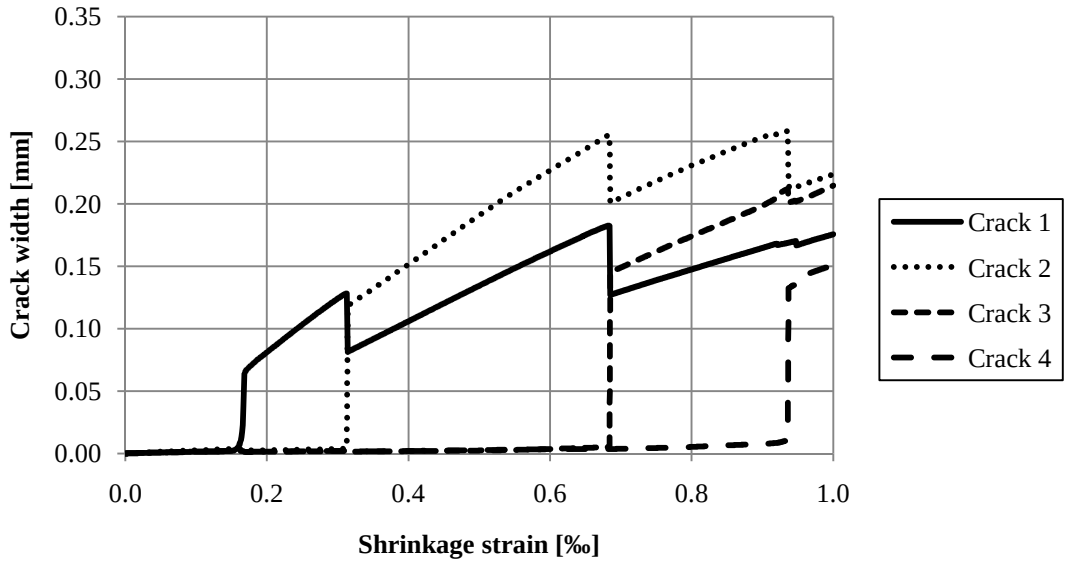

Figure 4.12 Example of graph showing crack width developments with increasing shrinkage strain.

Using the smeared crack approach, the stress-strain relation is given by assuming that cracks will concentrate to one single element row. This assumption is true for most of the cracks. However, in some cases, e.g. the second crack in Figure 4.10 at the top reinforcement level, the crack is smeared over two elements. An iterative process would be needed in order to capture a more realistic behaviour. A new specific stress-strain relation should be given for these elements, where the ultimate strain should be calculated according to Equation (4.4). Cracks obtained with this new stress-strain relation should smear over these two elements where the relation was changed. Otherwise it would be needed to redefine this relation until the cracks concentrate on the same number of elements that they were assumed to while defining the stress-strain relation, Johansson (2000).

$$\varepsilon_{cu} = \frac{w_u}{2 \cdot l_{el}} \tag{4.4}$$

Such an iterative solution with different stress-strain relation for some specific elements is considered to be very time consuming. Therefore, in this thesis project, crack widths due to fully open cracks smeared over more than one element will be treated as one single crack with a crack width contribution from each element, as seen in Equation (4.3).

4.3 Results

4.3.1 Influence of reinforcement configuration

In Johansson and Lantz (2009) ten different reinforcement arrangements were studied. It was concluded that the standard reinforcement, our reference case, is a good enough arrangement concerning restraint forces. This reinforcement case is shown in Figure 4.13 (a) and is henceforth referred to as cross-section 1 (CS1). However, since the bond at the joint interface contributes to the restraint at the bottom, it was also of

interest to study another reinforcement case. In this case one reinforcement bar was moved from the bottom level to the top level. Hence, for this case, hereby denoted cross-section 2 (CS2), there are five bars at the top level and two bars at the bottom level, see Figure 4.13 (b). With this rearrangement the longitudinal reinforcement ratio was kept constant. All results from the analyses on this subject can be found in Appendix C.

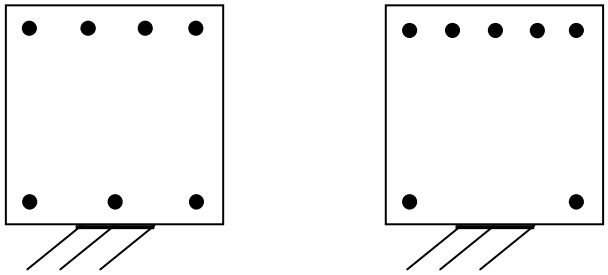

(a) Cross-section 1 (b) Cross-section 2

Figure 4.13 The two different reinforcement arrangements examined.

To compare the two different cases, crack patterns and crack widths were studied. In Figure 4.14 the shrinkage strain needed to create the cracks can be seen. It can be noticed that for cross-section 2 the second crack appeared somewhat earlier. However, both the third and forth cracks were delayed. This makes it possible for the crack width of the first and, particularly, the second crack to increase more than in cross-section 1.

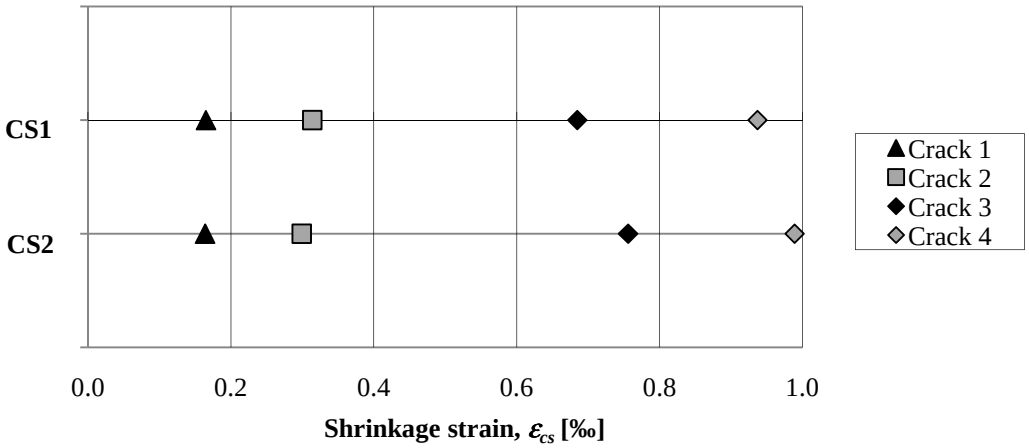

Figure 4.14 Shrinkage strain at which fully open cracks have developed for two different reinforcement arrangements.

The crack patterns for the two cases, presented in Figure 4.15, show some differences. Generally the cracks are straighter for cross-section 2, see Figure 4.15 (b). Furthermore, the small crack in the bottom between cracks 1 and 3 for cross-section 1 does not appear for cross-section 2. This is probably due to the decrease in restraint by the reinforcement in the bottom compared to cross-section 1.

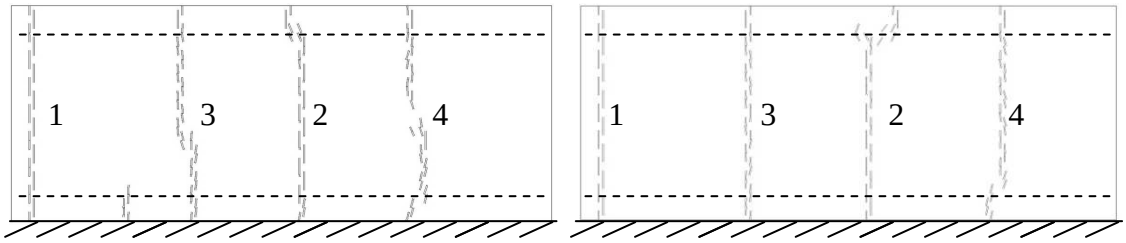

(a) Cross-section 1 (b) Cross-section 2

Figure 4.15 Crack pattern for fully open cracks for (a) cross-section 1 and (b) cross-section 2.

As can be seen in Figure 4.16, when a new crack occurs, crack widths for previous cracks decrease instantaneously and the stiffness is somewhat decreased.

When comparing the crack widths for the two cases, see Figure 4.16 and Figure 4.17, it can be noticed that, in general, crack widths are larger for cross-section 2. A difference can be seen for the second crack especially; this crack width is significantly larger in cross-section 2. Hence, there is a clear effect of the decrease in numbers of bars in the bottom.

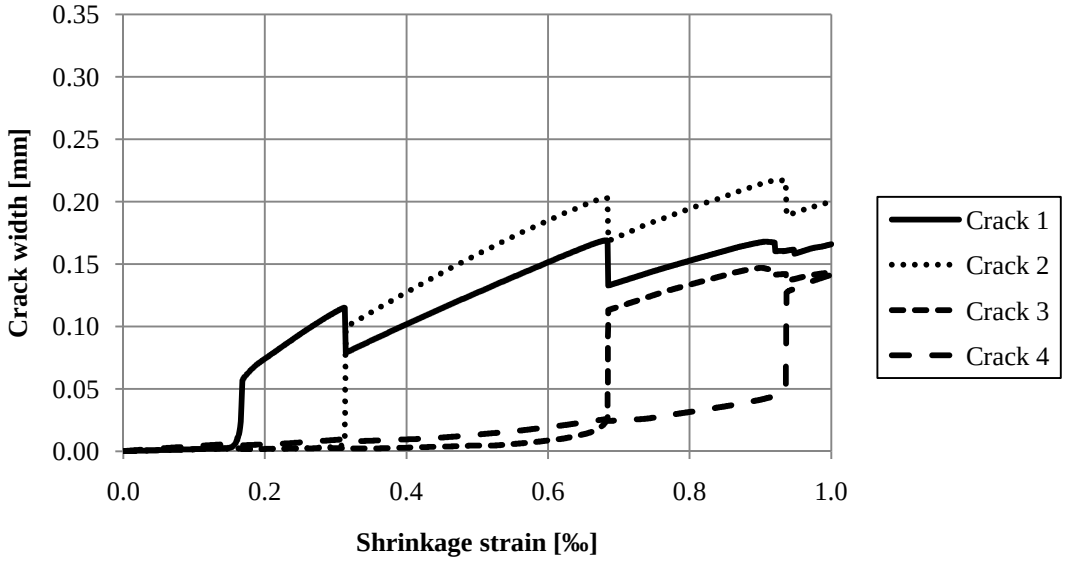

Figure 4.16 Crack width developments at the bottom reinforcement level for cross-section 1.

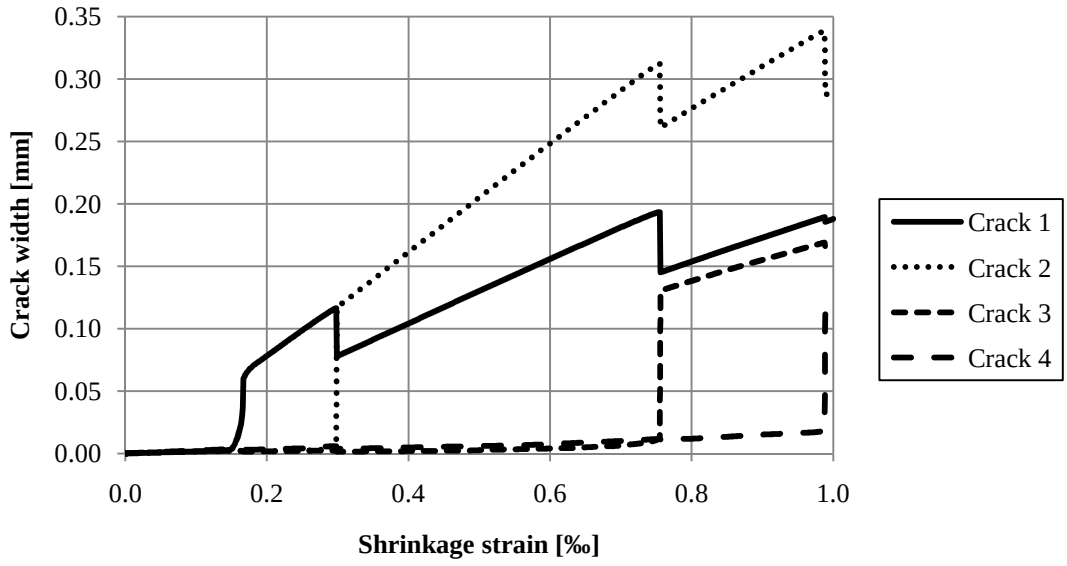

Figure 4.17 Crack width developments at the bottom reinforcement level for cross-section 2.

Since the results of the study above did not show an improved behaviour for the alternative reinforcement configuration (cross-section 2), new analyses were made with an increased transversal reinforcement ratio, ρ_t. By increasing the reinforcement ratio by 100 %, from $\rho_t = 0.6$ % to $\rho_t = 1.2$ %, the total restraint at the bottom was increased, and this could motivate rearranging the main reinforcement bars.

The shrinkage strain for which the cracks for the two different transversal reinforcement ratios appeared is shown in Figure 4.18. The effect of increasing the transversal reinforcement ratio is seen to be earlier cracking, especially for the forth crack. There is also a pretty clear difference when comparing the appearance of the third and second crack for cross-section 2. However, there is not such a clear effect of transversal reinforcement for the reference reinforcement configuration, where the third crack is an exception and appears at a higher shrinkage strain. The first crack appears almost at the same shrinkage strain for all cases.

Comparing different reinforcement configurations with higher transversal reinforcement ratio shows an improved behaviour for cross-section 2, as its latter cracks appear at lower shrinkage strains than for the reference case.

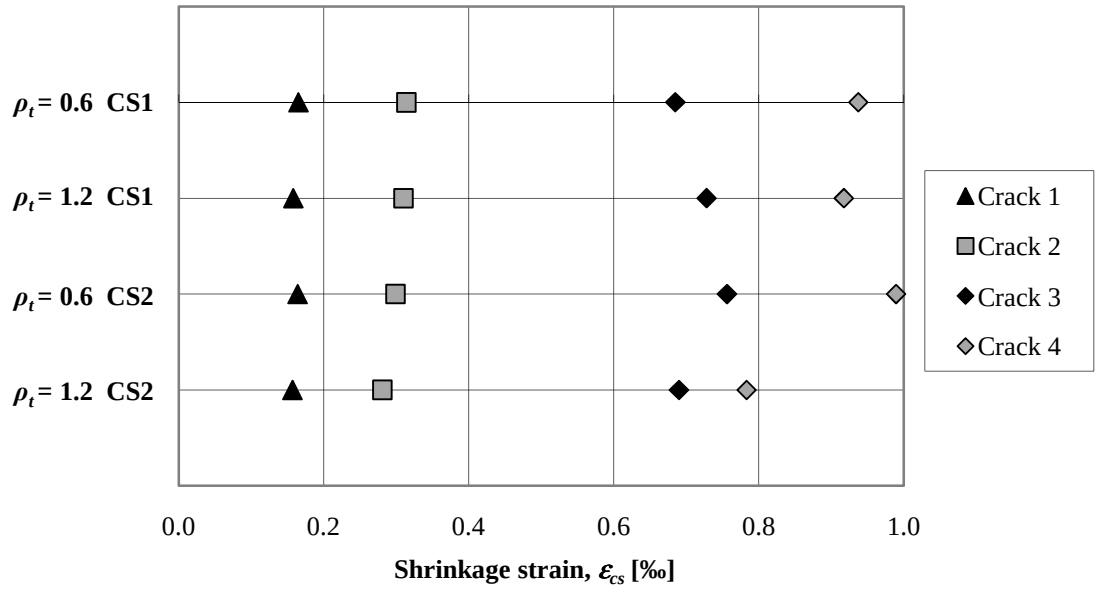

Figure 4.18 Shrinkage strains at which fully open cracks have developed for different reinforcement configurations and different transversal reinforcement ratios.

When analysing the crack pattern for cross-section 2, it can be seen that, by increasing the transversal reinforcement ratio to ρ_t = 1.2 %, a small crack has appeared in the bottom between cracks 1 and 3, seen in Figure 4.19 (d). This, together with the fact that the third crack is less straight with less transversal reinforcement make the crack pattern for ρ_t = 1.2 % more similar to the reference case, see Figure 4.15 (a) and (c). This indicates that the increased transversal reinforcement ratio, hence increased restraint, leads to an improved behaviour.

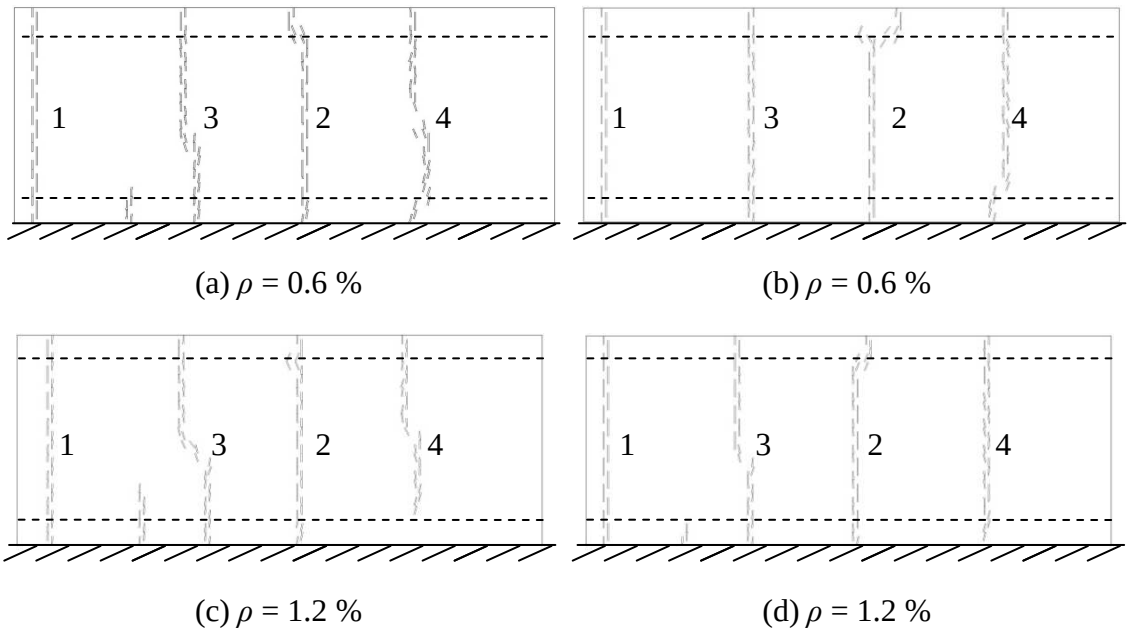

Figure 4.19 Crack patterns at ε_{cs} = 1 ‰ of fully open cracks for cross-section 1, (a) (c), and for cross-section 2, (b) (d), for different transversal reinforcement ratios.

By increasing the transversal reinforcement ratio for cross-section 2, the crack widths generally decreased to some extent. When comparing Figure 4.17 and Figure 4.21 it can be seen that the third and, especially, the forth crack appeared for a smaller shrinkage strain for the case of ρ_t = 1.2 %; something that keeps the crack widths at a lower level.

However, when increasing the transversal reinforcement ratio, crack widths are still smaller for cross-section 1, even when a third or fourth crack has appeared in cross-section 2 but not for cross-section 1. The reason for this might be that in cross-section 2 the deformation is more concentrated into the second crack than in cross-section-1, where the widths are more distributed between all cracks.

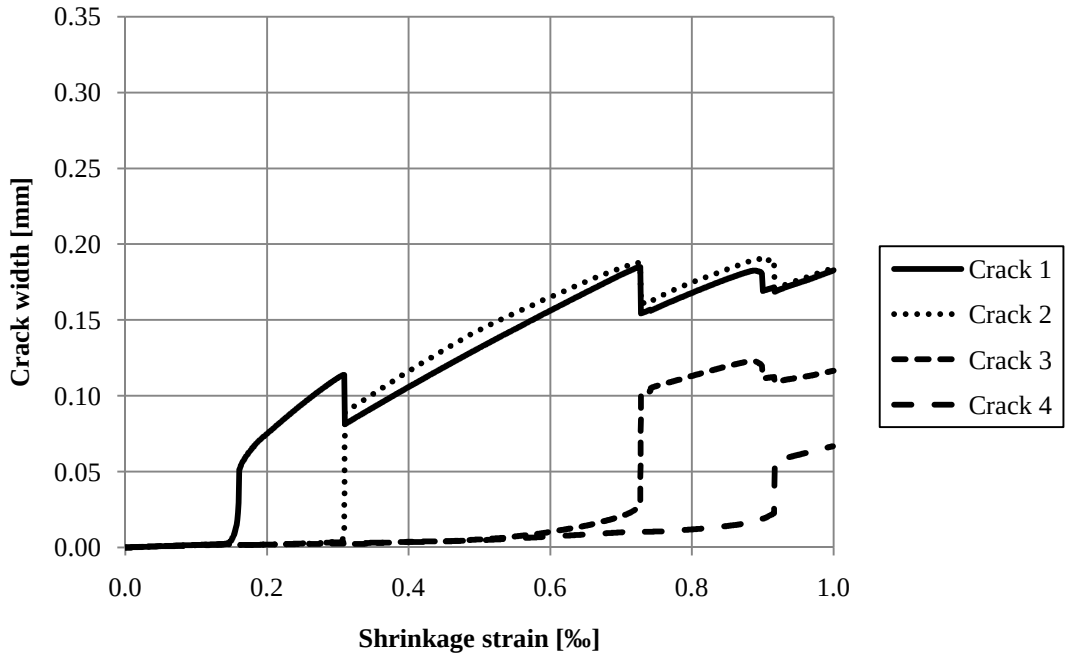

Figure 4.20 Crack width developments at the bottom reinforcement level for cross-section 1 with a transversal reinforcement ratio of ρ_t=1.2 %.

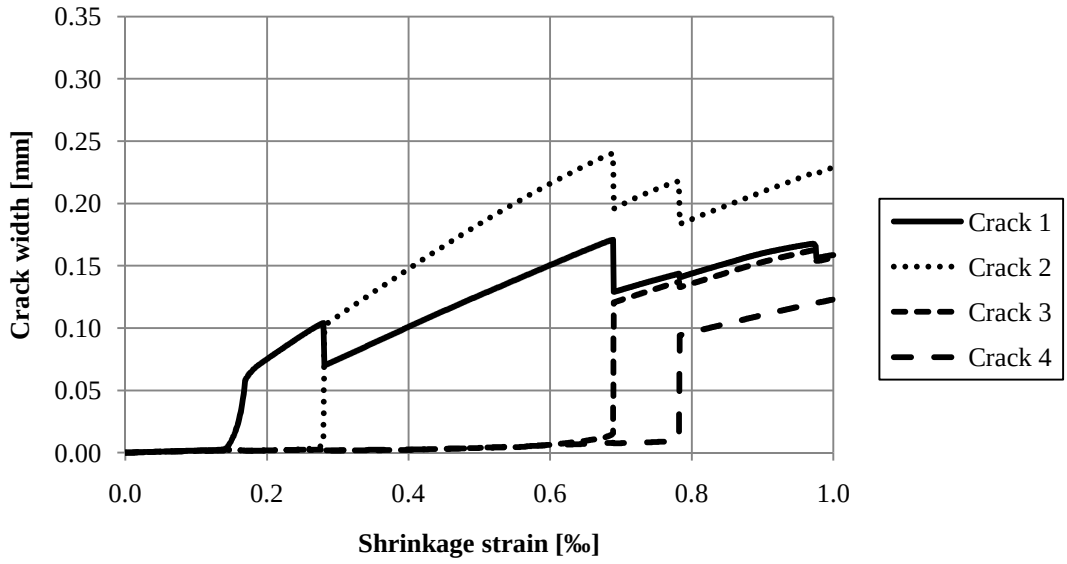

Figure 4.21 Crack width developments at the bottom reinforcement level for cross-section 2 with a transversal reinforcement ratio of ρ_t=1.2 %.

4.3.2 Influence of bar diameter

In order to study the influence of an increase in the bond force between the reinforcement and the surrounding concrete, analyses with different bar diameters were performed on the reference case. All results from these analyses are presented in Appendix D. While changing the bar diameters, the longitudinal reinforcement ratio was approximately kept constant. Hence, a decrease in bar diameter results in an increase of the number of bars. Apart from the bar diameter used in the reference case, 16 mm, three different bar diameters were investigated. The three other bar diameters were 12, 10 and 8 mm and the number of bars used in analysis of these four cases is presented in Table 4.2.

Table 4.2 Number of bars in the top and bottom for the four different bar diameters studied.

Bar diameter [mm]	Number of bars in the top	Number of bars in the bottom
8	16	12
10	10	8
12	7	5
16	4	3

In Figure 4.22 the shrinkage strain for which cracks appeared are shown for different bar diameters. From the figure it can be noticed that the general behaviour was a delayed cracking with increasing bar diameter, i.e. decreased bond force. However, the third crack for the case with a bar diameter of 12 mm is an exception.

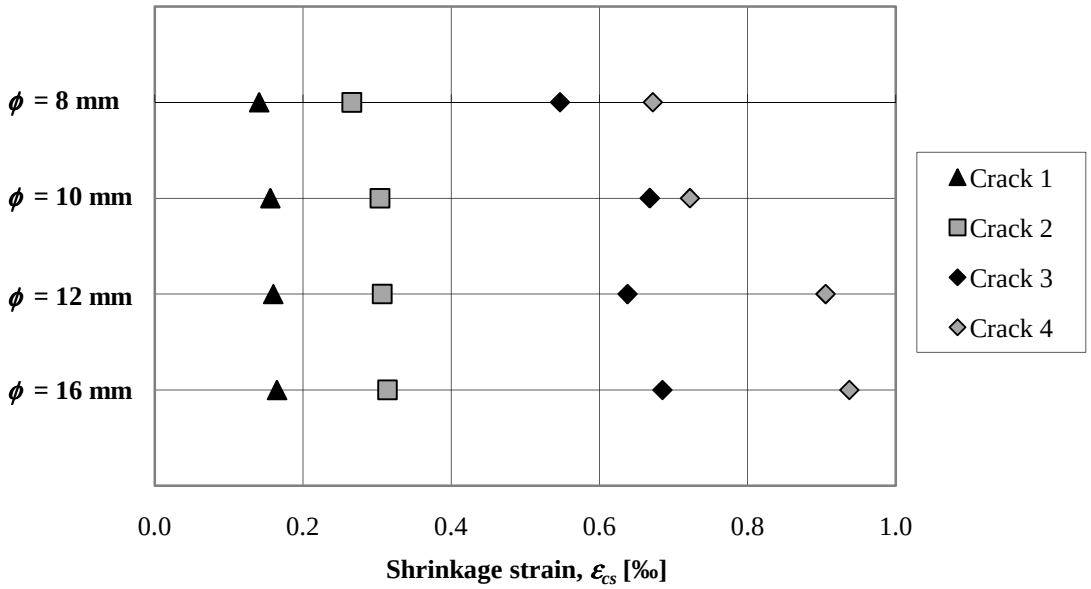

Figure 4.22 Shrinkage strains at which fully open cracks have developed for different bar diameters.

Reinforcement configurations with different bar diameters from 10 to 16 mm showed similar behaviour for the development of the second crack, which had the largest crack width for every case, see Figure 4.23. Even though the third crack appeared at different shrinkage strains, the crack widths were almost of the same magnitude. The case with bar diameter of 8 mm, on the other hand, showed lower crack widths than the other cases. This can partly be explained by earlier appearance of the second crack and theoretically, one can conclude that 8 mm bars show the best effect. However, due to the large number of ϕ 8 bars needed, in practice they can be excluded due to difficulties and extra work during construction. Since there are only small differences between the other three cases, it was concluded that 16 mm bars are the best option.

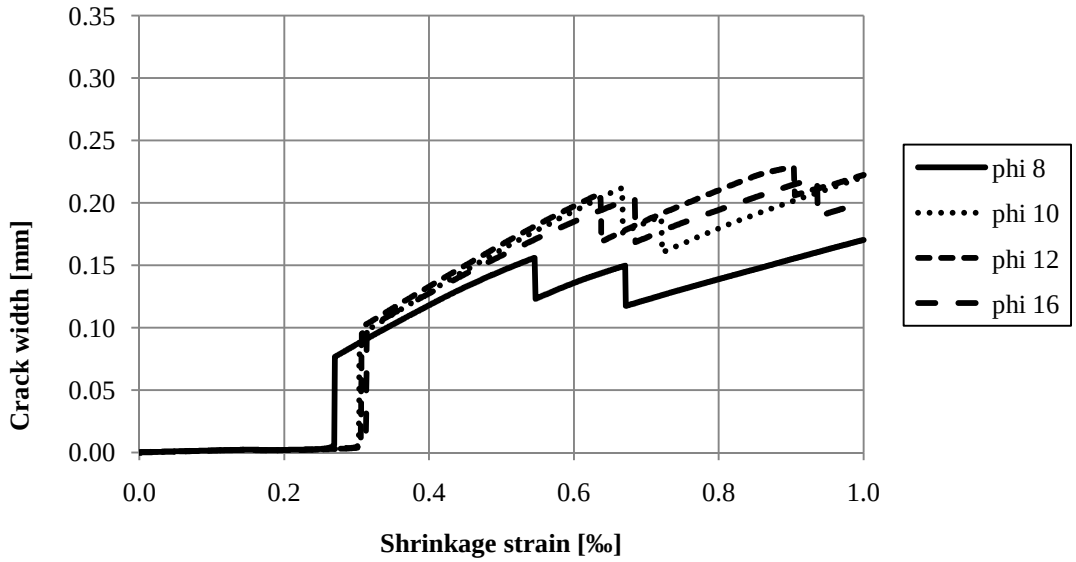

Figure 4.23 Comparison of development of the width of the second crack at the bottom reinforcement level for different bar diameters.

4.3.3 Influence of thickness of the concrete cover

For the reference case the reinforcement bars were placed at a distance from the edges to the centre of the reinforcement layers of 50 mm. The effect of increasing the concrete cover was studied by increasing this distance, a_s, see Figure 4.24. Results from these analyses are shown in Appendix E. The actual values of the concrete cover are half bar diameter lower than values presented in this section. Analyses to check the effect of location of reinforcement were carried out for larger values of a_s than the reference case. Smaller values were not considered as they may lead to durability problems. The distance from the edges to the reinforcement bars was increased stepwise with 50 mm for both reinforcement layers from 50 mm to a limit case of 200 mm. For this maximum value both layers merge into one at half height of the cross-section.

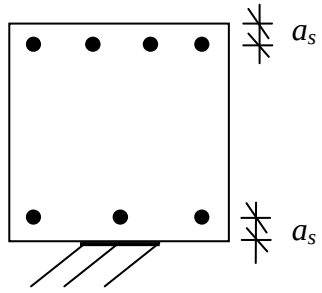

Figure 4.24 Definition of distances from the edges to the reinforcement layers, a_s.

Increasing the thickness of the concrete cover made the third crack appearing at a lower shrinkage strain, but it had a not such a clear effect on the fourth crack, see Figure 4.25. The first and second cracks appeared more or less for the same shrinkage strain for each concrete cover studied.

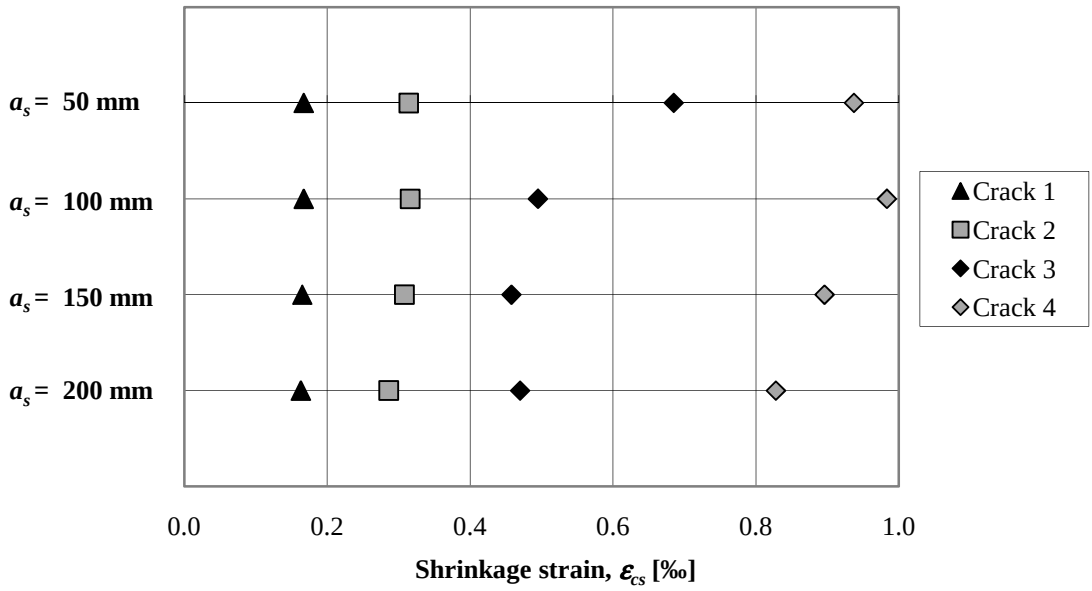

Figure 4.25 Shrinkage strains at which fully open cracks have developed for different values of a_s.

When looking at the crack patterns, it can be stated that when a_s was small, the cracks tended to bend in the big unreinforced area between the reinforcement layers, see Figure 4.26 (a). If the concrete cover was larger, some cracks developed just grow towards one edge; i.e. from the bottom to the top edge, see Figure 4.26 (c) and (d). More straight cracks were obtained for a more evenly distributed location of reinforcement; see Figure 4.26 (b). Almost perfectly straight cracks were formed independently of how the restraint degree varied across the cross-section.

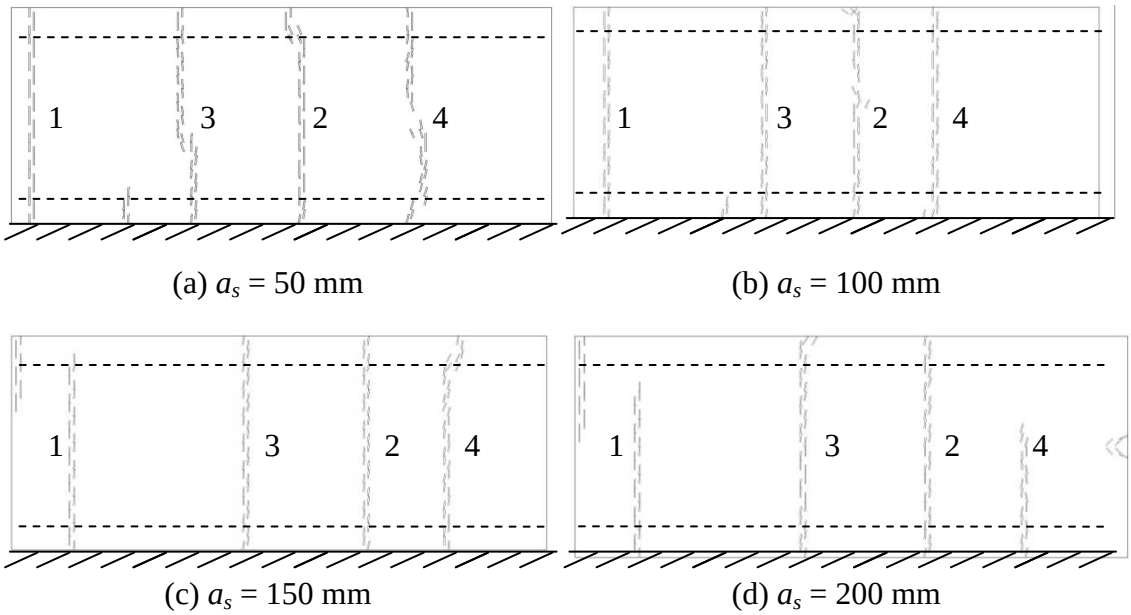

(a) a_s = 50 mm (b) a_s = 100 mm

(c) a_s = 150 mm (d) a_s = 200 mm

Figure 4.26 Crack patterns at ε_{cs}=1 ‰ for fully open cracks for different concrete values of a_s.

The crack widths were for all cases evaluated at a distance of 50 mm from both edges in order to be comparable with each other. It was also assumed that the two first cracks to the left in Figure 4.26 (c) and (d) behave as one single crack, as they appeared for the same shrinkage strain and their crack openings complement each other. Therefore, the crack width was calculated by adding them together.

The crack widths for the first crack from analyses of different values of a_s are presented in Figure 4.27. For certain shrinkage strain intervals, the crack widths were smaller for larger values of a_s than for the reference case. Since, for certain strain intervals, crack widths are lower for larger values of a_s than for the reference case, where even one more crack than for the reference case had appeared, no clear conclusion can be drawn from Figure 4.27. For the same number of cracks along the beam, however, the crack widths were smaller in the reference case. It would be of interest to do the same kind of analysis for longer edge beams where more cracks can form. Then the effect of more cracks appearing earlier could reduce crack widths to a larger extent for thicker concrete covers.

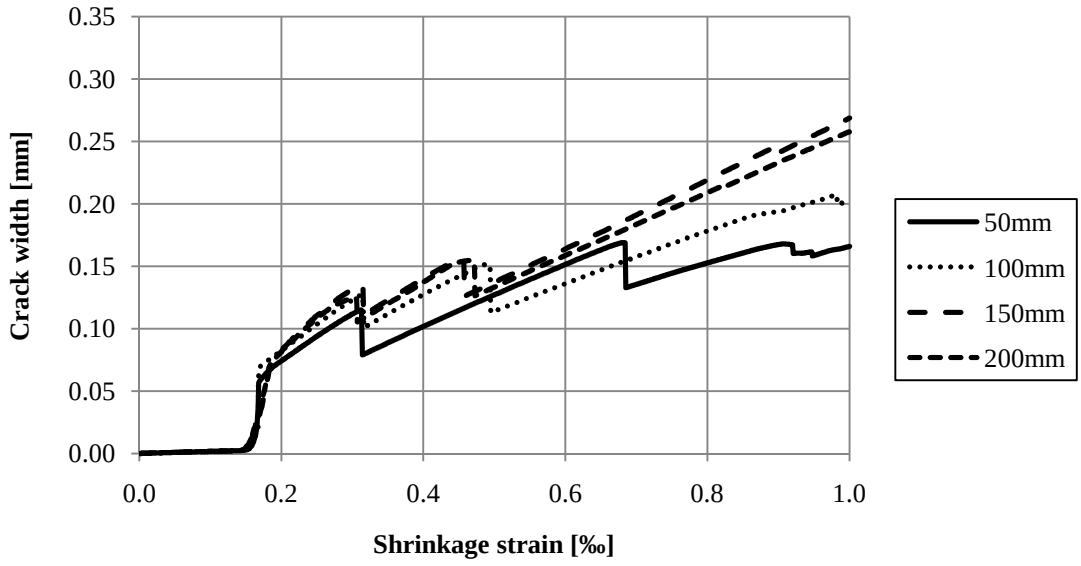

Figure 4.27 Comparison of width developments of the first crack for different values of a_s, determined at 50 mm from the bottom concrete edge.

4.3.4 Influence of fracture energy

One of the main effects of adding fibre reinforcement to concrete is that the fracture energy, G_f, increases. Because of that, it was of interest to perform a parametric study, concerning just the single influence of fracture energy on crack patterns and crack widths of concrete members with ordinary reinforcement. A variation of the fracture energy was obtained by varying the ξ value in Equation (4.5). Analyses were performed for four different values of the fracture energy; G_f = [100, 250, 375, 500] N/m. All results from these analyses can be seen in Appendix F.

According to the results of our analyses, see Figure 4.28, the main effect of increasing the fracture energy was a delayed and slower development of cracks. Even though the same shrinkage strain is needed to initiate cracking in the member, higher values of strain were needed to concentrate into one visible crack when the fracture energy is increased. Hence, more shrinkage was also needed to develop a crack zone into a fully developed crack, i.e. crack that is not any more able to transfer stresses, and less fully developed cracks formed, compare G_f = 100 N/m and 250 N/m in Figure 4.28. As a result of reducing the number of fully developed cracks, crack widths were increased for increased fracture energy. However, for even larger fracture energies, see G_f = 375 and 500 N/m in Figure 4.28, it was not possible for cracks to fully develop. In these situations, cracks at lower stages of development with less spacing were created, which helped to keep crack widths at a low value. However, if the shrinkage strain would had been large enough to develop at least one of those cracks to a fully developed crack, it would have concentrated all the deformation and become too large.

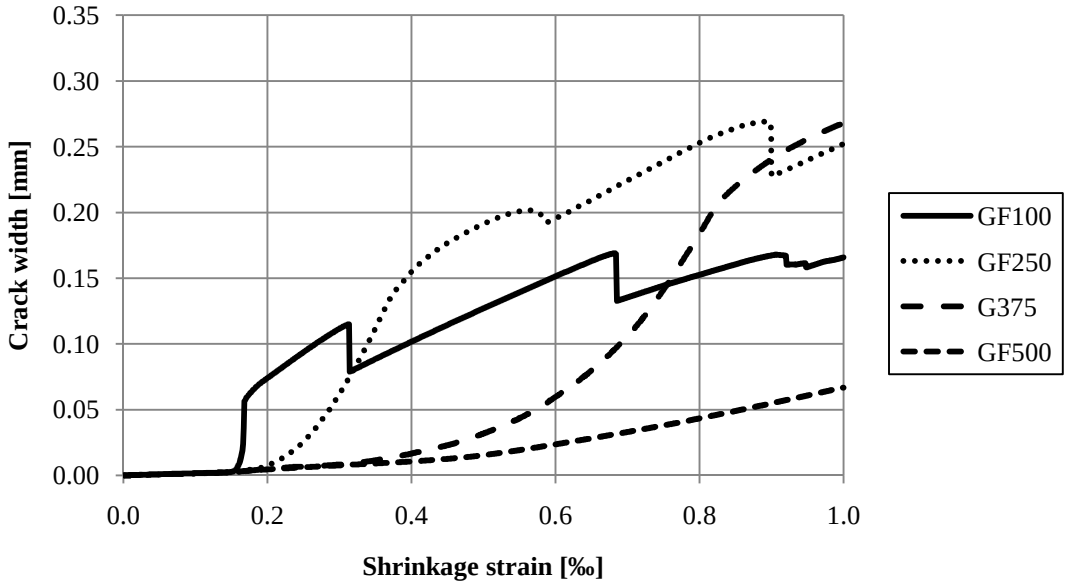

Figure 4.28 Comparison of width developments of the first crack at the bottom reinforcement level for different fracture energies.

The effect of creating more cracks at earlier states of development when the fracture energy is increased can be observed in Figure 4.29 (b) and (e), where more cracks were formed for a fracture energy of G_f = 500 N/m. However, these cracks were not fully developed, not even those shown in Figure 4.29 (f), as it was explained when defining the concept of 100 % open cracks for concrete with different fracture energies in Figure 4.9. For the reference case almost no cracks remain at an intermediate stage, except the fully developed ones, compare Figure 4.29 (a), (b) and (c).

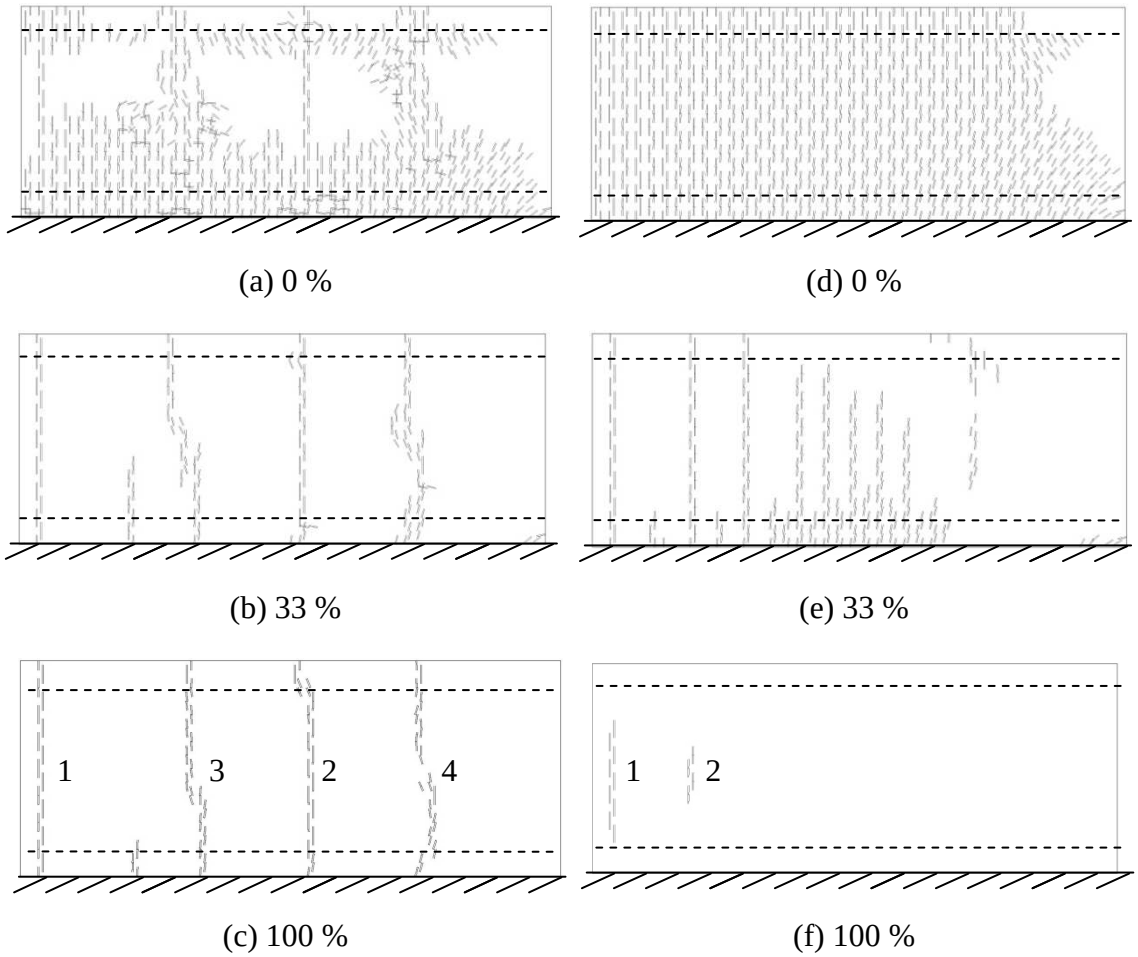

Figure 4.29 Crack pattern at ε_{cs} = 1 ‰ for 0 %, 33 % and 100 % open cracks for (a), (b), (c) with G_f = 100 N/m and (d), (e), (f) with G_f = 500 N/m.

4.3.5 Influence of fibre reinforcement

A possible application of adding fibre reinforcement to reduce crack widths was studied by using the heterogeneous material approach presented in Section 3.4.2. As it was discussed in Section 0, this does not necessarily correspond to any specific fibre dosage, but will help to understand the behaviour of fibre reinforced concrete and its applicability to concrete structures subjected to restraint forces. Results from analyses of edge beams when including fibre reinforcement are shown in Appendix G.

More and earlier cracks were formed when fibre reinforcement was added to the analysed edge beam. Fibre reinforced concrete is able to transfer large tensile stresses after through cracks have formed and then new cracks can be initiated for a small increase of the shrinkage strain. This is clearly seen in Figure 4.30, where the first crack was formed at the same shrinkage strain for cases but the second crack appeared much earlier for the fibre reinforced case. All cracks were developed at lower shrinkage strains and also a fifth crack was formed in the edge beam with fibre reinforcement, see Figure 4.31. Since tensile stresses are transferred through the cracks, the transmission length was decreased and therefore, cracks could appear closer to each other.

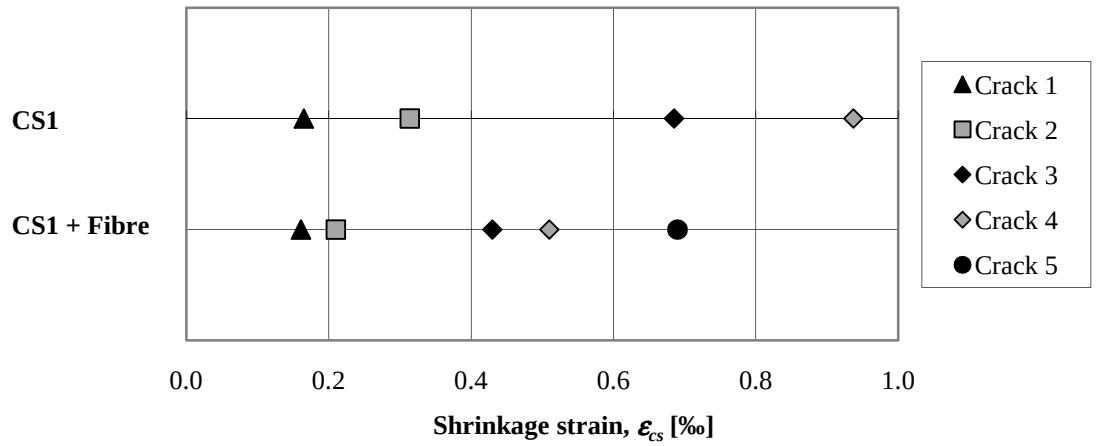

Figure 4.30 Shrinkage strain for which 100 % open cracks start to develop for edge beams with cross-section 1 with ordinary and fibre reinforcement.

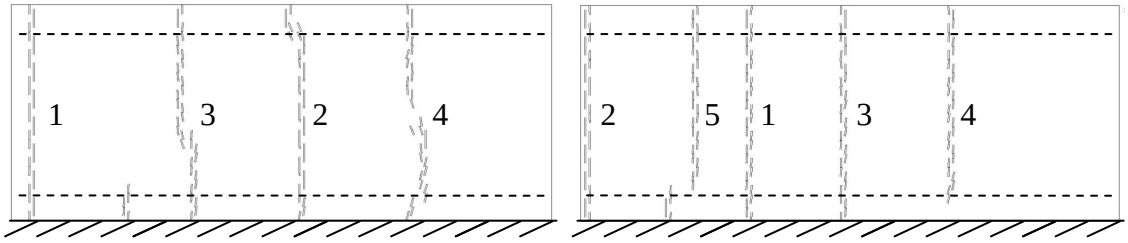

(a) Edge beam with ordinary reinforcement

(b) Edge beam with ordinary and fibre reinforcement

Figure 4.31 Crack patterns of 100 % open cracks at ε_{cs} = 1 ‰ for edge beams with cross-section 1 with ordinary and fibre reinforcement.

The crack widths were reduced significantly, when adding fibre reinforcement to the concrete, compare Figure 4.16 and Figure 4.32. It was also observed that cracks did not develop all of a sudden and that they had a more ductile behaviour. This was expected from the results shown in Section 4.3.4, as the same behaviour was obtained for materials with high fracture energy.

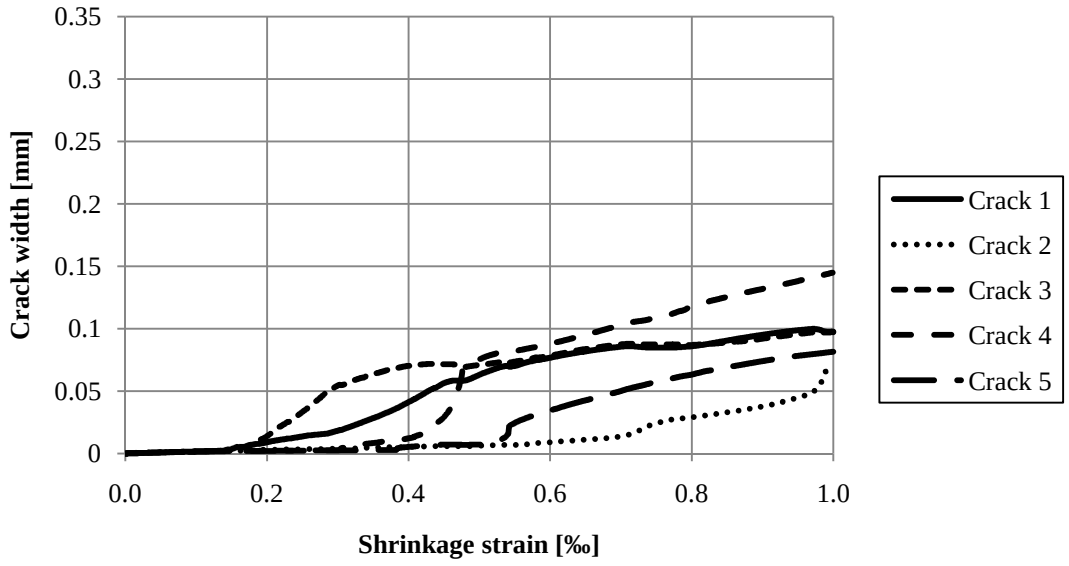

Figure 4.32 Crack widths at the bottom reinforcement level for fibre reinforced concrete with cross-section 1.

New analyses were carried out on edge beams without ordinary reinforcement bars in order to check the need of ordinary reinforcement when using fibre reinforcement. This unreinforced cross-section is referred to as cross-section 0 (CS0). More and earlier cracks were also obtained when using fibre reinforcement for this cross-section; see Figure 4.33. One additional straight crack appeared in the edge beam, but also more distributed cracks are formed close to the free end, see Figure 4.34.

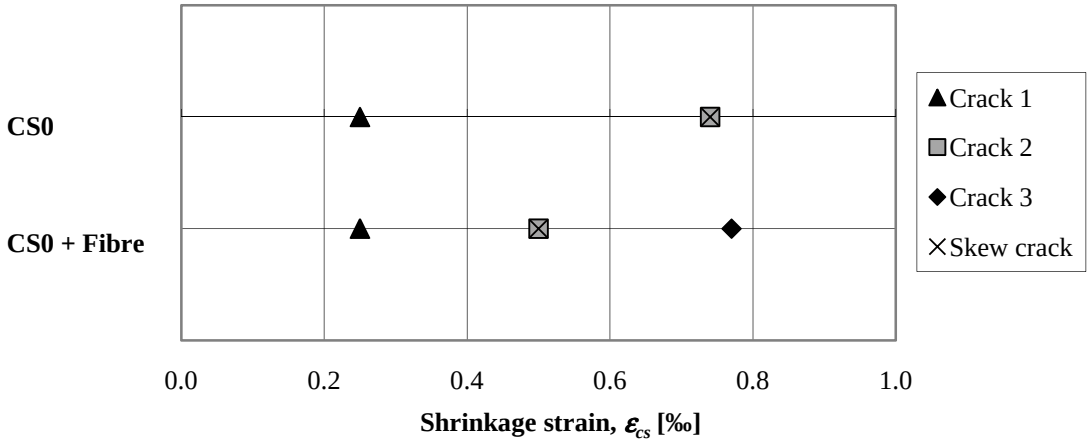

Figure 4.33 Shrinkage strain for which 100 % open cracks start to develop for the edge beam with cross-section 0, with or without fibre reinforcement.

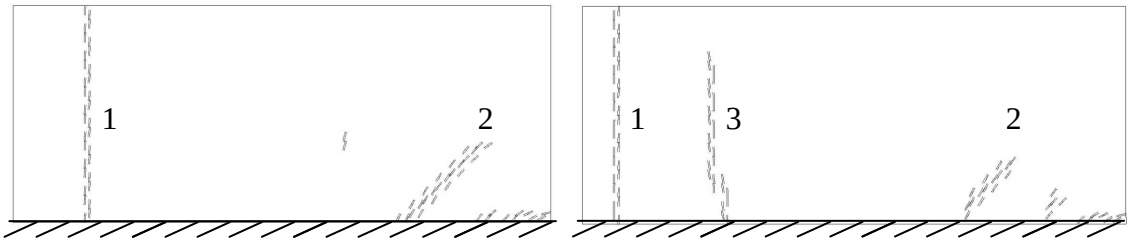

(a) Ordinary concrete (b) Fibre reinforced concrete

Figure 4.34 Crack pattern of 100 % open cracks for edge beam with cross-section 0, with or without fibre reinforcement.

When studying the crack width of the only through crack that was formed for both plain and fibre reinforced concrete, it is clearly seen that the crack width was reduced to almost half when fibre reinforcement was provided, see Figure 4.35. This effect is more apparent at a level close to the restrained edge, where more cracks not developing through the entire height have appeared in the case with fibre reinforcement. However, ordinary reinforcement may still be needed to force the cracks to develop through the whole cross-section and to control the crack widths at the top face.

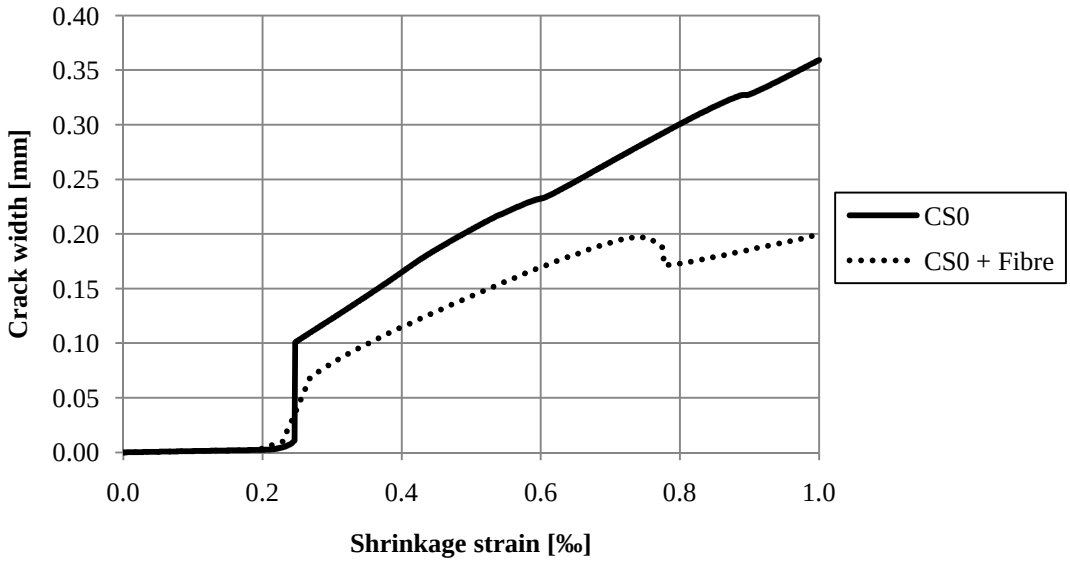

Figure 4.35 Crack widths 50 mm above joint interface for plain and fibre reinforced concrete.

4.3.6 Influence of concrete creep

The effect of creep was also studied, but in a simplified way. In Nesset and Skoglund (2007), influence of creep was studied analytically. They concluded that with creep the first cracking was delayed, i.e. more shrinkage was needed, but the crack widths increased compared to corresponding cases without creep. This observation was found interesting to be further checked by finite element analysis.

The effect of creep was considered by defining effective values of Young's modulus with different creep coefficients according to Equation (4.10). Due to limitations in ADINA the creep coefficient could not be added as a function of time, which would have resembled the influence of creep in a better manner. The investigation only considered a reduced value of Young's modulus that was constant with varying shrinkage strain, which is not reasonable in a real situation.

$$E_{c,ef} = \frac{E_{cm}}{1 + \varphi_i} \tag{4.10}$$

Two different values of the creep coefficient were chosen, $\varphi = 1$, $\varphi = 2$ and these cases were compared with the reference case, which did not include any effect of creep, $\varphi = 0$. All results from finite element analyses are presented in Appendix H.

When studying the effect of creep on at which shrinkage strain cracks appeared, see Figure 4.36, it can be seen that all cracks were delayed with increased value of the creep coefficient. For the cases with $\varphi = 1$ and $\varphi = 2$ a forth crack never developed, despite the fact that the analysis was expanded to a decrease in temperature of 200 °C, which resembles a shrinkage strain of 2.0 ‰. Since the cracking was delayed to a large extent, this was done in order to be able to study the full effect of creep.

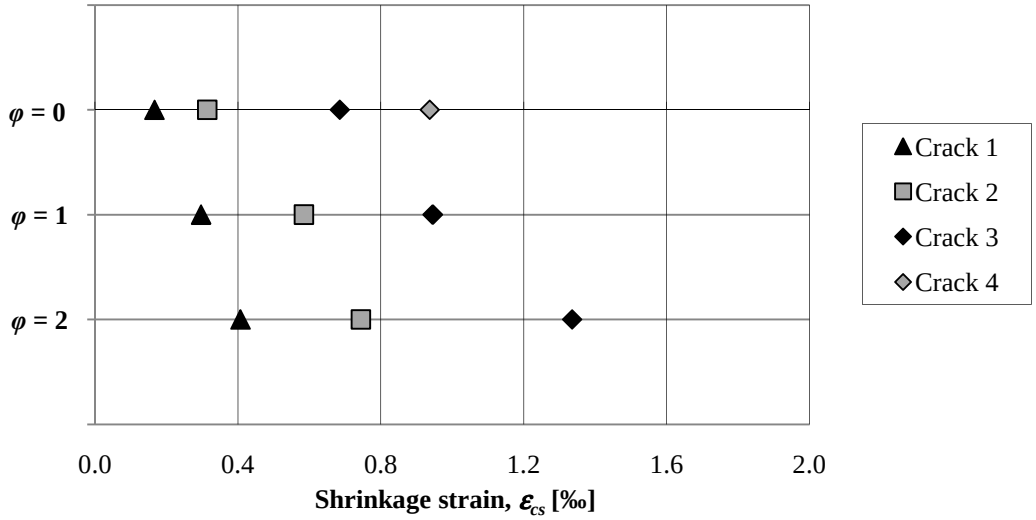

Figure 4.36 Shrinkage strains at which fully open cracks start to develop for different values of the creep coefficient.

A comparison of crack width developments of the first crack for these three cases is shown in Figure 4.37. It is clearly seen that the crack formation was delayed and the crack width development was slower when the creep coefficient was increased. Therefore, fewer cracks were formed, and accordingly the crack widths were markedly increased.

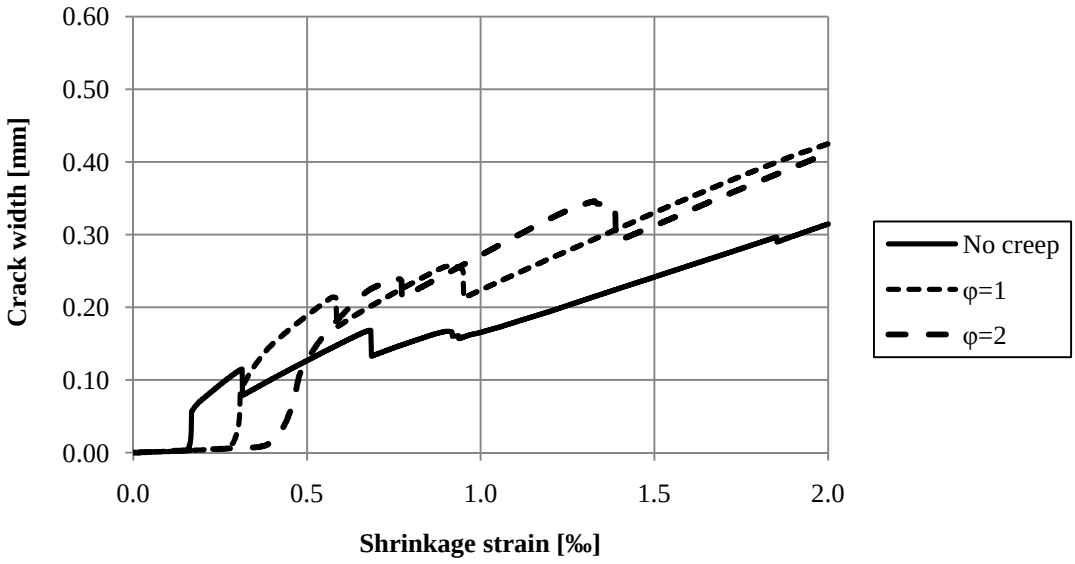

Figure 4.37 Comparison of crack width development of the first crack at the bottom reinforcement level for different values of the creep coefficient.

4.4 Concluding remarks

Finite element analysis carried out on edge beams have shown that the standard reinforcement case, i.e. four bars in the top and three at the bottom, was the best reinforcement arrangement concerning crack widths for the two different transversal reinforcement ratios studied. Doubling the continuous edge restraint is therefore not a reason to change the arrangement of the longitudinal reinforcement bars.

Concerning the diameter of the reinforcement bars, when the longitudinal reinforcement ratio was kept constant, the use of 8 mm bars resulted in the lowest crack widths. However, the number of bars needed is then four times larger than when using 16 mm bars, in which case the behaviour did not differ much from using 10 and 12 mm bars. Therefore, using 16 mm bars is considered as the best option for real application, as it will decrease the difficulties when placing reinforcement at the construction site.

When the concrete cover was increased, cracks appeared at lower shrinkage strains, but through cracks were not always developed and could concentrate towards just one surface. Therefore crack widths could be larger close to the surfaces.

A clear effect of increasing the fracture energy of concrete was the delay of crack development. Fully developed cracks were formed at larger shrinkage strains and cracks became wider. However, if the fracture energy was large enough, no fully developed cracks occurred and smaller and closer cracks formed instead.

With fibre reinforcement the crack widths decreased significantly. Large stresses were transferred through the cracks, the transmission length was reduced and more cracks were able to form. However, if ordinary reinforcement is not used at all it may not be sufficient to control cracks widths across the height of the cross-section. Use of fibre reinforcement together with a lower number of reinforcing bars may therefore be a way to achieve the desired resistance of the structure and control the crack widths

below an allowable value in aggressive environments, and then, the durability of the structure can be increased.

Due to the creep effect the concrete could withstand larger shrinkage strains before each new crack was formed. Hence, this lead to fewer cracks for this short member, but those that developed became larger. However, the concept of having a constant creep factor for restrained shrinkage is not a realistic assumption.

5 Non-linear FE analyses of concrete retaining walls with continuous edge restraint

5.1 Introduction

This chapter presents analyses of a wall with continuous edge restraint, shown schematically in Figure 5.1, subjected to shrinkage strain. The walls investigated in this thesis resemble concrete retaining walls in bridge and road constructions. When a retaining wall is cast against an already mature concrete foundation slab, the behaviour will be similar to an edge beam cast against an already existing bridge deck. There will be different thermal and shrinkage strains in the two members and the wall may crack due to the need of movement in combination with of the continuous restraint.

Non-linear finite element analyses were performed to investigate the influence of different reinforcement arrangements and geometries, as well as the influence of fibre reinforcement.

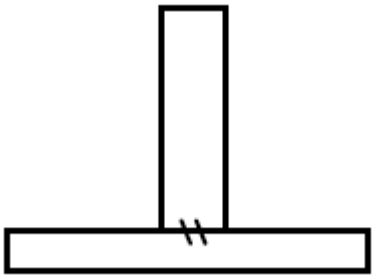

Figure 5.1 Concrete wall cast against a concrete foundation slab.

5.2 FE-model

5.2.1 Introduction

Since the wall in many ways resembles the edge beam, the FE-model of the wall was created based on the model of the edge beam. However, some differences needs to be explained and are presented here.

5.2.2 Geometry

The reference geometry of the wall was chosen to a length L = 6 m and a height of h = 2.9 m. However, analyses with different heights of the wall, according to Figure 5.2, were also performed. The heights of the wall were chosen to correspond approximately to different ratios between length and height; 1:1, 2:1 and 4:1. The wall heights where also chosen to be able to arrange the reinforcement in a suitable manner. Hence, some heights do not exactly correspond to the given length/height ratio.

Analyses were carried out without reinforcement as well as with different reinforcement arrangements, see Figure 5.2. In all reinforcement cases the

reinforcement bars were uniformly distributed over the entire height of the wall with a spacing of s = 200 mm.

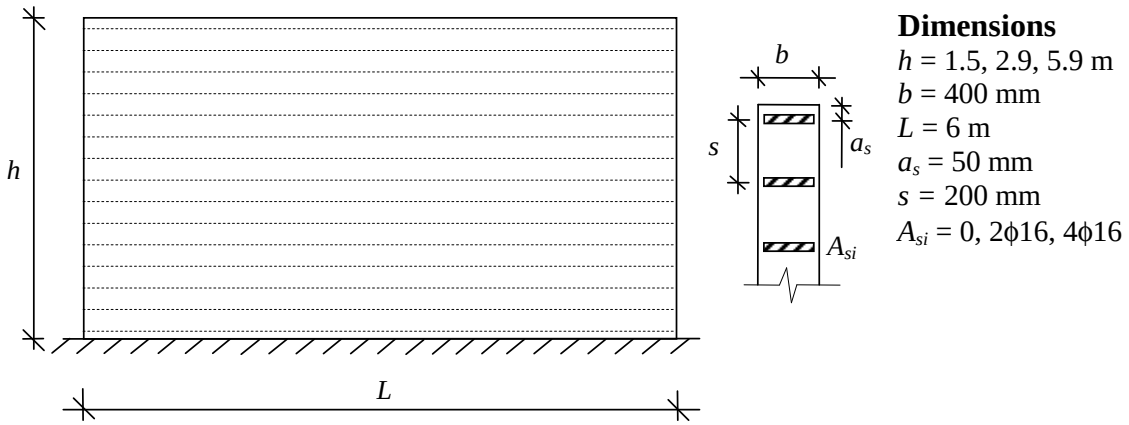

Figure 5.2 Geometry of the wall and schematic positioning of reinforcement.

5.2.3 Material model

The material models used for analysis of the wall was the same as the one described in Section 4.2.3. Walls including the behaviour of fibre reinforced concrete were modelled as described in Section 3.4.2.

5.2.4 Boundary conditions and load

The boundary conditions for the wall are described in Figure 5.3. Different from the modelling of the edge beam, for this application the whole wall was modelled. Thus, no symmetry line was used in these analyses. Furthermore, the reinforcement bars are not restrained at their edges, compare to Section 4.2.4. Apart from this the boundary conditions and the load are defined as in Section 4.2.4.

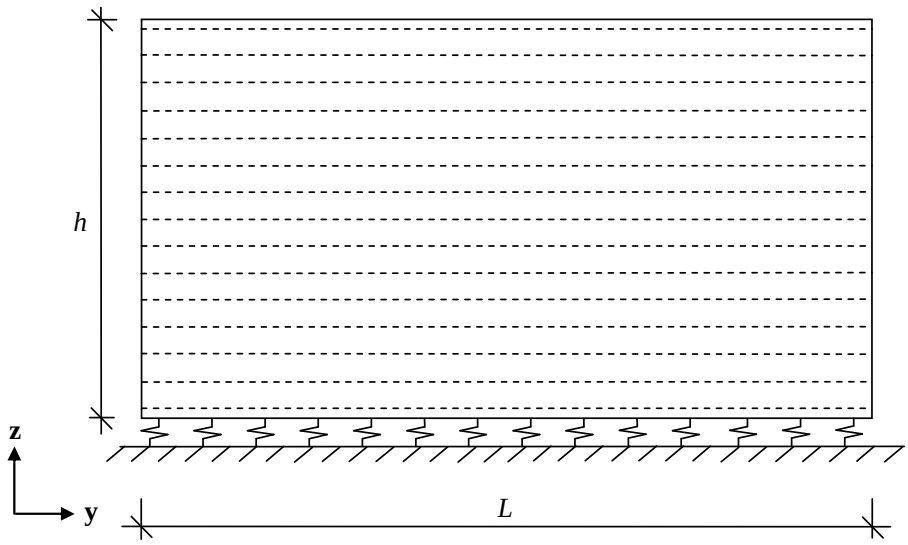

Figure 5.3 Boundary conditions for the retaining wall.

5.2.5 Mesh

The element length was chosen to l_{el} = 50 mm. Otherwise the mesh was created in the same way as described in Section 3.3.5.

5.2.6 Method

The same iteration method, the BFGS-method, as described in Section 3.3.6 was used.

The results in this chapter are presented by figures showing the crack patterns and the crack widths. The crack patterns are presented in figures in the same way as for the edge beam, described previously in Section 4.2.6. The cracks considered in these figures show 100 % open cracks, as explained in Section 3.3.6.

The crack widths in concrete structures subjected to shrinkage strain are calculated as described in Section 4.2.6. In this chapter the crack widths are plotted against the length of the wall at the final step of the analyses, ε_{cs} = 1.00 ‰, see example in Figure 5.4. This way of illustrating the crack widths was considered to be a clearer way for this application since many of the analyses resulted in a large number of cracks, compared to the case with edge beams.

Some of the analyses were stopped at an earlier shrinkage strain due to convergence problems. For these analyses the crack width are shown for the last reliable load step of the analysis. However, crack widths are shown for the end of the analysis, if nothing else is stated.

It should be noticed that this way of presenting the crack widths contains some inaccuracies concerning skew cracks. Since skew cracks also have a contribution from strains in the vertical direction, the crack widths shown for skew cracks are not always true. However, crack widths for vertical cracks are accurate and are the ones of largest interest concerning crack widths.

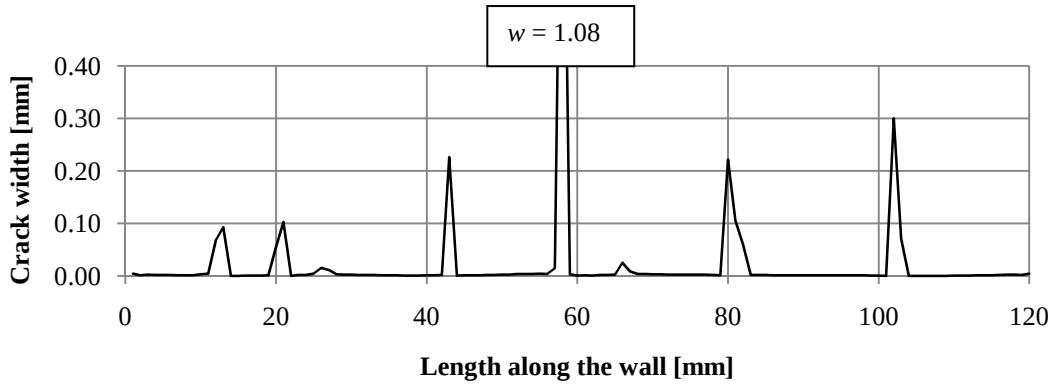

Figure 5.4 Example of graph showing crack widths for the analysed walls.

To make it easier to compare the different results, crack widths are only shown up to a width of 0.40 mm. Values of 0.40 mm and above are considered as undesirable. However, cracks with a width larger than this are still of interest in this study and the maximum crack widths for those cracks are presented as shown in Figure 5.4.

Crack widths in this chapter are presented and compared for different heights of the walls. Mainly three different levels are considered. The level of the bottom layer of reinforcement was chosen as one of these levels to be able to see the influence of the

edge restraint. This level is located 50 mm from the bottom edge and is in this chapter referred to as “level 1”. The other two levels were chosen to the fourth and sixth layer of reinforcement, since the maximum crack width was found at one of these two levels for all reinforcement and geometry cases. These levels are located 650 mm and 1050 mm from the bottom edge, respectively, and are in this chapter referred to as “level 4” and “level 6”, see Figure 5.5.

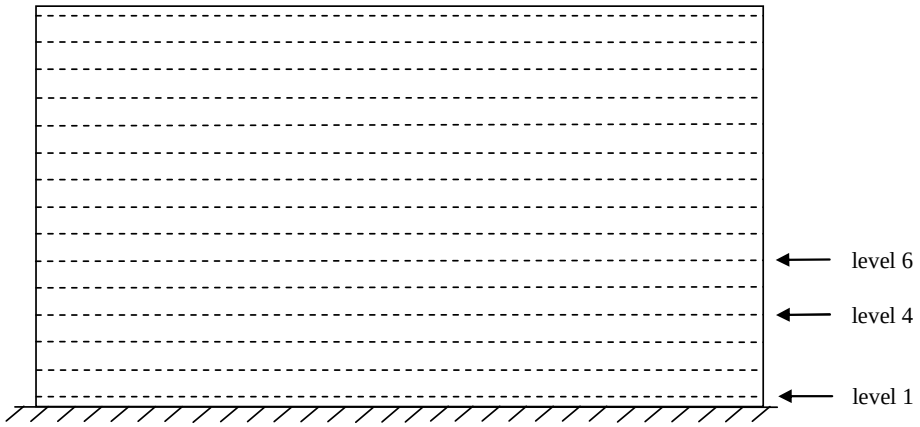

Figure 5.5 Levels for which crack widths are presented in this chapter.

5.3 Results

5.3.1 Influence of reinforcement amount and arrangement

In order to investigate how the amount of reinforcement influence a wall with continuous edge restraint subjected to shrinkage, three different reinforcement arrangements were studied. These cross-sections can be seen in Figure 5.6. A cross-section without reinforcement, cross-section 0, was analysed as a reference. Two reinforcement arrangements were analysed. Cross-section 1, Figure 5.6 (b), is provided with 2ϕ16 mm bars in 15 layers with a spacing of s = 200 mm, resulting in a reinforcement ratio of ρ_l = 0.5 %. This arrangement of reinforcement corresponds to the minimum amount of reinforcement according to Eurocode 2, CEN (2004). Cross-section 2, Figure 5.6 (c), is provided with the double reinforcement amount compared to cross-section 1. This reinforcement is arranged by adding 2ϕ16 mm bars in each layer, resulting in 4ϕ16 mm bars in 15 layers with a spacing of s = 200 mm, which resembles a reinforcement ratio of ρ_l = 1.0 %. All analyses in this section were performed on walls with the reference geometry, 6 x 2.9 m. In this section, only selected parts of the results are presented. All results from these analyses are presented in Appendix I.

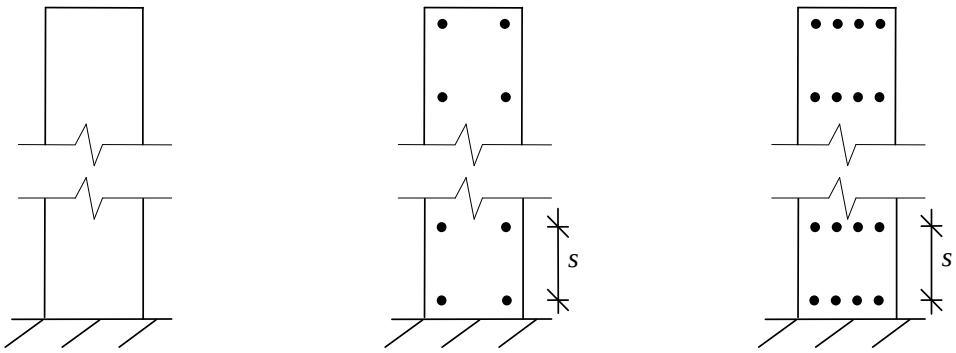

(a) Cross-section 0 (b) Cross-section 1 (c) Cross-section 2

Figure 5.6 The three different cross-sections analysed; (a) plain concrete, (b) minimum reinforcement, (c) doubled reinforcement.

The results concerning the crack patterns for cross-section 0, 1 and 2 are shown in Figure 5.7, Figure 5.8 and Figure 5.9 respectively. The general behaviour that can be seen is that there is one or several vertical cracks in the middle of the wall, while skew cracks appear towards the free edges. When comparing the crack patterns for cross-section 0 and cross-section 2, the main difference is the number of cracks. It can be noticed that while providing reinforcement or increasing the reinforcement amount, the number of cracks increased. The cracks also developed to larger heights while providing reinforcement or increasing the reinforcement amount.

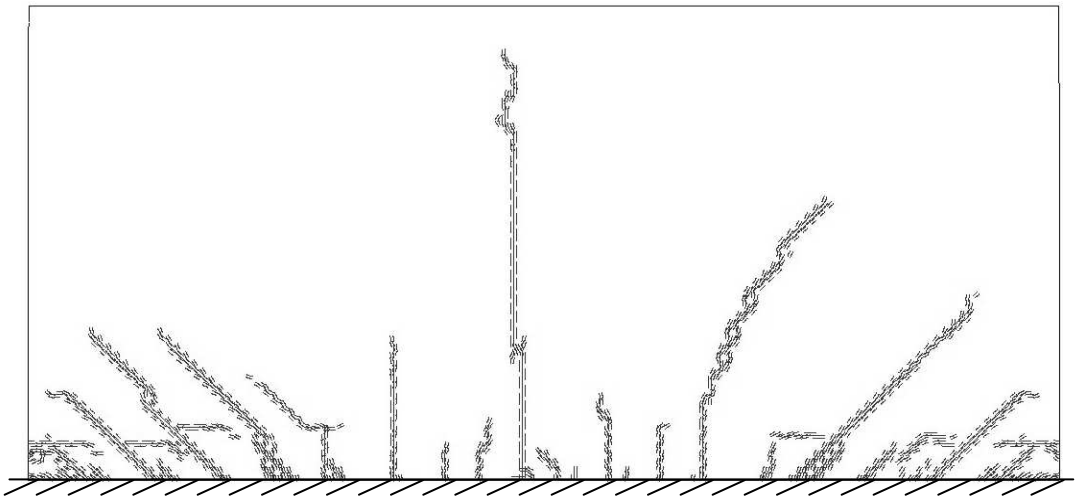

Figure 5.7 Crack pattern for cross-section 0 at shrinkage strain ε_{cs} = 1.00 ‰.

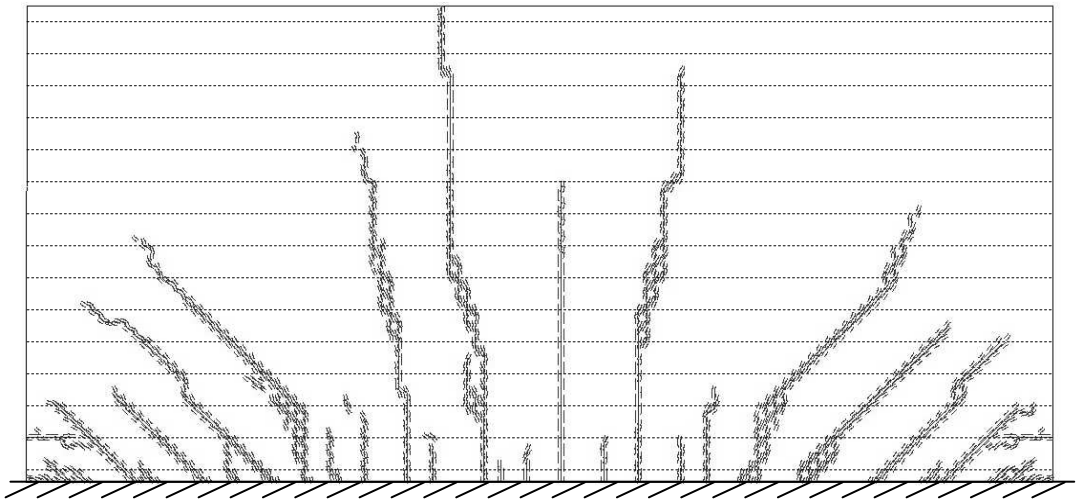

Figure 5.8 Crack pattern for cross-section 1 at shrinkage strain ε_{cs} = 1.00 ‰.

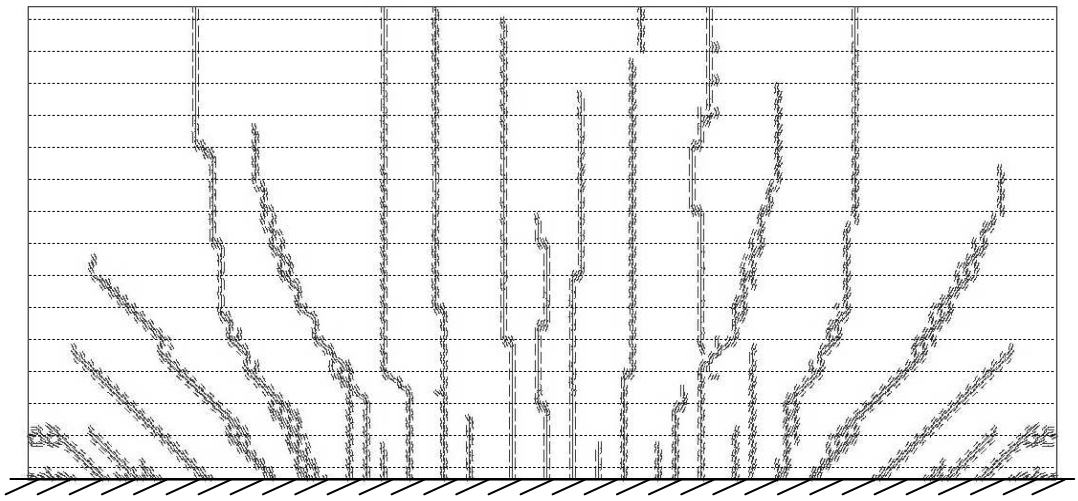

Figure 5.9 Crack pattern for cross-section 2 at shrinkage strain ε_{cs} = 1.00 ‰.

Figure 5.10 to Figure 5.12 show the crack widths at level 4, the level where the maximum crack widths were found. When comparing these figures it can be concluded that while adding reinforcement the crack widths were considerably decreased. The maximum crack width decreased from 1.08 mm to 0.42 mm when

providing reinforcement according to cross-section 1. By doubling the reinforcement amount the maximum crack width decreased further to a value of 0.24 mm. Of these, only the latter value can be considered a sufficiently small crack width when comparing to the limits given in Section 2.5.

Furthermore, it can be seen that the number of cracks increase at level 4 when reinforcement was provided and when the steel area was increased. This behaviour can be explained by the increase in bond force between the reinforcement bars and the concrete.

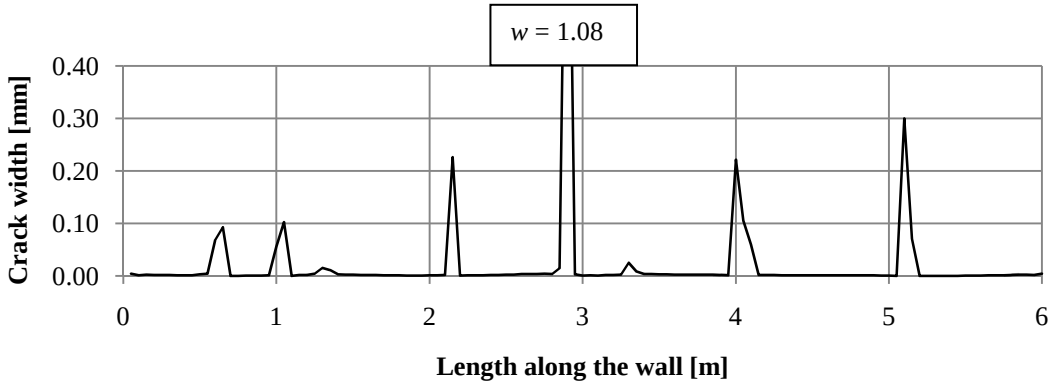

Figure 5.10 Crack widths for cross-section 0 at level 4 at shrinkage strain ε_{cs} = 1.00 ‰.

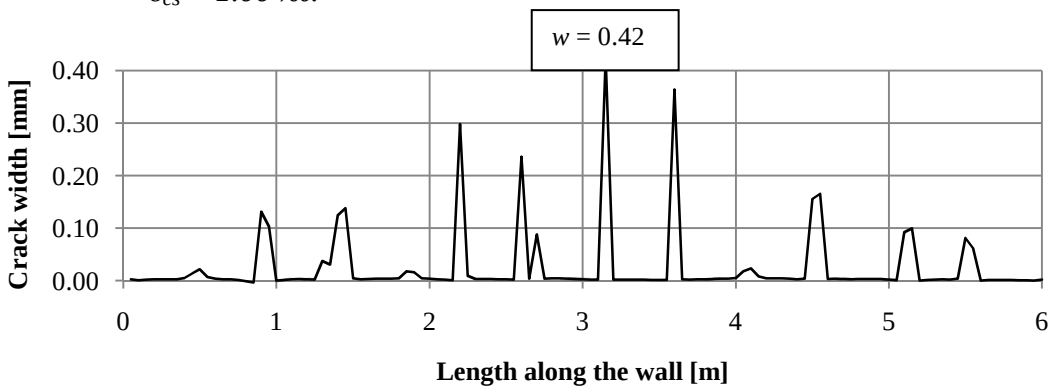

Figure 5.11 Crack widths for cross-section 1 at level 4 at shrinkage strain ε_{cs} = 1.00 ‰.

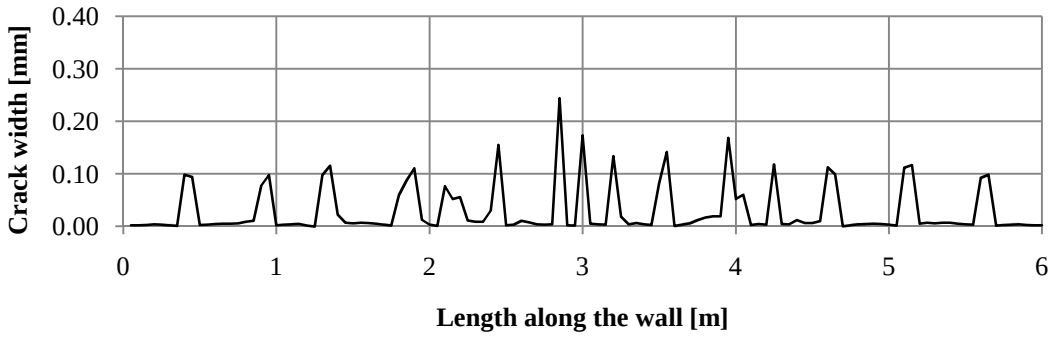

Figure 5.12 Crack widths for cross-section 2 at level 4 at shrinkage strain ε_{cs} = 1.00 ‰.

Studying the crack widths at level 1, see Figure 5.13 to Figure 5.15, it can be seen that they are generally significantly smaller than at level 4. The cause of this is the boundary condition present at the bottom edge. Restraint forces are created at the joint interface between the wall and the slab, acting as an external restraint, resulting in a larger amount of cracks.

Furthermore, the crack widths also at level 1 decreased when providing reinforcement. However, the decrease at this level was not as large as at level 4. By adding reinforcement the maximum crack width decreased from 0.36 mm to 0.26 mm and by doubling the reinforcement amount it decreased further to 0.18 mm. If comparing the maximum crack widths for the wall with plain concrete to the wall with cross-section 2, there is a difference of 50%, while the corresponding decrease at level 4 is almost 70%.

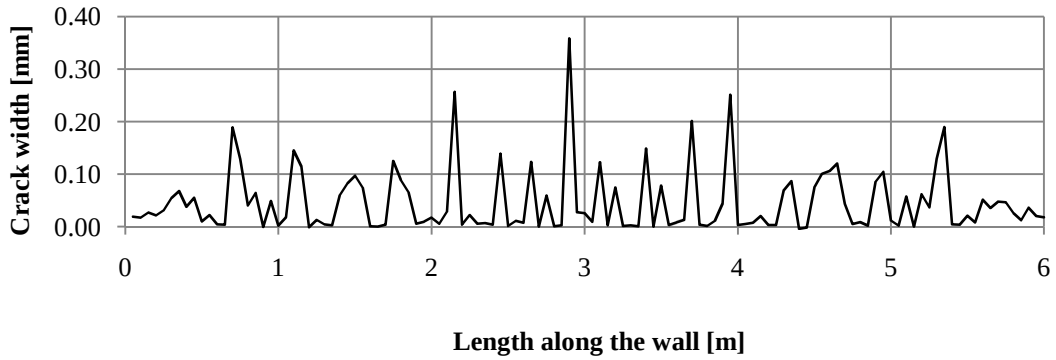

Figure 5.13 Crack widths for cross-section 0 at level 1 at shrinkage strain ε_{cs} = 1.00 ‰.

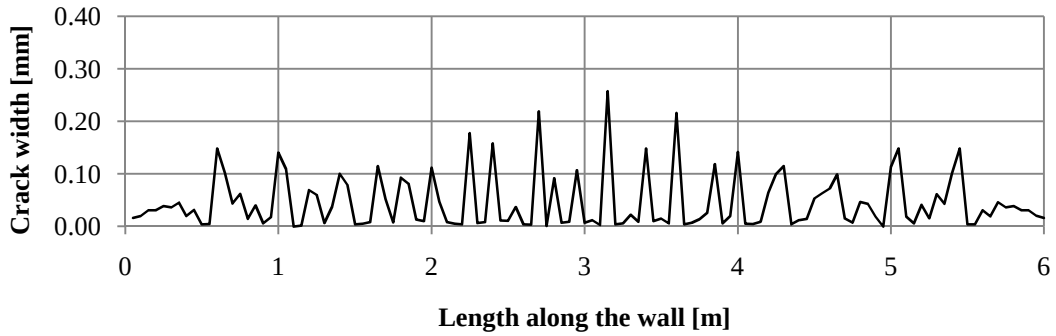

Figure 5.14 Crack widths for cross-section 1 at level 1 at shrinkage strain ε_{cs} = 1.00 ‰.

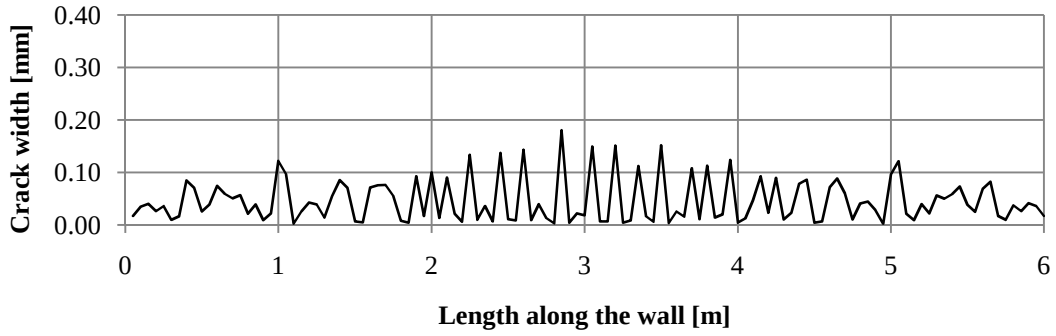

Figure 5.15 Crack widths for cross-section 2 at level 1 at shrinkage strain ε_{cs} = 1.00 ‰.

It can be observed that the restraint from the boundary condition at the bottom edge had a significant effect on the crack pattern. The presence of reinforcement bars at this level had the effect that more restraint forces were created and more cracks appeared. It can be stated that even though the bottom restraint helps keeping the cracks at a lower level, reinforcement is still needed to decrease the crack widths sufficiently.

Cross-section 1 showed somewhat large crack widths at certain levels, while cross-section 2 showed sufficiently small crack widths. The latter, however, showed a very large number of cracks and even through cracks. Due to this it was of interest to study an alternative reinforcement arrangement. A new cross-section, cross-section 3, was

introduced to see if a improved behaviour could be reached by doubling the reinforcement at three layers in cross-section 1. These three layers were chosen to layer 4 to 6 from the bottom, see Figure 5.16. In that way more reinforcement was provided in the region where the maximum crack widths were found for cross-section 1 and 2.

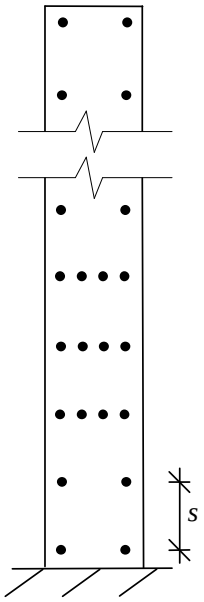

Figure 5.16 Cross-section of the combined reinforcement case, cross-section 3.

Figure 5.17 shows the crack pattern for this reinforcement arrangement. It can be seen that about the same number of cracks was formed as for the case with cross-section 1, previously shown in Figure 5.8. However, the cracks tend to develop to a more even, and intermediate, height than for the wall with cross-section 1, where heights of the cracks varied more.

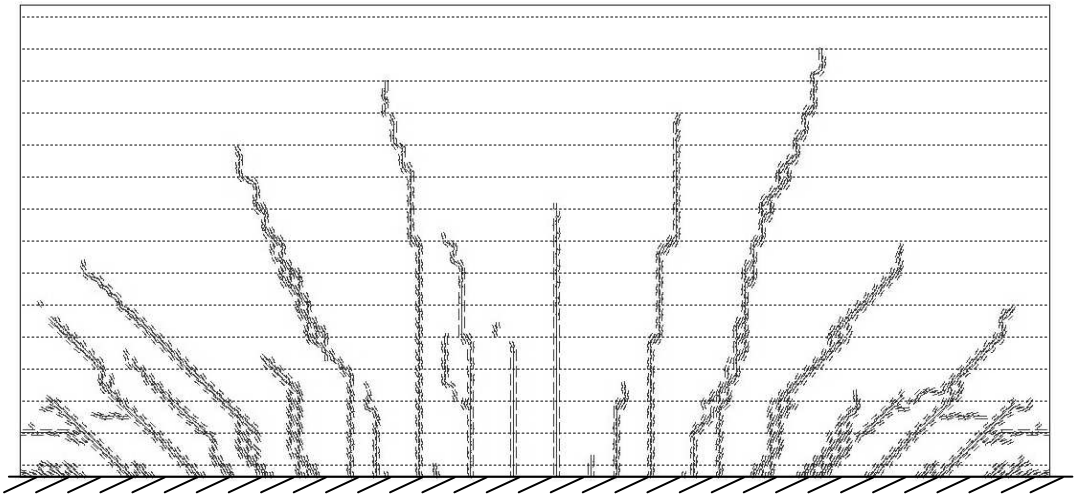

Figure 5.17 Crack pattern for cross-section 3.

The maximum crack width for cross-section 3 at level 4 was 0.28 mm, see Figure 5.18 (*a*). By comparing crack widths at level 4 for the three cross-sections it can be seen that cross-section 3 resulted in smalelr crack widths than for cross-section

1 at level 4, which is the level where the largest crack widths were observed. When comparing cross-section 3 with cross-section 2 there is a slightly wider maximum crack width for cross-section 3. However, the difference is small and the crack width can still be considered to be sufficiently small when comparing to the limits discussed in Section 2.5.

At level 6, see Figure 5.18 (*b*), the maximum value of the strain was found for cross-section 3. At this level the maximum crack width is, similar to level 4, found to be between the maximum values of the crack widths for the other two reinforcement cases. However, the crack width, 0.29 mm, is still considered reasonable, since it is below 0.3 mm. Hence, it can be concluded that the crack pattern and the crack widths can be improved by providing the three layers of four bars in the critical region.

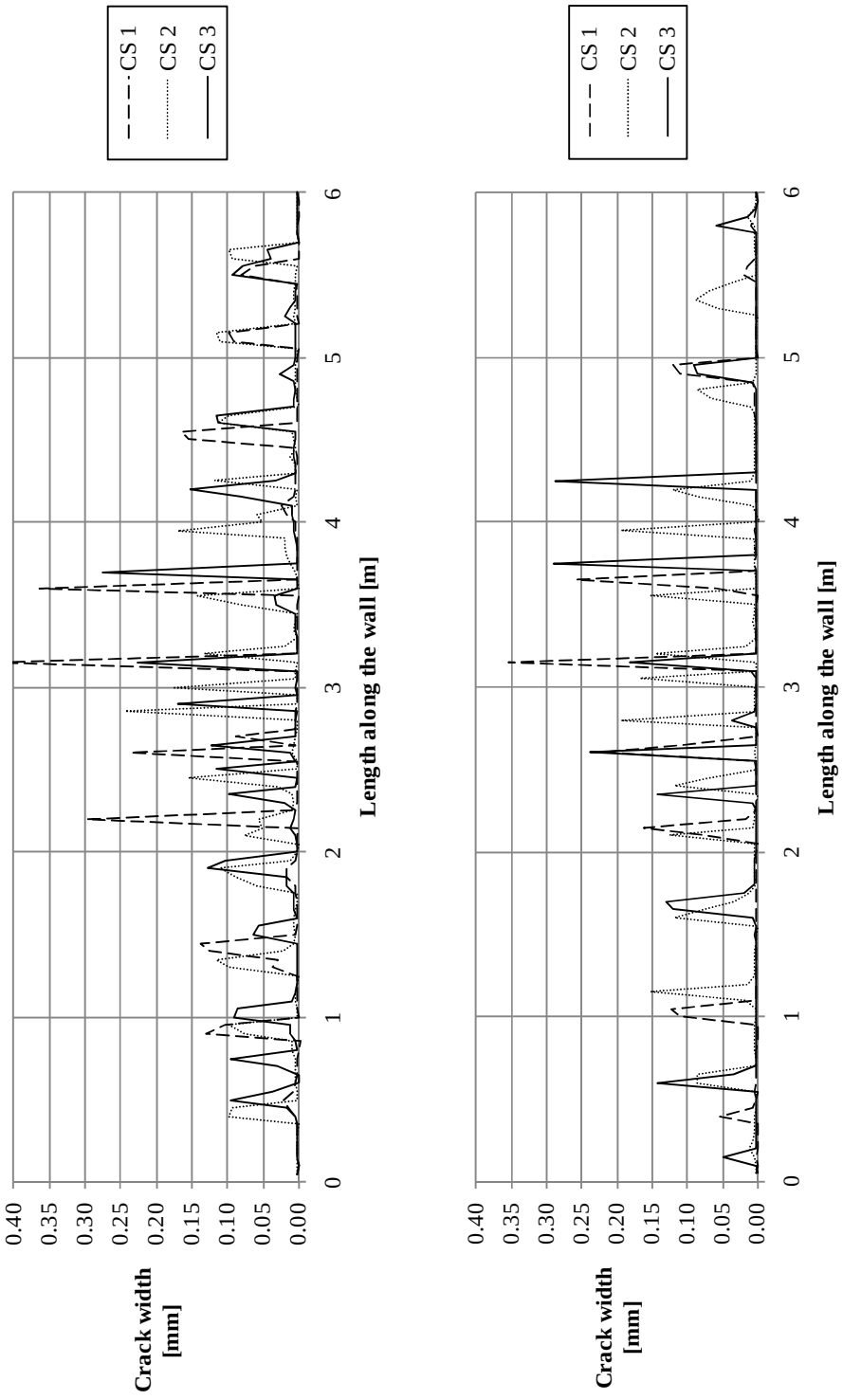

Figure 5.18 Comparison of crack widths for the three different cross-sections at level 4,(a), and level 6, (b).

5.3.2 Influence of geometry

In the previous section the study of the reinforcement arrangement was performed on only one specific case of geometry, the reference geometry 6 x 2.9 m. In order to study the influence of geometry, analyses were carried out on walls with different heights. Two other geometries were studied; one with half the height compared to the reference geometry and another with twice the height of the reference geometry. Thus, three cases with different ratios between length and height were chosen. The three different cases have the ratios 4:1, 2:1 and 1:1 and are shown in Figure 5.19.

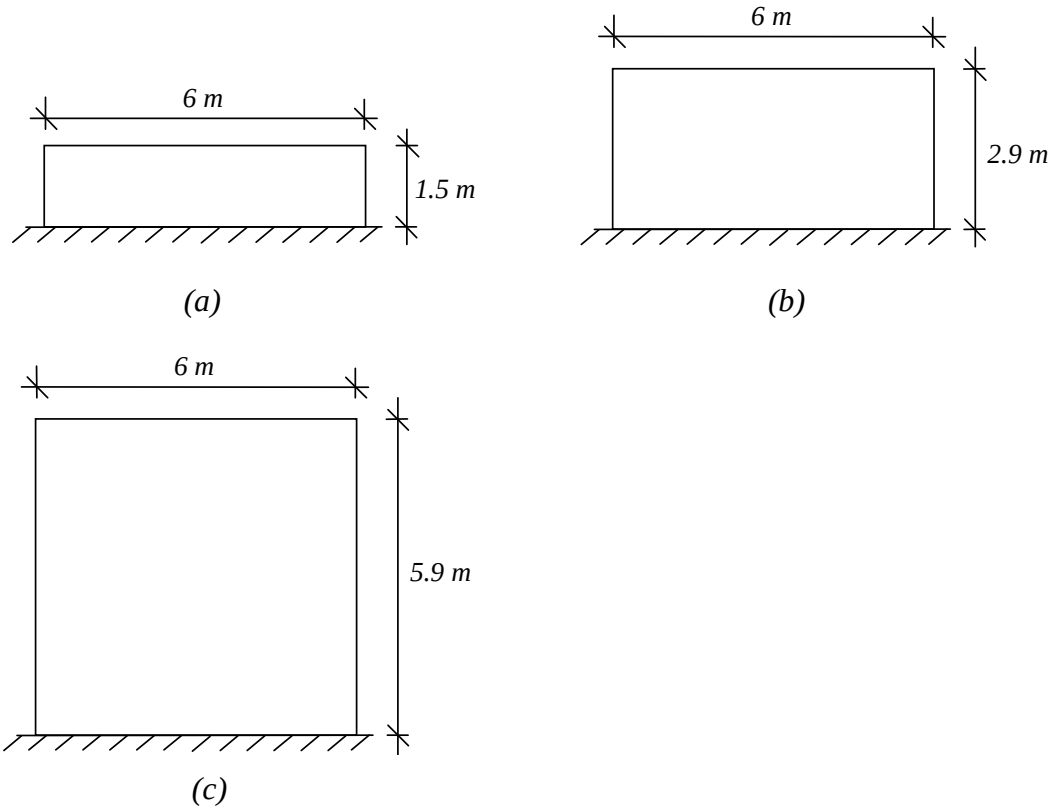

Figure 5.19 Three wall geometries studied with aspect ratio (a) 4:1, (b) 2:1, (c) 1:1.

The results in this section come from analyses carried out on these three different geometries using the reinforcement arrangement of cross-section 1, described in Section 5.3.1. Convergence problems was found for the wall with h = 5.9 m at a shrinkage strain of at ε_{cs} = 0.86 ‰. The results for all walls shown in this section are therefore at this shrinkage strain. Analyses were also performed on cross-section 0 and 2 for all geometries. The results from all analyses can be seen in Appendix I.

The crack patterns obtained in the analysis of the three geometries are shown in Figure 5.20 to Figure 5.22. It can from these figures be seen that the crack patterns for all three walls with different length/height ratio are rather similar. The general behaviour for all three cases is that there is one or several vertical cracks in the middle part of the wall, while skew cracks appeared towards the edges. It can also be noticed that the three different geometries show about the same number of cracks. However, it can be seen that for the height h = 1.5 m there are four cracks across the whole height, while no cracks go across the whole height for heights h = 2.9 and h = 5.9 m. Hence, a larger ratio between length and height resulted in more cracks developing through the entire height.

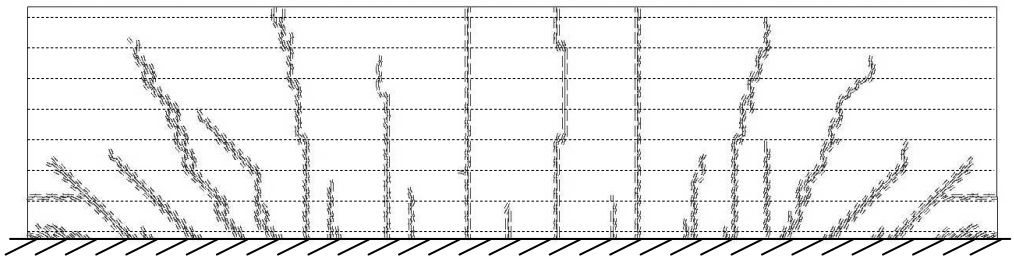

Figure 5.20 Crack pattern for wall with h = 1.5 m at ε_{cs} = 0.86 ‰.

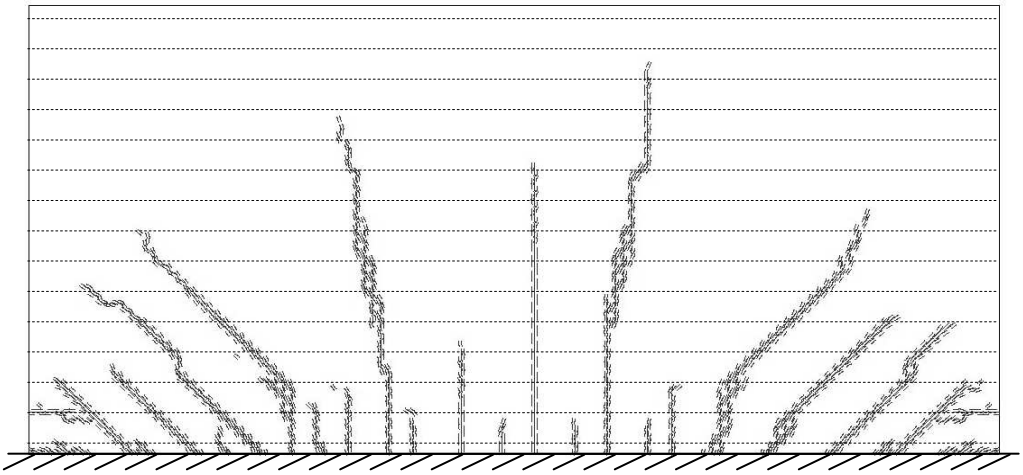

Figure 5.21 Crack pattern for wall with h = 2.9 m at ε_{cs} = 0.86 ‰.

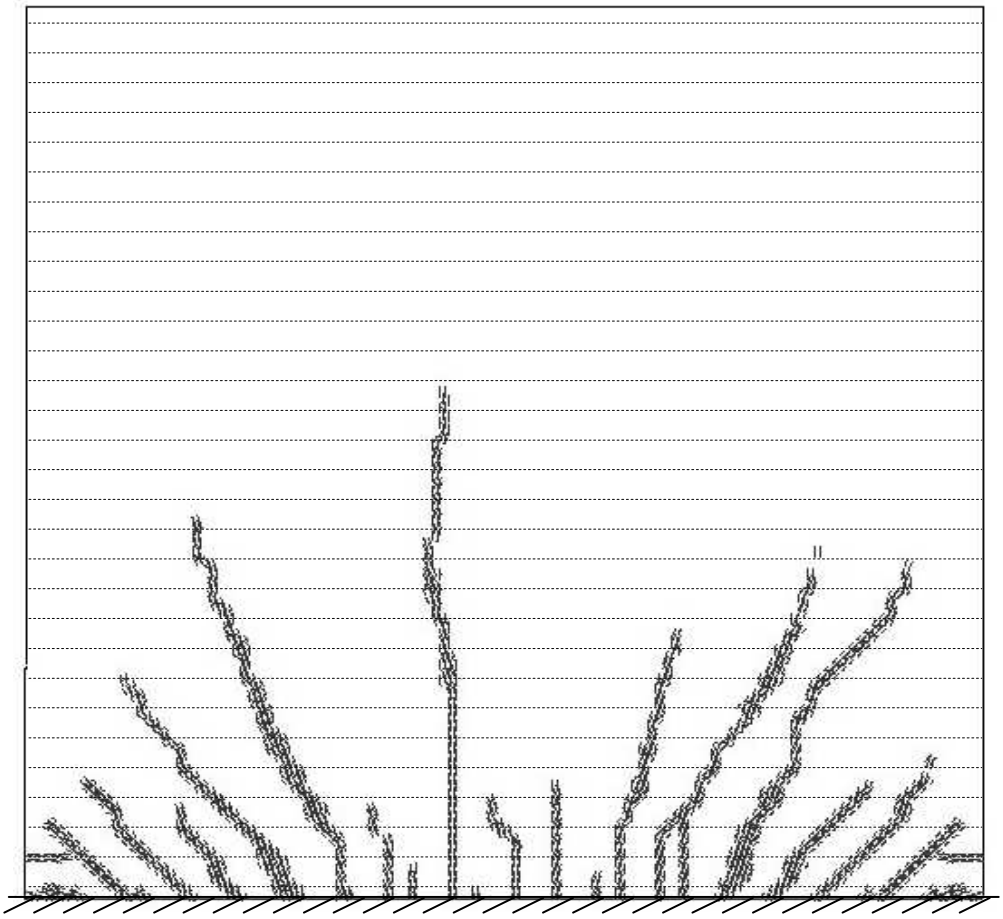

Figure 5.22 Crack pattern for wall with h = 5.9 m at ε_{cs} = 0.86 ‰.

The crack widths at level 1 for the three different cases are shown in Figure 5.23 to Figure 5.25. Similarities can be found between the three cases also by looking at these figures. All cases showed a large number of cracks at this level and the largest cracks appeared in the middle of the wall. The maximum crack widths for the three geometries are w = 0.27 mm, w = 0.24 mm and w = 0.22 mm for length/height ratios of 4:1, 2:1 and 1:1 respectively. Even though the crack widths are within a rather small interval a tendency that the maximum crack width decreased with increasing height of the wall can be observed.

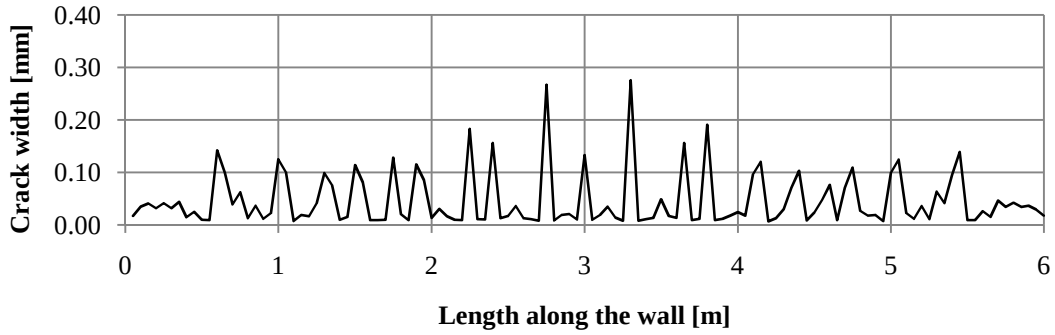

Figure 5.23 Crack widths at level 1 for wall with h = 1.5 m at ε_{cs} = 0.86 ‰.

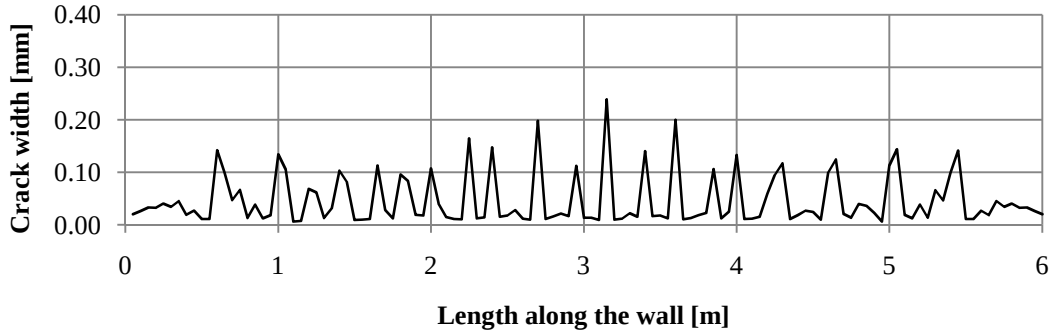

Figure 5.24 Crack widths at level 1 for wall with h = 2.9 m ε_{cs} = 0.86 ‰.

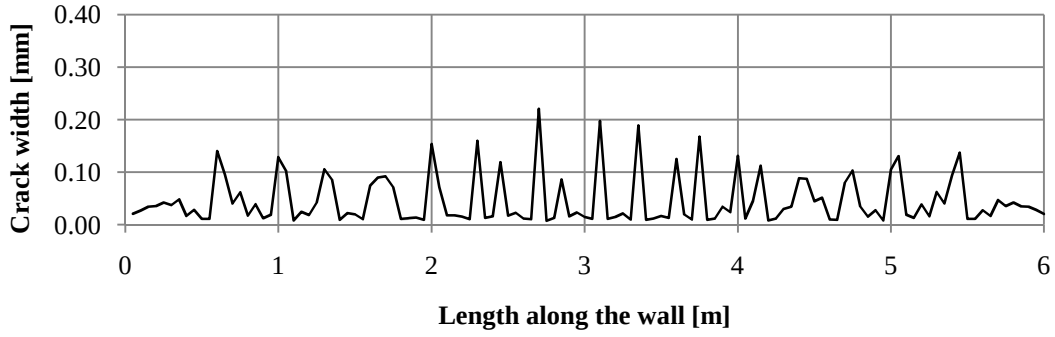

Figure 5.25 Crack widths at level 1 for wall with h = 5.9 m at ε_{cs} = 0.86 ‰.

The crack widths at level 4 are shown in Figure 5.26 to Figure 5.28. At this level more differences can be seen between the three wall geometries compared to the crack

widths at level 1. An increased number of cracks developed large crack widths for lower heights of the wall. It can be observed that for the length/height ratio of 4:1 there are eight cracks with crack widths larger than 0.20 mm. The corresponding numbers for the cases with ratios 2:1 and 1:1 are three and two, respectively. However, the maximum crack widths for the three cases are about the same.

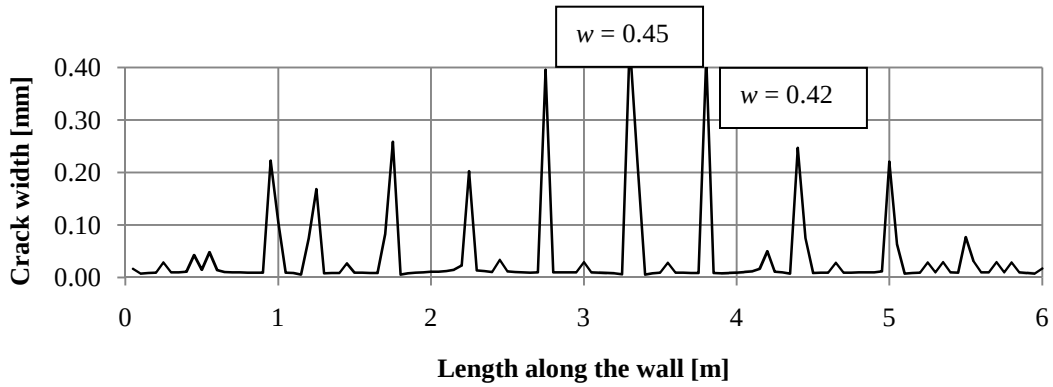

Figure 5.26 Crack widths at level 4 for wall with h = 1.5 m at ε_{cs} = 0.86 ‰.

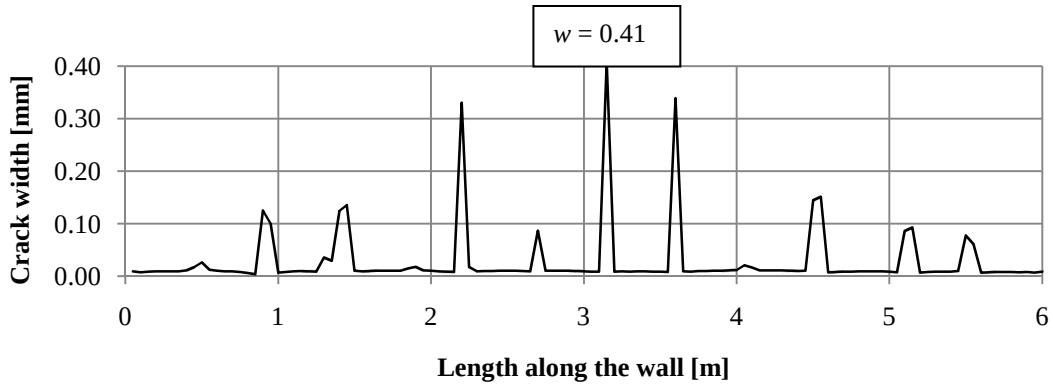

Figure 5.27 Crack widths at level 4 for wall with h = 2.9 m at ε_{cs} = 0.86 ‰.

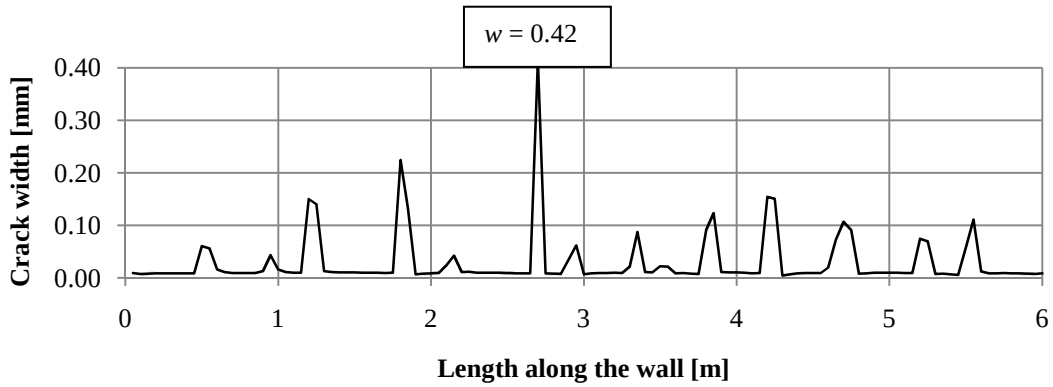

Figure 5.28 Crack widths at level 4 for wall with h = 5.9 m at ε_{cs} = 0.86 ‰.

Even though some differences were found for the walls with three different length/height ratios, it can be concluded that the effect of height was rather small

concerning the crack patterns and the crack widths. Studies on crack development due to imposed strains in concrete walls fully restrained at the base were carried out by Pettersson (2000). A conclusion drawn from his study was also that that the crack width was not highly influenced by the height of the wall, for walls with the same reinforcement ratio as in this section, ρ = 0.5 %.

5.3.3 Influence of fibre reinforcement

The FE model including material properties that simulates fibre reinforced concrete, as explained in Section 4.2.3.1, was also applied to the wall. This was done in order to study if providing fibre reinforcement would have the intended positive effect on the cracking behaviour of walls.

Analyses considering fibre reinforcement were performed on walls with the reference geometry. It was of interest to check the influence of fibre reinforcement for a wall without ordinary reinforcement, cross-section 0, as well as on a wall with reinforcement, cross-section 1. All results for these cases are presented in Appendix J.

The crack pattern obtained for the analysis on the wall, with fibre reinforced concrete only, is shown in Figure 5.29. The corresponding result for the wall with plain concrete, cross-section 0, shown previously in Section 5.3.1, is presented in Figure 5.30 to compare with. For the wall including fibre reinforcement it can be seen that more cracks appeared than in the case with plain concrete. For the wall with plain concrete there is mainly one crack in the middle of the wall developing almost across the height to the top edge. When fibres are added an increased number of more or less straight cracks in the middle developed to an intermediate height of the wall. This indicates that the fibres help to smear out the strains to create more cracks.

Towards the left and right edges, more skew cracks appeared for the fibre reinforced wall than for the plain concrete wall. Also this is in agreement with the expected effect of fibre reinforcement.

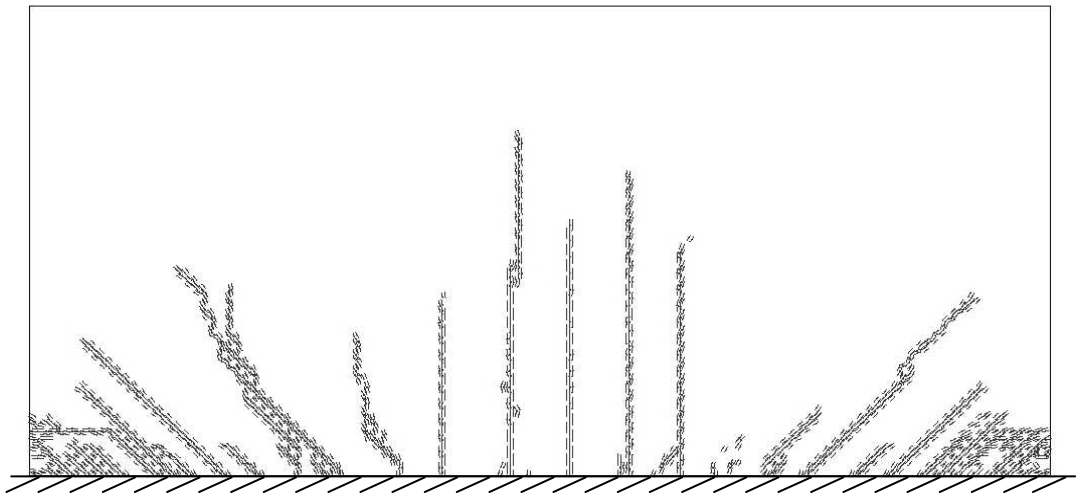

Figure 5.29 Crack pattern for wall with Cross-section 0 including fibre reinforcement.

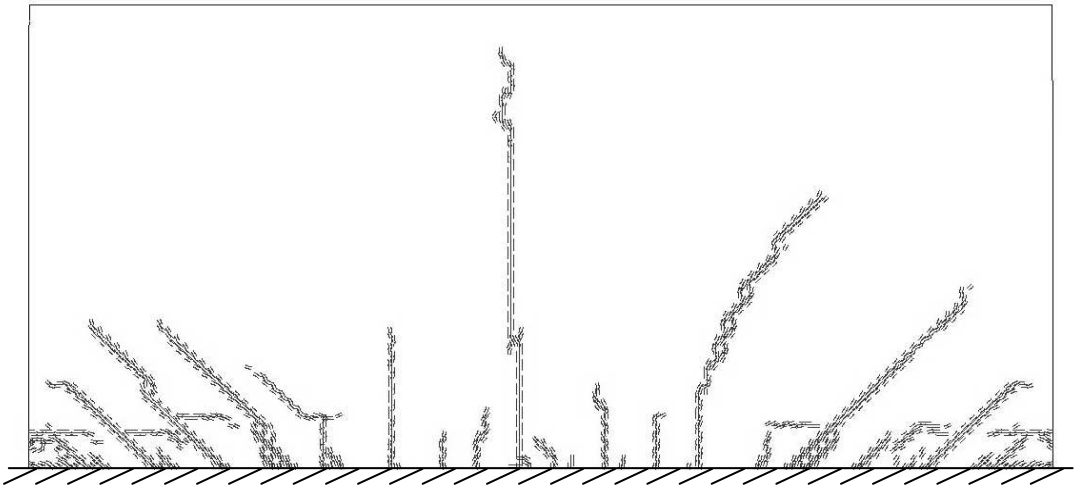

Figure 5.30 Crack pattern for wall with Cross-section 0, plain concrete.

The effect of more cracks while providing fibre reinforcement can be seen by analysing the crack widths. At the bottom level, level 1, where the bottom restraint had a large influence, the maximum crack width was 0.25 mm, see Figure 5.31. The corresponding value for the case without fibre reinforcement was 0.36 mm, shown previously in Figure 5.13. Apart from this difference in maximum crack widths the behaviour at level 1 was similar for the two cases; cracks were smeared out over almost the whole length.

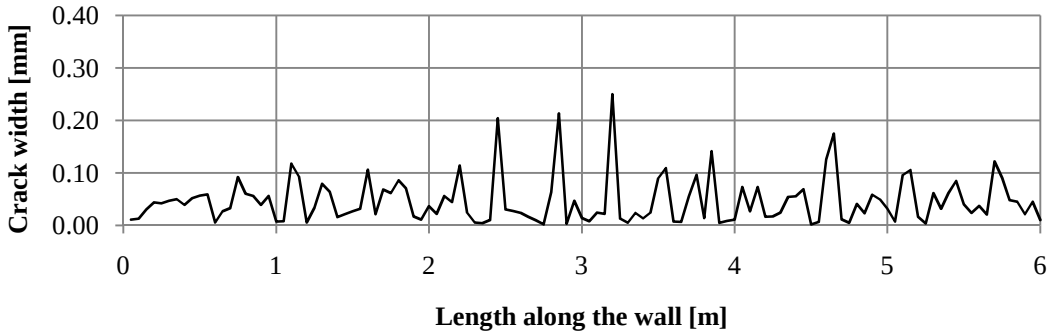

Figure 5.31 Crack widths at level 1 for cross-section 0 with fibre reinforcement.

The maximum crack width for the fibre reinforced wall, 0.36 mm, was found at level 6. At this level, see Figure 5.32, only three cracks in the middle showed crack widths above a value of 0.1 mm. However, the largest crack was markedly higher than the surrounding ones. When comparing these crack widths to the crack widths for the wall with the same cross-section but without fibre reinforcement, see Figure 5.33, a large difference can be found. When fibre reinforcement was added, the maximum crack width decreased from 1.08 mm to 0.36 mm, a decrease of 67 %. It can be seen that more cracks developed to level 6 when fibre reinforcement was included, which resulted in smaller crack widths.

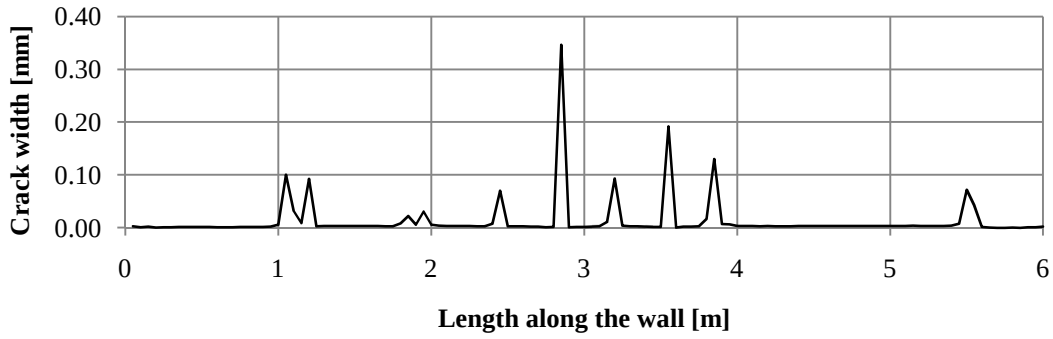

Figure 5.32 Crack widths at level 6 for cross-section 0 with fibre reinforcement.

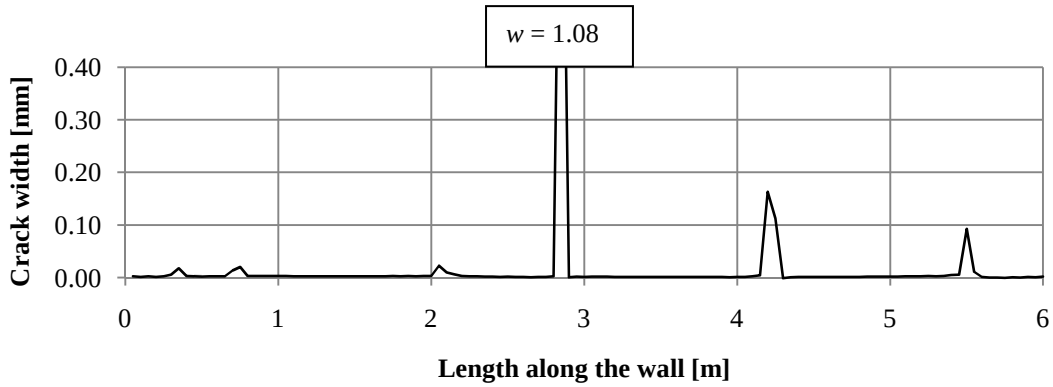

Figure 5.33 Crack widths at level 6 for cross-section 0, plain concrete.

The result concerning crack pattern from the analysis of the fibre reinforced wall with cross-section 1 is shown in Figure 5.34. It can be seen, when comparing to the same cross-section without fibre reinforcement, see Figure 5.35, that more cracks appeared when including fibre reinforcement. As for providing fibre reinforcement to the plain concrete, in this case also more straight cracks develop in the middle of the fibre reinforced wall. The heights of these cracks did not differ as much, though, as for the wall without fibre reinforcement and, generally, cracks were kept at a lower height. This indicates that strains were more smeared out over the length of the wall.

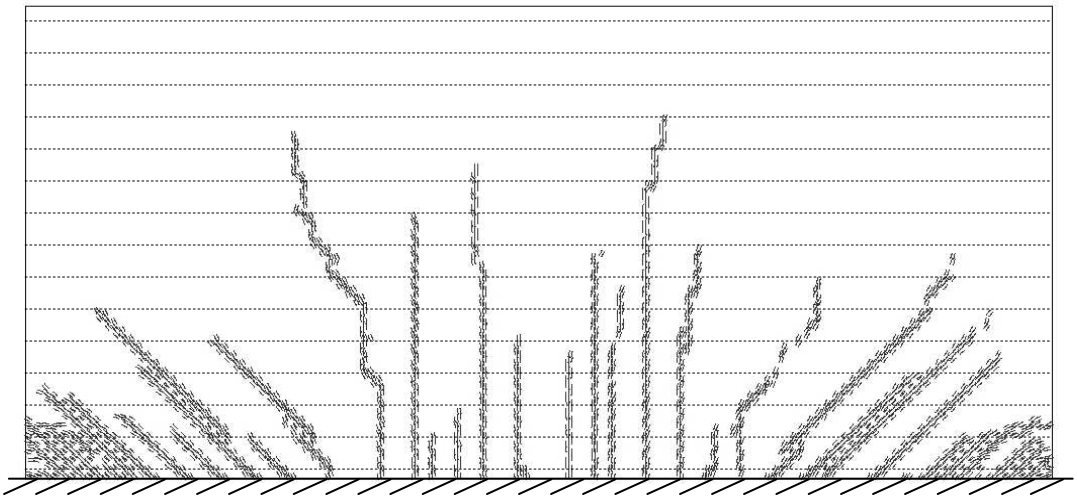

Figure 5.34 Crack pattern for wall with cross-section 1 including fibre reinforcement.

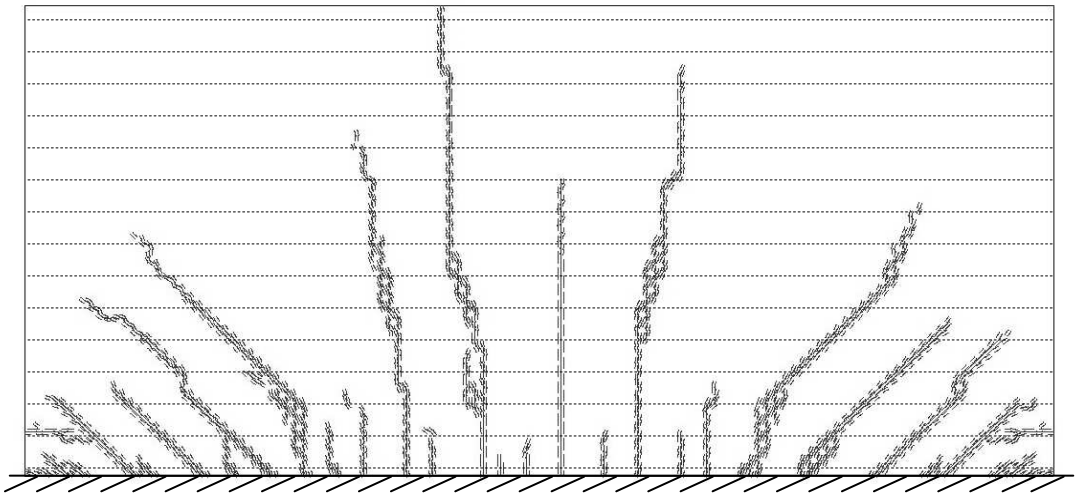

Figure 5.35 Crack pattern wall with cross-section 1.

The maximum crack width found for the fibre reinforced wall with cross-section 1 was 0.22 mm at level 6, see Figure 5.36. Compared to the wall with the same cross-section but without fibre reinforcement, previously shown in Figure 5.11, the maximum crack width was about 50 % lower for the fibre reinforced wall.

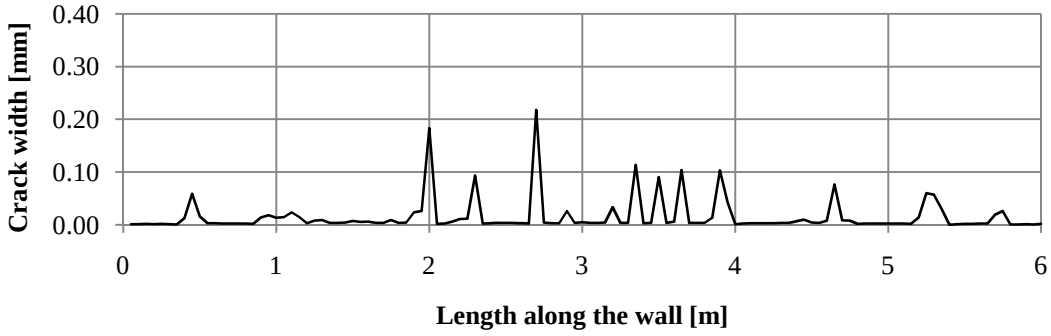

Figure 5.36 Crack widths at level 6 for cross-section 1 with fibre reinforcement.

Lastly, an interesting observation was found when the results from the fibre reinforced wall with cross-section 0 were compared to the results for the ordinarily reinforced wall with cross-section 1. The fibre reinforced wall without reinforcement bars generally showed a more favourable behaviour concerning crack widths. The maximum crack width for the fibre reinforced wall, 0.36 mm, was found to be smaller than the maximum crack width for the wall with cross-section 1, 0.42 mm, previously shown in Figure 5.32 and Figure 5.11 respectively. This indicates that by adding fibre reinforcement, in the way it was done in this project, the cracking behaviour was improved even compared to a wall reinforced with reinforcement bars as cross-section 1.

5.4 Concluding remarks

It was concluded that the restraint caused by the boundary condition at the bottom edge had a significant effect on the crack pattern. However, reinforcement is still needed at the bottom level to keep crack widths at sufficiently low levels. Concerning the influence of reinforcement it was observed that cross-section 2 showed an improved behaviour, with crack widths well below 0.30 mm, compared to cross-section 1. To see if a good cracking behaviour could be obtained with a smaller reinforcement amount than the one in cross-section 2, a third cross-section, cross-section 3, was introduced. Analyses of this cross-section, where more bars were provided at three levels in the region where the maximum crack width was expected, showed that crack widths can be kept at almost the same level as for cross-section 2. Hence, it can be concluded that the cracking behaviour can be improved by adding reinforcement bars at certain levels in a suitable manner.

Analyses of walls with different length/height ratios showed that the height of the wall did not have a significant influence on the crack patterns and crack widths.

The general behaviour observed when applying the fibre reinforced concrete model to the wall was that the number of cracks was increased and thereby the crack widths decreased. The largest improvement was found when a plain concrete wall was provided with fibre reinforcement only. This fibre reinforced wall showed even better behaviour concerning crack widths than the wall with reinforcement arrangement according to cross-section 1. However, since the crack widths in the fibre reinforced wall were still above 0.30 mm, reinforcement bars would still be needed to keep crack widths at a sufficiently low level. When fibre reinforcement was provided in the wall with cross-section 1, the maximum crack width was 0.22 mm, which can be considered to be sufficiently small.

The maximum crack widths at the three levels studied for all cross-sections investigated in this chapter are summarised in Table 5.1.

Table 5.1 Maximum crack widths at the three levels studied for all cross-sections of the wall. Bold numbers show the maximum crack width for each cross-section.

Cross-section case	Crack width [mm]		
	Level 1	Level 4	Level 6
CS0	0.36	**1.08**	**1.08**
CS1	0.26	**0.42**	0.35
CS2	0.18	**0.24**	0.19
CS3	0.22	0.28	**0.29**
CS0+fibre	0.25	0.27	**0.36**
CS1+fibre	0.15	0.21	**0.22**

What is not stated earlier but can be observed in this table is that the wall with fibre reinforcement and a reinforcement arrangement according to cross-section 1 showed a smaller maximum crack width than the wall with cross-section 2. This also indicates that a combined use of fibre reinforcement and ordinary reinforcement may be a way to optimise the control of cracking.

However, no optimal combination of ordinary reinforcement and ordinary reinforcement was determined and a more thorough investigation is still needed with different combinations before a certain combination can be recommended.

6 Final remarks

6.1 Conclusions

The FE model used in this and previous thesis projects on this subject was verified by comparisons with results from load tests on tie-rods. The following conclusions can be drawn:

- The FE model for ordinary concrete, with uniform material properties, has shown good agreement with test results.
- Use of material properties, based on tests results, applied uniformly the model was not enough to reproduce the behaviour of fibre reinforced concrete specimens by FE analysis.
- A combination of material models with two different material properties, corresponding to plain concrete and fibre response respectively, gave better agreement with test results and seems to be a good modelling approach to be further developed.

Conclusions drawn from the parametric studies carried out on edge beams are summarised as follows**:**

- The standard reinforcement arrangement, i.e. four 16 mm bars in the top and three 16 mm bars in the bottom, was found to be the best reinforcement arrangement concerning crack widths for the two different transversal reinforcement ratios studied. Doubling the continuous edge restraint by an increased amount of transverse reinforcement is therefore not found to be a reason to change the arrangement of the longitudinal reinforcing bars.
- When using 8 mm bars the smallest crack widths were found. However, the cracking behaviour with 10, 12 and 16 mm bars did not differ much. Therefore, 16 mm bars are considered to be the best option, as a significantly lower number of bars are needed, something that is practically preferable.
- The shrinkage strain needed to create fully open cracks decreased for increasing concrete cover. However, cracks across the whole section were not always developed and since they might concentrate towards only one face of the edge beam, their crack widths could be wider in these regions.
- An increase in fracture energy of concrete delayed the crack development. Fully developed cracks were formed at larger shrinkage strains, and those cracks that formed became wider since the total number of cracks was decreased. However, if the fracture energy was large enough, no fully developed cracks occured.
- Due to creep effect the concrete can withstand larger strains before each new crack is formed. This leads to fewer cracks for this short member, but the cracks that develop will be larger. Hence, creep has a negative effect on the resulting crack widths once a crack has occurred.

Parametric studies were also carried out on a retaining wall. Conclusions drawn from these analyses are as follows:

- The continuous edge restraint helped to create more and narrower cracks close to the bottom edge. However, reinforcement was still needed at a level close to this edge in order to keep the crack widths small enough.
- A configuration where reinforcement was concentrated at a certain distance away from the restrained edge was suggested to control crack widths in retaining walls cast on foundation slabs.
- It can be concluded that the effect of height was rather small concerning crack patterns and crack widths.

Based on the analyses carried out on edge beams and retaining walls considering the effect of fibre reinforcement by using the suggested heterogeneous material approach, it can be concluded that:

- Fibre reinforcement increased the number of cracks and decreased crack widths significantly. However, ordinary reinforcement was still needed to further decrease crack widths to sufficiently small levels and to distribute the cracks along the whole height of the wall.
- A combined use of fibre reinforcement and ordinary reinforcement may be a way to optimise the reinforcement arrangement while controlling the crack widths below an allowable value in aggressive environments. Then, the durability of the structure can be increased.

6.2 Further investigations

Since the time and resources for this thesis was limited, some subjects could not be investigated and are proposed for future research:

- Development of the FE model for fibre reinforced concrete by using a more suitable material model for elements simulating fibre behaviour. Determine the probability distributions for elements resembling concrete and fibre behaviour based on the total fracture energy or observed number of fibres per unit area.
- Study the possible influence of shrinkage induced stresses and long term effect during testing of plain and fibre reinforced concrete specimens.
- Further investigation on the effect of creep by including time dependent creep coefficients and corresponding material properties.
- Investigate the effect on crack widths and crack patterns of edge beams and retaining walls of different parameters, such as the concrete strength.
- Use results from this thesis project in deeper investigations on the effect of more parameters in order to develop the simplified method proposed by Johansson and Lantz (2009) for design of bridge edge beams.
- Include into the analysis the effect of external loads in the cracking process of concrete structures subjected to restraint forces.
- A more comprehensive investigation on combinations of fibre and ordinary reinforcement could be done in order to reach an optimised cross-section for the retaining walls.

7 References

ADINA (2010): *Theory and modeling guide*, Vol. 1: ADINA Solids & Structures Report ARD 10-7, ADINA R & D, Inc. Watertown, USA, 2010

Alfredsson H., Spåls J. (2008): *Cracking behaviour of Concrete Subjected to Restraint Forces.* Master's Thesis 2008:24. Division of Structural Engineering, Chalmers University of Technology, Brussels, Belgium, 2004.

Bentur A. and Mindess S. (1990): *Fibre reinforced cementitious composites*, Elsevier Applied Science, New York, USA, 1990.

Bigaj-van Vliet A.J. (2001): *Bond of Deformed Reinforcing Steel Bars Embedded in Steel Fiber Reinforced Concrete.* State-of-the Art Report, Delft Cluster, Delft, The Netherlands, 2001.

Bischoff P.H. (2003): *Tension stiffening and cracking of steel fibre reinforced concrete.* Journal of Materials in Civil Engineering, Vol. 15, No. 2, March/April 2003.

CEB-FIP (1993): *CEB-FIP Model Code 1990*. Comité Euro-International du Béton, EPF Lausanne. T Telford, London, Great Britain, 1993, 437 pp.

CEB (1997): *Serviceability Models, Behaviour and modelling in serviceability limit state including repeated and sustained loads*, CEB Bulletin 235, Lausanne, Switzerland 1997.

CEN (2004): *Eurocode 2: Design of concrete structures, Part 1-1, General rules and rules for buildings*, European Comittee for Standardization, Lausanne, Switzerland 1997.

Engström B. (2008): *Restraint cracking of reinforced concrete structures*. Division of Structural Engineering, Chalmers University of Technology, Göteborg, Sweden, 2008.

Fall D., Nielsen C.V. (2010): *Concrete reinforcement solutions*. Division of Structural Engineering, Chalmers University of Technology, Göteborg, Sweden, 2010.

fib (2009): *Structural concrete, Textbook on behaviour, design and performance*, Volume 1, International Federation of Structural Concrete, Bulletin 51, Lausanne, Switzerland, 2009.

Granju J-L., Balouch S.U. (2005): *Corrosion of steel fibre reinforced concrete from the crack*s. Cement and Concrete Research, Vol. 35, (2005)

Jansson A. (2008): *Fibres in reinforced concrete structures – analysis, experiments and design*. Licentiate Thesis. Division of Structural Engineering, Chalmers University of Technology, Göteborg, Sweden, 2008.

Jansson A. (2011): *Effect of Steel Fibres on Cracking of Reinforced Concrete*. Ph.D. Thesis. Division of Structural Engineering, Chalmers University of Technology, Göteborg, Sweden, 2011.

Johansson M. (2000): *Structural Behaviour in Concrete Frame Corners of Civil Defence Shelters*. Ph.D. Thesis. Division of Structural Engineering, Chalmers University of Technology, Göteborg, Sweden, 2000.

Johansson P., Lantz H. (2009): *Crack Control of Reinforced Concrete with Continuous Edge Restraint.* Master's Thesis 2009:43. Division of Structural Engineering, Chalmers University of Technology, Göteborg, Sweden, 2009.

Löfgren I. (2005): *Fibre reinforced Concrete for Industrial Construction*. Ph.D. Thesis. Division of Structural Engineering, Chalmers University of Technology, Göteborg, Sweden, 2005.

Magnusson J. (2000): *Bond and Anchorage of Ribbed Bars in High-Strength Concrete*. Ph.D. Thesis. Division of Structural Engineering, Chalmers University of Technology, Göteborg, Sweden, 2000.

Nesset J., Skoglund S. (2007): *Reinforced Concrete Subjected to Restraint Forces*. Master's Thesis 2007:23. Division of Structural Engineering, Chalmers University of Technology, Göteborg, Sweden, 2007.

Pettersson D. (2000): *Control of Cracking due to Imposed Strains in Concrete Structures*. Ph.D. Thesis. Division of Structural Engineering, Lund Institute of Technology, Lund, Sweden, 2000.

Plos M. (2000): *Finite element analyses of reinforced concrete structures*. Compendium 96:14. Division of Structural Engineering, Chalmers University of Technology, Göteborg, Sweden, 2000.

Schumacher P. (2006): *Rotation Capacity of Self-Compacting Steel Fiber Reinforced Concrete*. Ph.D. Thesis. Concrete Structures Group, Faculty of Civil Engineering and Geosciences, Delft University of Technology, Delft, The Netherlands, 2006.

Svensk byggtjänst (1994): *Betonghandbok – Material (Concrete handbook – Material), Chapter 16, pp. 54*7-607, Sweden 1994.

Vägverket (2001): *Utbyte av kantbalk (Replacement of edge beam)*. Drawing number: 584:1G-i rev. C. Vägverket tekniska avdelningen brosektionen, Borlänge, Sweden 2001.

Appendix A Randomised material properties study

Some problems while localizing cracks were found while simulating tie-rod tests of fibre reinforced concrete with uniform properties. In order to try to avoid this, new material properties, where tensile strength was varied following a normal distribution, were defined. Normal distribution parameters, i.e. mean value and standard deviation, were determined by results from uni-axial tensile tests described in Section 3.2.1 and are shown in Table A.1.

Table A.1 Parameters used to determine the tensile strength normal distribution.

f_{ctm}	3.630 MPa
s_N	0.295 MPa

To transform the continuous probability function of the normal distribution into discrete values, 12 different tensile strength values were established. The cumulative probability for each interval is shown in Figure A.1. Highest and lowest intervals got higher probability as they also include all values above and below them, respectively. Same number of material definitions was created in ADINA. For each of them, the fracture energy was kept constant at 10500 N/m by varying the parameter ξ and the post tensile strength was equal to 85 % of its corresponding tensile strength, according to the mean values observed during testing of fibre reinforced specimens.

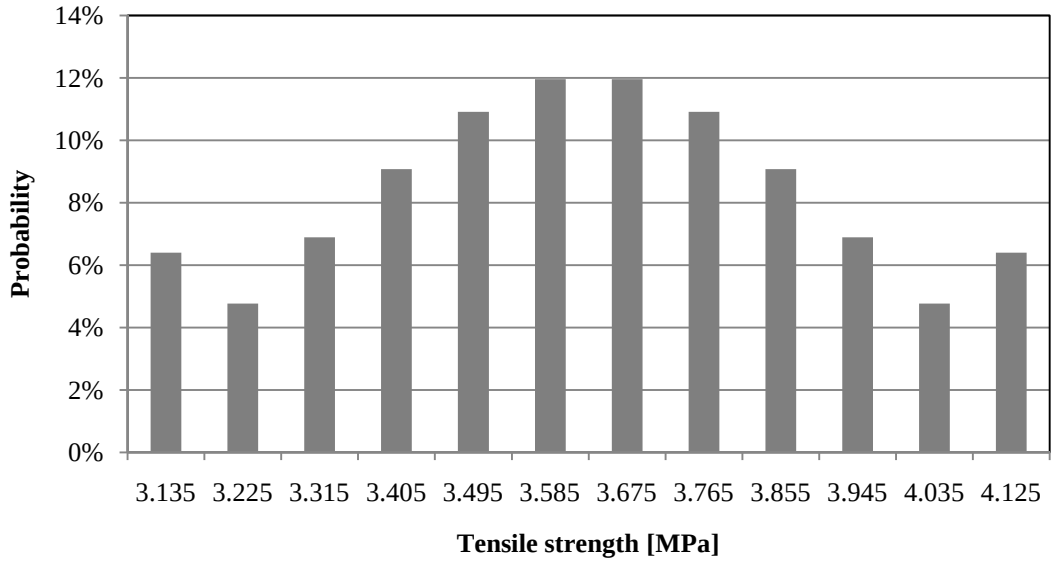

Figure A.1 Cumulative probability for each tensile strength interval used in analysis of fibre reinforced concrete with random material properties.

All elements in the model were randomly assigned a material definition according to its probability of appearance. Three different samples, i.e. R1, R2 and R3, with different material properties distribution were created. The number of elements which were assigned for each material definition is compared for each sample with the theoretical normal distribution in Figure A.2.

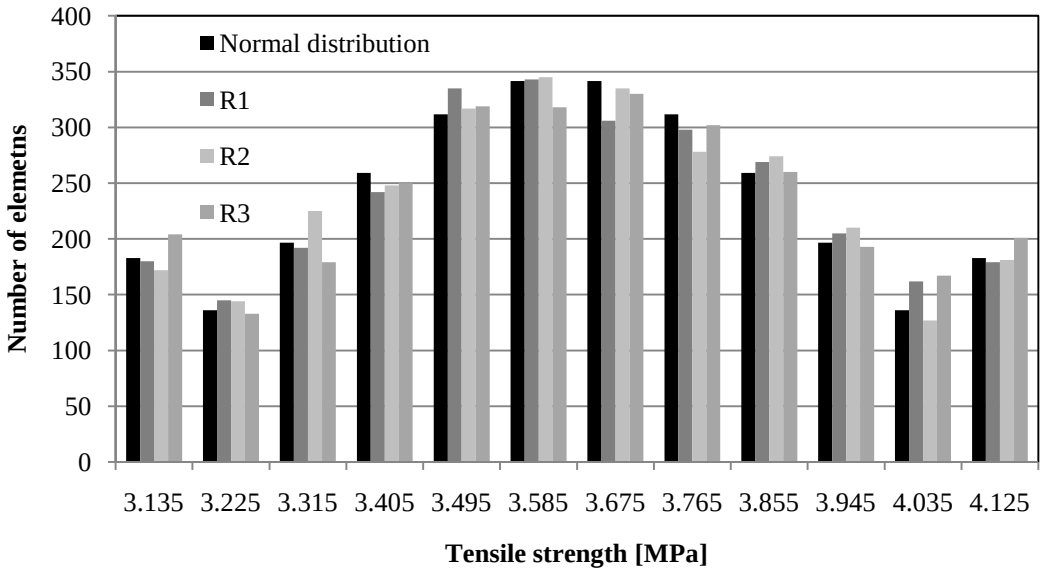

Figure A.2 Distribution of elements with each material definition in all three samples.

In Figure A.3 to Figure A.5, crack patterns and crack widths graphs are presented for each sample. Although some small localization has occurred, most of the central region of the model is still cracked. As material properties are not uniform in the model, crack widths may vary along the section. Therefore, it is needed to check crack widths at the surface, rather than at the steel level, which were not visible during the tests. If crack widths graphs are observed, it can be seen that crack widths are too small and localization of cracks is too small to form 100 % developed cracks.

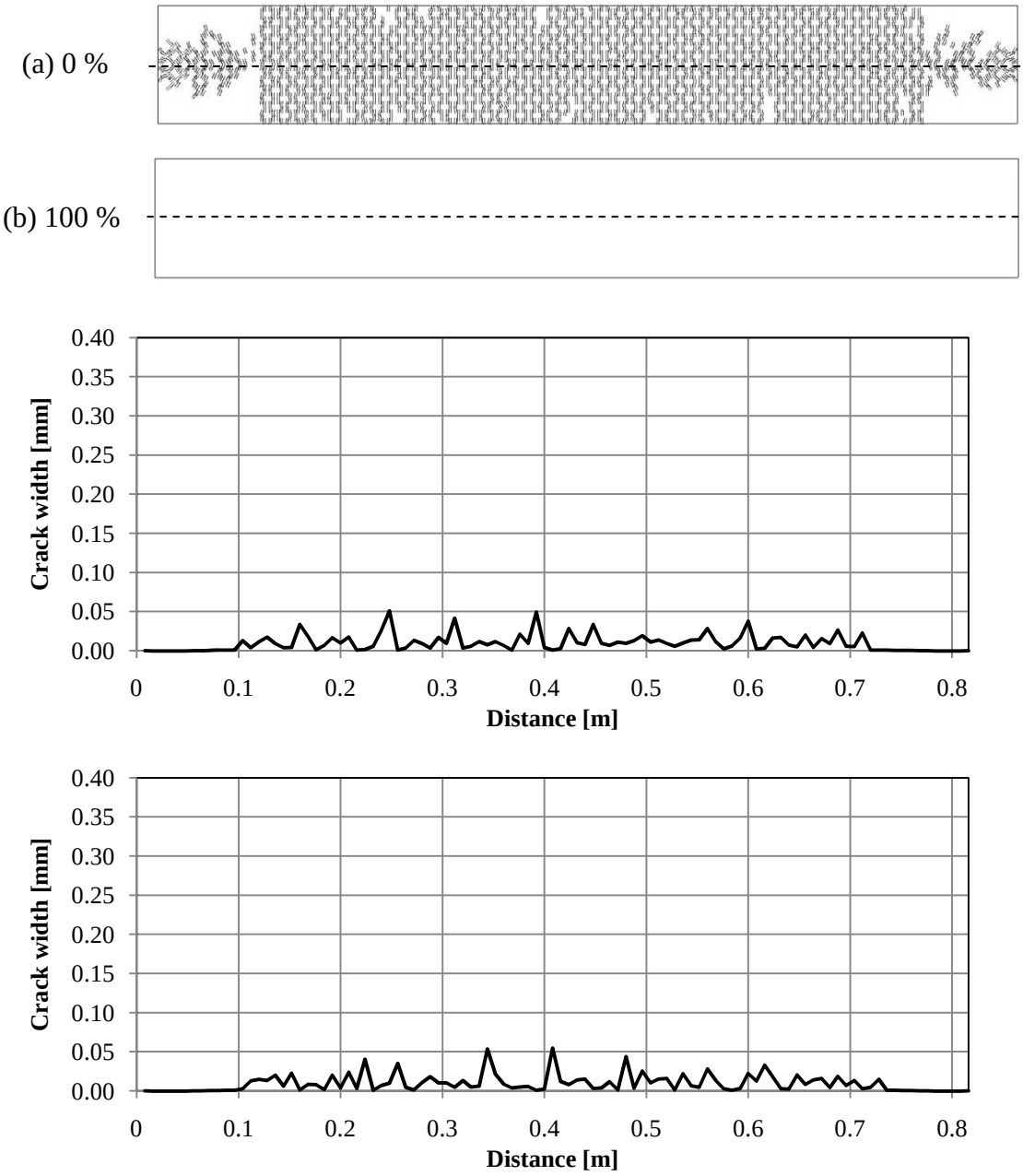

Figure A.3 Crack pattern and crack widths at top (top figure) and bottom surface (bottom figure) of fibre reinforced concrete analyzed with random material properties R1 for u = 1.05 mm.

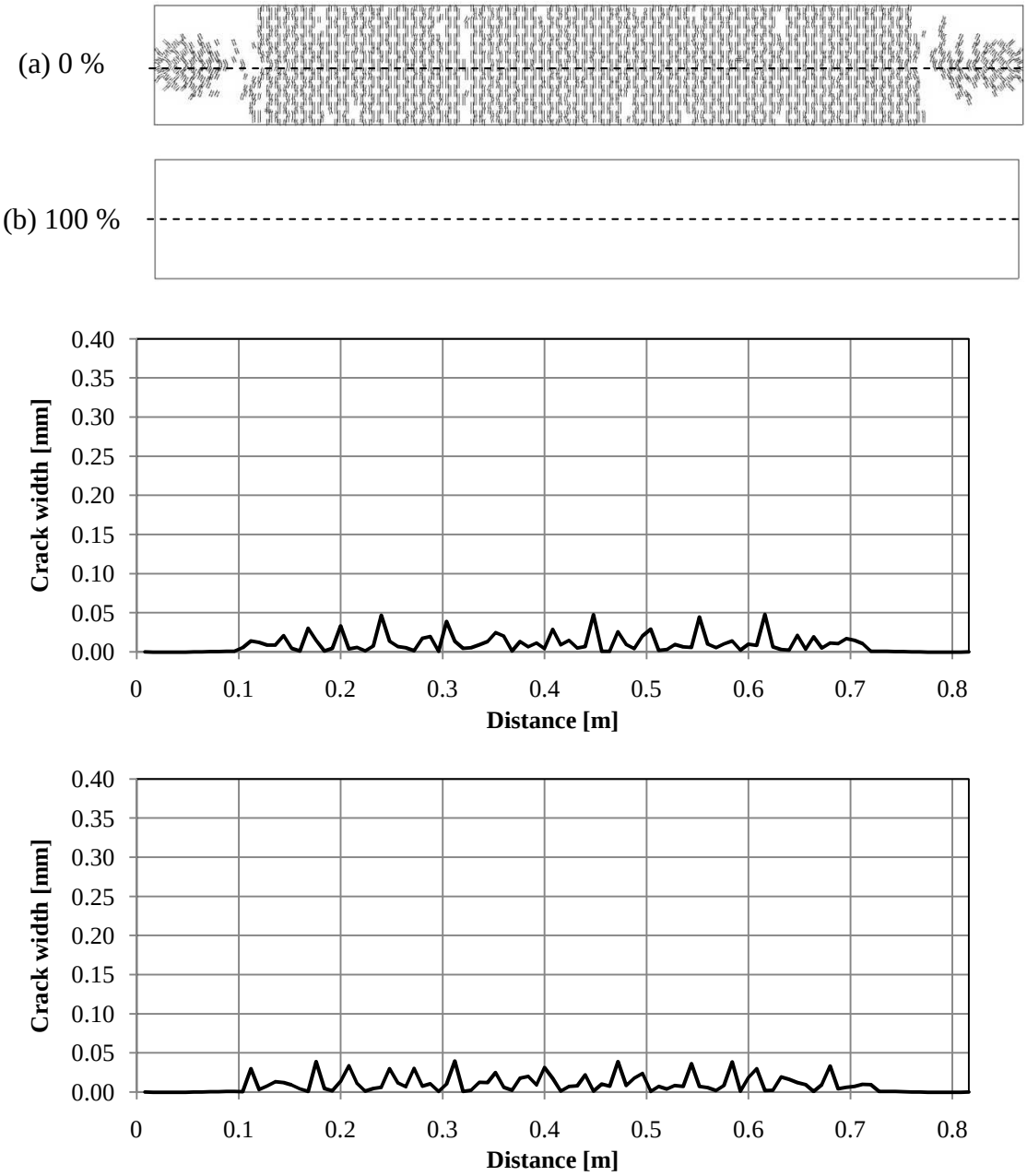

Figure A.4 Crack pattern and crack widths at top (top figure) and bottom surface (bottom figure) of fibre reinforced concrete analyzed with random material properties R2 for u = 1.05 mm.

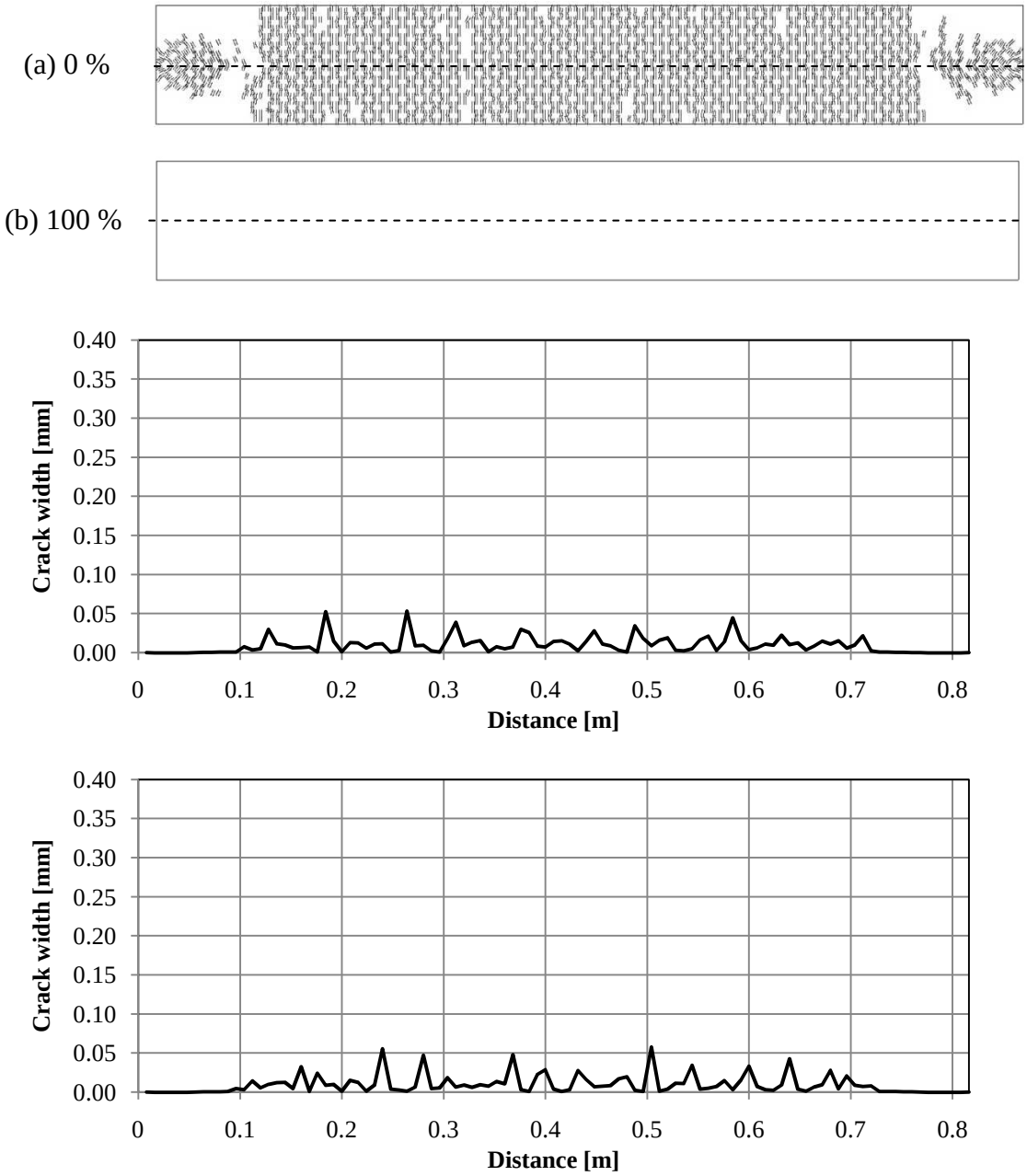

Figure A.5 Crack pattern and crack widths at top (top figure) and bottom surface (bottom figure) of fibre reinforced concrete analyzed with random material properties R3 for u = 1.05 mm.

In Figure A.6, the load elongation response obtained during analysis with random and uniform material properties are compared with the test results. Use of random material properties reduces difficulties to calculate the solution after cracking and had a better behaviour compared to the tests. However, although the tensile strength has been decreased in some elements, the cracking load is still too high. This could be explained because of an element with low tensile strength has the same probability of being surrounded by a weak or strong element, while in reality it can be expected to concentrate into weaker sections.

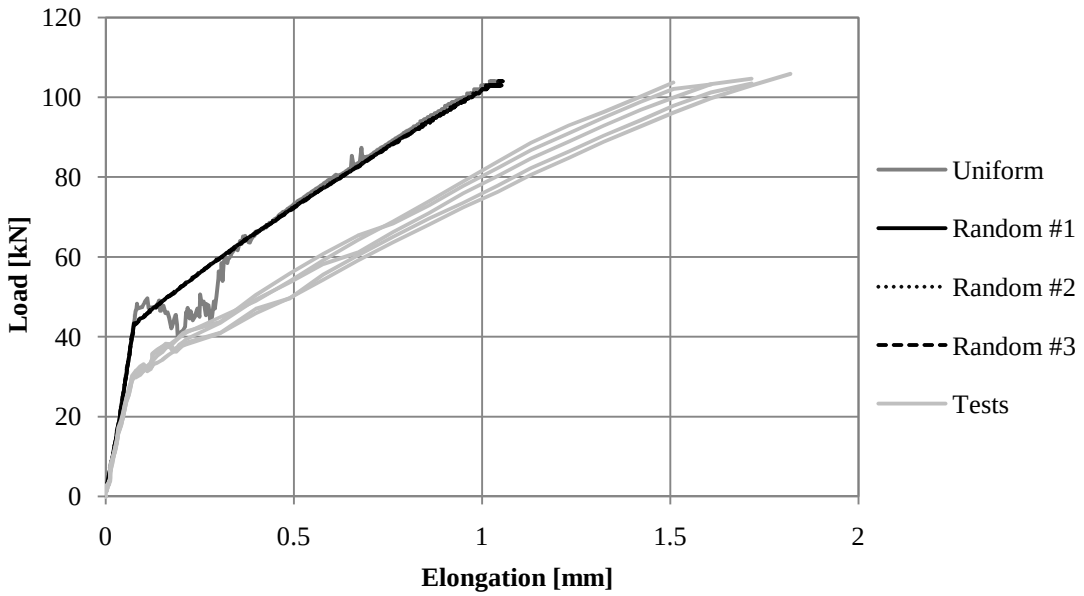

Figure A.6 Comparison of load-elongation relation obtained during testing and finite element analysis.

In conclusion, use of randomized tensile strength helps the finite element analysis by providing weaker sections where the cracks can start to grow. However, it is not enough in order to simulate behaviour of fibre reinforced concrete, as the whole model still has a very ductile behaviour and no large stresses are redistributed due to crack formation.

Appendix B Heterogeneous material approach

In this Appendix, results from non-linear finite element analyses using heterogeneous material approach on tie-rods are presented. Two material properties were assigned along the model with the same probability of appearance for both of them. Three different distributions were analysed.

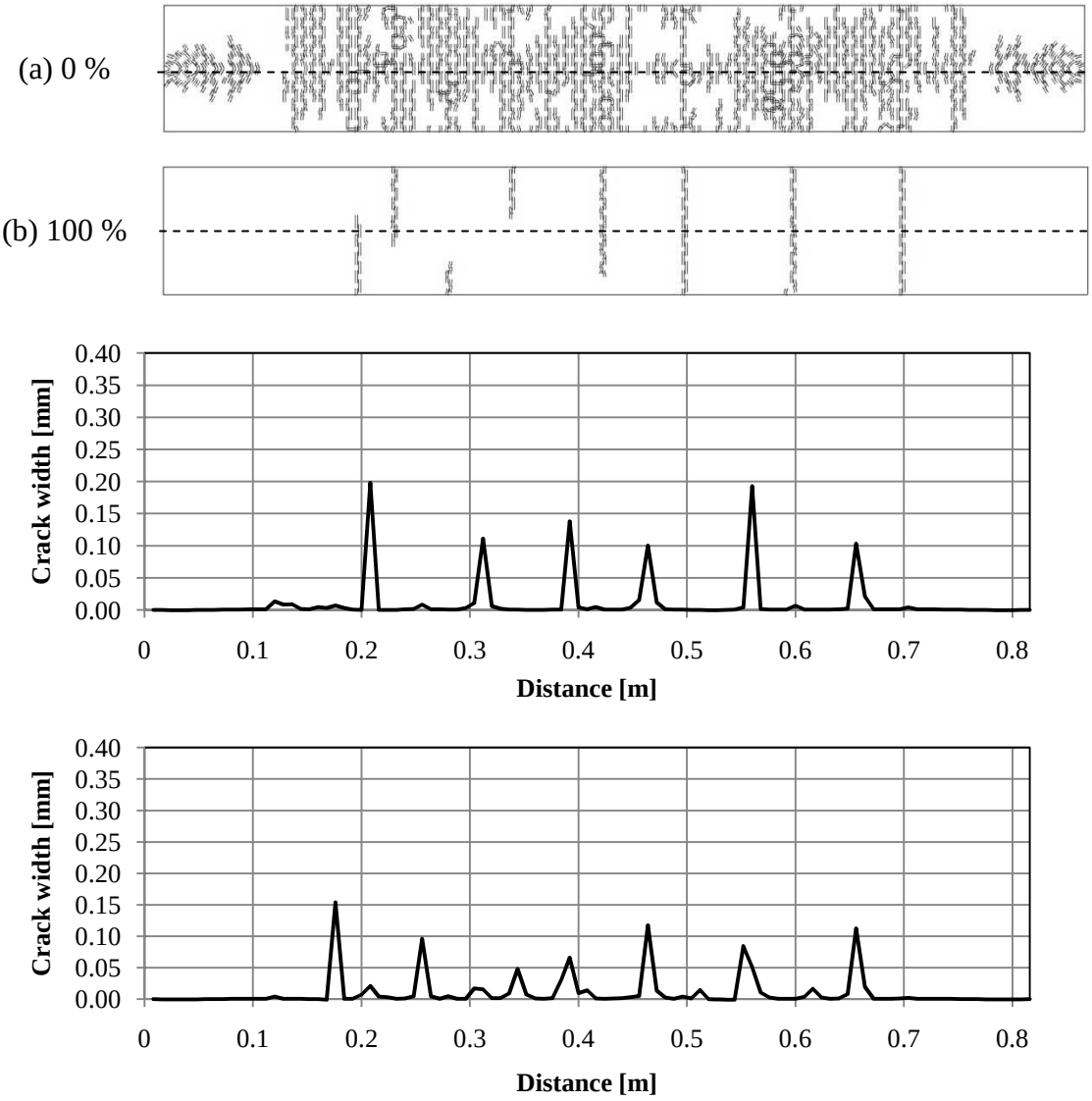

Figure B.1 Crack pattern and crack widths at top (top figure) and bottom surface (bottom figure) of fibre reinforced concrete analyzed with heterogeneous material approach and material properties distribution R1 for u = 1.10 mm.

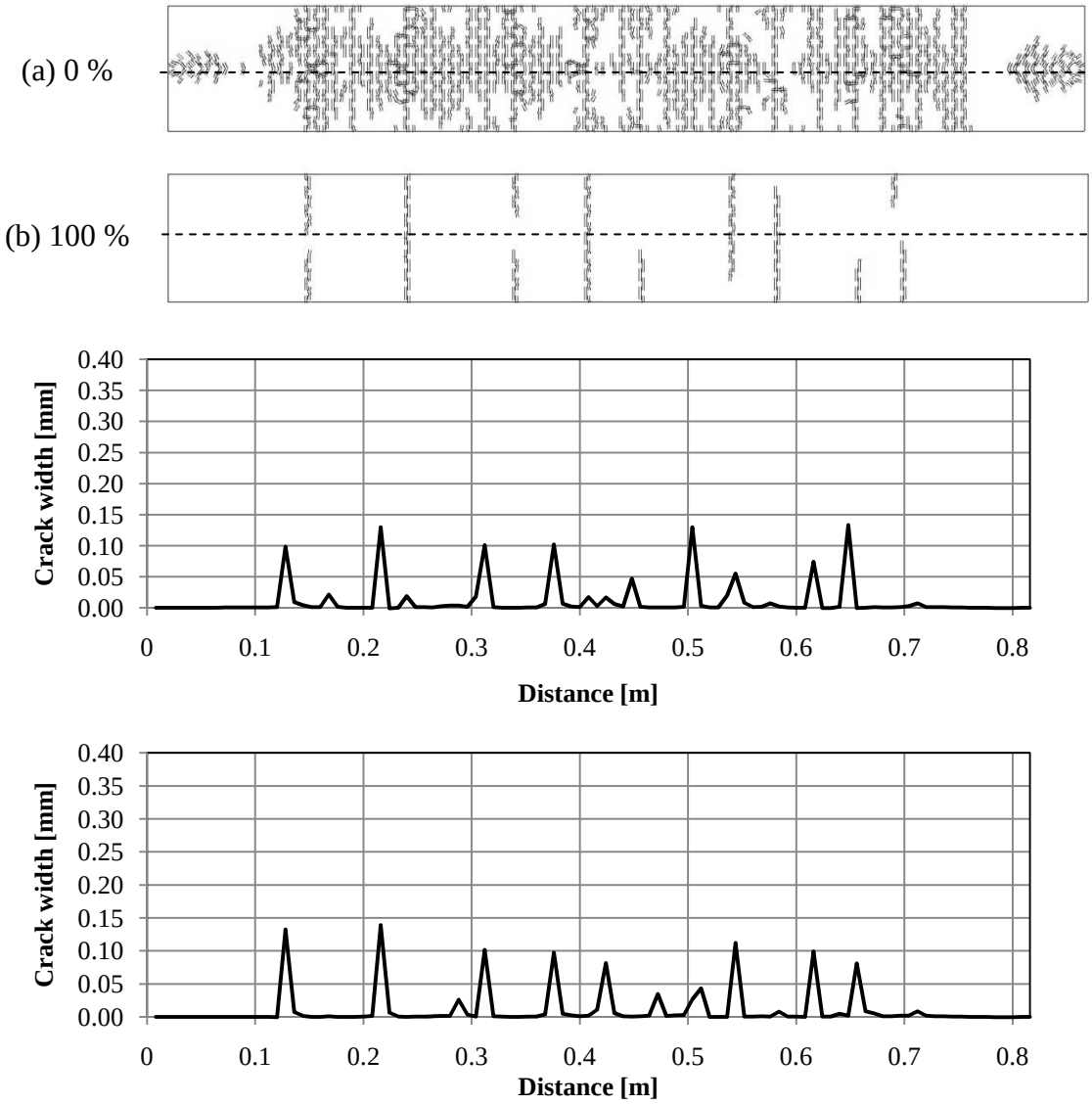

Figure B.2 Crack pattern and crack widths at top (top figure) and bottom surface (bottom figure) of fibre reinforced concrete analyzed with heterogeneous material approach and material properties distribution R2 for u = 1.14 mm.

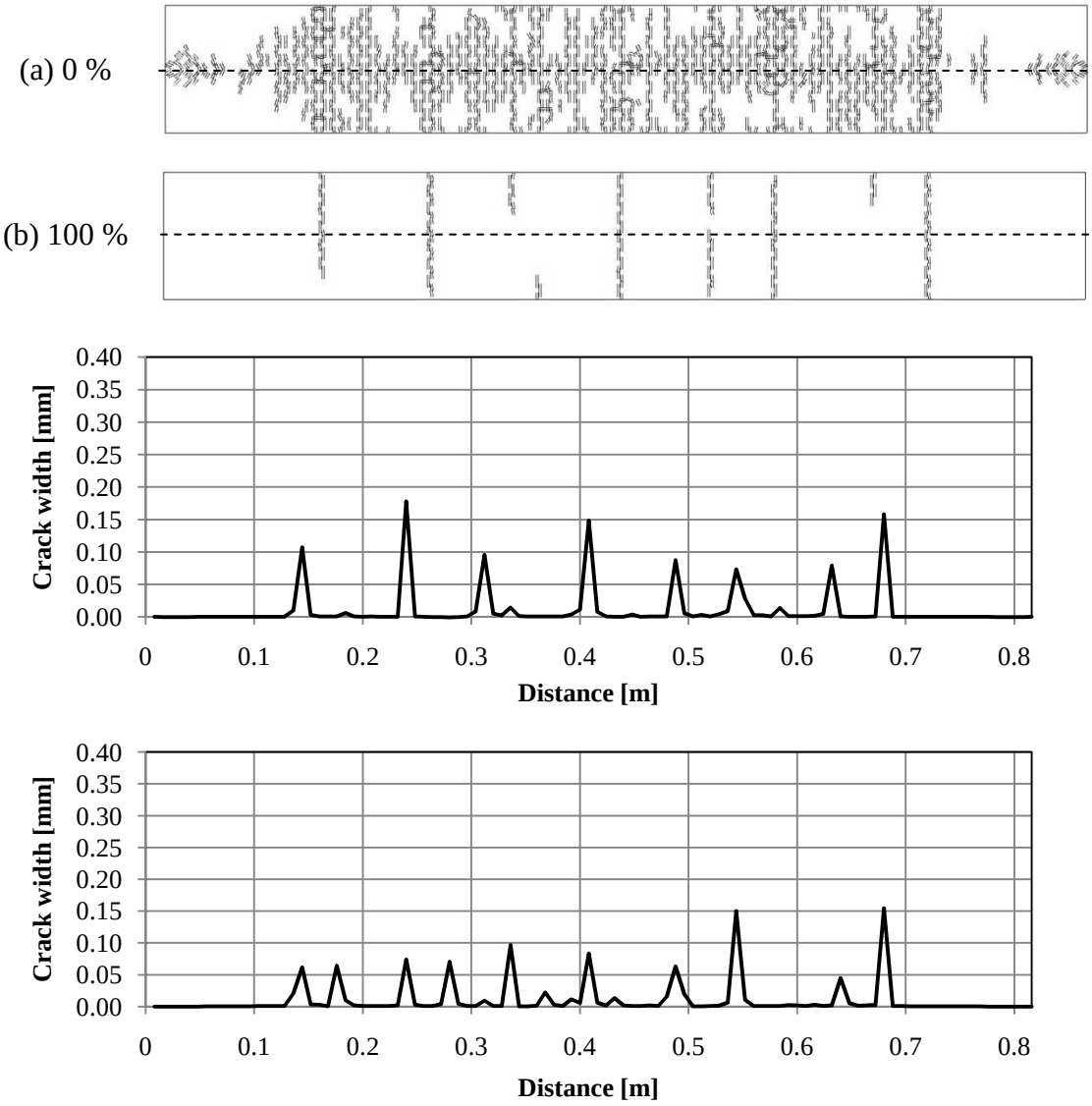

Figure B.3 Crack pattern and crack widths at top (top figure) and bottom surface (bottom figure) of fibre reinforced concrete analyzed with heterogeneous material approach and material properties distribution R3 for u = 1.14 mm.

Appendix C Influence of reinforcement configuration

Two different reinforcement configurations, which can be seen in Figure C.1, for edge beams were analysed by non-linear finite element analyses on edge beams. Results from these analyses are presented in this Appendix.

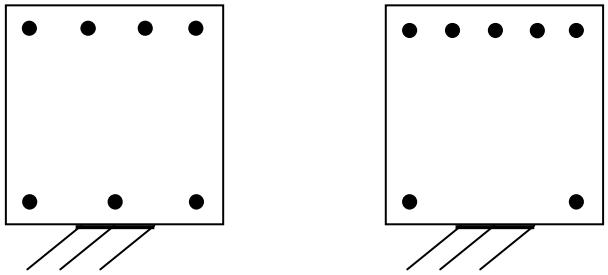

(a) Cross-section 1 (b) Cross-section 2

Figure C.1 Different cross-sections analysed.

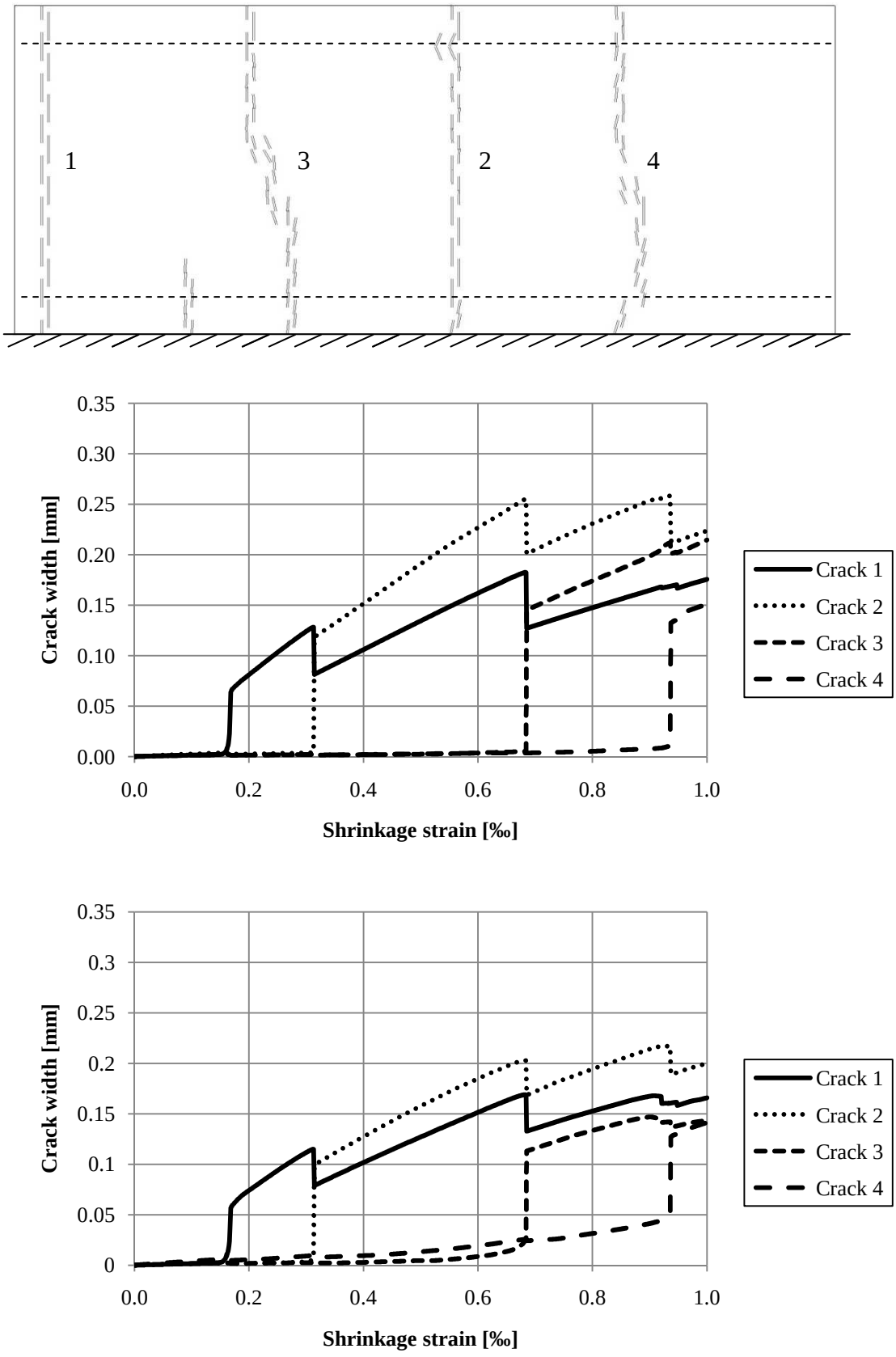

Figure C.2 100 % open cracks pattern at ε_{cs} = 1 ‰ and crack widths at the top (top figure) and bottom reinforcement level (bottom figure) for cross-section 1 with a transversal reinforcement ratio of ρ_t = 0.6 %.

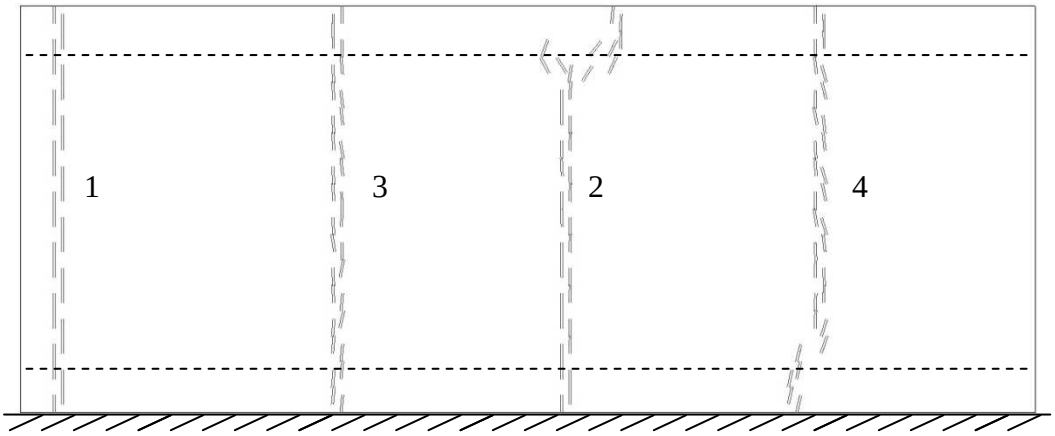

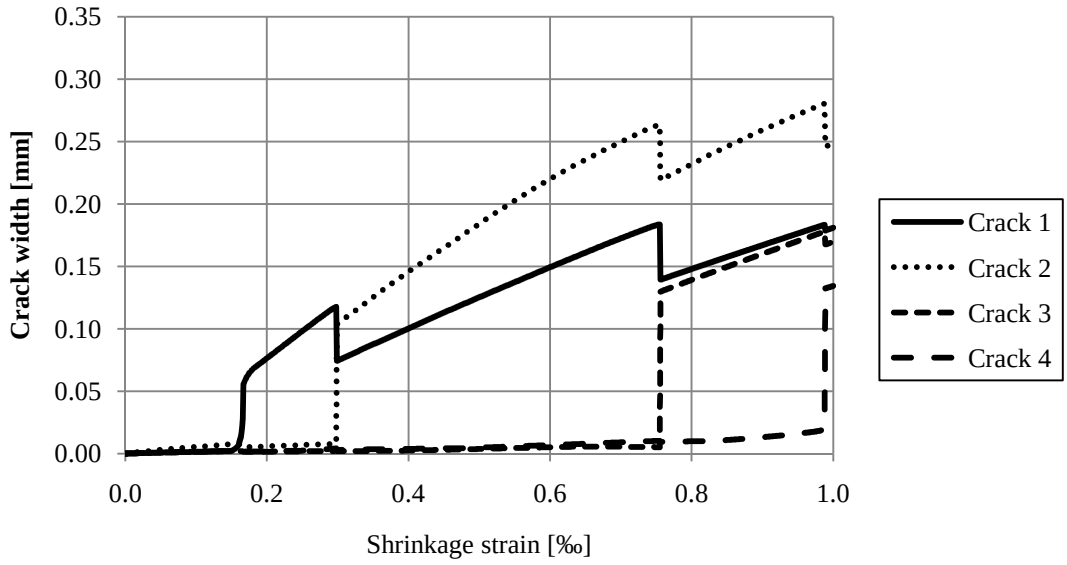

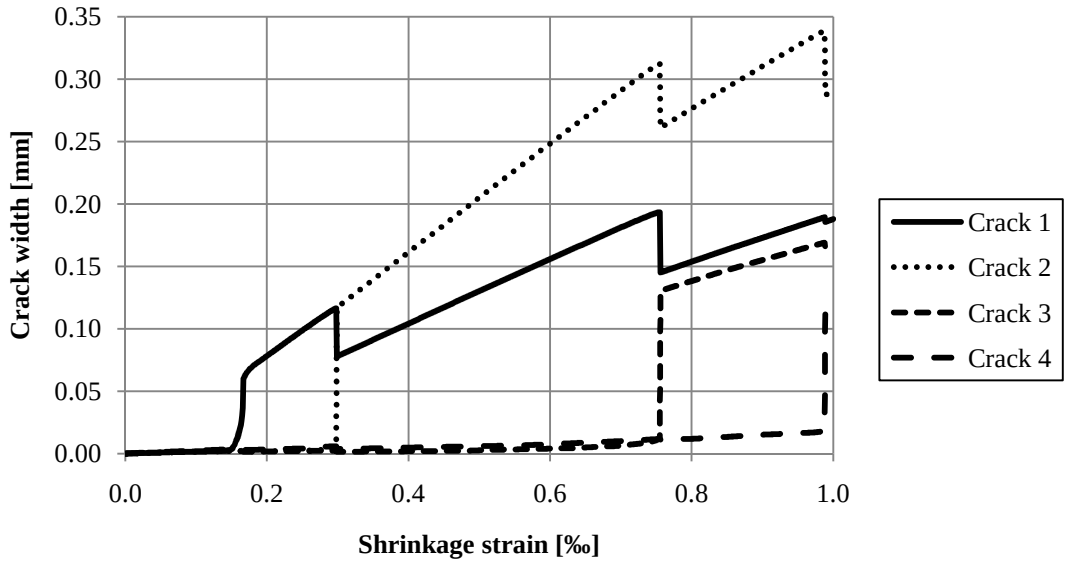

Figure C.3 100 % open cracks pattern at ε_{cs} = 1 ‰ and crack widths at the top (top figure) and bottom reinforcement level (bottom figure) for cross-section 2 with a transversal reinforcement ratio of ρ_t = 0.6 %.

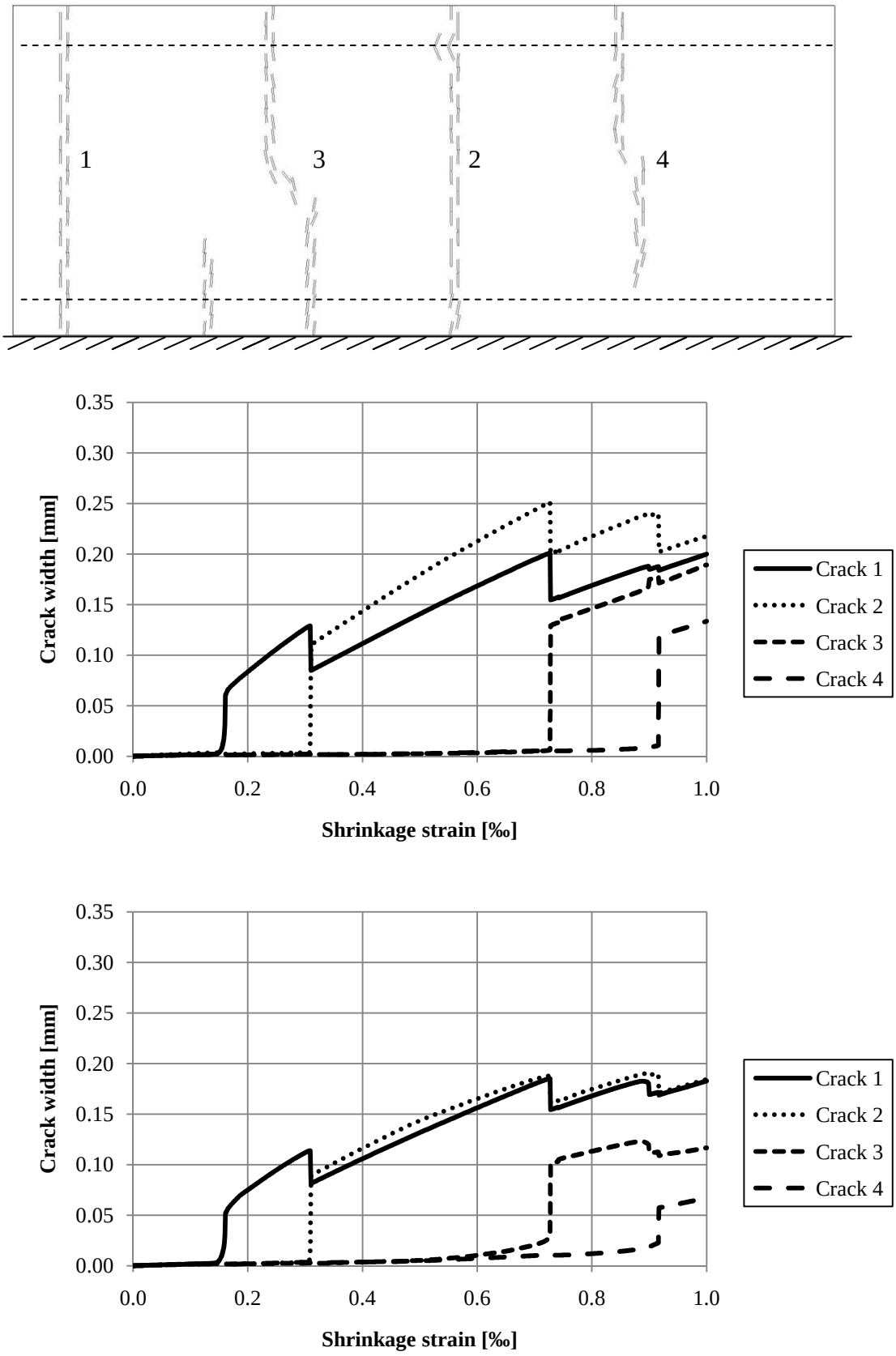

Figure C.4 100 % open cracks pattern at ε_{cs} = 1 ‰ and crack widths at the top (top figure) and bottom reinforcement level (bottom figure) for the cross-section 1 with a transversal reinforcement ratio of ρ_t=1.2 %.

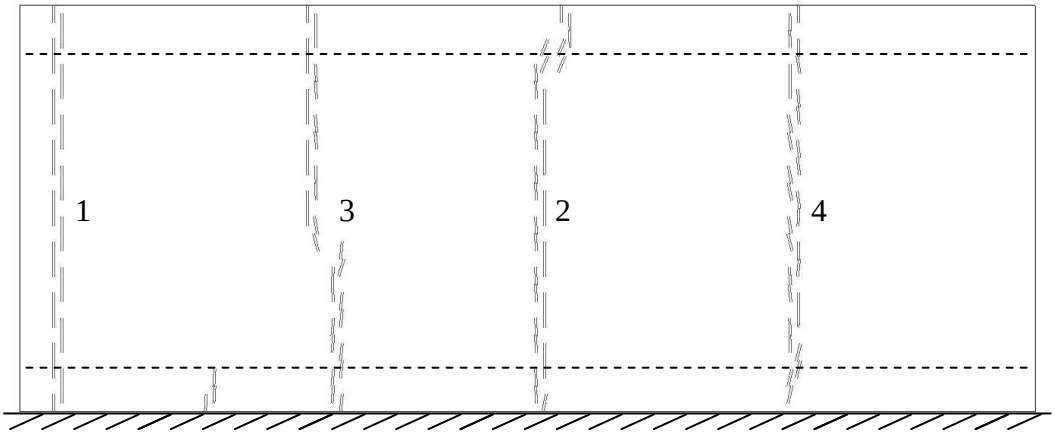

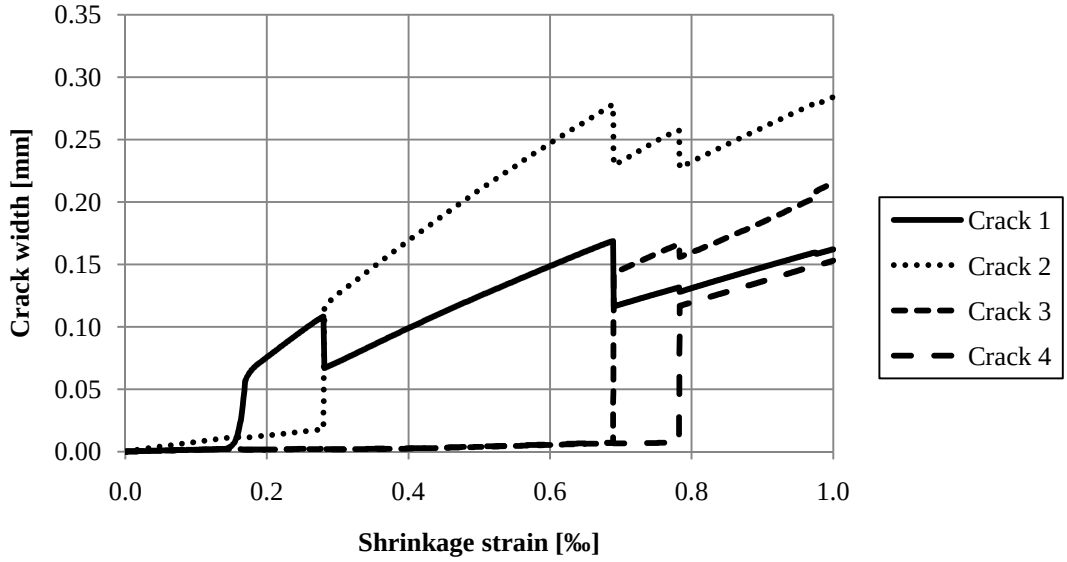

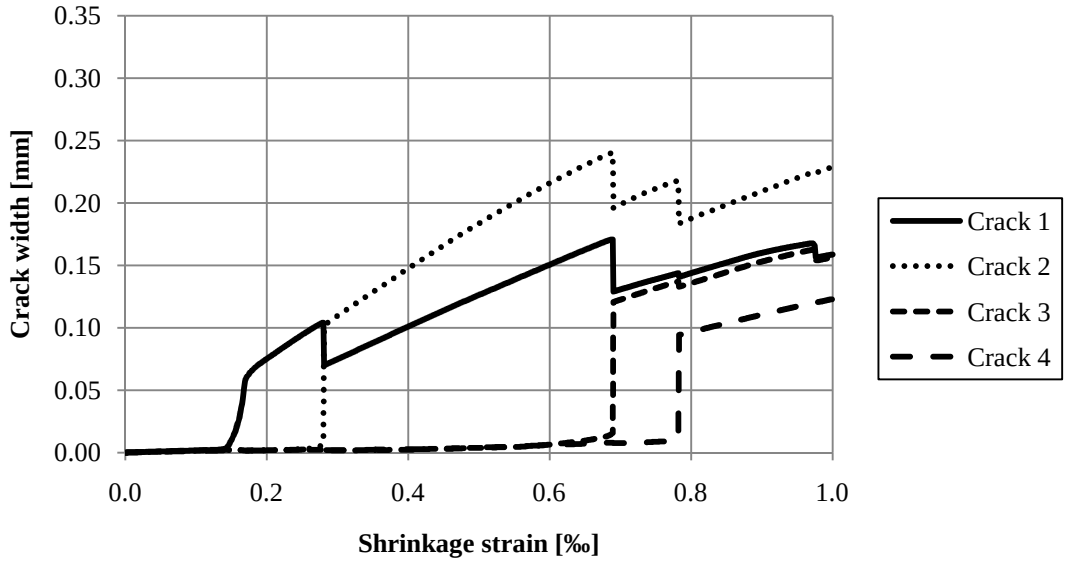

Figure C.5 100 % open cracks pattern at ε_{cs} = 1 ‰ and crack widths at the top (top figure) and bottom reinforcement level (bottom figure) for cross-section 2 with a transversal reinforcement ratio of ρ_t=1.2 %.

Appendix D Influence of bar diameter

In this Appendix, results from non-linear finite element analyses carried out on edge beams with different reinforcement diameters are shown. Longitudinal reinforcement ratio was kept constant by changing the total amount of bars for each case studied. Results for a bar diameter of 16 mm are not presented in this Appendix as they were already shown in Appendix C for cross-section 1 with transversal reinforcement ratio of ρ_t = 0.6 %.

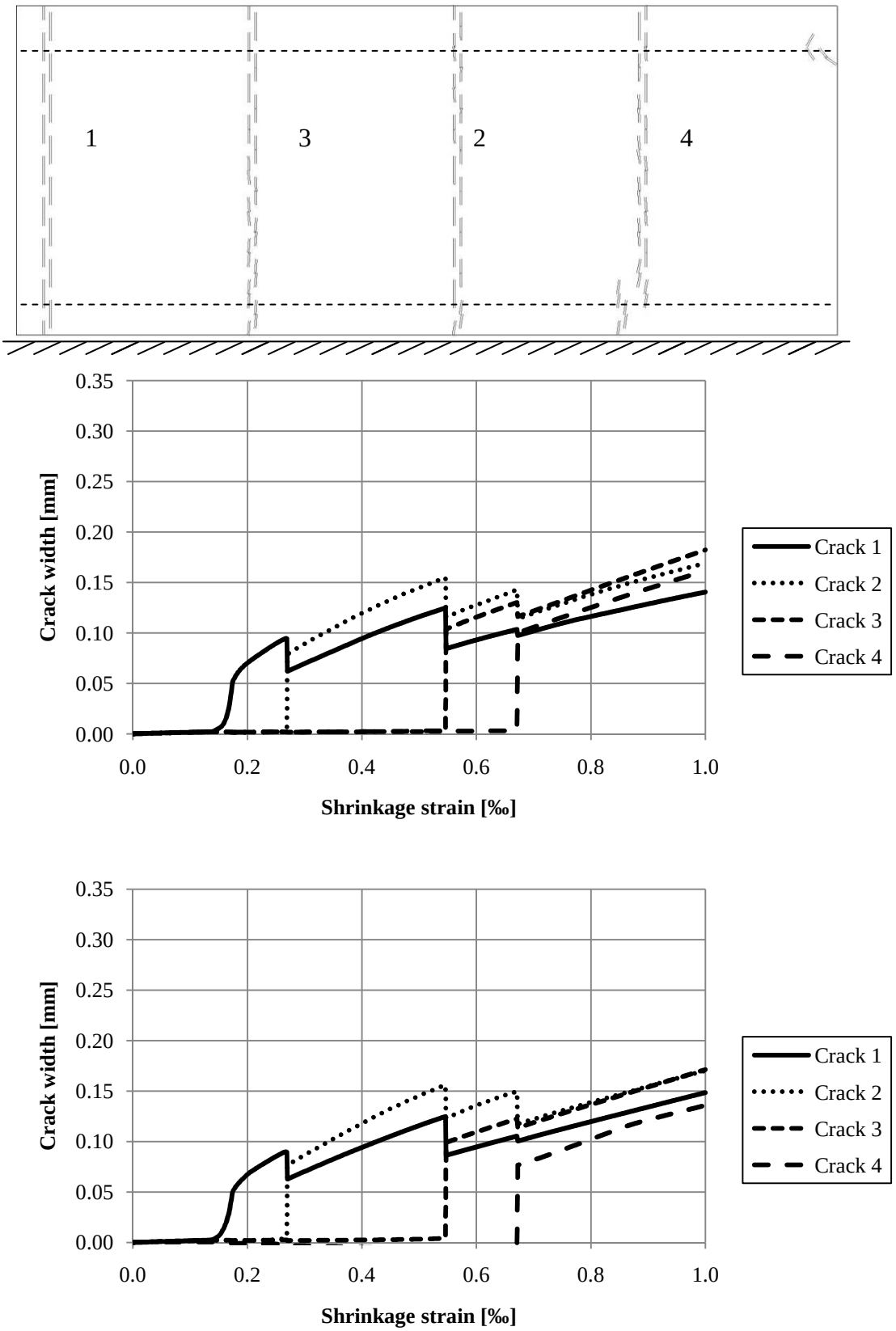

Figure D.1 100 % open cracks pattern at ε_{cs} = 1 ‰ and crack widths at the top (top figure) and bottom reinforcement level (bottom figure) when diameter of the bars is 8 mm.

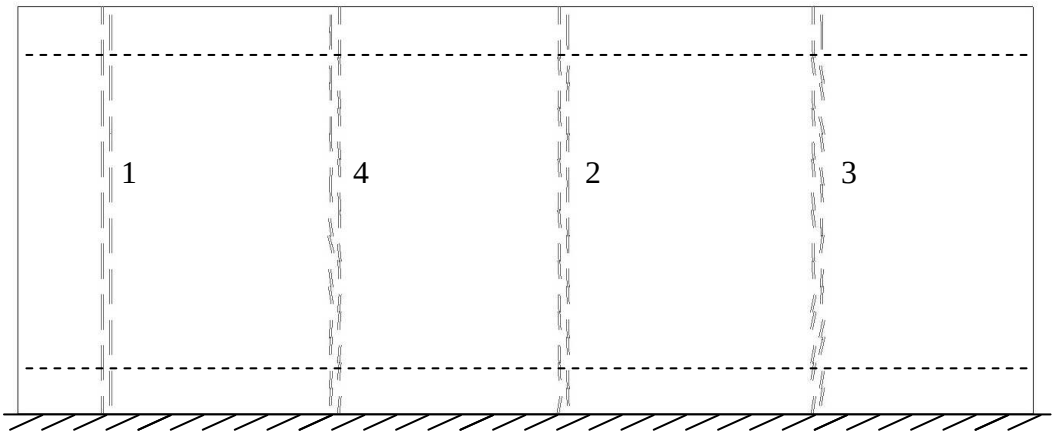

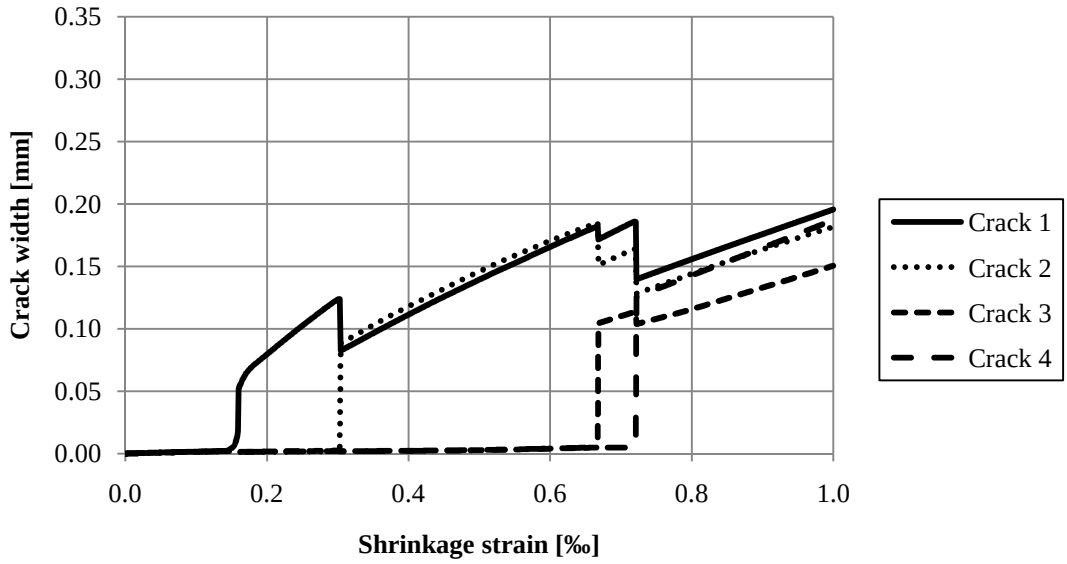

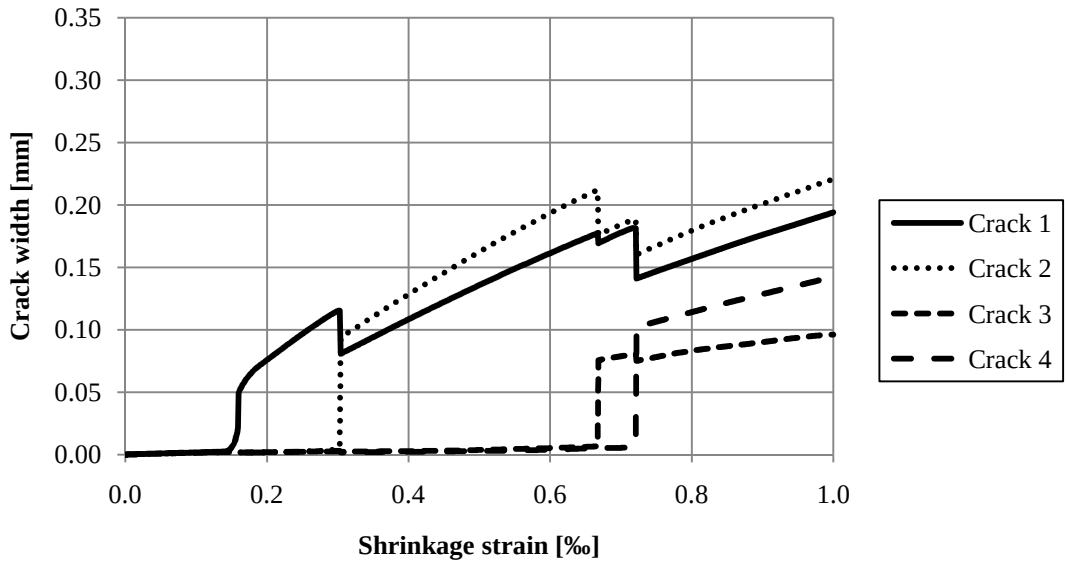

Figure D.2 100 % open cracks pattern at ε_{cs} = 1 ‰ and crack widths at the top (top figure) and bottom reinforcement level (bottom figure) when diameter of the bars is 10 mm.

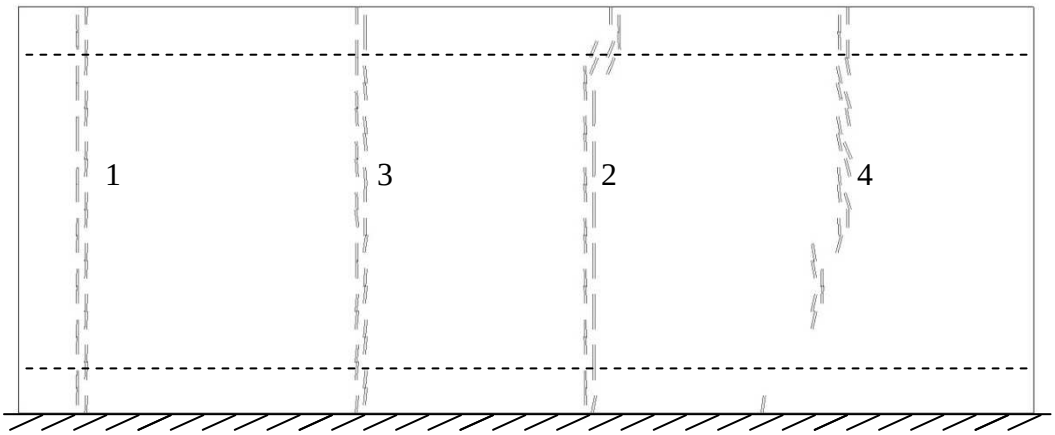

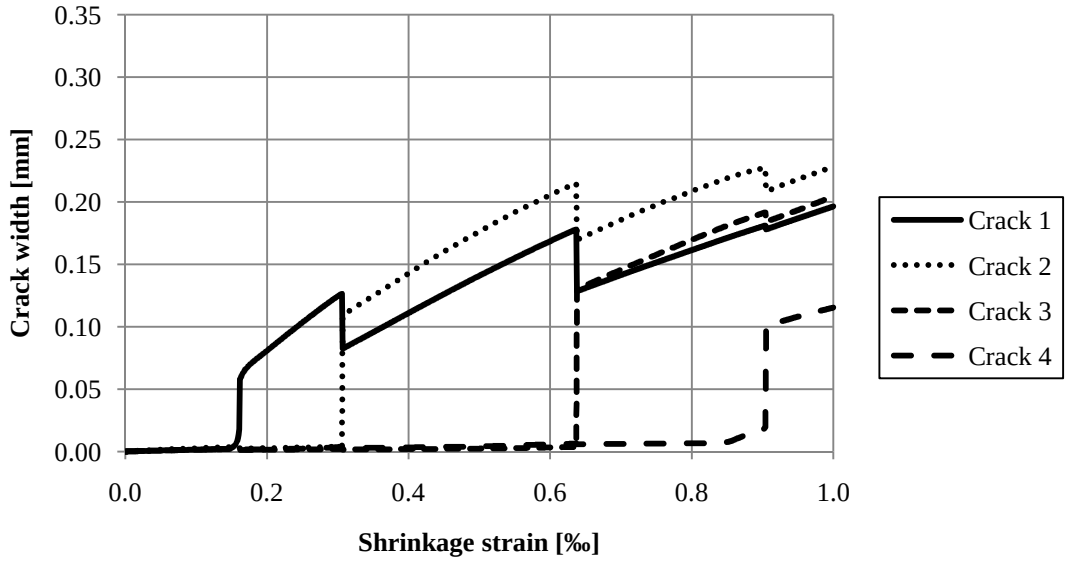

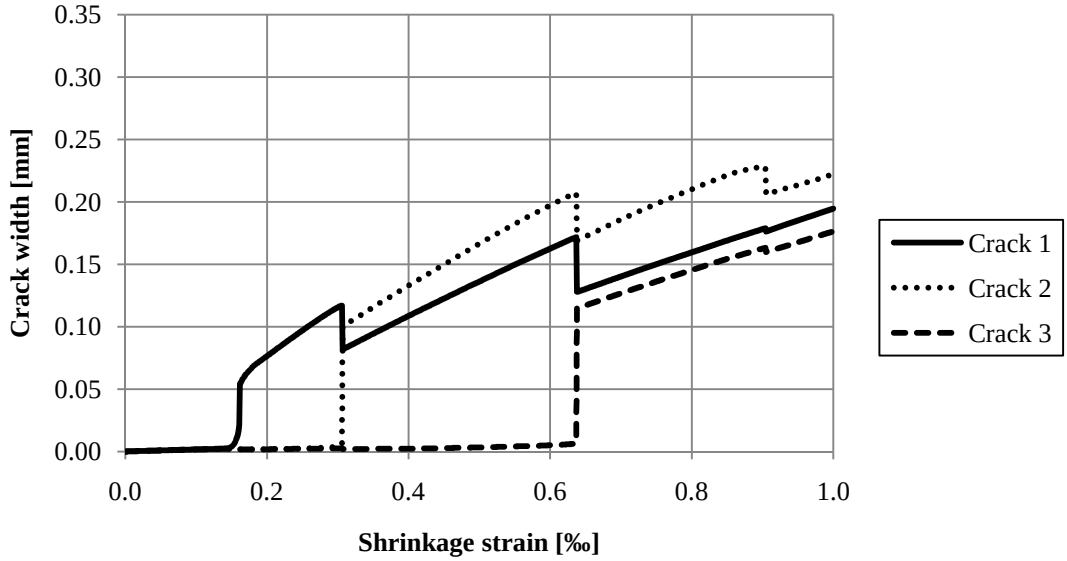

Figure D.3 100 % open cracks pattern at ε_{cs} = 1 ‰ and crack widths at the top (top figure) and bottom reinforcement level (bottom figure) when diameter of the bars is 12 mm.

Appendix E Influence of concrete cover

Results from analyses concerning influence of concrete cover in edge beams are shown in this Appendix. It should be stated that values of a_s presented do not directly correspond to the depth of the concrete cover, but to the distance from the edges to the reinforcement level, as shown in Figure E.1. Half of the diameter of the bar should be subtracted from this value in order to get the real value of the concrete cover.

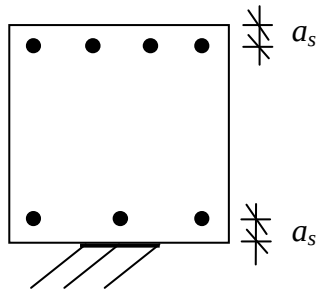

Figure E.1 Definition of the distance to the reinforcement level, a_s.

Results for a_s = 50 mm are not shown in this Appendix as they were previously presented in Appendix C for the case with cross-section 1 with transversal reinforcement ratio of ρ_t = 0.6 %.

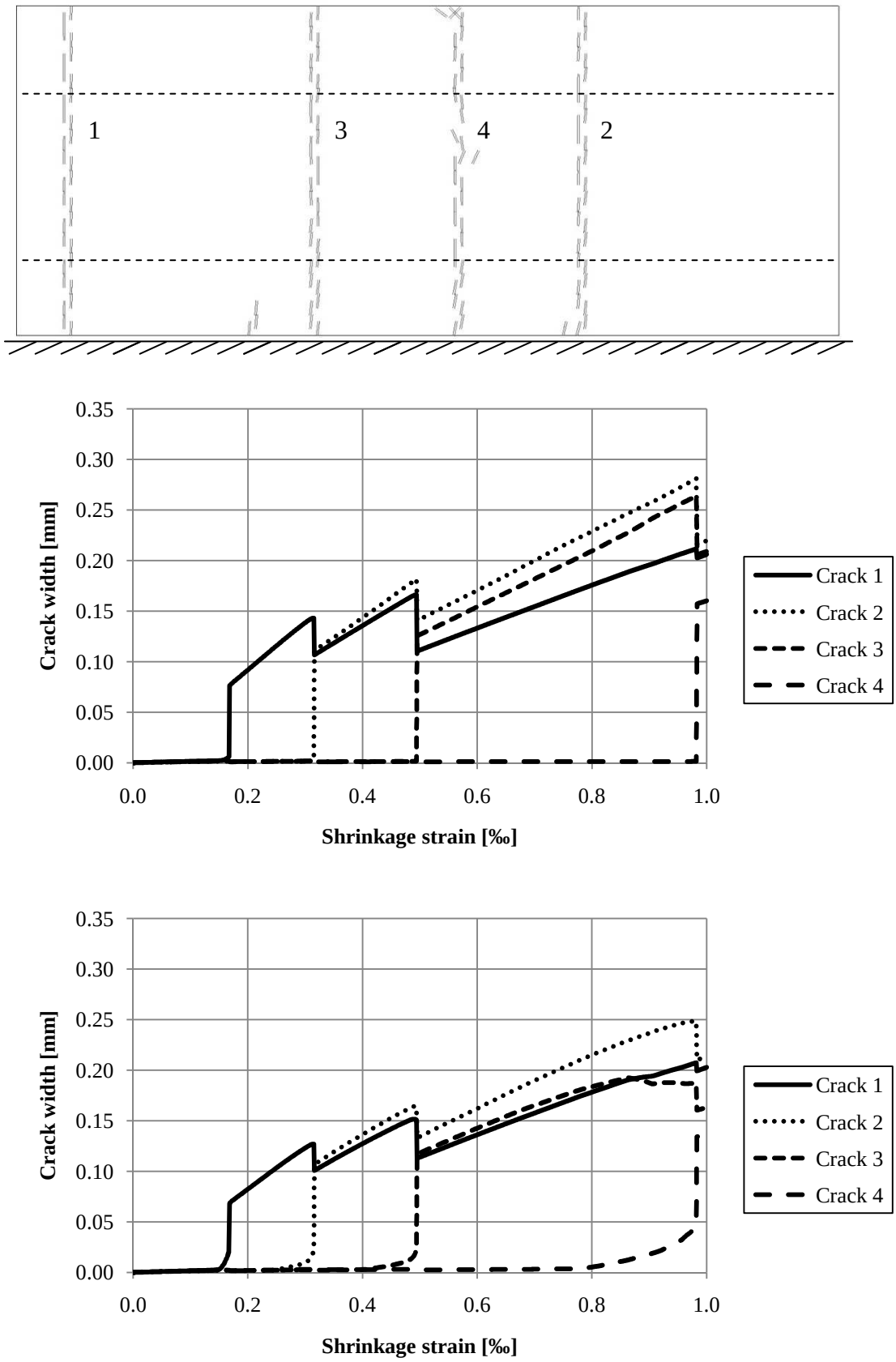

Figure E.2 100 % open cracks pattern at ε_{cs} = 1 ‰ and crack widths at 50 mm from top (top figure) and bottom concrete edge (bottom figure) for a_s = 100 mm.

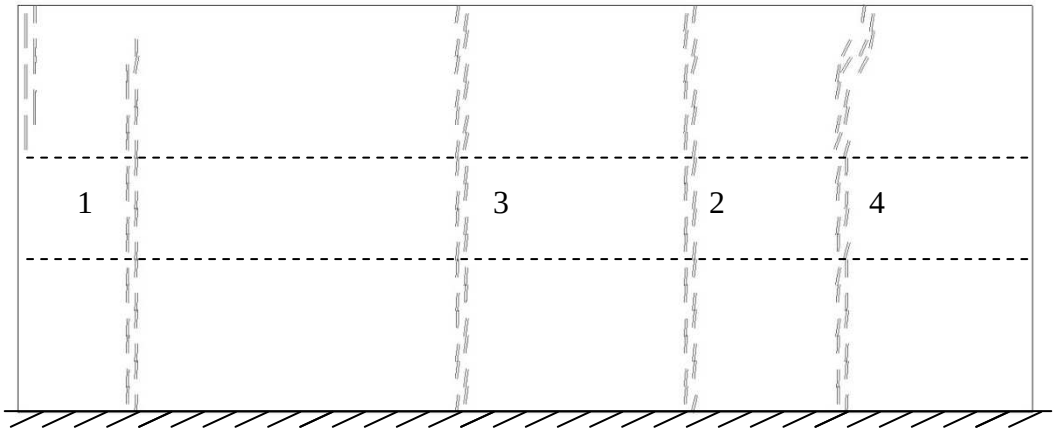

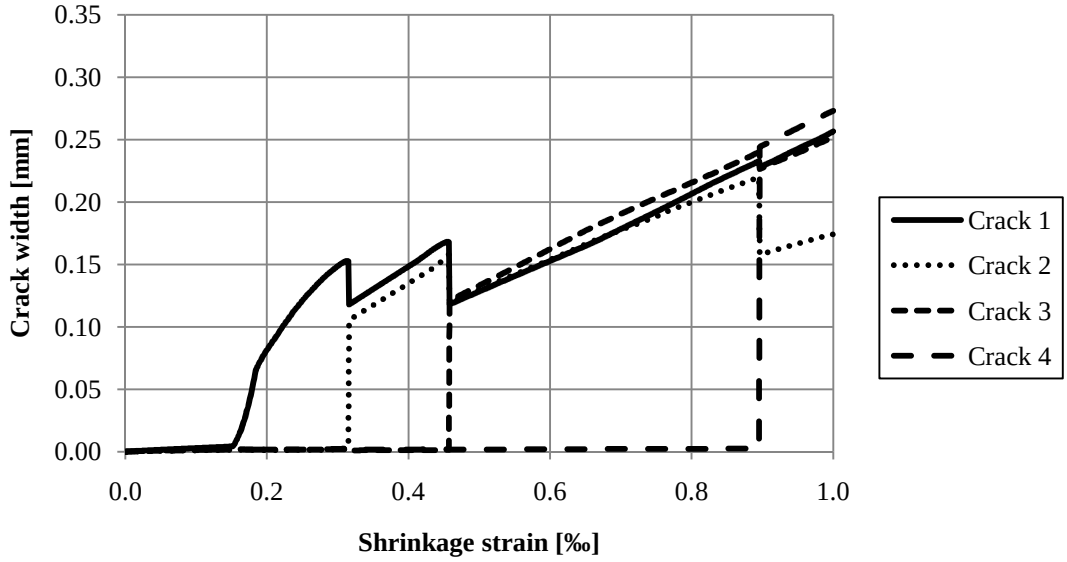

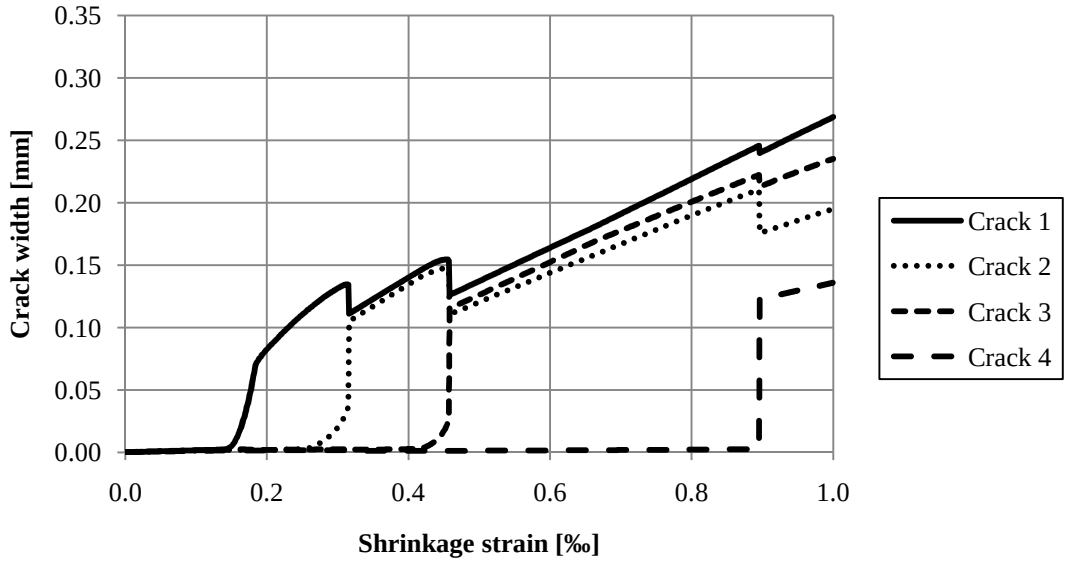

Figure E.3 100 % open cracks pattern at ε_{cs} = 1 ‰ and crack widths at 50 mm from top (top figure) and bottom concrete edge (bottom figure) for a_s = 150 mm.

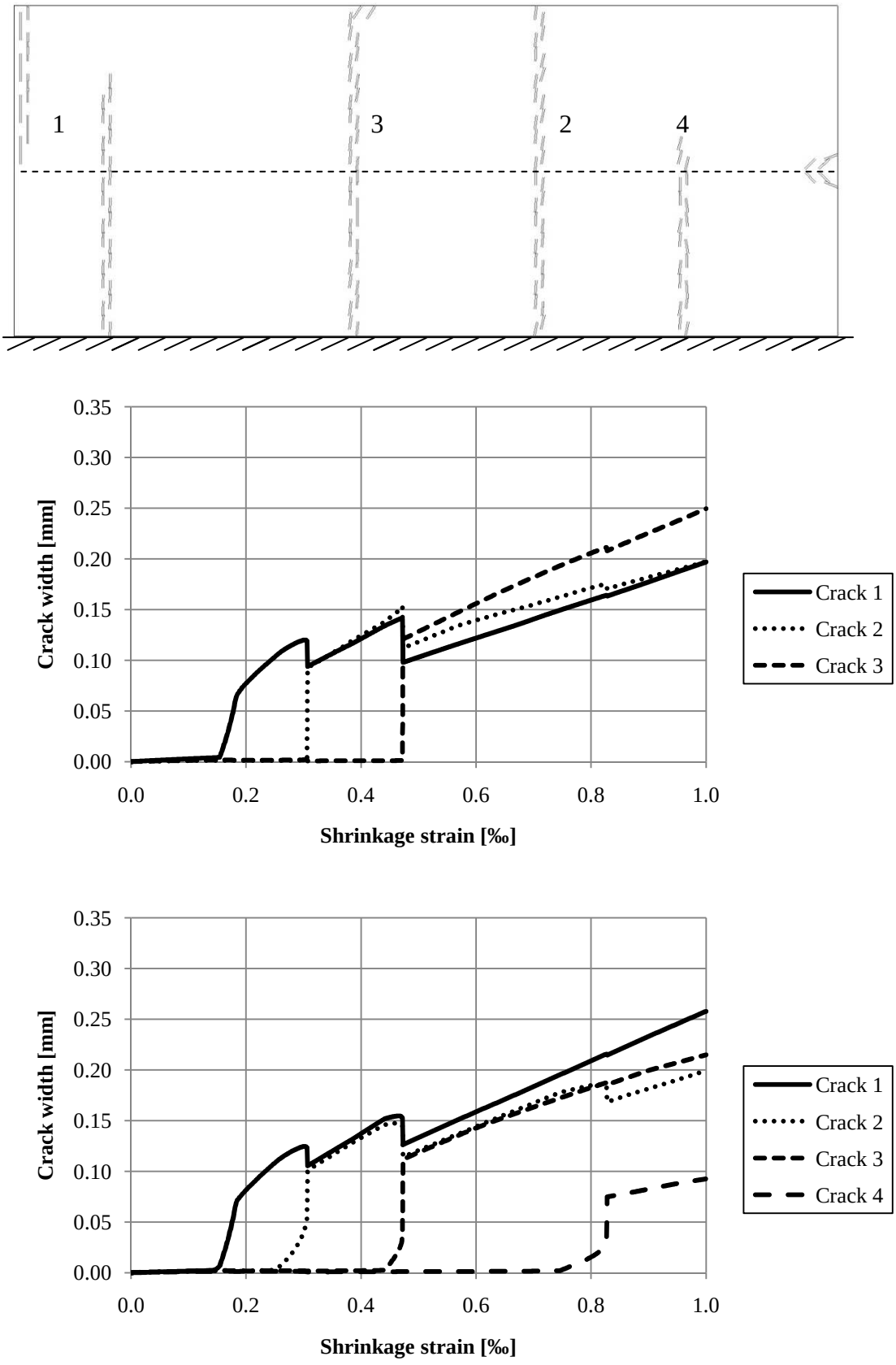

Figure E.4 *100 % open cracks pattern at ε_{cs} = 1 ‰ and crack widths at 50 mm from top (top figure) and bottom concrete edge (bottom figure) for a_s = 200 mm.*

Appendix F Influence of fracture energy

In this Appendix results from finite element analyses on edge beams with different fracture energies are presented. Crack width graphs for *GF* = 100 N/m are not shown in this Appendix as they were previously presented in Appendix C for the case with cross-section 1 with transversal reinforcement ratio of ρ_t = 0.6 %.

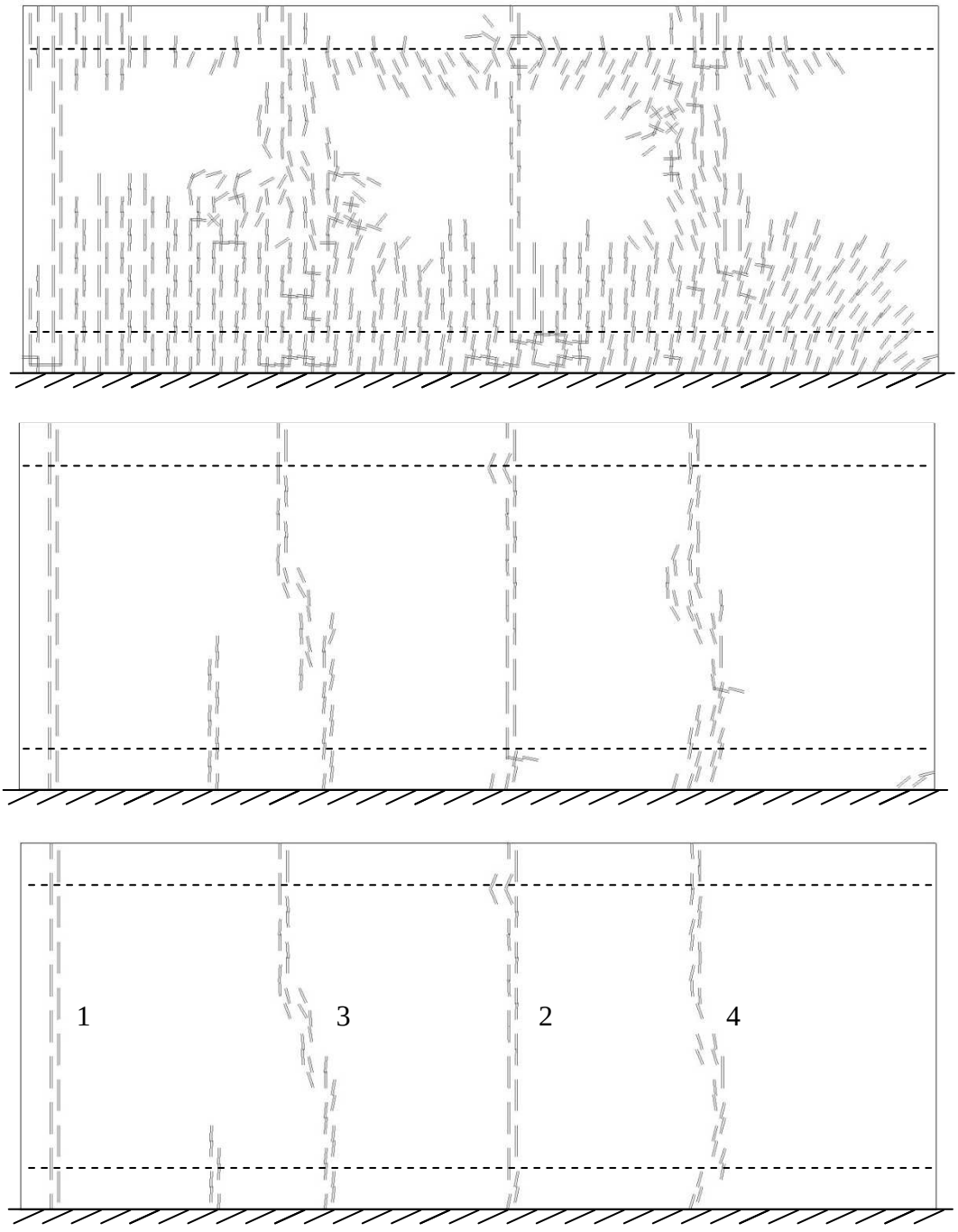

Figure F.1 Crack pattern at ε_{cs} = 1 ‰ for 0, 33 and 100 % fully developed cracks for G_f = 100 N/m.

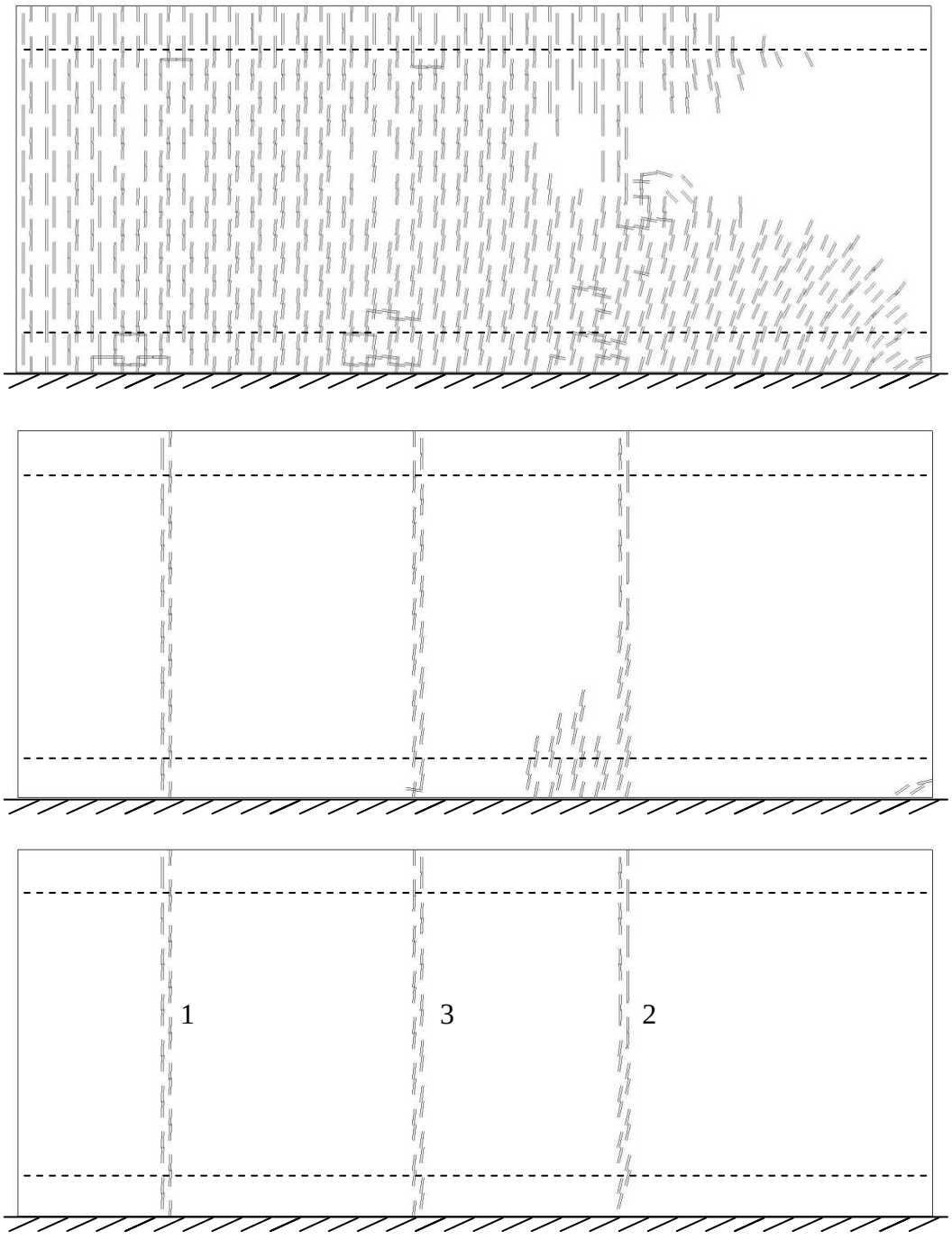

Figure F.2 Crack pattern at ε_{cs} = 1 ‰ for 0, 33 and 100 % fully developed cracks for G_f = 250 N/m.

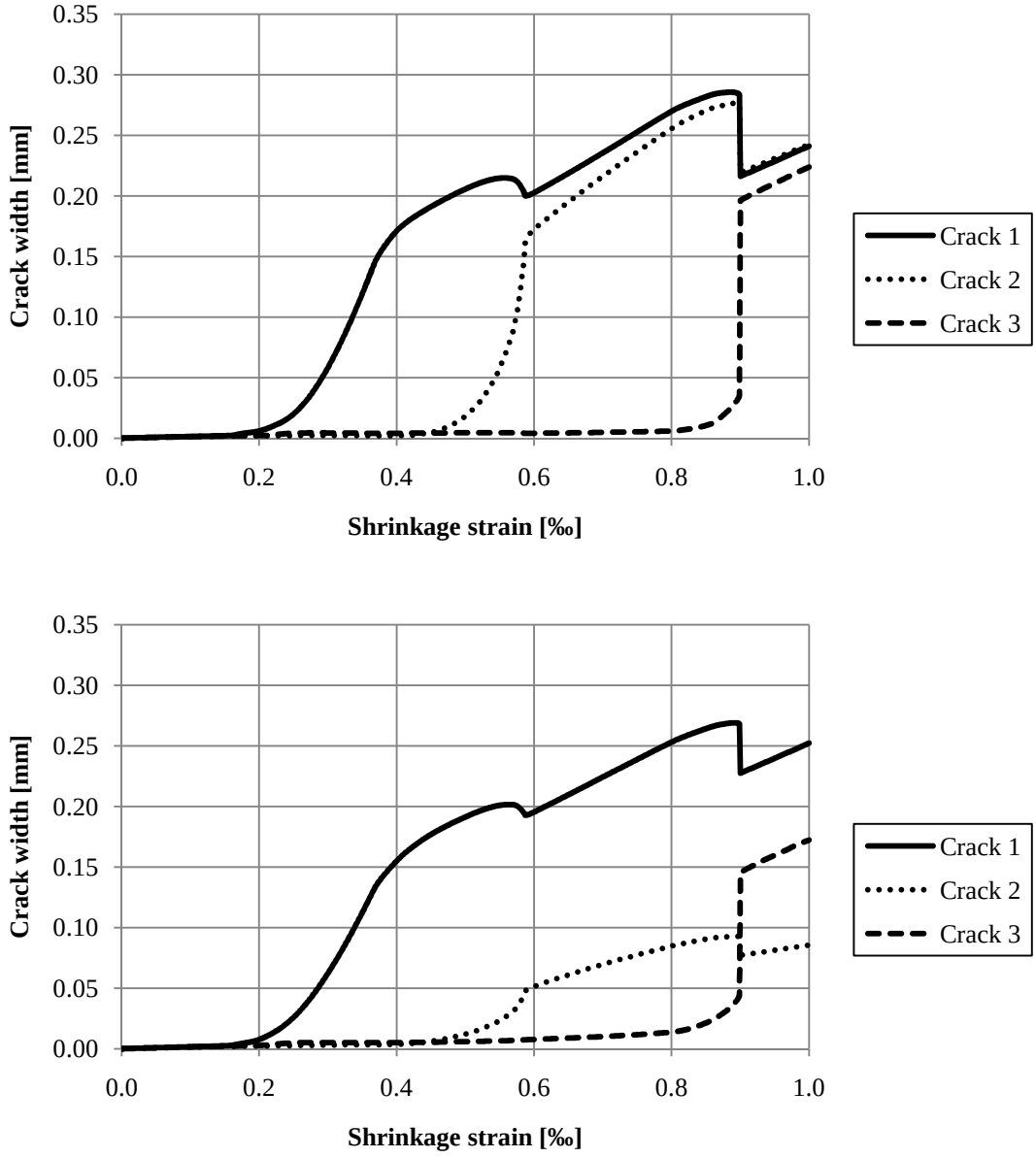

Figure F.3 Crack widths at top (top figure) and bottom reinforcement level (bottom figure) for G_f = 250 N/m.

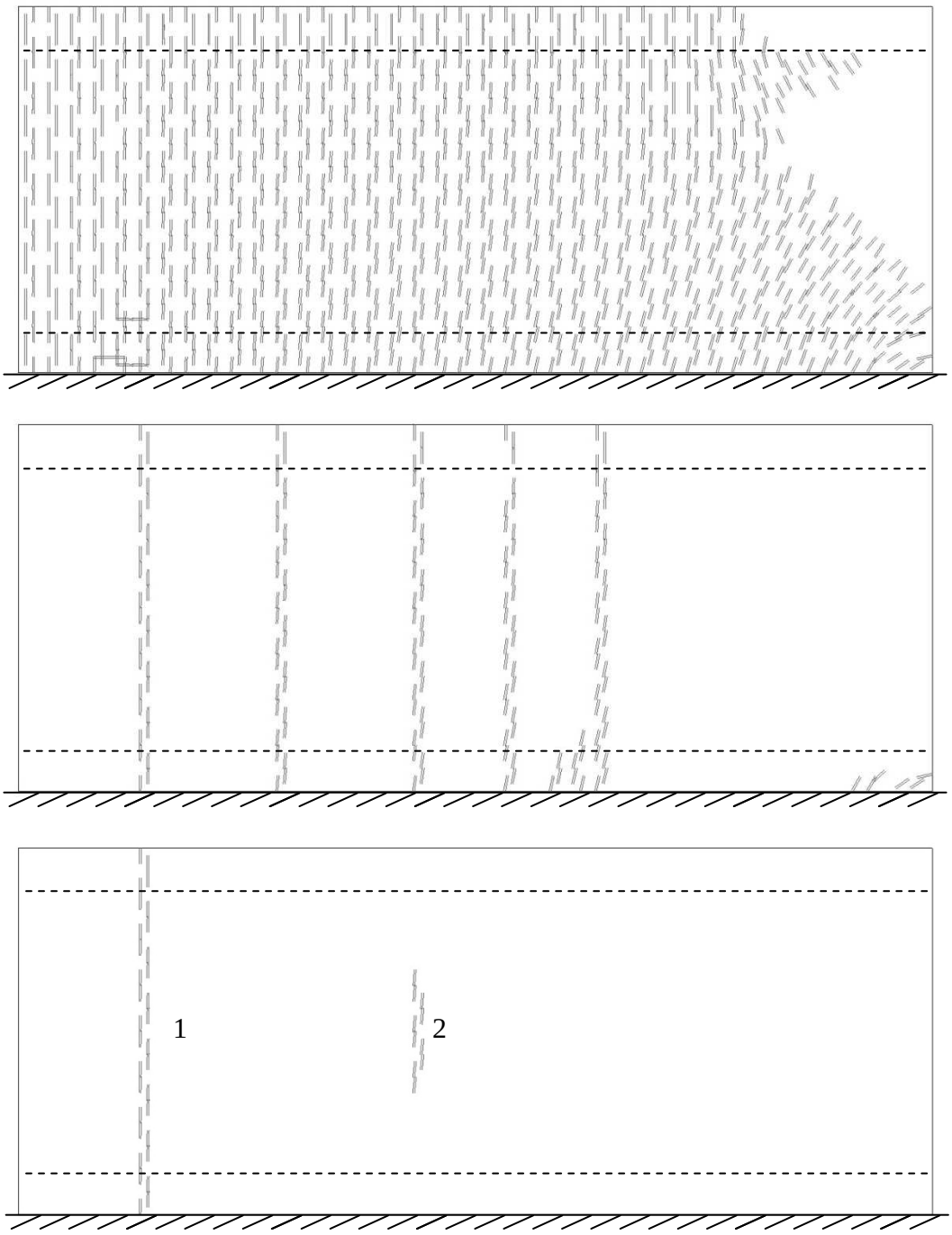

Figure F.4 Crack pattern at ε_{cs} = 1 ‰ for 0, 33 and 100 % fully developed cracks for G_f = 375 N/m.

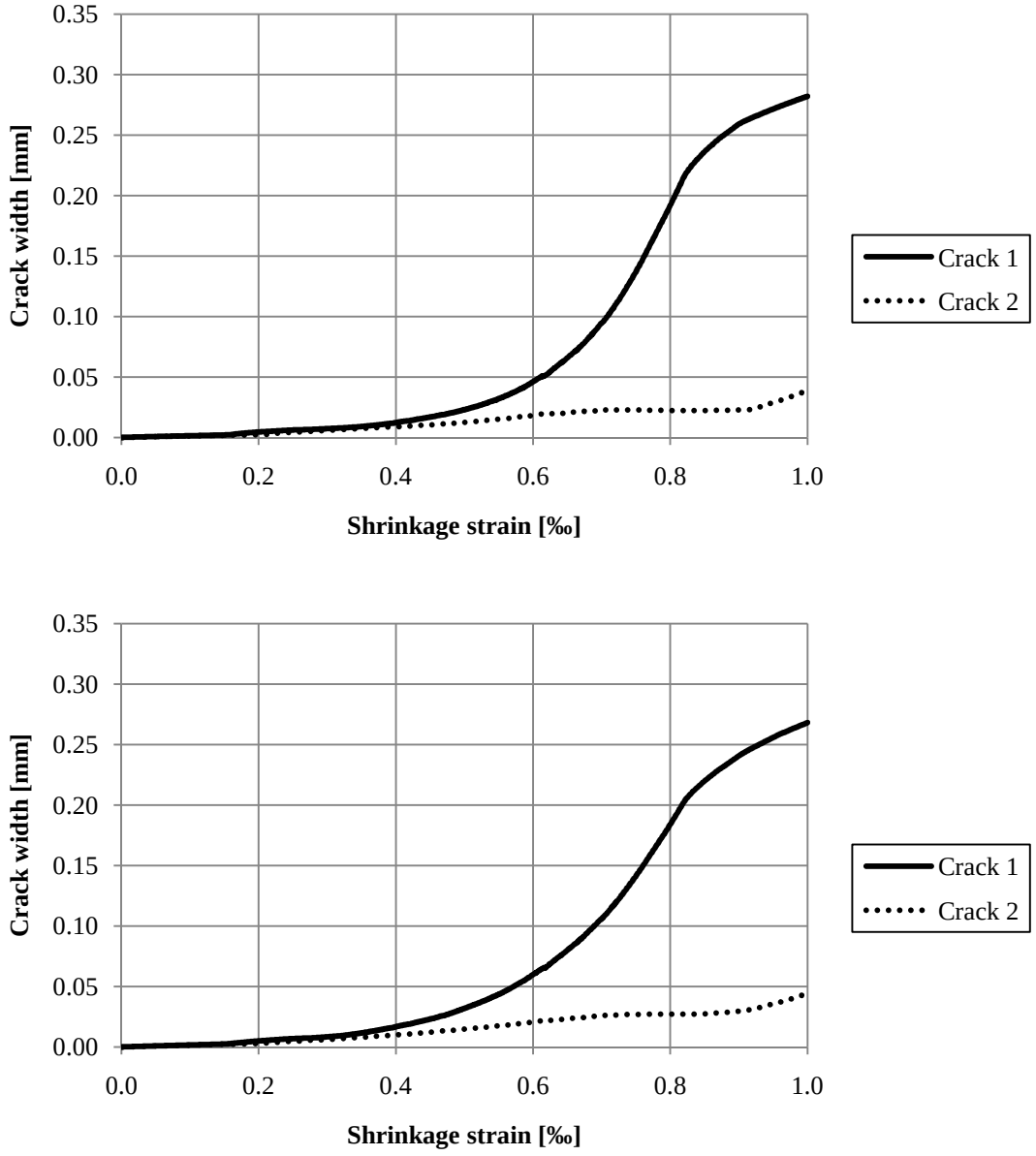

Figure F.5 Crack widths at top (top figure) and bottom reinforcement level (bottom figure) for G_f = 375 N/m.

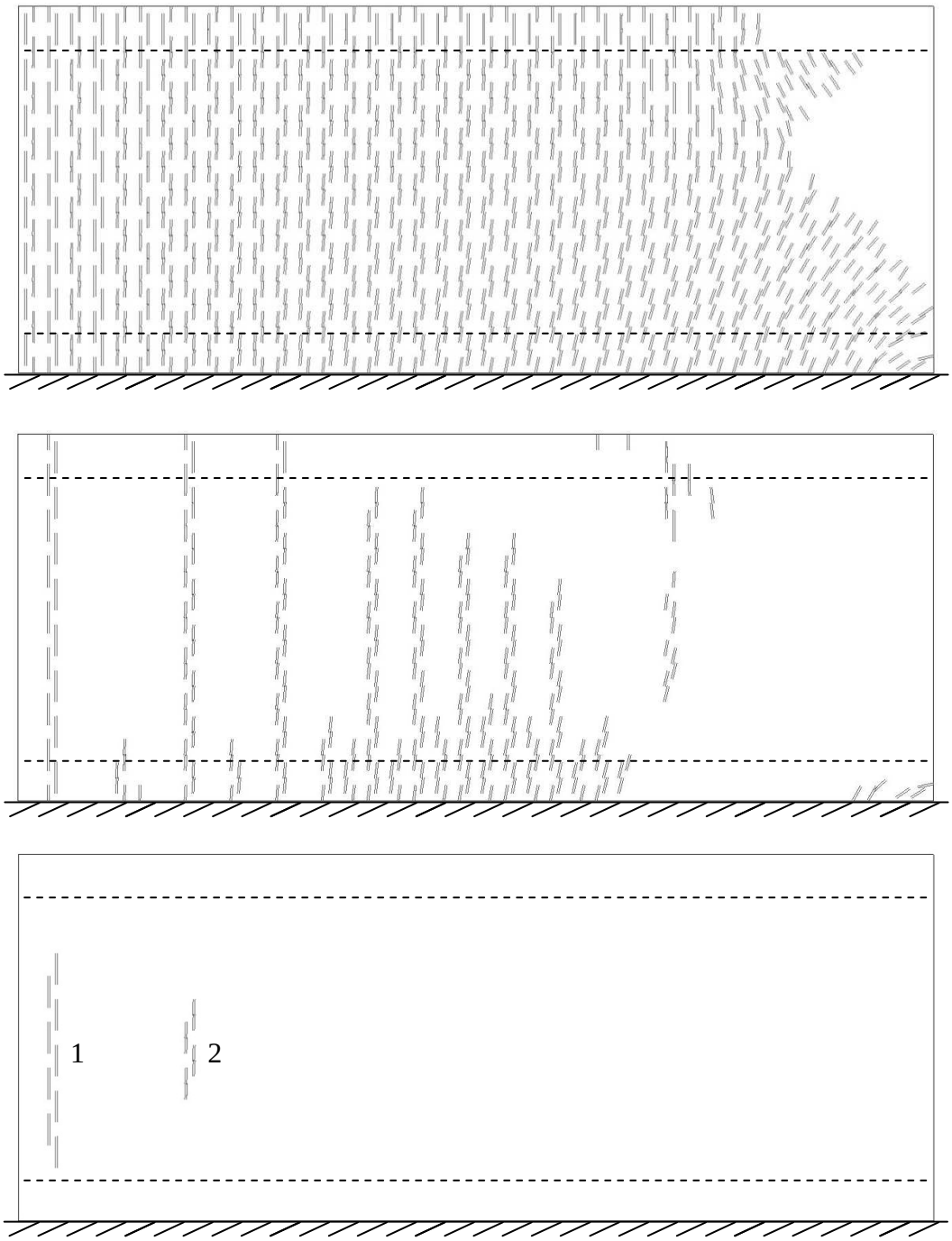

Figure F.6 Crack pattern at ε_{cs} = 1 ‰ for 0, 33 and 100 % fully developed cracks for G_f = 500 N/m.

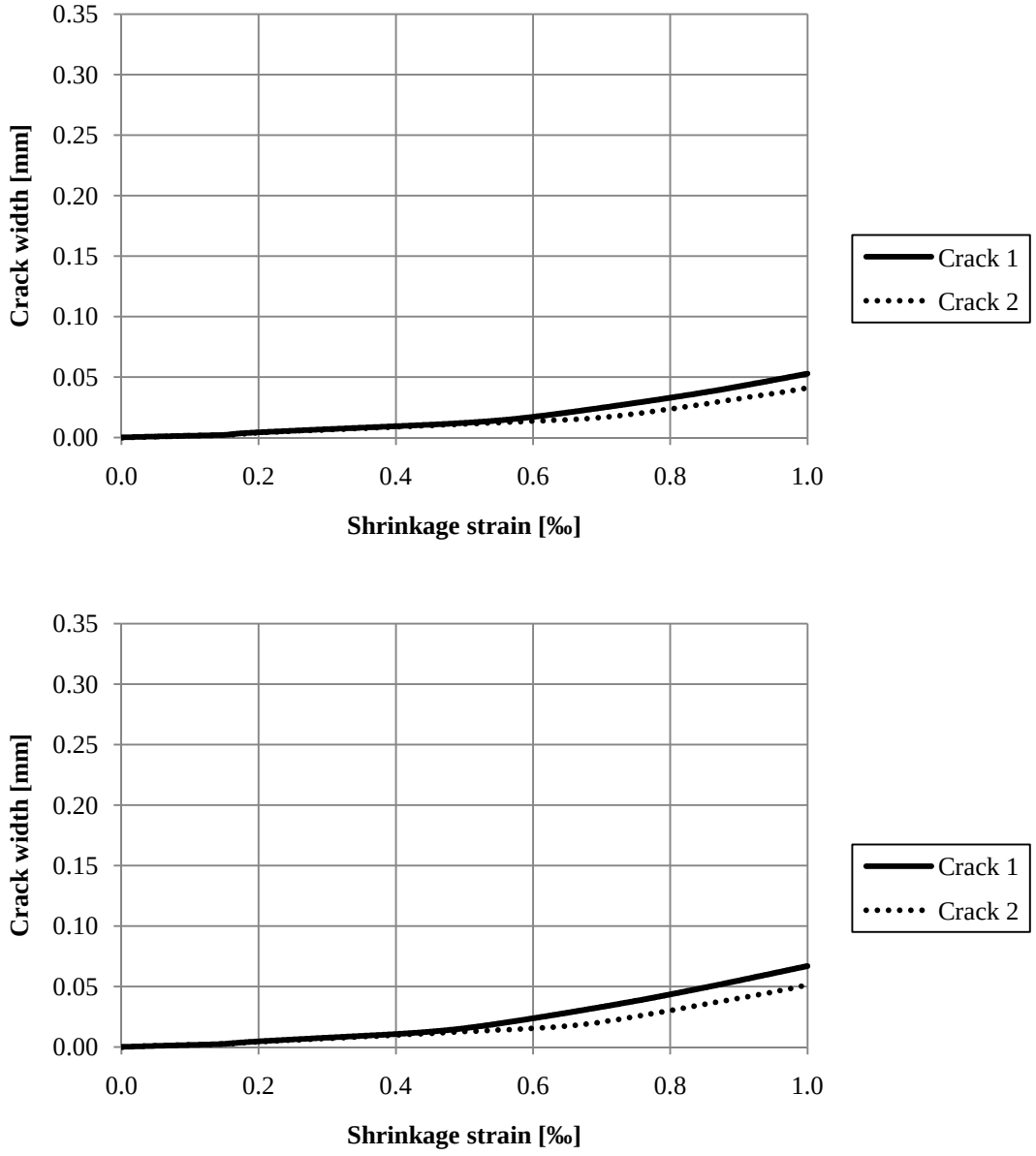

Figure F.7 Crack widths at top (top figure) and bottom reinforcement level (bottom figure) for G_f = 500 N/m.

Appendix G Influence of fibre reinforcement on edge beam

Results from non-linear finite element analyses using the heterogeneous material approach for edge beams are shown in this Appendix. Effect of adding fibre reinforcement is analysed for both reinforced and unreinforced edge beams. Results for the ordinarily reinforced edge beam are not shown in this Appendix as they were previously presented in Appendix C for the case with cross-section 1 with transversal reinforcement ratio of ρ_t = 0.6 %.

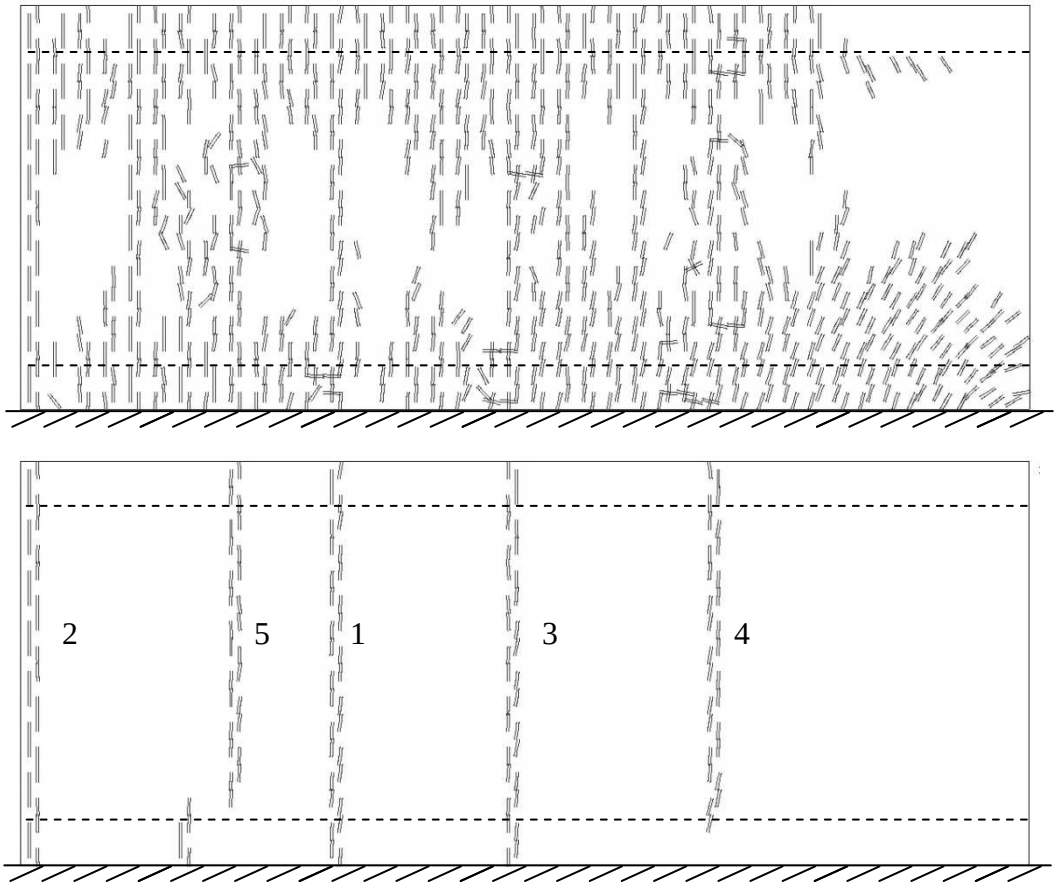

Figure G.1 Crack pattern at ε_{cs} = 1 ‰ for 0 and 100 % fully developed cracks for fibre reinforced concrete with cross-section 1.

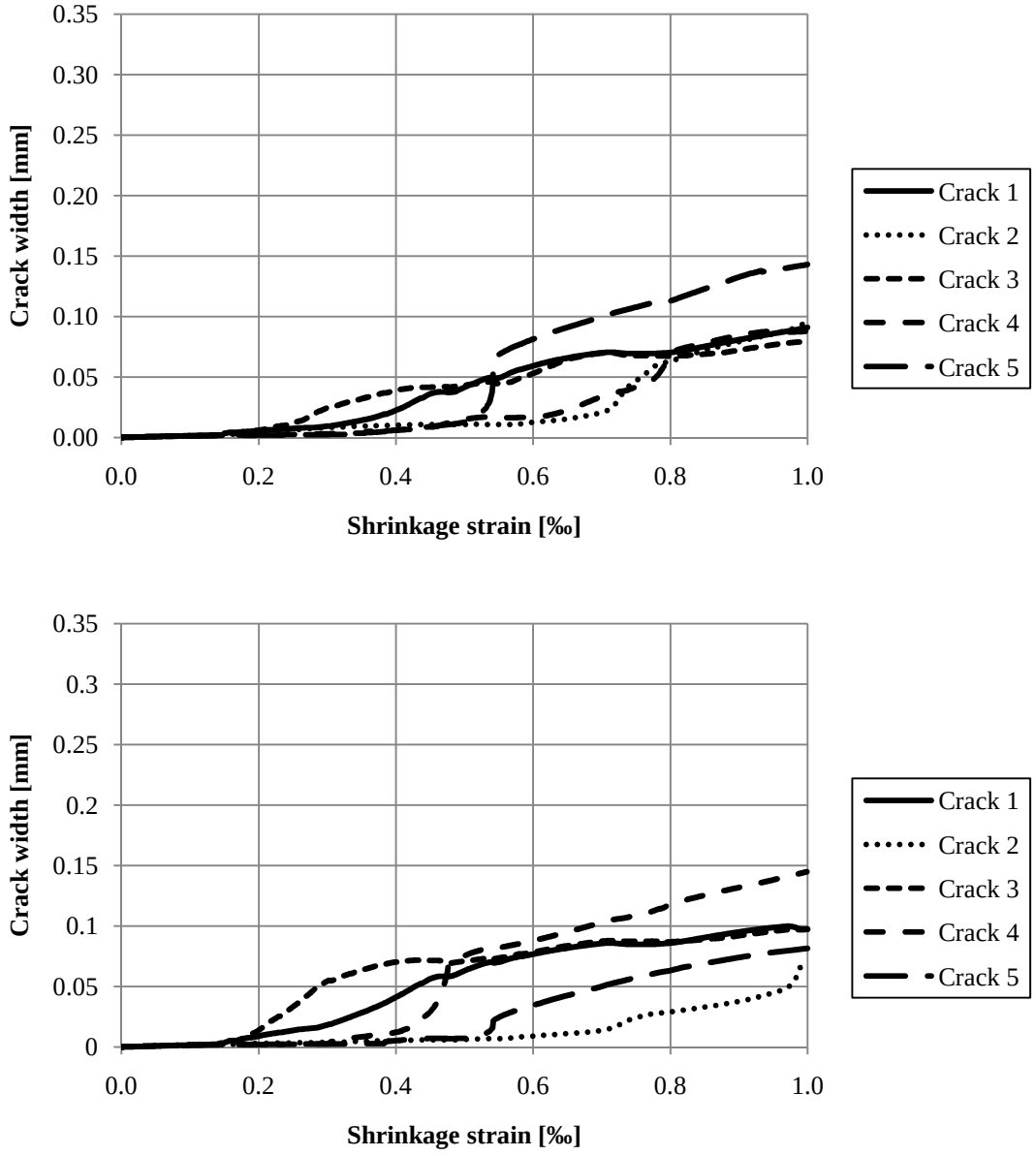

Figure G.2 Crack widths at the top (top figure) and bottom reinforcement level (bottom figure), respectively, for fibre reinforced concrete with cross-section 1.

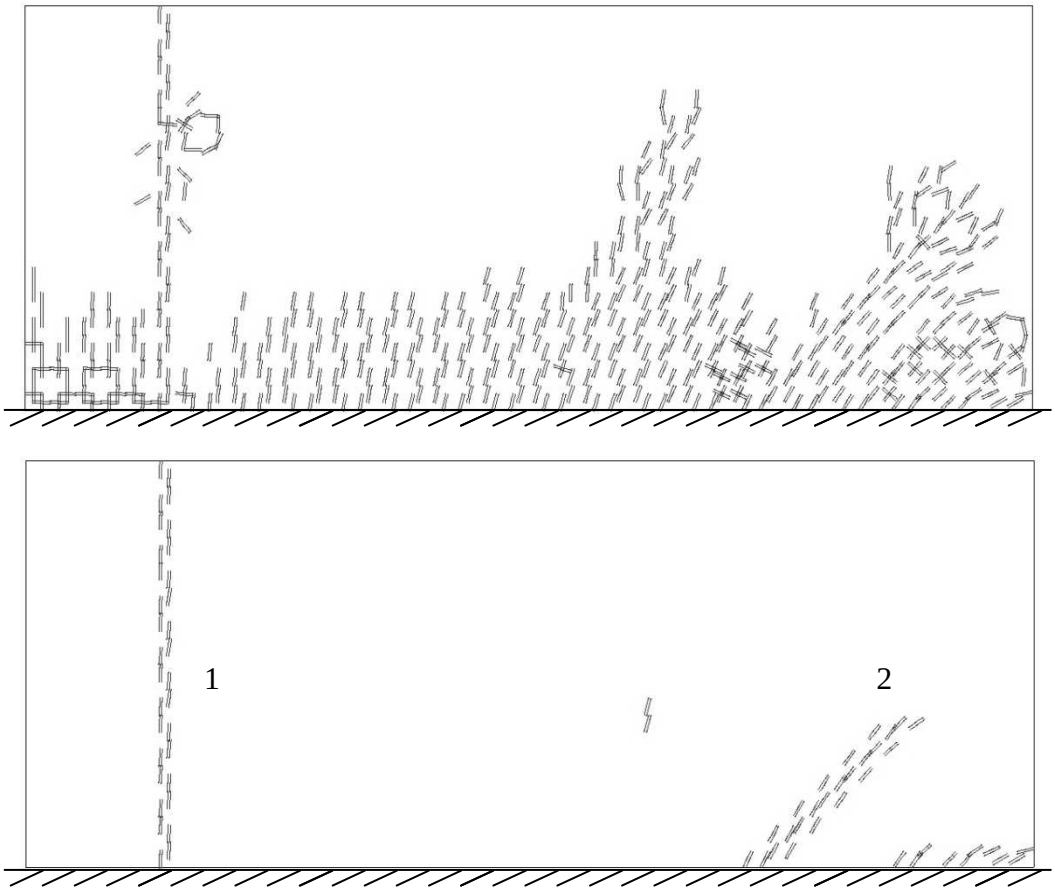

Figure G.3 Crack pattern at ε_{cs} = 1 ‰ for 0 and 100 % fully developed cracks for ordinary concrete with cross-section 0.

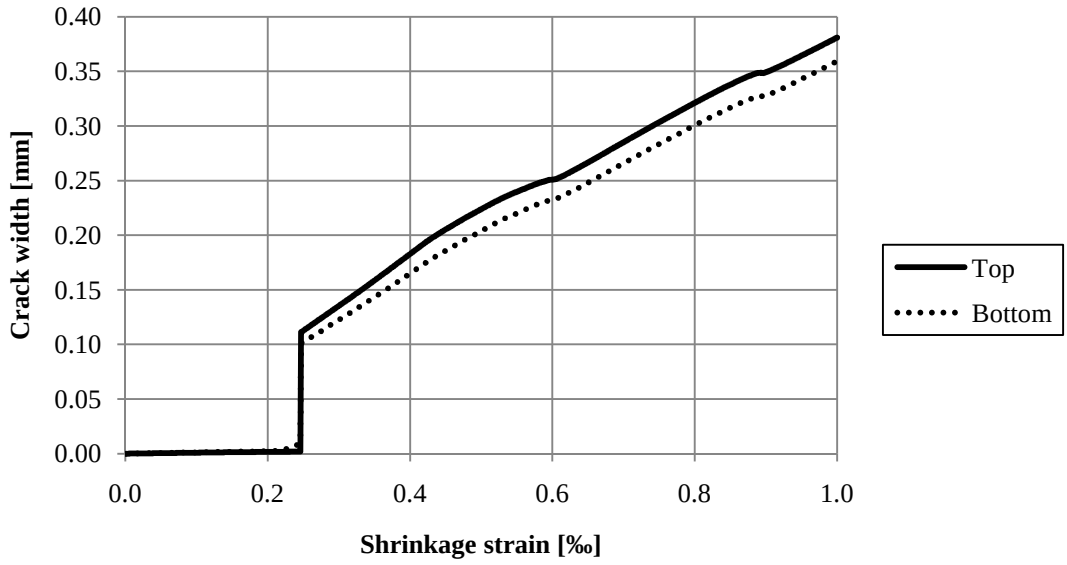

Figure G.4 Crack widths at the original reinforcement levels for ordinary concrete with cross-section 0.

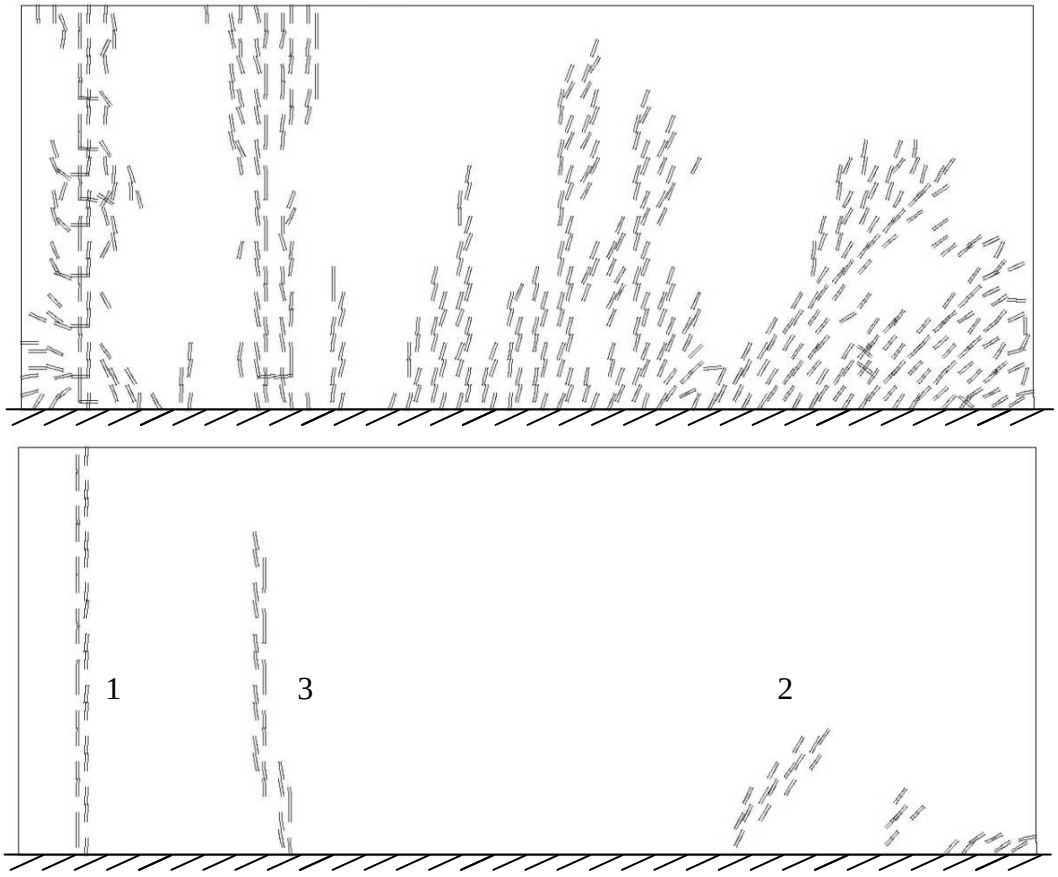

Figure G.5 Crack pattern at ε_{cs} = 1 ‰ for 0 and 100 % fully developed cracks for fibre reinforced concrete with cross-section 0.

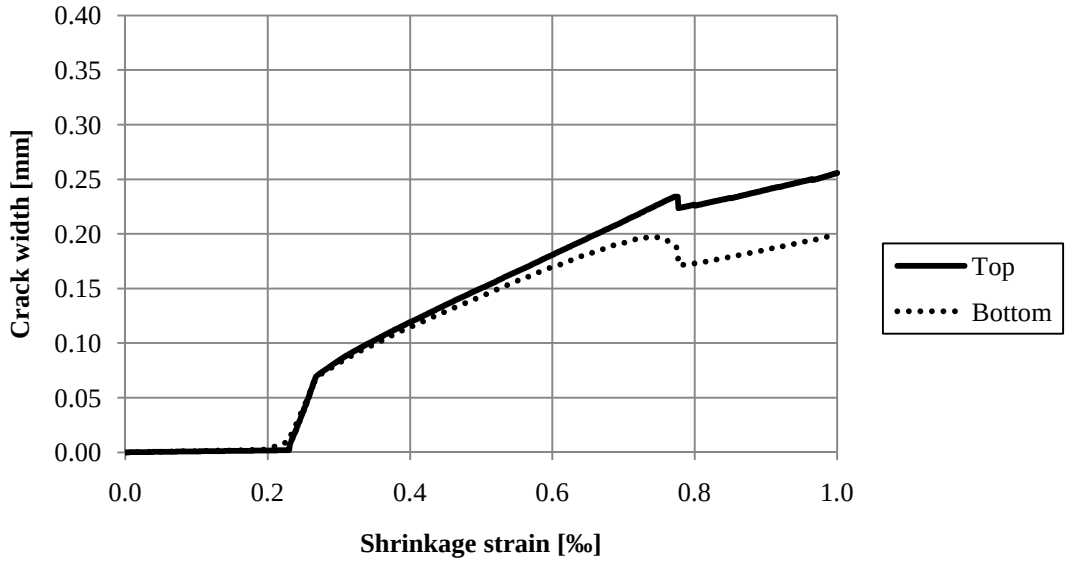

Figure G.6 Crack widths at the original reinforcement levels for fibre reinforced concrete with cross-section 0.

Appendix H Influence of creep

Effect of concrete creep on an edge beam was analysed by non-linear finite element analyses. Results from these analyses are shown in this Appendix, except for $\varphi = 0$, as they were already presented in Appendix C for the case with cross-section 1 with transversal reinforcement ratio of $\rho_t = 0.6$ %.

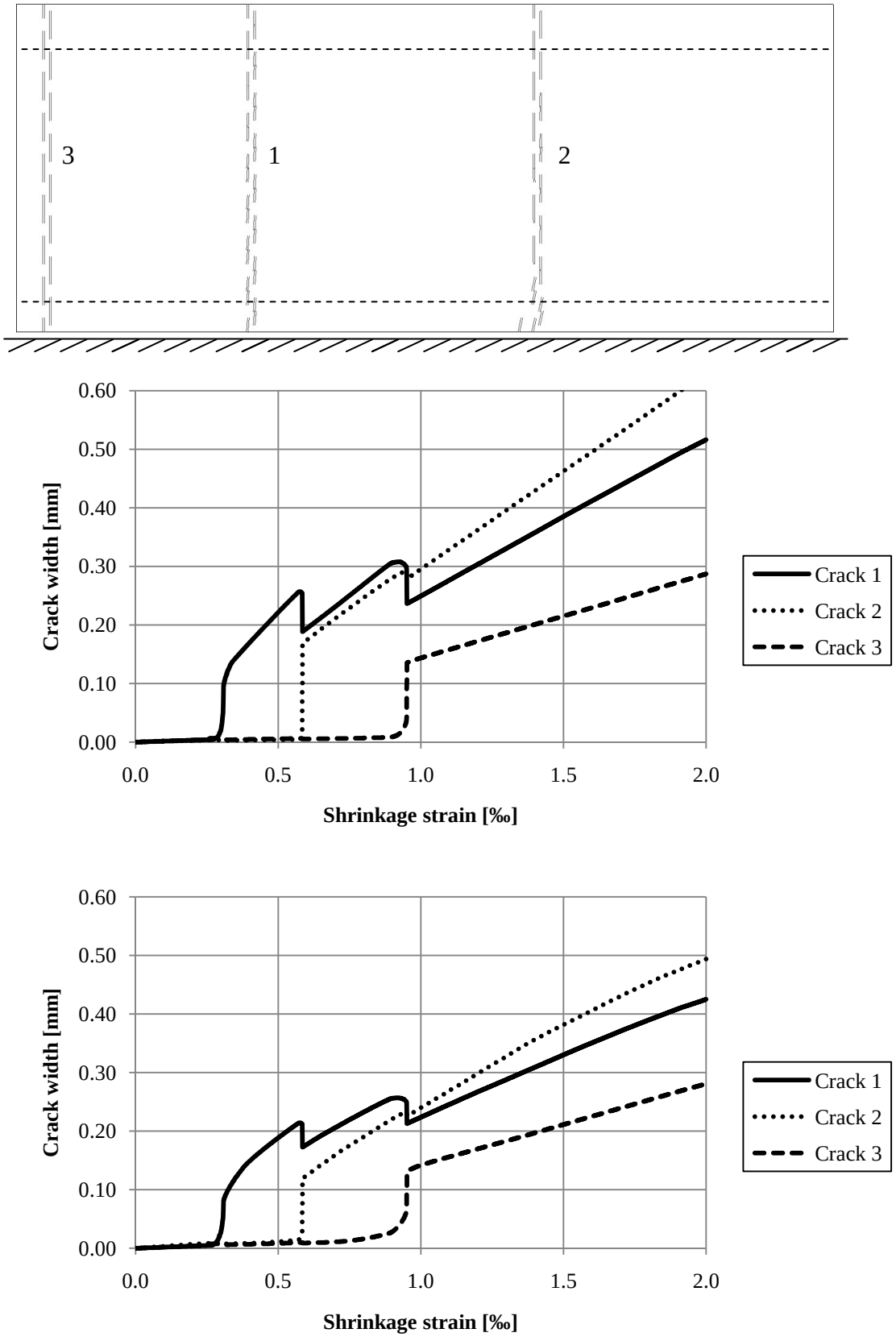

Figure H.1 Fully developed cracks pattern at ε_{cs} = 2 ‰ and crack widths at the top (top figure) and bottom reinforcement level (bottom figure) for φ = 1.

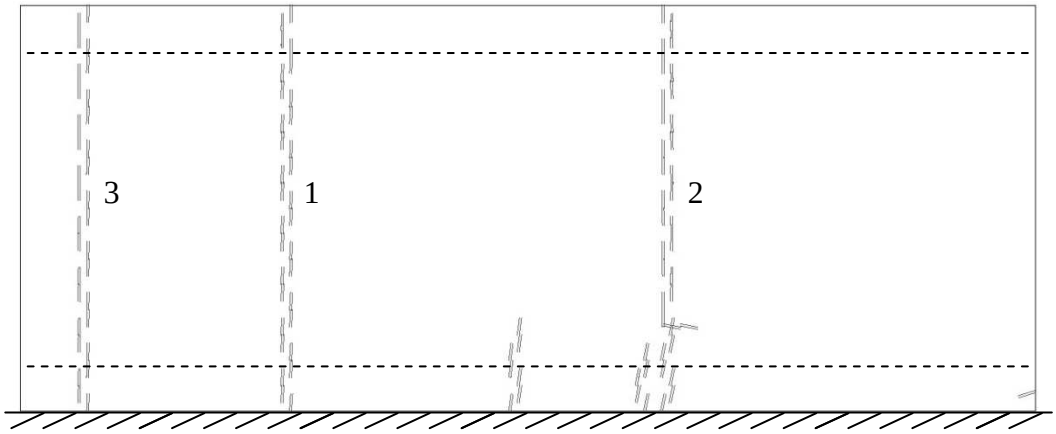

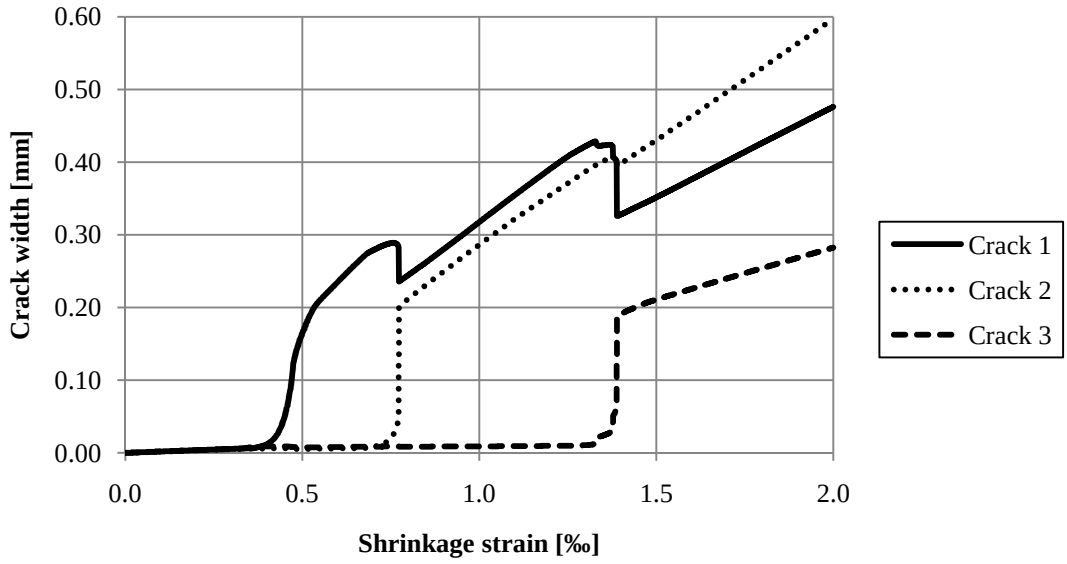

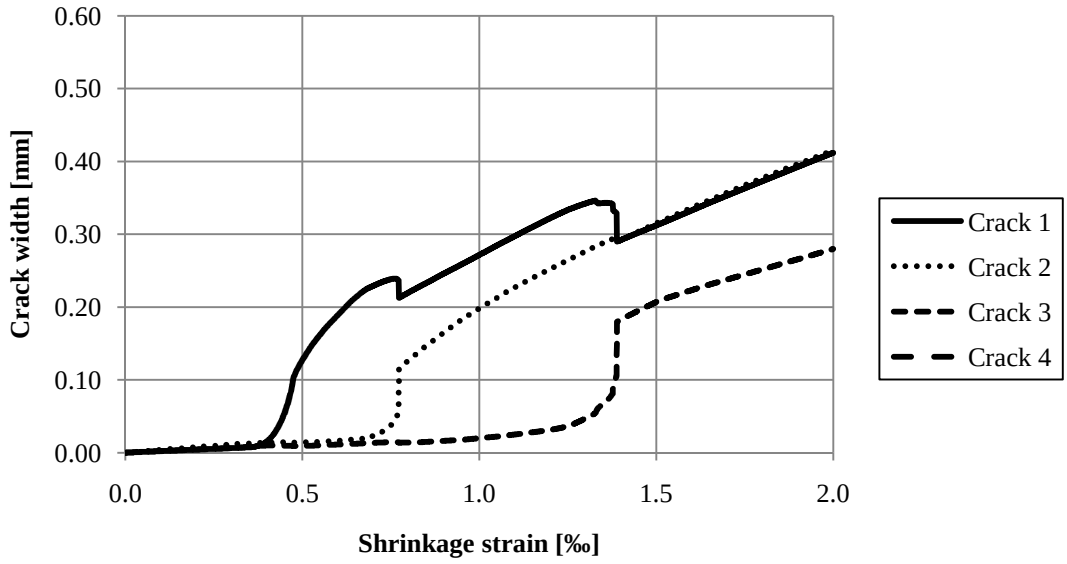

Figure H.2 Fully developed cracks pattern at ε_{cs} = 2 ‰ and crack widths at the top (top figure) and bottom reinforcement level (bottom figure) for φ = 2.

Appendix I Crack patterns and crack widths for retaining walls with different geometries and cross-sections

In Section 5.3 selected parts from the analyses of the wall was presented. In this appendix, all results concerning the crack patterns and the crack widths for different reinforcement arrangement and geometries are presented.

It shall be stated that numerical problems occurred for some of the analyses. Hence, the results from the last reliable step for each of these cases are shown in the figures in this appendix. At what shrinkage strain the results are presented is stated in the caption of each figure. Different geometries and reinforcement arrangement should be compared with this in mind.

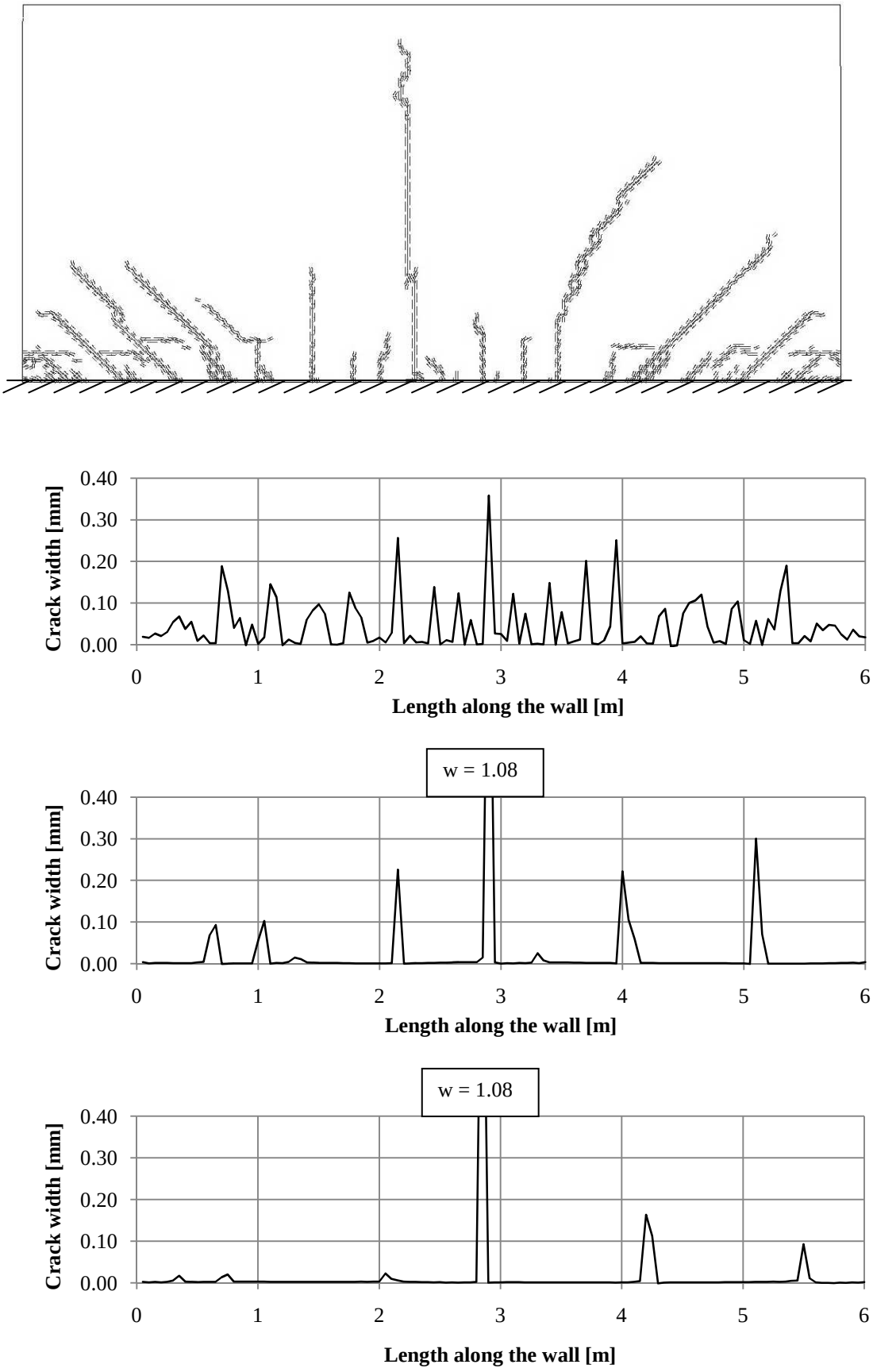

Figure I.1 Crack pattern for ε_{cs} = 1.00 ‰ and crack width at level 1 (top), 4 (middle) and 6 (bottom) for wall with h = 2.9 m and cross-section 0.

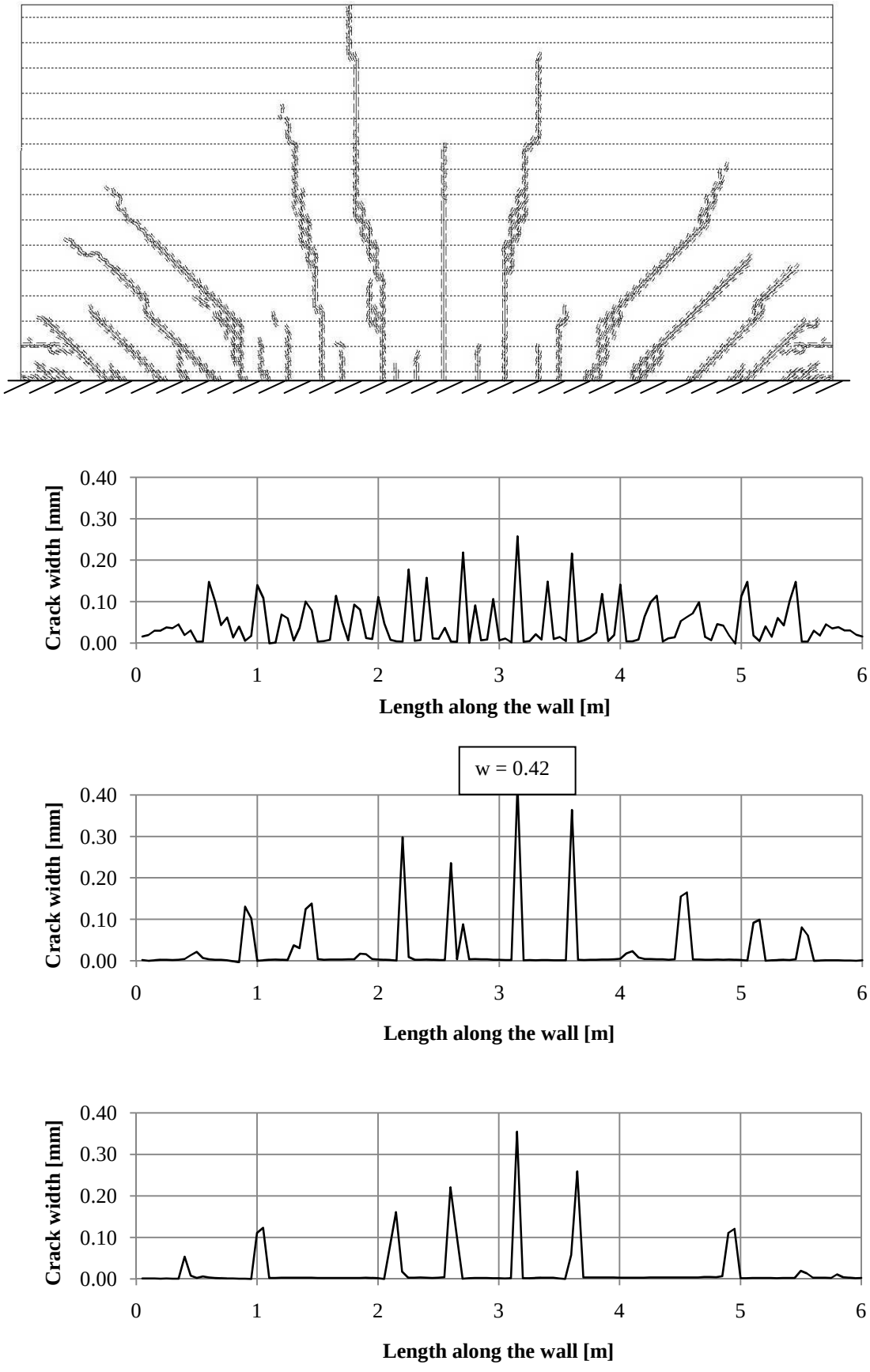

Figure I.2 Crack pattern for ε_{cs} = 1.00 ‰ and crack width at level 1 (top), 4 (middle) and 6 (bottom) for wall with h = 2.9 m and cross-section 1.

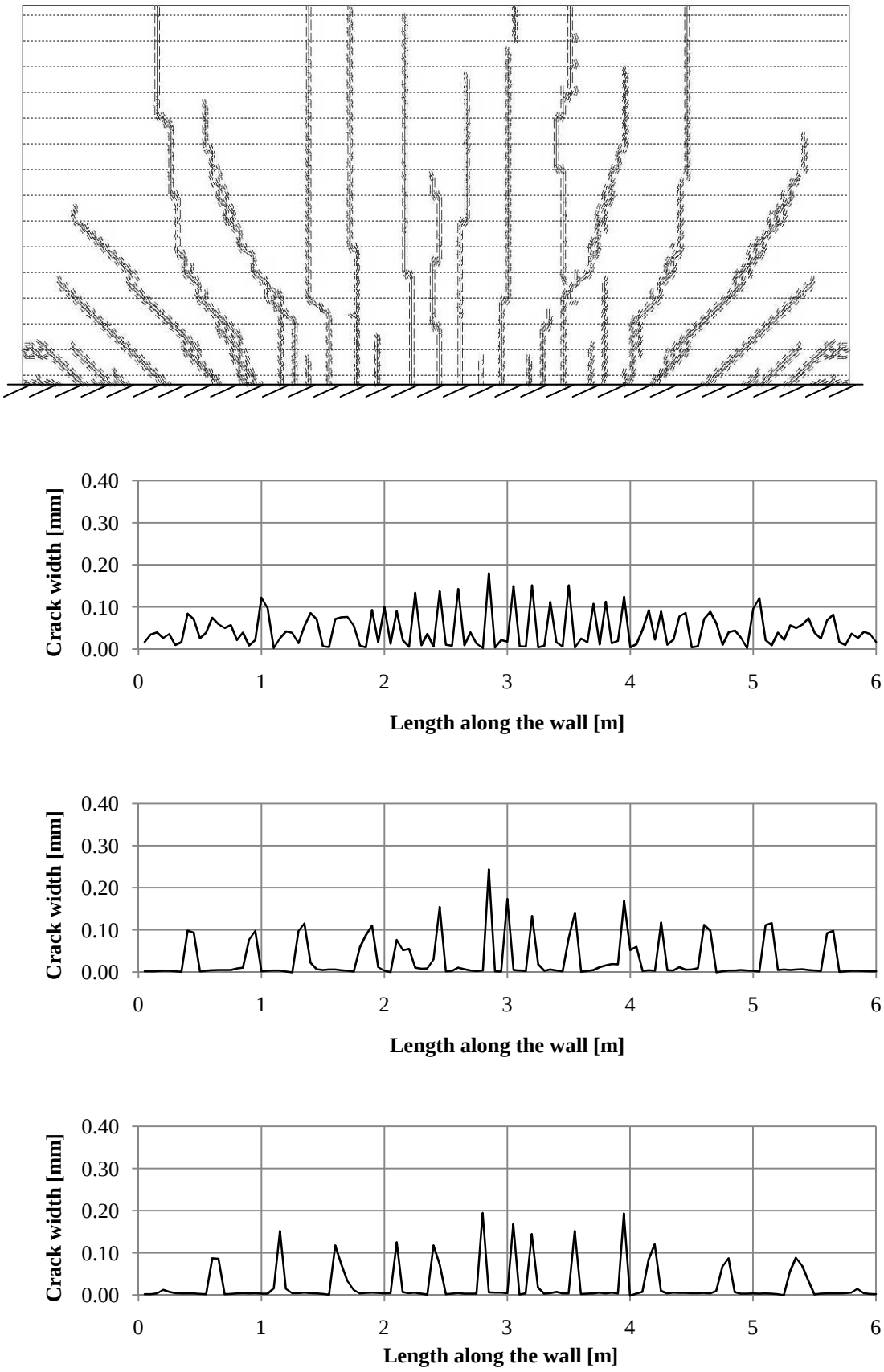

Figure I.3 Crack pattern for ε_{cs} = 1.00 ‰ and crack width at level 1 (top), 4 (middle) and 6 (bottom) for wall with h = 2.9 m and cross-section 2.

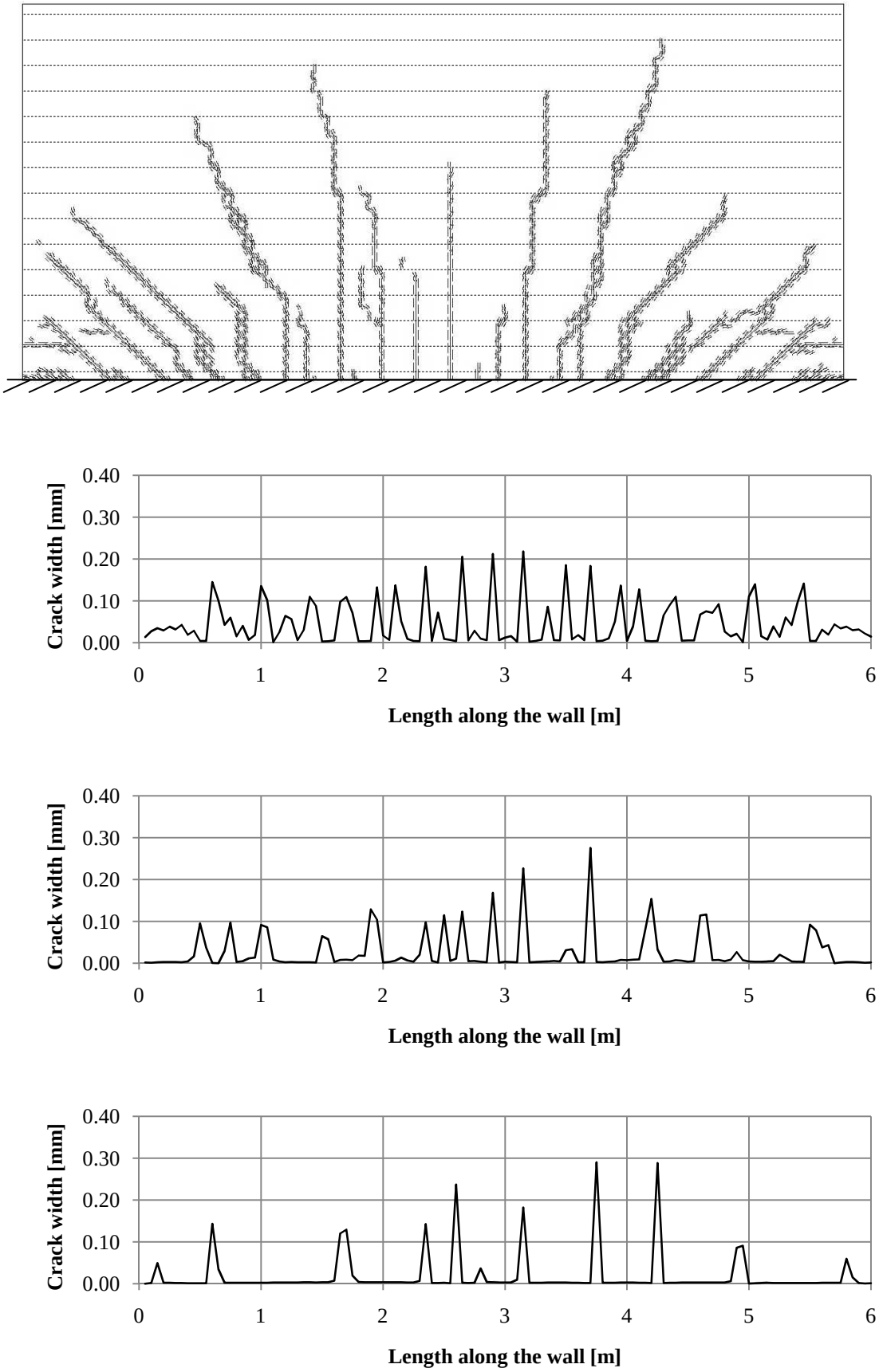

Figure I.4 Crack pattern for ε_{cs} = 1.00 ‰ and crack width at level 1 (top), 4 (middle) and 6 (bottom) for wall with h = 2.9 m and cross-section 3.

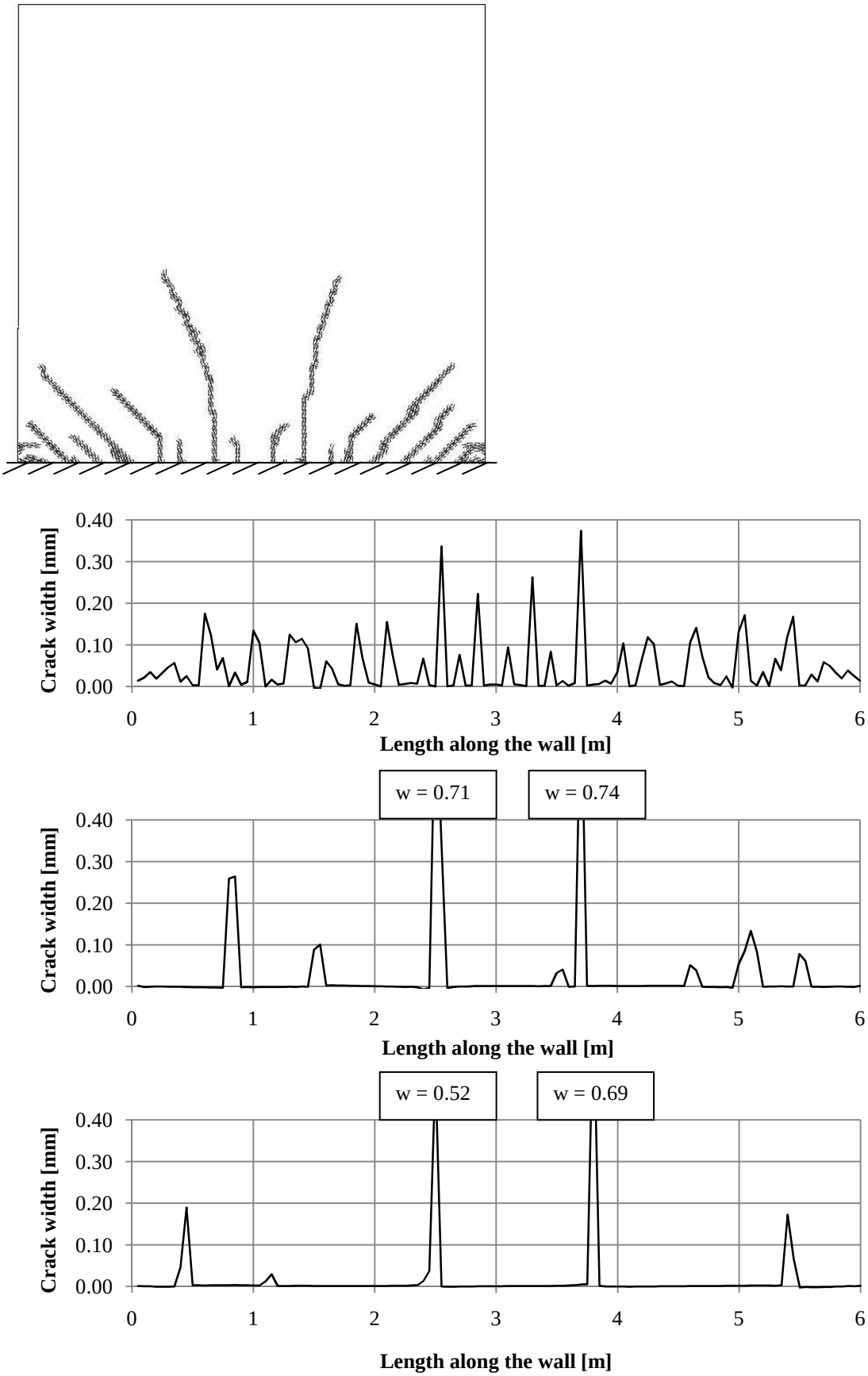

Figure I.5 Crack pattern for ε_{cs} = 0.86 ‰ and crack width at level 1 (top), 4 (middle) and 6 (bottom) for wall with h = 6 m and cross-section 0.

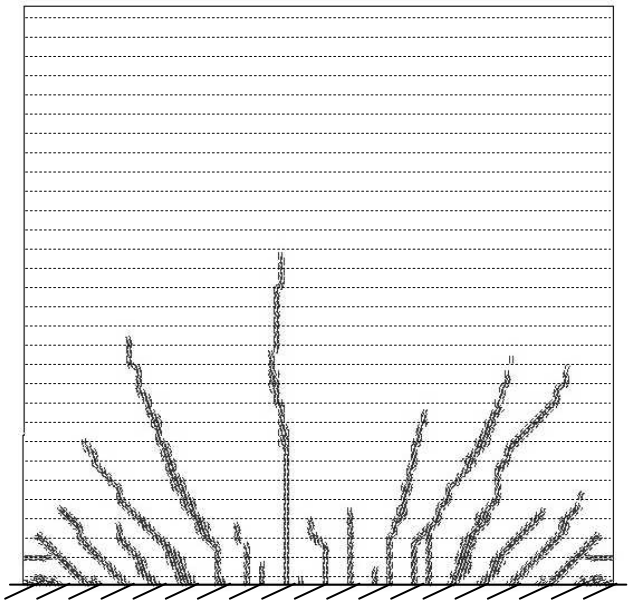

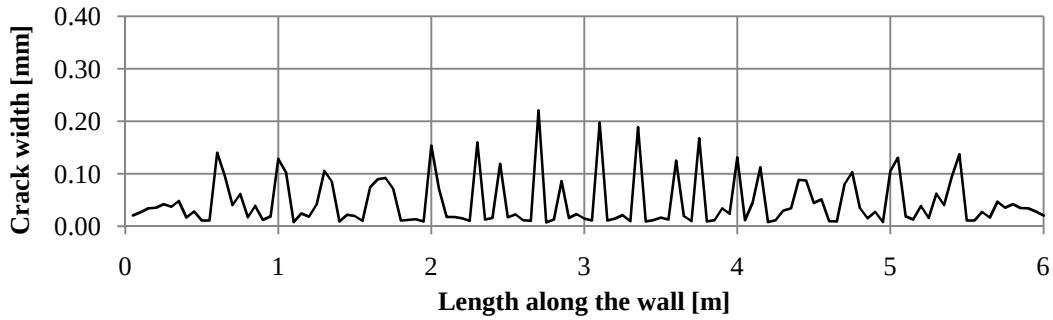

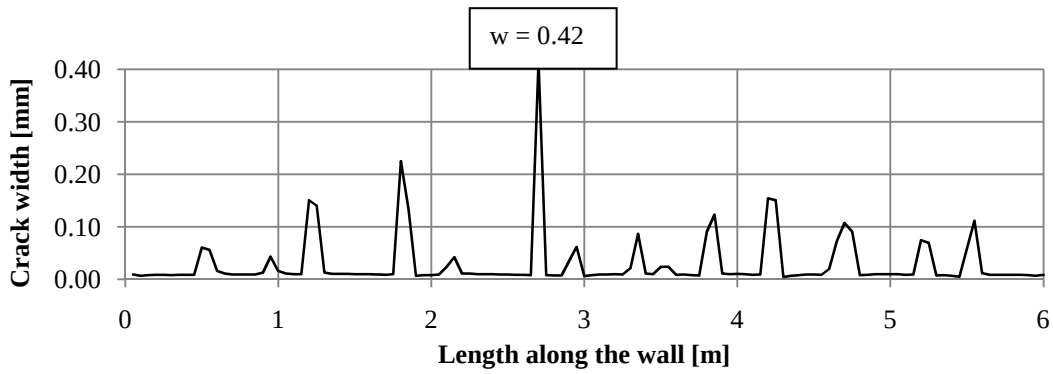

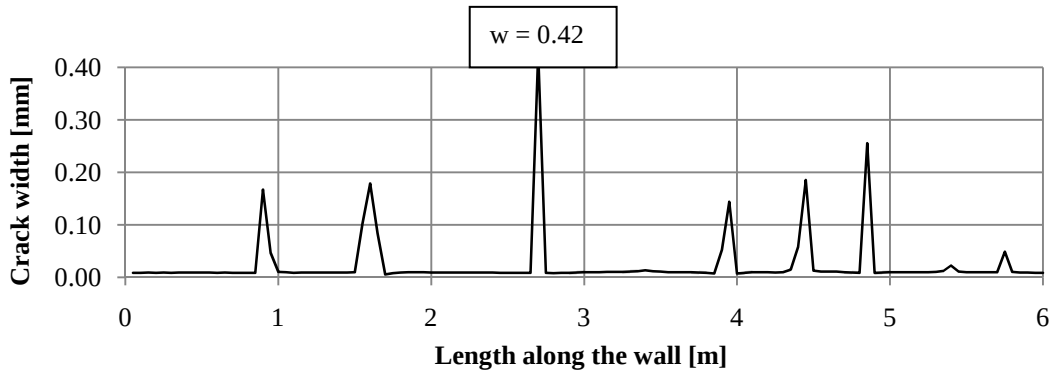

Figure I.6 *Crack pattern for ε_{cs} = 0.86 ‰ and crack width at level 1 (top), 4 (middle) and 6 (bottom) for wall with h = 6 m and cross-section 1.*

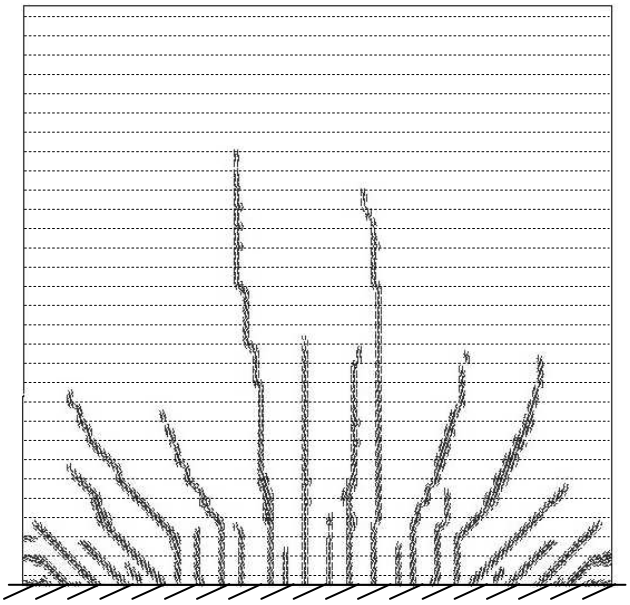

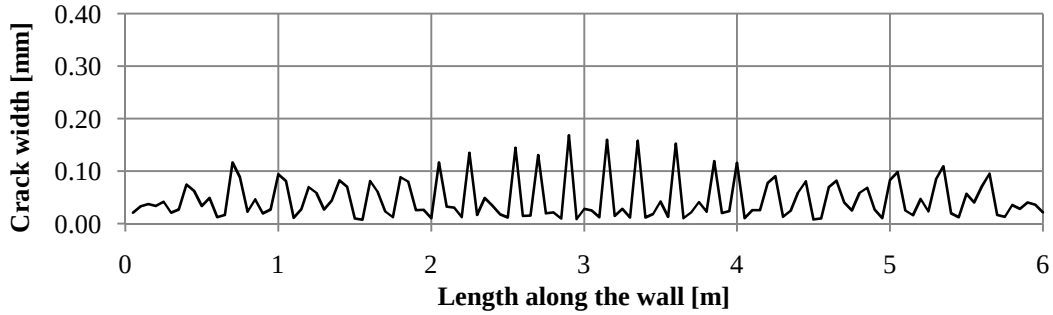

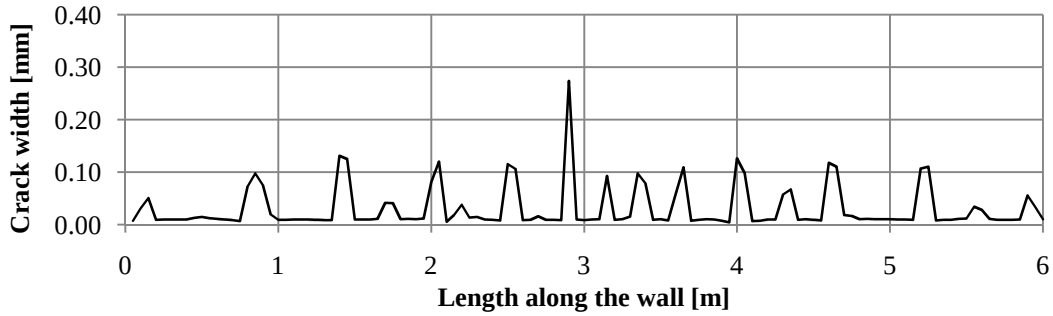

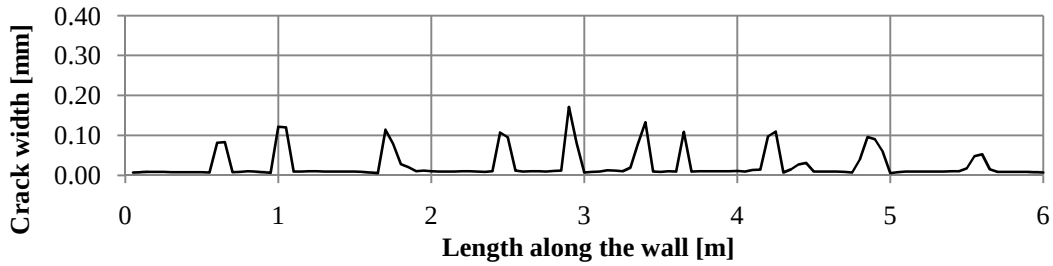

Figure I.7 Crack pattern for ε_{cs} = 0.86 ‰ and crack width at level 1 (top), 4 (middle) and 6 (bottom) for wall with h = 6 m and cross-section 2.

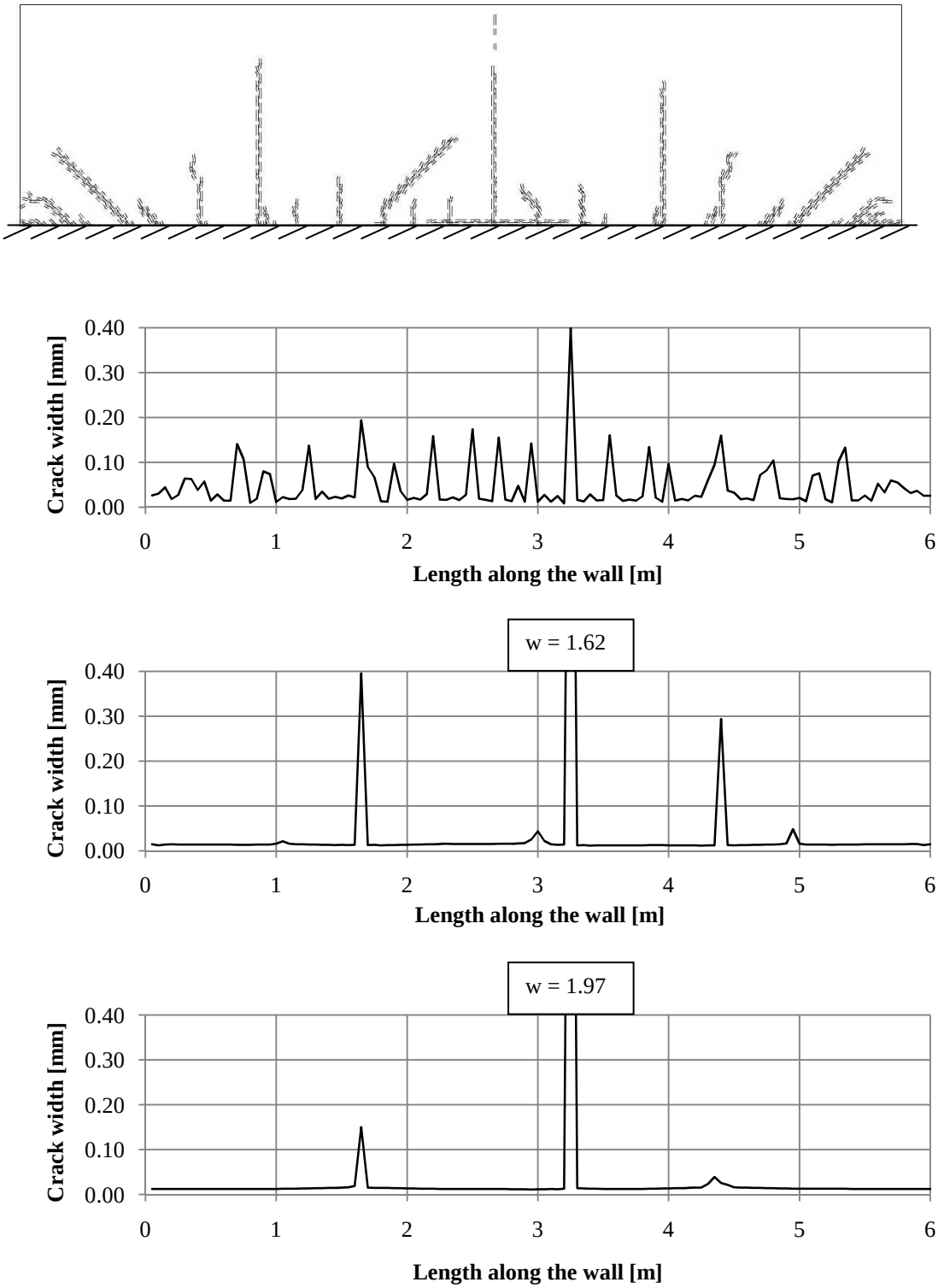

Figure I.8 *Crack pattern for ε_{cs} = 0.76 ‰ and crack width at level 1 (top), 4 (middle) and 6 (bottom) for wall with h = 1.5 m and cross-section 0.*

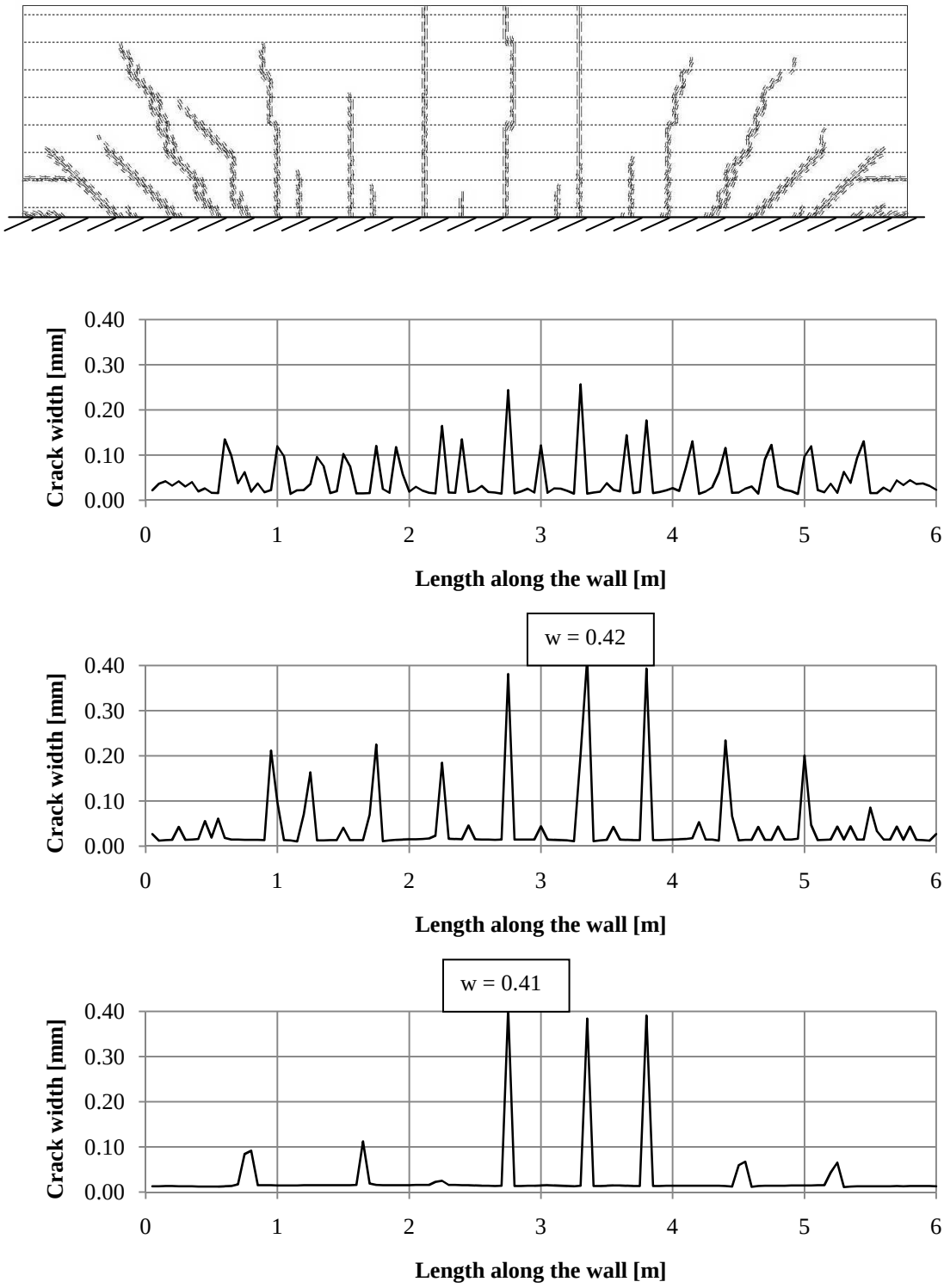

Figure I.9 Crack pattern for ε_{cs} = 0.76 ‰ and crack width at level 1 (top), 4 (middle) and 6 (bottom) for wall with h = 1.5 m and cross-section 1.

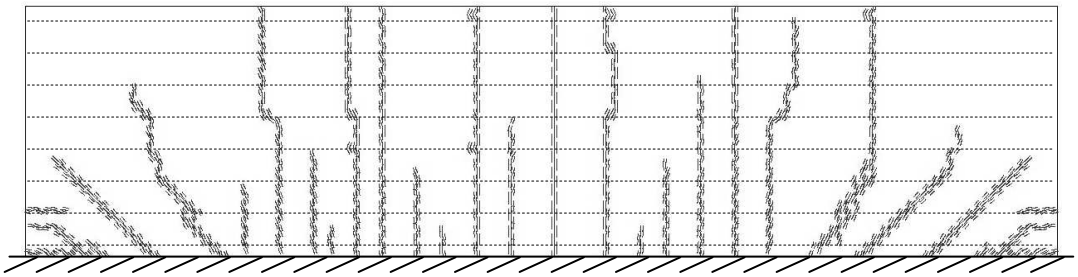

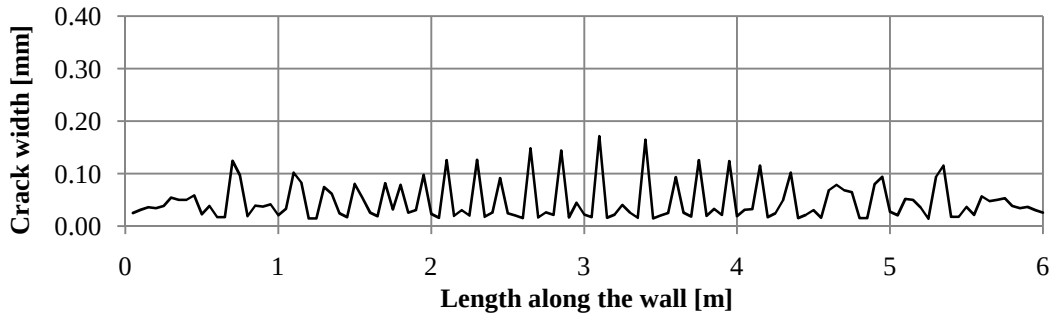

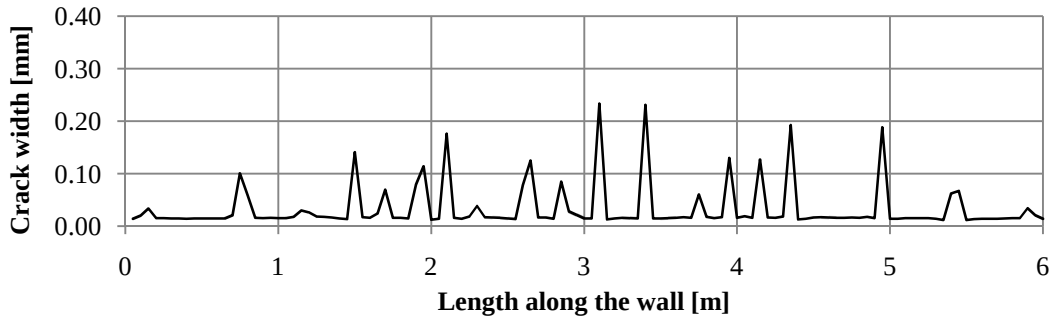

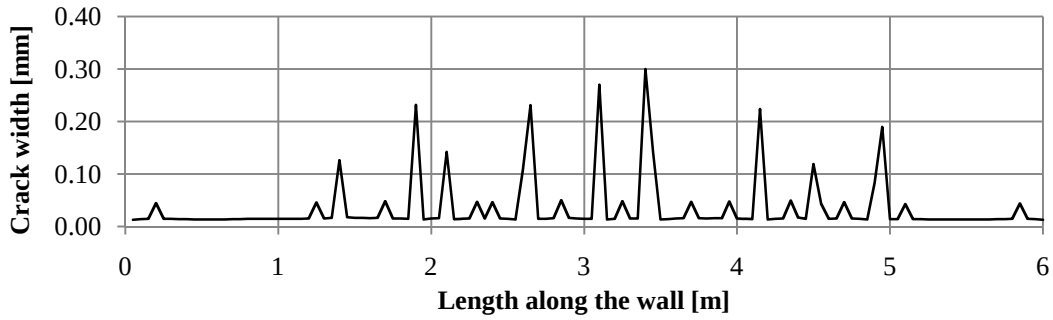

Figure I.10 Crack pattern for ε_{cs} = 0.76 ‰ and crack width at level 1 (top), 4 (middle) and 6 (bottom) for wall with h = 1.5 m and cross-section 2.

Appendix J Crack patterns and crack widths for retaining wall with fibre reinforced concrete

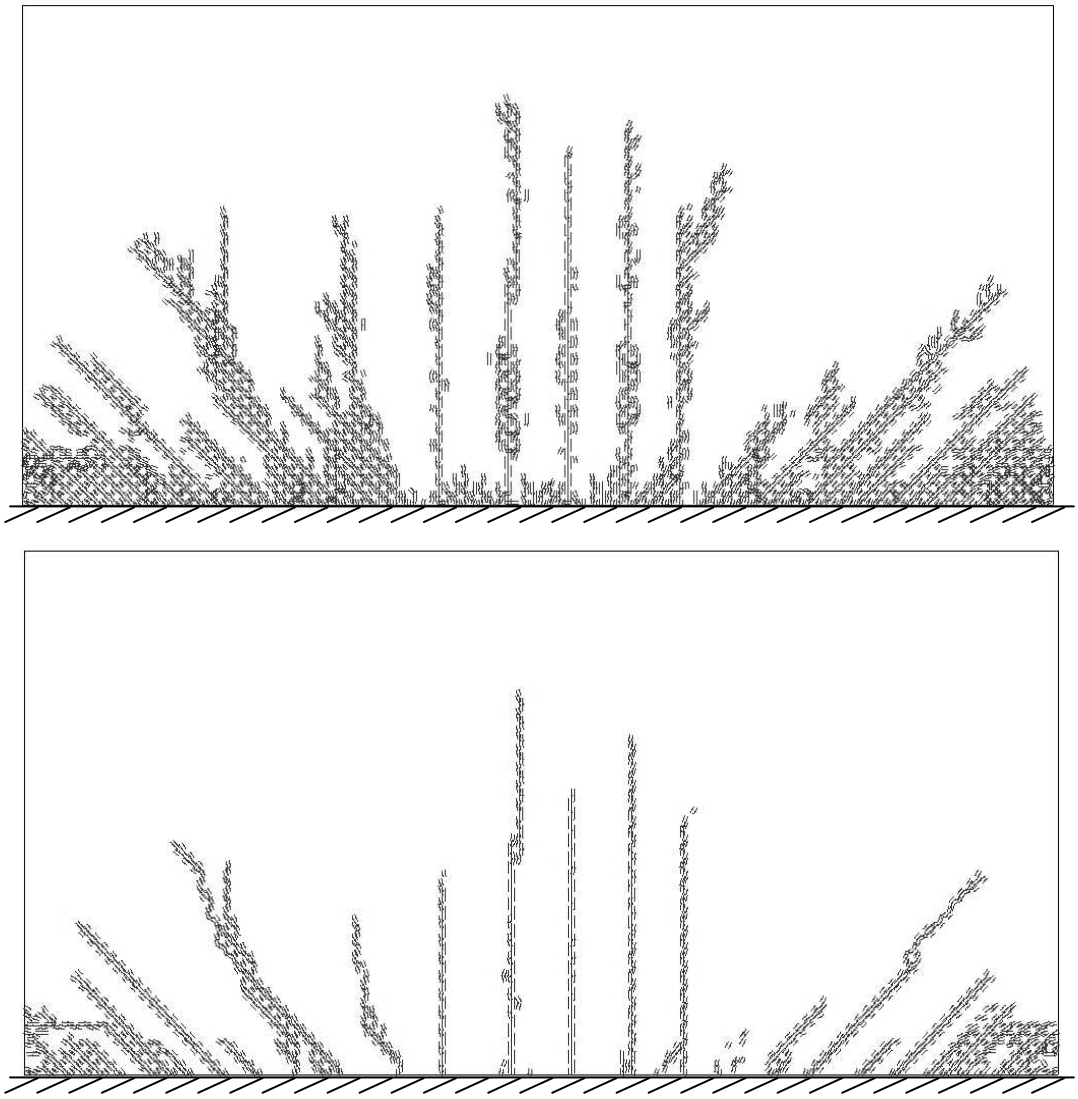

Figure J.1 Crack pattern for 0 (top figure) and 100 % (bottom figure) open cracks at ε_{cs} = 1.00 ‰ for wall with h = 2.9 m and cross-section 0 with fibre reinforced concrete.

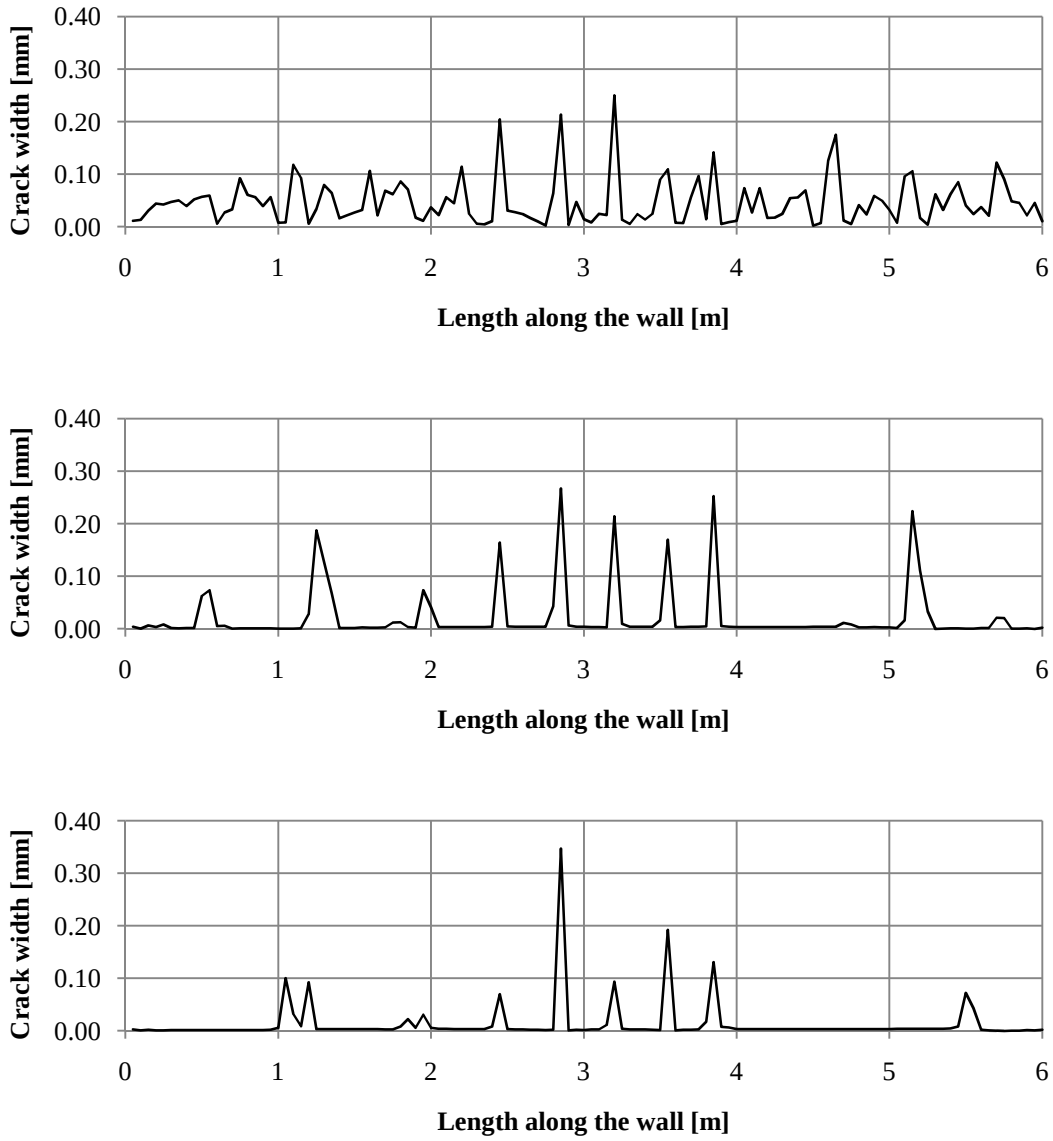

Figure J.2 *Crack width for ε_{cs} = 1.00 ‰ at level 1 (top), 4 (middle) and 6 (bottom) for wall with h = 2.9 m and cross-section 0 with fibre reinforced concrete.*

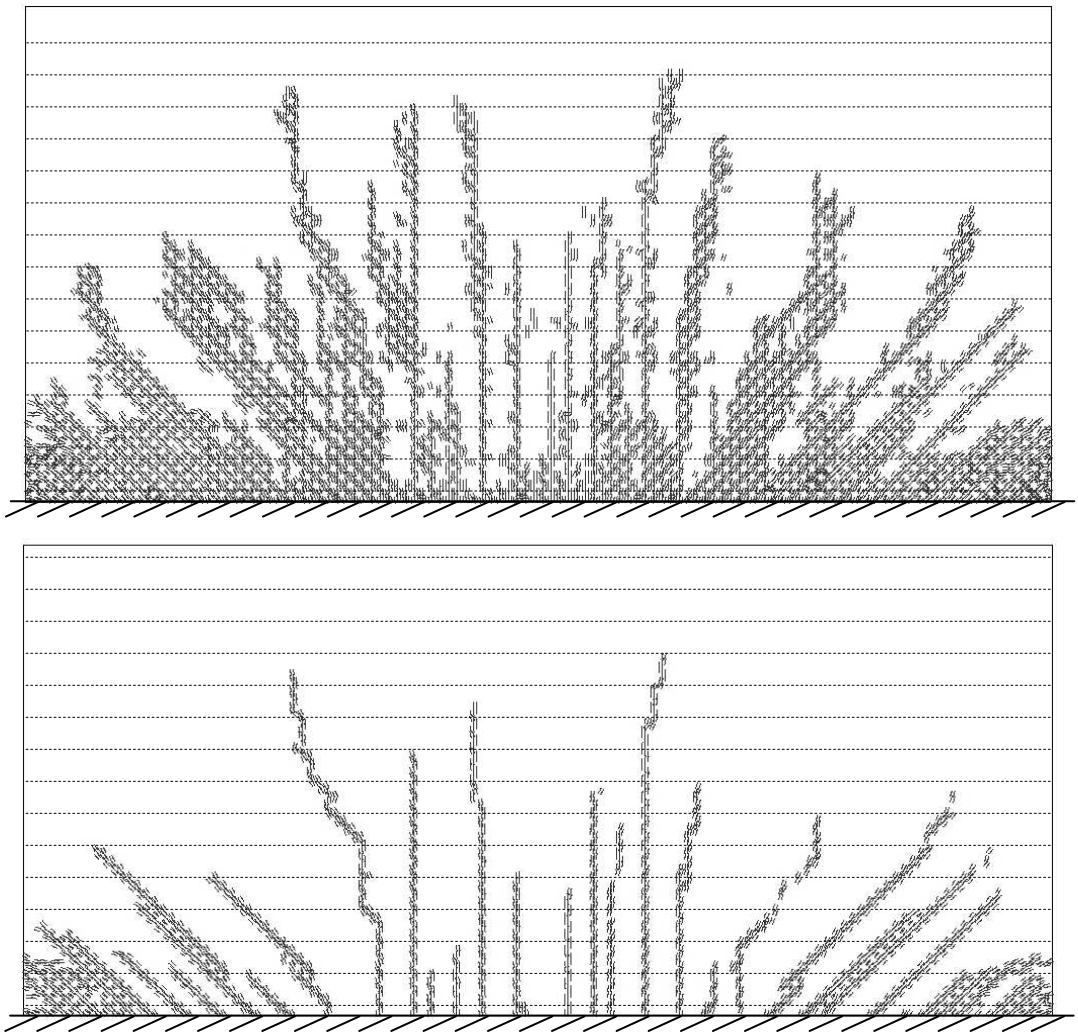

Figure J.3 Crack pattern for 0 (top figure) and 100 % (bottom figure) open cracks at ε_{cs} = 1.00 ‰ for wall with h = 2.9 m and cross-section 1 with fibre reinforced concrete.

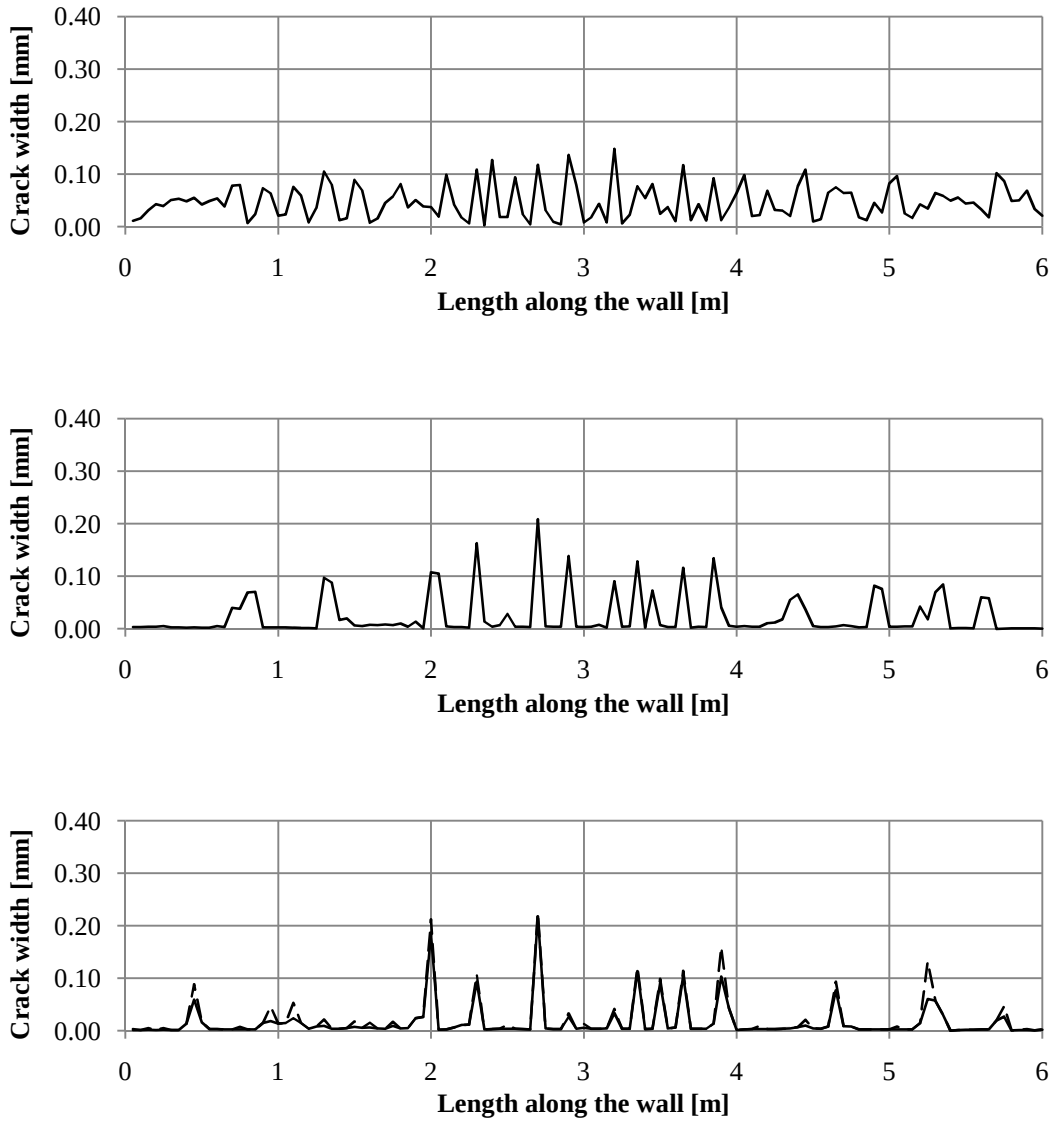

Figure J.4 *Crack width for ε_{cs} = 1.00 ‰ at level 1 (top), 4 (middle) and 6 (bottom) for wall with h = 2.9 m and cross-section 1 with fibre reinforced concrete.*

Appendix K Input files for ADINA

K.1 Introduction

In this Appendix an example is presented of the input text files as introduced in ADINA. They correspond with analysis of tie-rod test carried out on specimen with ordinary reinforcement. However, changes in the files needed to be included in order to simulate tie-rod tests on fibre reinforced concrete specimens are also presented.

K.2 Coordinates

```
*
SYSTEM NAME=1 TYPE=CARTESIAN MODE=1,
   XORIGIN=0 YORIGIN=0 ZORIGIN=0,
   AX=1 AY=0 AZ=0,
   BX=0 BY=1 BZ=0,
   MOVE=NO
*
COORDINATES POINT SYSTEM=1
@CLEAR
*
*** GEOMETRY BOUNDARIES ***
*
1       0       0       0       1
2       0       0.816   0       1
3       0       0.816   0.112   1
4       0       0       0.112   1
*
*** REINFORCEMENT POINTS ***
*
210     0       -0.002  0.056   1
211     0       0.01    0.056   1
.
.
311     0       0.81    0.056   1
312     0       0.818   0.056   1
@
```

K.3 Lines

```
*
*** GEOMETRY BOUNDARIES ***
*
LINE STRAIGHT NAME=   1       P1=    1       P2=    2
LINE STRAIGHT NAME=   2       P1=    2       P2=    3
LINE STRAIGHT NAME=   3       P1=    3       P2=    4
LINE STRAIGHT NAME=   4       P1=    4       P2=    1
*
*** REINFORCEMENT LINES ***
*
LINE STRAIGHT NAME=   5       P1=    210     P2=    211
LINE STRAIGHT NAME=   6       P1=    211     P2=    212
.
.
.
LINE STRAIGHT NAME=   105     P1=    310     P2=    311
LINE STRAIGHT NAME=   106     P1=    311     P2=    312
```

K.4 Surface

```
*
SURFACE VERTEX NAME=       1       P1=    1       P2=    2       P3=    3
        P4=    4
*
SFTHICKNESS
@CLEAR
1       0.1120 0       0       0       0
@
*
SURF-ELEMDAT    TWODSOLID

@CLEAR
1       1       0       'DEFAULT'   'DEFAULT'   0       0       'NO'    0
@
*
```

K.5 Material properties (for analysis of ordinary concrete)

```
*
*** CONCRETE NON-LINEAR MATERIAL PROPERTIES ***
*
MATERIAL CONCRETE NAME=1 OPTION=KUPFER E0=3.000E+10,
    NU=0.200 SIGMAT=3084600,
    SIGMATP=0 SIGMAC=-10.00E+07,
    EPSC=-0.01 SIGMAU=-9.700E+07,
    EPSU=-0.0135 BETA=0.750,
    C1=1.400 C2=-0.400 XSI=92.22,
    STIFAC=0.0001 SHEFAC=0.500,
    ALPHA=0.0 TREF=0.000 INDNU=CONSTANT,
    GF=0.0 DENSITY=2400.000 TEMPERAT=NO,
    MDESCRIP='Concrete'
*
*** STEEL MATERIAL PROPERTIES ***
*
MATERIAL PLASTIC-BILINEAR NAME=2 HARDENIN=ISOTROPIC,
    E=2.0E+11 NU=0.3,
    YIELD=5.0E+08 ET=2.0E+08,
    EPA=0.01 STRAINRA=0 DENSITY=7800,
    ALPHA=0.0 TREF=0.0 DEPENDEN=NO,
    TRANSITI=0.0001 EP-STRAI=0.0 BCURVE=0,
    BVALUE=0.0 XM-INF=0.0,
    XM0=0.0 ETA=0.0 MDESCRIP='Steel'
```

K.6 Material properties (for analysis of fibre reinforced concrete)

```
*
*** CONCRETE NON-LINEAR MATERIAL PROPERTIES ***
*
MATERIAL CONCRETE NAME=1 OPTION=KUPFER E0=3.000E+10,
    NU=0.200 SIGMAT=3632420,
    SIGMATP=0 SIGMAC=-10.00E+07,
```

```
    EPSC=-0.01 SIGMAU=-9.700E+07,
    EPSU=-0.0135 BETA=0.750,
    C1=1.400 C2=-0.400 XSI=66.5051,
    STIFAC=0.0001 SHEFAC=0.500,
    ALPHA=0.0 TREF=0.000 INDNU=CONSTANT,
    GF=0.0 DENSITY=2400.000 TEMPERAT=NO,
    MDESCRIP='Concrete'
*
*** STEEL MATERIAL PROPERTIES ***
*
MATERIAL PLASTIC-BILINEAR NAME=2 HARDENIN=ISOTROPIC,
    E=2.0E+11 NU=0.3,
    YIELD=5.0E+08 ET=2.0E+08,
    EPA=0.01 STRAINRA=0 DENSITY=7800,
    ALPHA=0.0 TREF=0.0 DEPENDEN=NO,
    TRANSITI=0.0001 EP-STRAI=0.0 BCURVE=0,
    BVALUE=0.0 XM-INF=0.0,
    XM0=0.0 ETA=0.0 MDESCRIP='Steel'
*
*** FIBRE REINFORCED CONCRETE MATERIAL PROPERTIES ***
*
MATERIAL CONCRETE NAME=3 OPTION=KUPFER E0=3.000E+10,
    NU=0.200 SIGMAT=3632420,
    SIGMATP=3117800 SIGMAC=-10.00E+07,
    EPSC=-0.01 SIGMAU=-9.700E+07,
    EPSU=-0.0135 BETA=0.750,
    C1=1.400 C2=-0.400 XSI=6953.5447,
    STIFAC=0.0001 SHEFAC=0.500,
    ALPHA=0.0 TREF=0.000 INDNU=CONSTANT,
    GF=0.0 DENSITY=2400.000 TEMPERAT=NO,
    MDESCRIP='Concrete'
```

K.7 Reinforcement

```
*
*** REINFORCEMENT CROSS-SECTION PROPERTIES ***

*
CROSS-SECTIO PIPE NAME=1 DIAMETER=      0.0160000000 THICKNES=
          0.0080000000 SC=0     TC=0     TORFAC=1     SSHEARF=0     TSHEARF=0
SOLID=YES
*
@
*
*** REINFORCEMENT  ELEMENTS***

*
LINE-ELEMDAT PIPE
@CLEAR
5       2       1       'DEFAULT'   'DEFAULT'   0       0       'NO'    0
6       2       1       'DEFAULT'   'DEFAULT'   0       0       'NO'    0
.
.
.
105     2       1       'DEFAULT'   'DEFAULT'   0       0       'NO'    0
106     2       1       'DEFAULT'   'DEFAULT'   0       0       'NO'    0
@
```

K.8 Boundary conditions

```
FIXITY NAME=SURFACE
@CLEAR
 'X-TRANSLATION'
 'X-ROTATION'
 'Y-ROTATION'
 'Z-ROTATION'
 'OVALIZATION'
@
```

```
*
FIXBOUNDARY SURFACES FIXITY=ALL
@CLEAR
1       'SURFACE'
@
*
FIXITY NAME=REINFORCEMENT
@CLEAR
 'X-TRANSLATION'
 'X-ROTATION'
 'Y-ROTATION'
 'Z-ROTATION'
 'OVALIZATION'
@
*
FIXBOUNDARY LINES FIXITY=ALL
*
5       'REINFORCEMENT'
6       'REINFORCEMENT'
.
.
.
105     'REINFORCEMENT'
106     'REINFORCEMENT'
*
FIXITY NAME=GROUND
@CLEAR
 'X-TRANSLATION'
 'Y-TRANSLATION'
 'Z-TRANSLATION'
 'X-ROTATION'
 'Y-ROTATION'
 'Z-ROTATION'
 'OVALIZATION'
@
```

```
*
FIXBOUNDARY POINTS FIXITY=ALL
*
210     'GROUND'
@
*
*** REINFORCEMENT CONSTRAINTS ***
*
CONSTRAINT      NAME=       1       SLAVETYP=POINT SLAVENAM=
        210     SLAVEDOF=Z-TRANSLATION    MASTERTY=POINT SBODY=0
        OPTION=0    GENERALI=NO     /       @CLEAR      /       107     'Z-
TRANSLATION'    1       0       /       @
CONSTRAINT      NAME=       2       SLAVETYP=POINT SLAVENAM=
        211     SLAVEDOF=Z-TRANSLATION    MASTERTY=POINT SBODY=0
        OPTION=0    GENERALI=NO     /       @CLEAR      /       108     'Z-
TRANSLATION'    1       0       /       @
.
.
.
CONSTRAINT      NAME=       102     SLAVETYP=POINT SLAVENAM=
        311     SLAVEDOF=Z-TRANSLATION    MASTERTY=POINT SBODY=0
        OPTION=0    GENERALI=NO     /       @CLEAR      /       208     'Z-
TRANSLATION'    1       0       /       @
CONSTRAINT      NAME=       103     SLAVETYP=POINT SLAVENAM=
        312     SLAVEDOF=Z-TRANSLATION    MASTERTY=POINT SBODY=0
        OPTION=0    GENERALI=NO     /       @CLEAR      /       209     'Z-
TRANSLATION'    1       0       /       @
```

K.9 Load

```
*
LOAD DISPLACEMENT NAME=1 DX=FREE DY=5E-03 DZ=FREE AX=FREE
AY=FREE AZ=FREE
*
APPLY-LOAD BODY=0
@CLEAR
1       'DISPLACEMENT'  1       'POINT'     312     0       1       0       0
        -1      0       0       0       'NO'    0       0       1       0
@
*
```

K.10 Element groups

```
*
EGROUP TWODSOLID NAME=1 SUBTYPE=STRESS2 DISPLACE=DEFAULT,
   STRAINS=DEFAULT MATERIAL=1 INT=DEFAULT RESULTS=STRESSES DEGEN=NO,
   FORMULAT=0 STRESSRE=GLOBAL INITIALS=NONE FRACTUR=NO,
   CMASS=DEFAULT STRAIN-F=0 UL-FORMU=DEFAULT PNTGPS=0 NODGPS=0,
   LVUS1=0 LVUS2=0 SED=NO RUPTURE=ADINA INCOMPAT=DEFAULT,
   TIME-OFF=0 POROUS=NO WTMC=1,
   OPTION=NONE DESCRIPT='Concrete' THICKNES=1,
   PRINT=DEFAULT SAVE=DEFAULT TBIRTH=0,
   TDEATH=0 TMC-MATE=1
*
EGROUP PIPE NAME=2 DISPLACE=DEFAULT MATERIAL=2 RINT=1 SINT=1 TINT=4,
   RESULTS=STRESSES OVALIZAT=DEFAULT INITIALS=NONE ICALRA=0,
   RADTOL=0.001 CMASS=DEFAULT RUPTURE=ADINA,
   TIME-OFF=0 OPTION=NONE,
   BOLT-TOL=0.01 DESCRIPT='NONE' SECTION=1,
   PRINT=DEFAULT SAVE=YES TBIRTH=0,
   TDEATH=0 BOLTFORC=0 BOLTNCUR=0,
   TMC-MATE=1
```

K.11 Meshing

```
SUBDIVIDE SURFACE NAME=1 MODE=LENGTH 0.008
@CLEAR
1
@
*
SUBDIVIDE LINE NAME=2 MODE=LENGTH 0.008
5
to
106
@
```

*

GSURFACE NODES=3 PATTERN=8 NCOINCID=BOUNDARIES NCEDGE=1234,

NCVERTEX=1234 NCTOLERA=1.0E-05 SUBSTRUC=0 GROUP=1,

PREFSHAP=AUTOMATIC MESHING=MAPPED SMOOTHIN=NO DEGENERA=NO,

COLLAPSE=NO MIDNODES=CURVED METHOD=ADVFRONT FLIP=NO

@CLEAR

1

@

*

GLINENODES=2 AUXPOINT=4 NCOINCID=ENDS NCENDS=12,

NCTOLERA=1.0E-05 SUBSTRUC=0 GROUP=2 MIDNODES=CURVED

5

to

106

@

K.12 Random material model distribution (only for fibre reinforced concrete)

EDATA SUBSTRUC=0 GROUP=1 UNDEFINE=IGNORE

@CLEAR

1 1

2 3

3 3

4 1

5 3

6 1

7 1

8 1

9 3

10 3

.

.

.
2847 1
2848 3
2849 3
2850 3
2851 1
2852 1
2853 3
2854 1
2855 1
2856 3
@

K.13 Non-linear springs

*
*** INNER NODES SPRING PROPERTIES ***
*
PROPERTY NONLINEAR-K NAME=11 RUPTURE=NO
-0.00100000 -7403.8442
-0.00080000 -7400.4865
.
.
.
-0.00001000 -1789.1456
-0.00000500 -1637.8103
0.00000000 0.0000
0.00000500 1637.8103
0.00001000 1789.1456
.
.
.
0.00080000 7400.4865
0.00100000 7403.8442
@
*

```
*** OUTER NODES SPRING PROPERTIES ***
*
PROPERTY   NONLINEAR-K      NAME=12     RUPTURE=NO
-0.00100000   -3701.9221
-0.00080000   -3700.2432
.
.
.
-0.00001000   -894.5728
-0.00000500   -818.9051
0.00000000    0.0000
0.00000500    818.9051
0.00001000    894.5728
.
.
.
0.00080000    3700.2432
0.00100000    3701.9221
@
*
*** DEFINING SPRING PROPERTIES ***
PROPERTYSET NAME=11 K=0 M=0 C=0 NONLINEA=YES NK=11 NM=0 NC=0
*
PROPERTYSET NAME=12 K=0 M=0 C=0 NONLINEA=YES NK=12 NM=0 NC=0
*
*** SPRING ELEMENT GROUP ***
*
EGROUP SPRING NAME=4 PROPERTY=1 RESULTS=FORCES
NONLINEA=MNO OPTION=NONE DESCRIPT='Spring' PRINT=DEFAULT
SAVE=DEFAULT TBIRTH=0 TDEATH=0
*

*** OUTER NODES SPRINGS ***

*
```

SPRING POINTS

1 1070 2 0 2100 0 12 'DEFAULT' 'DEFAULT' 0 0

2 2090 2 0 3120 0 12 'DEFAULT' 'DEFAULT' 0 0

@

*

*** INNER NODES SPRINGS ***

*

SPRING POINTS

3 1080 2 0 2110 0 11 'DEFAULT' 'DEFAULT' 0 0

4 1090 2 0 2120 0 11 'DEFAULT' 'DEFAULT' 0 0

.

.

.

102 2070 2 0 3100 0 11 'DEFAULT' 'DEFAULT' 0 0

103 2080 2 0 3110 0 11 'DEFAULT' 'DEFAULT' 0 0

@

K.14 Solution process

*

KINEMATICS DISPLACE=SMALL STRAINS=SMALL UL-FORMU=DEFAULT PRESSURE=NO INCOMPAT=NO RIGIDLIN=NO

*

ITERATION METHOD=BFGS LINE-SEA=YES MAX-ITER=999 PRINTOUT=ALL PLASTIC-=1

*

TIMEFUNCTION NAME=1 IFLIB=1 FPAR1=0 FPAR2=0 FPAR3=0 FPAR4=0 FPAR5=0 FPAR6=0

@CLEAR

```
0 0
1 1
@
*
TIMESTEP NAME=DEFAULT
@CLEAR
1000 0.001
@
*
MASTER ANALYSIS=STATIC MODEX=EXECUTE TSTART=0.0 IDOF=0,
   OVALIZAT=NONE FLUIDPOT=AUTOMATIC CYCLICPA=1 IPOSIT=STOP,
   REACTION=YES INITIALS=NO FSINTERA=NO IRINT=DEFAULT CMASS=NO,
   SHELLNDO=AUTOMATIC AUTOMATI=ATS SOLVER=SPARSE,
   CONTACT-=CONSTRAINT-FUNCTION TRELEASE=0.0,
   RESTART-=NO FRACTURE=NO LOAD-CAS=NO LOAD-PEN=NO MAXSOLME=0,
   MTOTM=2 RECL=3000 SINGULAR=YES STIFFNES=0.0001,
   MAP-OUTP=NONE MAP-FORM=NO NODAL-DE=" POROUS-C=NO ADAPTIVE=0,
   ZOOM-LAB=1 AXIS-CYC=0 PERIODIC=NO VECTOR-S=GEOMETRY EPSI-FIR=NO,
   STABILIZ=NO STABFACT=1.0E-10 RESULTS=PORTHOLE,
   FEFCORR=NO BOLTSTEP=1 EXTEND-S=YES CONVERT-=NO DEGEN=YES,
   TMC-MODE=NO ENSIGHT-=NO
*
AUTOMATIC TIME-STEPPING MAXSUBD=10 ACCURACY=NO,
   DISTOL=0.001 DTMAX=3.0,
   RESTORE=AUTOMATIC RESPS=NO RESFAC=0.0001,
   DIVFAC=2.0 LSMASSF=1.0
```